# An application of a phenomenological triple mechanism driven direct cyclic fatigue analysis in composites

Alexander Verhoeven

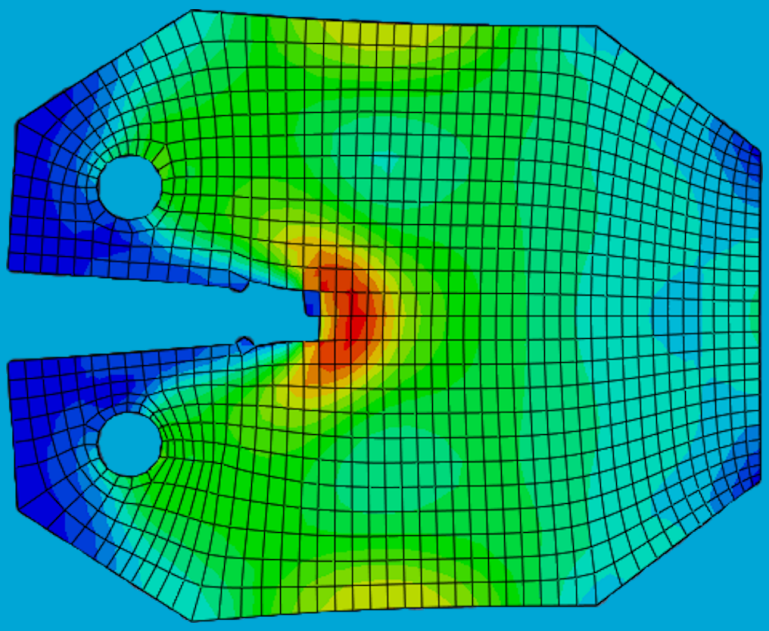

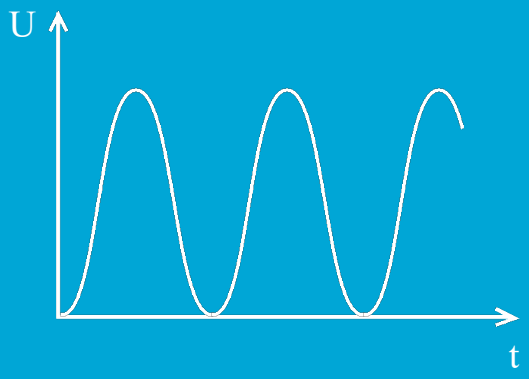


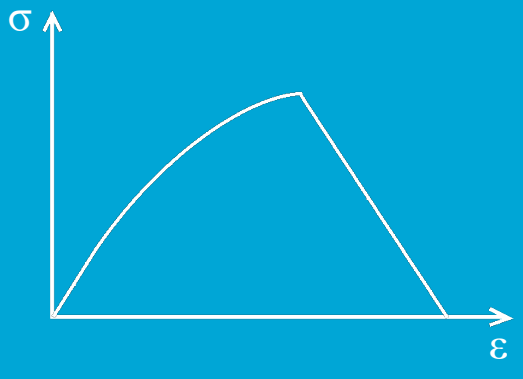


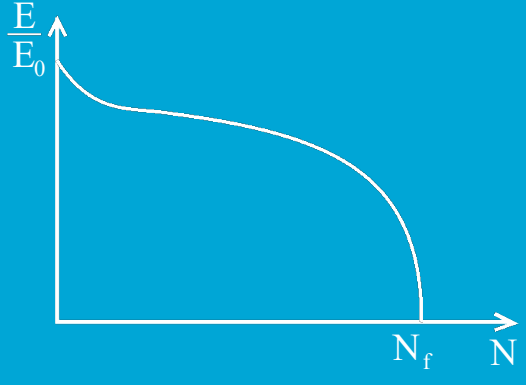


TU Delft
Delft University of Technology

# An application of a phenomenological triple mechanism driven direct cyclic fatigue analysis in composites

by

**Alexander Verhoeven**

to obtain the degree of Master of Science

at the Delft University of Technology,

to be defended publicly on Monday October 26, 2020 at 14:30.

| | | |
|---|---|---|
| Student number: | 4270177 | |
| Project duration: | 2 September 2019 – 26 October 2020 | |
| Thesis committee: | Dr. Ir. M. Pavlovic, | TU Delft, Chair of committee |
| | Dr. Ir. F. P. van der Meer, | TU Delft, Supervisor |
| | Ir. W. Feng, | TU Delft, PhD |

*This thesis is confidential and cannot be made public until 23 October 2020.*

An electronic version of this thesis is available at `http://repository.tudelft.nl/`.

TU Delft

# Preface

The first time I encountered composite materials was at my rowing club D.S.R. Proteus-Eretes. Their fleet of over 100 boats is almost entirely made of fibre reinforced polymers. I became a member of Proteus in my freshman's year at the Delft University of Technology (TU Delft) and was immediately intrigued by the fact that a skiff of 8 [m] long had a weight of only 14 [kg]. In my third year I became member of the MatCie, a group of students at Proteus who repair and maintain the boats. Every repair I executed made me more fascinated by the material. Not only is it stiff and strong in use, but it also has a large freedom in geometry for instance the ability to make 90 [°] corners. After obtaining two years of experience in handling composite materials, I participated as the structural engineer in the TU Delft Solar Boat Team of 2018 where I was put in charge of designing and producing the composite parts of the solar boat which were mainly for use in the hull and the solar deck. That year every day felt like a dream come true: designing, modelling and handling composites. After that year I knew I wanted to continue my journey to understand the material better.

This thesis is written mainly for my research group, especially to my successor who has to continue the work that I have started. Therefore the starting point of knowledge and skills of the reader is that of a master Structural Engineering student at the TU Delft. It is expected to know how to perform a static linear elastic analysis. Furthermore, the report contains a vast content of the knowledge currently available on fatigue behaviour in composites and of the non-linear finite element modelling techniques. More research groups are investigating the issue as we speak as is demonstrated by the fact that the papers of Brod et al.[1] and Bartkowiak et al.[2] were published several months ago in March and April of 2020. Their papers confirmed the idea which I had in mind in September 2019 about addressing the fatigue behaviour in composites to the individual stages of stiffness degradation with for each stage its respective dominating failure mechanism. This idea is the main argument for my model of the fatigue behaviour in composites.

My sincere gratitude to Marko Pavlovic for being patient enough to let me deal with the hurdles I had to take. I understand it is frustrating if people have a slow progress, because they want to tackle the problem in their own way. Also we had sometimes different opinions about certain issues. Hopefully the discussions about these issues were enlightening to both of us. Finally, perhaps the result of the project is not yet at the point we wished for, but creating something useful out of nothing always takes a lot of time. Let this be the first step to that something useful.

I would like to take this opportunity to thank Iris Verouden for helping me out to improve my introduction and conclusion by posing critical questions. Also thank you to Esther Spruit and Kimberley van Batenburg to read the report to see if there were any parts that needed further clarification and report back the message that was conveyed in the report. And my specials thanks to Mieke Witjens and Bart de Cleyn for proofreading this report not only to check if the overall structure conveys the message, but also thoroughly to every little detail.

# Table of Contents

# List of abbreviations

| Abbreviation | Complete terminology | Definition |
|---|---|---|
| BDSTAT | Bond status | The visualisation in colour if a nodes are separated along an interface or not as output of Abaqus[3]. |
| BK | Benzeggagh-Kenane law | One of the three laws to find equivalent energy release rates. |
| CAFL | Constant amplitude fatigue limit | The stress level at which infinite fatigue life is observed. |
| CHS | Circular hollow section | The description of the type of cross-section for the (steel) member |
| COD | Crack opening displacment | The maximum distance between two points that are across the crack perpendicularly to centre line of the crack pattern. |
| CT specimen | Compact tension specimen | A coupon for fatigue testing with the standardised geometry described in ISO-norm 15850[4]. |
| CZM | Cohesive zone modelling | A modelling tehcnique that describes a bondline between two part of the material based on contact stresses. |
| DBT | Bond time | The time that is required to debond two elements along the surface as output of Abaqus[3]. |
| DEL | Delamination | The significant failure mechanism between the plies causing a pair of layers to split. |
| EFENRRTR | Effective energy release rate | The equivalent effective energy release rate between two element based on the mixed mode law in a certain increment as output of Abaqus[3]. |
| ENNRRT | Energy release rate | The energy release rate in a certain mode as output of Abaqus[3]. |
| FAT | Fatigue | Type of loading |
| FF | Fibre failure | The last significant mechanism that occurs within the composite layer where the amount of fibres in a cross-section progressively break |
| FEM | Finite element method | An analysis method that discretises the material is small parts and uses linear approximations for these small parts to estimate the structural response. |
| FHC | First half cycle | The tensile part of the first load cycle. |
| HAZ | Heat affected zone | The area in the steel parent material that is affected by the heat of the welding process. |
| HPC | High performance cluster | A strong computer that has multiple nodes that allows to run computationally heavy models. |
| IFF | Inter fibre failure | The first significant mechanism that occurs within the composite layer as link up of the ovalised holes. |

| Abbreviation | Complete terminology | Definition |
|---|---|---|
| LEFM | Linear elastic fracture mechanics | An approach to estimate the crack propagation in a cross-section using piece-wise linear extrapolation. |
| OPENBC | Opening behind crack tip | The COD as output of Abaqus[3]. |
| Proteus | D.S.R. Proteus-Eretes | The student rowing club in Delft of which the author was member of. |
| S,N-curve | Wöhler curve | A visualisation of the number of cycles till failure for a certain constant applied stress level. |
| SDEG | Stiffness degradation parameter | The damage parameter in the element as output of Abaqus[3]. |
| TU Delft | Delft University of Technology | The university at which the research was performed. |
| U,N-curve | Displacement Wöhler curve | A variation of the S,N-curve based on displacements instead of stresses. |
| VCCT | Virtual crack closure technique | A modelling technique that describes the separation of nodes along the interface based on the local forces. |
| XFEM | Extended finite element method | A modelling technique that allows to enrich an element that could be split if the fracture criterion is met. |

# List of symbols

| Symbol | Name | Definition |
|---|---|---|
| $\alpha_f$ | Fatigue stress limit ratio | Describes the ratio between the stress level of the CAFL and the ultimate stress of the material. |
| $\beta$ | Global geometry factor | The factor that takes into account the global/structural geometry and relative crack length |
| $\Delta\sigma$ | Stress difference | The difference between the maximum and minimum stress of the cycle |
| $\Delta G$ | Difference between $G_{max}$and $G_{min}$ | The change in energy release rate between the maximum and minimum load of a cycle. |
| $\Delta G$ | Load cycle energy release rate | The difference between the maximum and minimum energy release rate of the cycle |
| $\Delta K$ | Load cycle stress intensity factor | The difference between the maximum and minimum stress intesity factor of the cycle. |
| $\eta$ | Stress triaxiality | The change in yield stress if the materialis stress dependent. |
| $\eta$ | BK law exponent | The exponent used in the BK law to define the fatigue crack propagation. |
| $\gamma$ | Load aspect ratio | The ratio between the longitudinal and transverse applied stress. |
| $\gamma$ | Surface quality ratio | Ratio describing the applied surface quality with the standardised surface quality. |
| $\gamma$ | Second kinematic hardening parameter | Describes how fast the kinematic hardening of backstress $n$ takes place. |
| $\nu_{ij}$ | Poisson's ratio | The transverse contraction in direction j of the material loaded in direction i, it relates the Young's modulus with the shear stiffness. |
| $\phi$, $\theta$ | Angle of fibre | The angle of main fibres in the layer of the composite material. |
| $\rho$ | Notch radius | The radius of the crack or notch observedin the specimen. |
| $\sigma_a$ | Amplitude stress | Half of the difference between the maximum and minimum stress of the cycle. Different notation of $S_a$. |
| $\sigma_{eff}$ | Effective stress | The amount of stress that is applied on the reduced cross-section due to damage or transverse contraction. |
| $\sigma_{eq}$ | Von Mises equivalent stress | The equivalent stress condition between different stress loads based on the Von Mises yield contour to define whether a material should yield or not. |
| $\sigma_{i,0}$ | Initial crack initiation stress | The stress level at which cracking occurs for the first time in an element. |
| $\sigma_{i,k}$ | Crack initiation stress | The stress level at which damage starts to evolve further in cycle $k$. |
| $\sigma_{ii}$ | Normal yield stress | The yield stress along the normal vector of a plane for anisotropic hardening on surfacewith the normal $i$ direction of the material and the stress also in direction $i$. |

| Symbol | Name | Definition |
|---|---|---|
| $\sigma_{ij}$ | Shear yield stress | The yield stress for an inplane shear stress for anisotropic hardening on surface $i$ in the normal direction of the plane and $j$ the direction of the stress. |
| $\sigma_m$ | Mean stress | The average of the maximum and minimum stress of the cycle. |
| $\sigma_{ij}$ | Shear yield stress | The yield stress for an inplane shear stress for anisotropic hardening on surface $i$ in the normal direction of the plane and $j$ the direction of the stress. |
| $\sigma_m$ | Mean stress | The average of the maximum and minimum stress of the cycle. |
| $\sigma_{max}$ | Maximum stress | The maximum amount of (local) stress applied to the material. |
| $\sigma_{min}$ | Minimum stress | The minimum amount of (local) stress applied to the material. |
| $\sigma_{N,\sigma_{m=0}}$ | Stress amplitude with fatigue life $N$ for zero mean stress | The level of stress that has a fatigue life of $N_f = N$ with no mean stress if applied as a constant amplitude. |
| $\sigma_{N,R}$ | Stress amplitude with fatigue life $N$ for given load ratio | The level of stress that has a fatigue life of $N_f = N$ for a load ratio stress if applied as a constant amplitude. |
| $\sigma_N$ | Stress amplitude with fatigue life $N$ for given mean stress | The level of stress that has a fatigue life of $N_f = N$ for a given mean stress if applied as a constant amplitude. |
| $\sigma_{nom}$ | Nominal stress | The applied stress if the force was exerted on a non-deformed or non-damaged cross-section. |
| $\sigma_{opening}$ | Opening stress | The tensile stress level required to open the crack. |
| $\sigma_u$, $\sigma_{ult}$, $\sigma_{ultimate}$ | Ultimate stress | The maximum stress applicable to a specimen loaded with one cycle. Different notation for $\sigma_{ult}$ |
| $\sigma_{y,\varepsilon^p_{eq}}$ | Von Mises equivalent plastic stress | The Von Mises equivalent yield stress for certain plastic equivalent strain based on the hardening. |
| $\sigma_{y,0}$ | Initial yield stress | The yield stress at the start of the analysis, input yield stress. |
| $\sigma_{y,n}$ | Current yield stress | The yield stress at cycle $N = n$ in the analysis. |
| $\sigma_y$ | Yield stress | The stress at which the material no longer follows the linear elastic response due to a stiffness reduction. |
| $\varepsilon$ | Strain | The amount of relative extension a material has obtained to deform. |
| $\dot{\varepsilon}$ | Strain rate | The speed at which the yield contour hardens if the material is strain dependent. |
| $\varepsilon^p_{eq}$ | Plastic equivalent strain | The equivalent strain of the material according to the Von Mises yield contour. It is the strain equivalent of the equivalent Von Mises stress. |
| $\varepsilon_f$ | Fracture strain | The final strain at which the material is considered to reach zero resistance. |
| $\varepsilon_{i,0}$ | Initial crack initiation strain | The strain at which cracking occurs for the first time in the material. |
| $\varepsilon_{i,k}$ | Crack initiation strain | The strain level at which damage starts to evolve further in cycle $k$. |
| $\varepsilon_{p,observed}$ | Observed plastic strain | The plastic strain observed from the nodal output of the model (engineering strain). |

| Symbol | Name | Definition |
|---|---|---|
| $\varepsilon_{p,true}$ | True plastic strain | The true plastic strain taking into account the necking of the material. |
| $\varepsilon_{ult}$,$\varepsilon_{ultimate}$ | Ultimate strain | The strain at which the ultimate stress occurs. |
| $\varepsilon^p_{ult}$, $\varepsilon^p_{ultimate}$ | Ultimate plastic strain | The plastic strain observed at ultimate stress. |
| $\varepsilon_{y,input}$ | Input yield strain | The given strain at which the material starts to yield. |
| $A$, $a*$ | Surface roughness parameter | The parameter dependent on the ultimate stress to provide a relative surface roughness. |
| $a$ | Crack length | The sum of the length of the crack created by the fatigue load, premade cracks and cut-outs. |
| $\frac{da}{dN}$ | Crack propagation rate | The speed that a crack moves through a cross-section: the change in crack length divided by the change in number of cycles. |
| $b$ | Material constant 2 of Paris law | The material constant that describes the power of the Paris law. |
| $b$ | Stress change speed | Describes how fast the isotropic hardening takes place. |
| $C$ | Material constant 1 of S,N-curve | The material constant that describes the multiplicative of the Basquin relation. |
| $C$ | Material constant 1 of Paris law | The material constant that describes the multiplicative of the Paris law. |
| $c$ | Viscosity | The numerical applied viscosity to stabilise the model. |
| $c_1$ | Paris law material constant 3 | The material constant that describes the multiplicative of the critical energy release rate in the Paris law. This notation is used in Abaqus[3] to describe the Paris law for crack initiation in fatigue. |
| $c_2$ | Paris law material constant 4 | The material constant that describes the power of the critical energy release rate in the Paris law. This notation is used in Abaqus[3] to describe the Paris law for crack initiation in fatigue. |
| $c_3$ | Paris law material constant 3 | The material constant that describes the multiplicative of the critical energy release rate in the Paris law. This notation is used in Abaqus[3] to describe the Paris law for crack propagation in fatigue. |
| $c_4$ | Paris law material constant 4 | The material constant that describes the power of the critical energy release rate in the Paris law. This notation is used in Abaqus[3] to describe the Paris law for crack propagation in fatigue. |
| $C_n$ | First kinematic hardening parameter | In combination with $\gamma_n$ as denominator, it describes how much additional in applied stress is allowed above the yield stress for the kinematic hardening of backstress $n$ |

| Symbol | Name | Definition |
|---|---|---|
| $D$ | Damage | The relative amount of material in an element that is no longer able to resist loads. |
| $\frac{dD}{dN}$ | Damage propagation rate | The speed that a damage accumulates in a cross-section: the change in damage accumulation divided by the change in number of cycles. |
| $E_{ii}$ | Young's modulus | The initial material stiffness parameters describing the elasticity of the material in normal direction on surface with the normal i direction of the material and the stress also in direction $i$. |
| $f$ | Unity check crack propagation | The (equivalent) crack driving force over the (equivalent) crack resisting force. |
| $f$ | Unity check crack propagation | The (equivalent) crack driving force over the (equivalent) crack resisting force. |
| $f^{tol}$ | Allowed tolerance on the crack propagation | The tolerance for stable crack growth to determine a cut-back in the increment or not. |
| $f_{(\sigma)}$ | Yield function | The formulation of the yield contour as a limit state for the elastic response of the material at certain hardening levels. |
| $f_U$ | Load frequency | How many times the load is applied per second. |
| $f_u$ | Ultimate stress | The maximum stress applicable to a specimen loaded with one cycle. Different notation for \sigma_{ult} |
| $f_u^{tol}$ | Additional allowed tolerance on the crack propagation | The tolerance additional for unstable crack growth to determine a cut-back in the increment or not. |
| $f_{y,observed}$ | Observed yield stress | The current yield stress that is observed in the nodal output of the model. |
| $G$ | Energy release rate | The amount of energy released as a result of breaking of the material to allow crack propagation. |
| $G_{eq,c}$ | Equivalent critical energy release rate | The equivalent energy release rate based on one of the three mix laws determining when final failure during fatigue occurs. |
| $G_{eq}$ | Equivalent energy release rate | The sum of the energy release rates of the three modes. |
| $G_f$ | Fracture energy | The energy stored in the material that will be released during non-linear deformation beyond the ultimate stress. |
| $G_I$ | Energy release rate mode I | The amount of energy released in mode I as a result of breaking of the material to allow crack propagation as normal crack. |
| $G_{I,c}$ | Critical energy release rate mode I | The amount of energy the material cross-section could resist before final rupture due to lack of resistance in mode I will occur. |
| $G_{II}$ | Energy release rate mode II | The amount of energy released in mode II as a result of breaking of the material to allow crack propagation as in-plane shear crack. |

| Symbol | Name | Definition |
|---|---|---|
| $G_{II,c}$ | Critical energy release rate mode II | The amount of energy the material cross-section could resist before final rupture due to lack of resistance in mode II will occur. |
| $G_{III}$ | Energy release rate mode III | The amount of energy released in mode III as a result of breaking of the material to allow crack propagation as out-of-plane shear crack. |
| $G_{III,c}$ | Critical energy release rate mode III | The amount of energy the material cross-section could resist before final rupture due to lack of resistance in mode III will occur. |
| $G_{ij}$ | Shear modulus | The initial material stiffness parameters describing the shear elasticity of the material on the surface i in normal direction of the plane and j the direction of the stress. |
| $G_p$ | Plastic energy release rate | The value of the energy release rate at which plasticity has large influence on the material loaded with fatigue. It indicates when stage III of the Paris law starts. |
| $G_{th}$ | Threshold energy release rate | The reduction of energy release rate due to the truncation of accounted crack propagation in the material. |
| $h$ | Element size | The nominal size of the element, generally equal for the height and width of the element. |
| $k$ | Material constant 2 of S,N-curve | The material constant that describes the power of the Basquin relation. |
| $K$ | Stress intensity factor | A description of how much higher the stress is compared to the nominal stress of the cross-section due to the geometry influence, load level and crack length during the crack propagation phase. |
| $k$ | Cycles of crack development | The number of cyces since cracks initiated in an element. |
| $K_{eff}$ | Effective stress intensity factor | The remainig $\Delta K$ after reduction of the opening and threshold values. |
| $K_f$ | Notch sensitivity factor | A description of the influence of $K_t$ on the material due to notches. |
| $K_{max}$ | Maximum stress intensity factor | The maximum stress intensity factor observed during a load cycle. |
| $K_{min}$ | Minimum stress intensity factor | The minimum stress intensity factor observed during a load cycle. |
| $K_{opening}$ | Opening stress intensity factor | The reduction of stress intensity factor due to the delayed opening of the crack as result of the load history. |
| $K_t$ | Stress concentration factor | A description of how much higher the stress is compared to the nominal stress of the cross-section due to the geometry influence, originally only in the crack initiation phase. |
| $K_{th}$ | Threshold stress intensity factor | The reduction of stress intensity factor due to the trunctation of accounted crack propagation in the material. |
| $M$ | Schütz constant | Material value given to the tangens of $R$ as a sensitivity value for the different load ratios. |
| $n$ | Arbitrary cycle number | The number of cycles that have passed that equals to an predefined number. |
| $N$ | Number of cycles | The number of cycles that have passed. |

| Symbol | Name | Definition |
|---|---|---|
| $N_f$ | Fatigue life | The total number of cycles required to let the structure fail under a certain applied load spectrum. |
| $Q_\infty$ | Stress change | The change in stress between the yield stress and the ultimate stress of the material. |
| $R$ | Load ratio | The minimum load divided by the maximum load. Load could either be stress, force, strain or displacement. |
| $R_{ij}$ | Anisotropic yield stress ratios | The ratio between the yield (shear) stress in a certain direction divided by the Von Mises yield stress. |
| $S_a$ | Amplitude stress | Half of the difference between the maximum and minimum stress of the cycle. Different notation of $\sigma_a$. |
| $t$ | Time | The perception of how long something will last. |
| $T$ | Temperature | The applied temperature in the model in $[^\circ C]$ |
| $tan(\phi)$ | Tangens of R | The tangens of the angle that $R$ makes in a $\sigma_m$,$\sigma_a$-plot. |
| $U$ | Displacement | Either the maximum displacement that is applied or the observed displacement in the model. |
| $u$ | Displacement | The required displacement to obtain infinite life in a pure plastic one element model. |
| $U_{max}$ | Maximum displacement | The maximum observed displacement in the model. |
| $U_{min}$ | Minimum displacement | The minimum observed displacement in the model. |
| $v_{1,6,i}$ | COD at points 1 and 6 at time i | The COD in the VCCT model for nodes 1 and 6 at cycle $i$ |
| $v_{1,6,i+1}$ | COD at points 1 and 6 at time i+1 | The COD in the VCCT model for nodes 1 and 6 at cycle $i+1$ |

# Summary

Wrapped composite joints are being developed to replace the design with welded joints in offshore jacket structures. Many problems arise with welding mainly due to an uncontrolled environment and the inevitable side effect of a heat affected zone (HAZ). Wrapped composite joints are created by first wrapping glass fibre around the circular hollow sections (CHS) such that a bond is created between the tube and the glass fibre. A joint will be created upon connecting the glass fibres of the multiple laminated tubes with additional layers of glass fibre. The joints could be made with or without welding the CHS prior to laminating the fibres in a thick package around the CHS. Laminating the fibres does not require immense heat to cure, thus it avoids creating a HAZ. Additionally, larger geometries allow for a smoother transition of stresses and less severe notches which reduce stress concentrations. However, composites behave differently than metals, therefore extra considerations have to be taken into account.

Assessing the fatigue behaviour of composites based on the residual stiffness diagram allows non-destructive testing to obtain the required information. Also less fatigue tests are required once the relation is known between the residual stiffness and the residual strength. Therefore a model is desired that predicts the residual strength based on the residual stiffness. In order to mimic the stiffness degradation and predict the residual strength, simulations are required that use models that extent the linear elastic computations. So the main questions are: which model is most suited to this approach of fatigue assessment with the readily available tools in Abaqus[3]? And which parameters have the most influence on the fatigue behaviour of that model?

The chosen model is a phenomenological model that generates simulations of the structure on a meso-scale level with the focus on predicting the onset of strength degradation. Three mechanisms were observed by Brod et al.[1] in out-of-plane bending fatigue tests: inter fibre failure (IFF), delamination (DEL) and fibre failure (FF). Bartowiak et al.[2] observed the same three mechanisms, but had observed only two stages upon testing an in-plane tension-tension fatigue loaded coupon. As such it is expected that these mechanisms are also present in the compact tension specimen (CT specimen). A CT specimen test is a standardised test that is described in ISO-norm 15850[4] in order to determine the crack growth resistance parameters of a certain layup of composite material. A CT specimen is loaded with in-plane bending. Therefore it is expected that the delamination mechanism will not occur separately during the fatigue test of the CT specimen. One model for each mechanism is chosen, resulting in three models included in the simulations. First the intraply mechanisms (IFF and FF) are simulated on a model with one element for better understanding of these models. Later the one element model is upgraded on its material properties and geometry before introducing the interply mechanism (DEL). The residual stiffness diagram is used to display the effect of the significant mechanisms. The research focuses heavily on the first stage of the residual stiffness diagram. This first stage is the most important part in predicting the total stiffness degradation up to the point where the strength degradation effectively starts in the final stage.

IFF is a micro-mechanism that generates cracks which are nearly invisible to the naked eye. These cracks cause to degrade the stiffness rapidly but not significantly the strength. This effect stabilises after a few cycles. In contrast to the readily available damage models, the plasticity model is capable of defining the degradation of stiffness without creating visible separation or deletion of elements, nor degradation in structural strength. Therefore the plasticity model is chosen to describe the IFF that dominates stage I of the stiffness degradation. The effect of the plasticity model is first checked on a single element since the direct cyclic analysis in combination with the plasticity model was an unconfirmed

case. One major choice had to be made regarding the formulation of hardening to be used: isotropic or kinematic hardening. Tests with a load ratio of $R = -1$ should point out which type of hardening is the most suited to describe the IFF. The parametric formulation of the hardening is preferred over tabular formulation for guaranteed compatibility with the ductile damage model. A remark has to be given to the use of the plasticity model. The plasticity model has to be taken with caution as it will lead to the crack overclosure effect which is present in metals, but not in composites.

The ductile damage model is used to describe the meso-scale cracks of the FF that dominates stage III. In stage III both the stiffness and the strength deteriorate progressively. The plasticity model is compatible with the ductile damage model since the ductile damage model is an augmentation of the plasticity model. It implies that stage I and III will not occur together in a model with one element. In all the models with a CT specimen geometry it is possible to have one element in stage I and the adjacent element in stage III. For that reason on a structural level the transition from stage I to stage III is defined as the moment that the residual stiffness degradation has stabilised itself for the first time and now progresses slowly and linearly on a logarithmic scale. On that point stage III starts. This transition point coincides with the first element in the model failing completely due to the ductile damage model.

The delamination is modelled using the Virtual Crack Closure Technique (VCCT). Since the DEL is occurring on the interface between two layers during fatigue loading, the VCCT criterion is the most suited model. During the delamination pairs of layers are pulled apart step-by-step as an interply mechanism.

The model that includes all three mechanisms for the CT specimen geometry with a layup of [0|-45|90|45|0] shows results that are consistent with the requirements as long as the quasi-isotropic stiffness is used to describe each layer. The cracks are in the horizontal direction from the crack tip which is the weakest direction bases on the quasi-isotropic stiffness and the isotropic strength. The shape of the stiffness degradation curve shows stages I and III with delamination present in both stages. Also the peak stress at the crack tip of $284$ [MPa] matches closely with that of the defined maximum stress in the plasticity model of $289.5$ [MPa]. Together with the nominal stresses based on the applied forces and the net cross-section, a stress intensity factor of about $6$ is observed in the first cycle. Only the crack propagation rate over the number of cycles $\frac{da}{dN}$ of the intraply does not follows the Paris law and $\frac{da}{dN}$ of the interply follow a Paris law with different material constants $c_3$ and $c_4$.

The fatigue life of the CT specimen is influenced by many factors. Changing one of the influencing parameters related to a certain mechanism will change the fatigue life of an element that endures that mechanism. With this in mind the shape of the stiffness degradation curve of the one element model and the CT specimen could be adjusted to match that of the future test results. The total fatigue life depends on the speed of the slowest mechanism at any given moment. If the intraply cracking is lagging behind, then the most influential parameters on the fatigue life are: fracture energy $G_f$, fracture strain $\varepsilon_f$ and stress change $Q_\infty$. Furthermore the fatigue life is increased during the ductile damage model by increasing $G_f$ or $\varepsilon_f$. The fatigue life for a certain stage is increased by increasing one of these parameters correlated to the mechanism of that stage. That will therefore influence when stage I has ended. If the interply cracking is lagging behind, then the most influential parameters are the material constants $c_3$ and $c_4$ of the Paris law. The fatigue life is increased by increasing $c_3$. Increasing $c_4$ will generally decrease the fatigue life as the equivalent exerted effective energy release rate at the crack tip is generally lower than $1$.

The mesh refinement study revealed that for both the VCCT models and the tie models of the CT specimen an element size of $1$ [mm] is sufficiently small to obtain converged solutions. An element size of $2$ [mm] could be used for quick simulations, but is somewhat less accurate.

However, the both type of models (VCCT and TIE) do not take into account certain mechanisms that have a lesser influence. It assumes these mechanisms do not occur. Also the phenomenological model only mimics the mechanisms instead of describing the real mechanism. Additionally, the model is only capable of handling quasi-isotropic composites since no strength differences in different material orientations are defined. Furthermore, the hardening and fracture parameters are based on static tests and estimated values, hence fatigue testing is desired to calibrate the model. Finally, the most important limitation is the fact that the model is not capable of performing (controlled) cycle jumping.

All in all, the VCCT MS2 models describe the fatigue behaviour of composites based on the different failure mechanisms within the given limitations. Therefore the most suited model with readily available techniques in Abaqus [3] is to use the plasticity formulation for the IFF, the VCCT for delamination and the ductile damage formulation for FF. Currently the model is not ready to fully describe the fatigue behaviour in composites. The improvements that have to be made are cycle jumping and including the different strengths for each material orientation as is present in the Hashin model for static analysis.

# Chapter 1: Introduction

## 1.1. Background and motivation

In off-shore structures the type of foundation is based on the depth of the water underneath the surface as summarised by Dvorak[5]. In medium shallow waters jacket structures are the most economical solution. Jacket structures are made of hollow sections that create a three dimensional truss system that is light, strong and rigid. Generally these are made of circular hollow sections (CHS) that are connected by welding. In the past some major disasters happened with oil platforms such as the Alexander Kielland in 1980 as is written in a report of the Officer of the Watch[6]. The cause of these disasters were often related to a bad quality of welding. The welding has to be done on site, which means that it is likely to obtain poor quality welds and misplaced beams. In case of the Alexander it was because of an incomplete welding resulting in a cross-section reduction of the weld of more than $50\%$. Even if the welding is performed with a high level of quality, there is still a heat affected zone (HAZ) present in the parent material caused by rapid cool down resulting in residual stresses.

Creating a connection using composite materials would be a solution. Winding the fibres around the steel hollow section and fixating these with resin does not require large amounts of heat. On top of that, composite connections have a larger freedom in geometry, especially in the thickness direction of the fillet. For that reason also lower stress concentrations could be achieved which is advantageous when designing against fatigue failure as stated by Alderliesten[7]. Additionally, the crack propagation works as a warning on site for failure as the crack creates loud noises during growth.

## 1.2. Scope and problem statement

The fatigue behaviour in composites is a relatively new field of study. At first composite fatigue behaviour was assessed as steel. However, when it became evident that composite have short crack initiation phase, other methods were required. The crack propagation methods showed that composites is a material that initially shows a quick degradation in stiffness of a couple of percent, but that stabilises to a slow and steady degradation up to a certain point where the stiffness and strength deteriorates progressively as was observed by Brod et al.[1] and other research groups. This allows to monitor failure more accurately once fully understood according to Van Paepegem and Degrieck[8]. However, the fatigue behaviour in composites is not yet fully understood, therefore an accurate prediction method is not yet obtained.

The goal is to create a finite element model that predicts the stiffness degradation and fatigue life of a glass fibre reinforced compact tension specimen. The compact tension specimen is generally investigated in a more pragmatic manner that considers the entire composite layup as one material. Then Paris law[9] is often used to predict how many cycles are required to propagate a crack through the entire cross-section. This thesis will apply the research of Brod et al.[1] of the out-of-plane bending fatigue test and Bartowiak et al.[2] of the in-plane tension-tension fatigue test on the compact tension specimen for fatigue load. That will provide a better insight on how the compact tension specimen fails. If that is well understood, then these techniques could be applied on larger scale, for instance to investigate the fatigue

failure of the wrapped composite joints.

In order to achieve that goal, a definition has to be set to the stiffness degradation and fatigue life of composites. The stiffness degradation is defined as the reduction in stiffness between cycle $N = n$ and cycle $N = 1$. The stiffness of cycle $N$ will be measured as an average stiffness of the structure during that cycle: $\frac{F_{max}-F_{min}}{U_{max}-U_{min}}$. Often the residual stiffness will be normalised to the first cycle to compare the results for different load levels. The fatigue life of composites is defined as the final cycle that the structure is able to withstand the imposed load. This implies that the cycle after will let the crack propagate through the specimen in one cycle for the remainder of the cross-section. This coincides with no residual stiffness being present.

These definitions will be applied in a finite element model (FEM) to investigate the fatigue performance of a glass fibre reinforced compact tension specimen. Although the applications for FEM in structural engineering is very extensive, only a limited amount of possibilities will be investigated. The research will limit itself to the readily available tools in Abaqus[3]. The readily available tools are options in Abaqus[3] that do not require any user-defined subroutine or user-defined material.

## 1.3. Research questions and model requirements

This report will focus first on the fundamental understanding of how to address fatigue failure in composites, then on the assessment using finite element models. From the master study Structural Engineering a lot is emphasised on recognising failure mechanisms and that each change in response indicates that a new failure is governing. In order to fully understand the composite reaction to fatigue loading, every significant failure mechanism needs to be addressed. So first of all, what are the significant failure mechanisms that need to be identified? Also how do they influence the fatigue behaviour? **In the next step the main question arises: which model is the most suited for simulating the fatigue mechanisms in composites in a compact tension specimen with the readily available tools in Abaqus [3]?** How much potential does this model have in predicting fatigue failure in glass fibre composites?

In order to grade the potential of this model certain requirements have been set from most to least important:

- The fatigue model has to generate a crack pattern for every layer in direction of the weakest direction for that layer of composite material. This weakest link is based on the stress field due to the orthotropic stiffness and the orthotropic strength of the composite material of that layer, the influence of the layup and the geometry of the specimen.
- The fatigue model has to perform (partial) cycle jumping in order to handle a million number of cycles within a week for a compact tension specimen.
- The fatigue model should include the orthotropic stiffness formulation for the material properties to predict the stress and the deformation field accurately for the different material orientations in a similar manner as the orthotropic elastic stiffness formulation for static models.
- The fatigue model should include orthotropic strength formulation for the material properties to predict the onset of cracking more accurately based on the stress field for the different material orientations in a similar manner as the Hashin damage[10] model for the static models.
- The fatigue model has to include the brittle material properties (failure strain of less than $1\%$) in

the damage model to mimic the brittle behaviour of the composite material in a similar manner as a damage criteria in a static model.

- The crack propagation speed in the fatigue compact tension specimen model should correlate with the critical energy release rate or the stress intensity factor to the Paris law[9] as is often observed in compact tension fatigue tests.
- The fatigue model should visualise the effects of the three significant mechanisms identified in chapter 2 in a different manner for each mechanism for easy identification in determining in which stage the material is.

The last requirement listed above is a preference instead of a boundary condition. If some of these requirements are not met now, then it is interesting to know: what are the possibilities in future research to meet the lacking requirements? In the model certain parameters will be used that influence the crack behaviour of the elements in the model, therefore they also influence the fatigue life prediction. In order to reduce the work load during calibration of the model, which parameters have the most influence on the expected fatigue life?

The research questions will be listen below, once more, in chronological order in which the thesis is build up:

1. What are the significant failure mechanisms and how do they influence the fatigue behaviour of composites?
2. Which model is the most suited for simulating the fatigue mechanisms in composites in a compact tension specimen with the readily available tools in Abaqus [3]?
3. How much potential does this model have in predicting fatigue failure in glass fibre composites based on these mechanisms based on the requirements set?
4. What are the possibilities in future research to meet the lacking requirements?
5. Which parameters have the most influence on the expected fatigue life and how do they influence the fatigue life of the model?

The overall conclusion in chapter 7 will answer these questions in this order as well.

## 1.4. Thesis outline and guide

Each chapter will be readable as a stand-alone with its own introduction and conclusion that poses and discusses the research questions related to that chapter. This allows to read only certain chapters of the report. The overall introduction and conclusion mainly focus on the ideas that will span multiple chapters and answer the main research questions discussed earlier. Chapters 3, 4 and 5 will also have a set of hypotheses that will be investigated during that chapter. At the end of the chapter these hypotheses will be answered concisely with a reference to the paragraphs in the chapter that will discuss it in detail. After that, new hypotheses will be stated based upon the theory and hypotheses of that chapter. These hypotheses will be accompanied with an explanation on how these hypotheses are derived and in which section the answer will be given.

The chapters are written in this order to capture first a general idea of fatigue assessment that then will be narrowed down to the final application. This results in starting off with the theory about fatigue and ending with the implementation of the model. Chapter 2 will be the starting point to provide additional knowledge for students and engineers who have basic knowledge about finite element methods, composites and fatigue. It will particularly be addressed to the research group of composites on the faculty of Civil Engineering at the Delft University of Technology. This chapter provides the most important characteristics of a fatigue assessment in composites. It will discuss the various failure mechanisms that are present and how these mechanisms influence the fatigue behaviour of the composite. Chapter 3 will show which model is suited to simulate each failure mechanism and why it is suitable. This will be a guideline to numerically simulate fatigue failure in composites. Chapter 4 will continue on this by focusing on how it is implemented in Abaqus [3] and what the influence of each parameter is on a single element. This one element model needs to be upgraded to a full compact tension specimen model. That is done in chapter 5. In that chapter the requirements are implemented step-by-step. The final model will be judged on the earlier described requirements, therefore it answers the question if it has the potential of simulating the fatigue failure after calibration or not. It will also provide possible solutions to the requirements that are not met.

# Chapter 2: Theory of fatigue in composites

## 2.1. Introduction

In order to let the simulations aid the fatigue assessment of composites, first the fatigue assessment should be defined. What are the characteristics of a fatigue assessment in composites? Basic knowledge if often lacking as most engineers only understand what an S,N-curve is and what stress concentration factors are. To start off, a generic material independent idea of the fatigue assessment will be discussed, assuming the reader already knows the existence of an S,N-curve and the influence of stress concentrations. Secondly the fatigue assessment of a metal will be presented as it is much easier with only one fatigue failure mechanism.

Afterwards the transition to composites is made by answering the question: which fatigue mechanisms are present in composites? These mechanisms will be elaborated further by observing the literature about their influence on the fatigue failure of composites. Composites are often assessed on a relative residual stiffness or strength curve where each stage is dominated by a different mechanism. For out-of-plane bending this is already investigated, but how does it translate to in-plane bending? Moreover, how is it related to the Paris law?

## 2.2. Generic concept of fatigue assessment

In a fatigue assessment a cyclic load is applied on a structure. The load could be from as simple as a sinusoidal load with a constant amplitude to as complex as an applied spectrum with a variable amplitude which only has unique load cycles. Although the latter is more realistic to structures loaded by forces caused by nature, the former is often used in design and research. The constant amplitude load is used so often, because fatigue assessment in general is already complex. Currently fatigue assessment during the design phase of a new structure is usually done by carefully comparing the new structure with a related existing structure of which the fatigue performances are known. There are a lot of factors influencing the fatigue behaviour of a structure ranging from the quality of the material to the global load bearing structure. Notice that the word structure is often used instead of material as fatigue failures are $80\%$ caused by the performance of the structural design and $20\%$ caused by the material that has been used as stated by Alderliesten[7]. Therefore the fatigue assessment is often simplified to the applied stress range that has the most impact on for the structure. The most impact on the structure is not necessarily related to the highest applied stress range, but is related to the stress range that leads to the shortest fatigue life. This is not only dependent on how large the difference in maximum and minimum stress is, but is also dependent on how often each stress range occurs. The fatigue life $N_f$ is defined as the number of load cycles it endures until final failure occurs, which is the moment just before the structure is fully cracked. Figure 2.1 visualises the general approach to a fatigue assessment. As more cycles of the load are applied, the cracks in the structure will grow causing the residual strength to decrease. If the residual strength remains larger than the applied stress, then no failure will occur. Failure only occurs at the moment that the applied stress is equal to the residual strength of the structure.

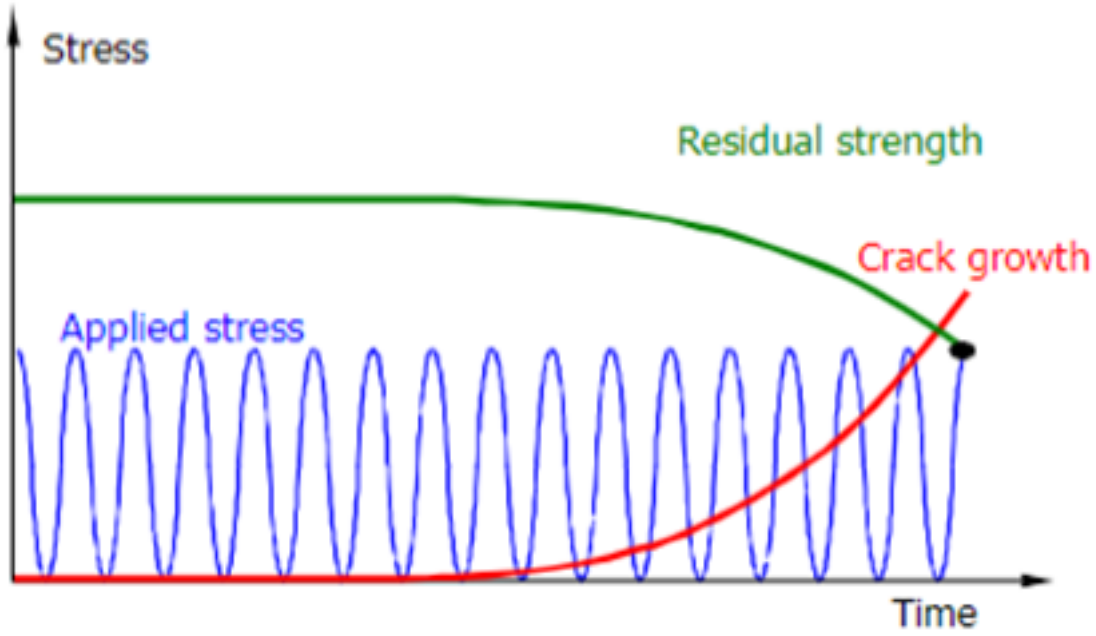


**Figure 2.1:** The general representation of a fatigue assessment: the blue line is the applied load over time on the structure with the value of the stress on the vertical axis, the red line represents the crack length over time in the structure with on the vertical axis the length of the crack and the green line is the residual strength over time of the structure showing a reduction due to the crack growth. Failure happens if the residual strength and the applied stress are equal as is represented by the black dot. This figure is retrieved from the lectures by Alderliesten[7].

During any fatigue analysis there are a couple of definitions used that makes it easier to communicate. First of all a load cycle has a maximum stress $\sigma_{max}$ and minimum stress $\sigma_{min}$. These are corresponding to the extreme values of each cycle. In a load sequence with a constant amplitude these are easy to spot since the cycles are easy to distinguish, for a load spectrum it is more difficult. There exist several methods to count cycles in a spectrum. The two most common counting methods are reservoir counting as described in the BS 5400-10 norm[11] and rainflow counting as explained by Schijve[12]. The reservoir counting is easier to perform during hand calculations, but the rainflow counting is easier to program. Both methods give the same answers. The stress range $\Delta\sigma$ is defined as the difference between the maximum and minimum stress as is given in equation 2.1. Often the load ratio $R$ is used in fatigue assessments as many failure mechanisms and other fatigue life determining aspects are related to the load ratio. The load ratio is defined as the minimum stress over the maximum stress as is shown in equation 2.2. One could also define a certain mean stress $\sigma_m$ which is not the average of stress over time, but simply the mean of the maximum stress and minimum stress of a load cycle as is given in equation 2.3. In fatigue assessment the load time is of limited influence compared to the stress range. The stress amplitude $\sigma_a$ could either be defined by the absolute of the difference between the mean stress and maximum or minimum stress, or be defined as half of the stress range as both definitions are equal as proven in equation 2.4. Although equations 2.1 and 2.2 are described for the stresses in a load controlled test or analysis, these equations are analogous for strains in a displacement controlled test or analysis. Figure 2.2 illustrates the different possible regimes of the load ratio related to the mean stress and the stress amplitude. Some regularly used load ratios are: $R = -1$ for a fully reversed load cycle, $R = 0$ for a pure tensile load cycle with $\sigma_{min} = 0$ and $R = +\infty$ for a pure compressive load cycle with $\sigma_{max} = 0$. In practice a slightly different ratio than $R = 0$ is used to prevent external compressive loading with potentially different mechanisms activated due to an overshoot of the jacket. $R = 0.1$ is used instead of $R = 0$ which results in a minimum stress at an amplitude of a tenth of the maximum stress. For compressive cycles $R = 10$ is used as a substitute for $R = \infty$ for the same reasons as is mentioned

by Alderliesten[7]. This is certainly of greater importance for composites than for metallic structures as composites behave much worse under compressive load cycles than under tensile load cycles compared to metals.

$$\Delta\sigma = \sigma_{max} - \sigma_{min} \tag{2.1}$$

$$R = \frac{\sigma_{min}}{\sigma_{max}} \tag{2.2}$$

$$\sigma_m = \frac{\sigma_{max} + \sigma_{min}}{2} \tag{2.3}$$

$$\sigma_a = \sigma_{max} - \sigma_m = \sigma_m - \sigma_{min} = \sigma_{max} - \frac{\sigma_{max} + \sigma_{min}}{2} = \frac{\sigma_{max} - \sigma_{min}}{2} = \frac{\Delta\sigma}{2} \tag{2.4}$$

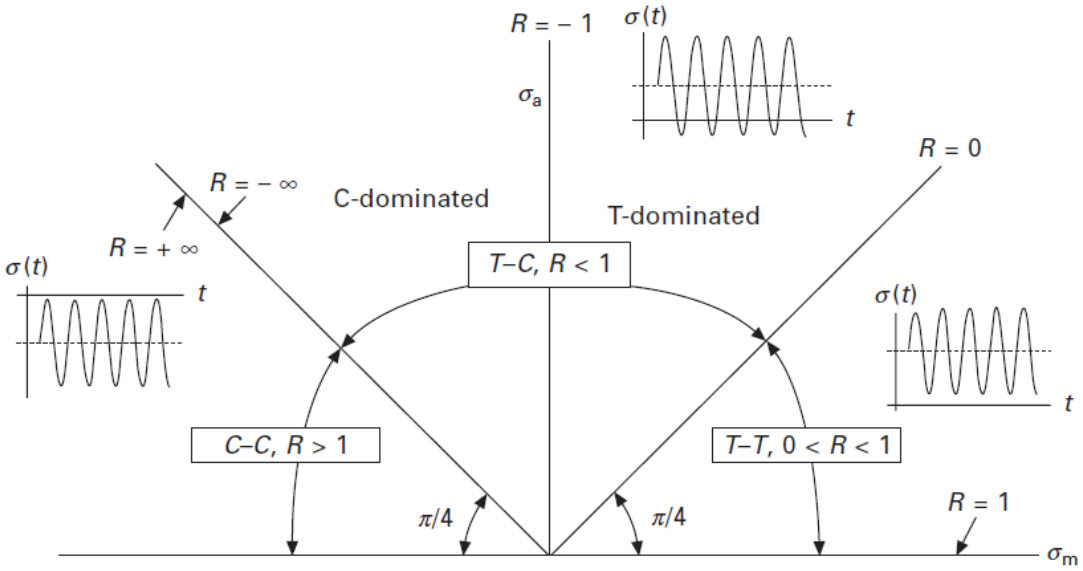


**Figure 2.2:** The different fatigue amplitude loading ratios $R$ sketched for different mean stress and stress amplitudes. The capital letter "T" is short for tensile and the capital letter "C" is short for compression. The diagonal lines are at an angle of $\frac{\pi}{4}$ which means that the amplitude equals the absolute value of the mean stress. The figure has been retrieved from Vassilpoulos and Nijssen[13].

May it now be clear that fatigue is mainly a structural problem. However, the research performed is focused on the fundamentals of a finite element model (FEM) that describes the fatigue failure mechanisms of the material. In essence finite element models divide the structure into small pieces which are direct transformations of isoparametric elements. The isoparametric elements are elements with basic shapes that have unit size dimensions on which the constitutive relations are defined. Thus little to no numerical calibration is expected during up-scaling from a CT specimen model to the full size joint model. Therefore the focus will be on the material behaviour with respect to fatigue loading which is described in the constitutive relations.

## 2.3. Common practise to address fatigue assessment

There is still much unknown about fatigue behaviour, let alone about fatigue behaviour in composite structures as much repeated by Alderliesten[7]. Still one of the design requirements is that the structure will not prematurely fail due to fatigue mechanisms. The fatigue mechanisms are material depended and in theory for each mechanism a set of constitutive relations is required as is mentioned by Shokrieh and Lessard[14]. Each set of constitutive relations will be implemented in the material model as a module [7]. Especially in composites it will mean that multiple modules are needed to assess the fatigue behaviour since many mechanisms are present in composites. For that reason simplifications are made by grouping fatigue mechanisms that result into the same failure mode and neglecting the mechanisms that have little influence on the fatigue life estimation. It are the load cycles which determine what fatigue mechanism is governing and which failure mode will prevail. Important aspects of the load cycles are: load range, load ratio, direction of loading, length of specimen, ageing, environment (lab, vacuum, saltwater), frequency and opening time as stated by Alderliesten[7]. Since these mechanisms are assessed pragmatically by comparing results from tests to verify if there is sufficient fatigue life or to estimate the fatigue life from it, currently all the widely used existing models are phenomenological. Progress is made in the fundamental models that describe the true behaviour of each occurring mechanism as for instance Brod et al.[1] and Shorieh and Blessard[14] have focused their research on. Additionally progress is made in statistical models that will aid to reduce the amount of tests needed as is investigated by Kaminski[15], Naderi and Maligno[16] and Kassapoglou[17]. Both type of models are useful, but the fundamental models that describe the mechanisms are more desired at the moment.

### 2.3.1. Fatigue life of a structure

Often the fatigue life is split in a crack initiation phase and a crack propagation phase. According to the definition of fatigue life all the cycles from $t = 0$ in the crack initiation stage till $t = t_{failure}$ in the crack propagation stage must be included. The crack initiation stage is the period of fatigue loading where no visible crack is observable. Only after failure striation marks will be visible with an electron microscope. Each striation mark indicates a cycle and the size of the striation mark is proportional to the size of the load as is shown in figure 2.3. The crack nuclei start to form at local imperfections as these imperfections cause stress concentrations. The imperfection starts the crack as a local slip band creating alternating intrusions and extrusions due to the cyclic loading as is drawn in figure 2.4. Generally cracks start at the surface as these imperfections are generally larger. Hence the crack initiation period could be extended not only by which material is used, but also by how well the surface is polished as is illustrated in figure 2.5.

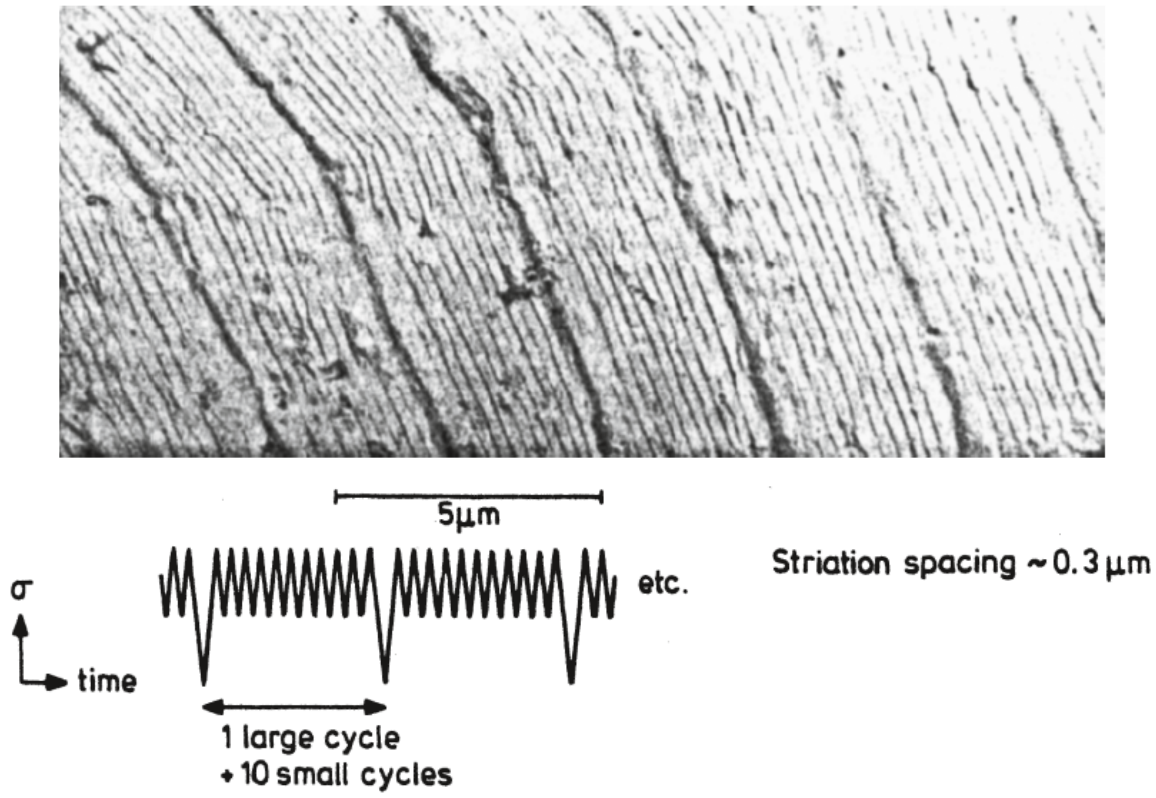


**Figure 2.3:** An electron microscope revealing the striation marks on the fracture surface of a fatigue failed specimen of metallic material. The figure has been retrieved form the book of Schijve[12].

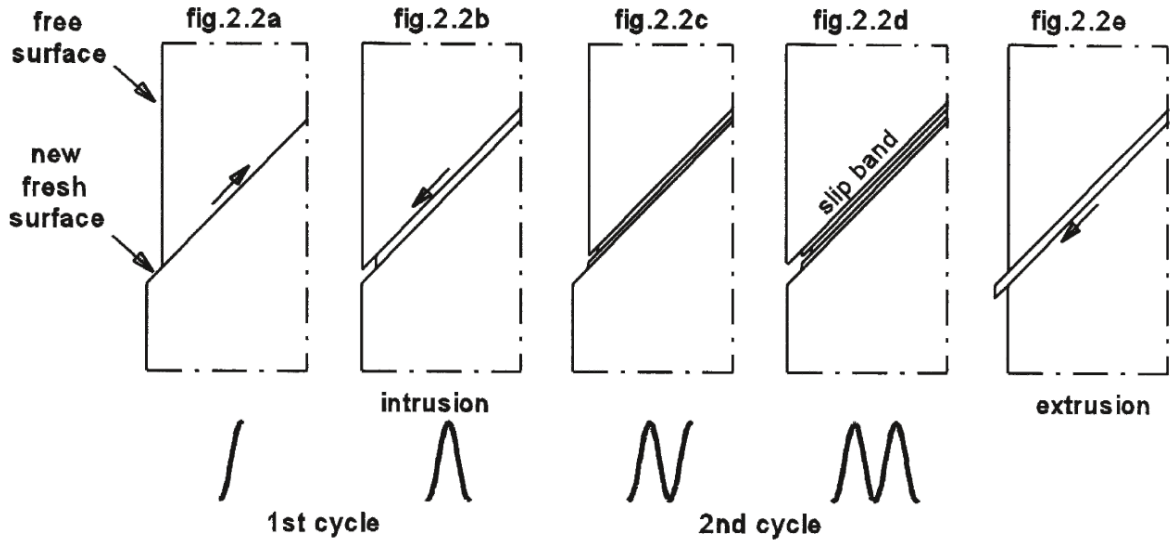


**Figure 2.4:** One or more of the local slip bands are excited by the cyclic loading. During the first half cycle the internal slip creates a new surface until the grains on microscopic level are arranged in such a way that the imperfection is moved out. Hence the material becomes stronger locally. This creates an intrusion. Now the parallel grains are excited as the next weak spot and upon by completing the next cycle a slip band forms which results in an extrusion. The figure has been retrieved form the book of Schijve[12].

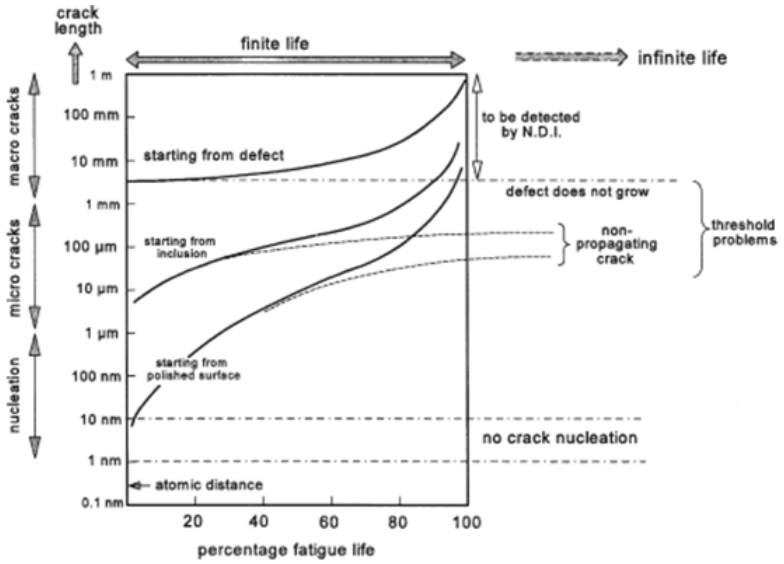


**Figure 2.5:** Different sizes of initial flaw lead to different numbers of cycles till failure. The smaller the initial flaw, the more cycles in the crack nucleation stage is needed until the crack propagation phase starts, thus the longer the fatigue life. The figure has been retrieved form the book of Schijve[12].

### 2.3.2. Crack initiation phase of a structure

The numerical assessment for the crack initiation phase is often performed with an S,N-curve. The S,N-curve was first formulated by August Wöhler in 1867 [12]. The basic idea is to use a material constant that relates the stresses in logarithmic order with the number of cycles till failure. This is also know as the Basquin relation. The Basquin relation is given in equation 2.5.

$$(S_a)^k N = C \tag{2.5}$$

Upon plotting the relation on a double logarithmic scale, a straight line is observed. The S,N-curve describes the number of cycles till failure on the x-axis for a certain constant maximum stress on the y-axis as is represented in figure 2.6. The Basquin relation is said to be true between $100$ cycles and one million cycles for metals. Below $100$ cycles an upper limit is reached which is the ultimate strength of the metal itself. This upper limit is caused by the plastic shakedown effect that allows the plastic response of the material to redistribute stresses accordingly such that a negligible amount of fracture happens. At about $100$ cycles on maximum load the metal will still fail due to the amount of plastic strain. If the analysis is below $10^4$ cycles, then it is called a low-cycle fatigue analysis and if it is above $10^4$ cycles, then it is high cycle fatigue. Above $10^6$ cycles the constant amplitude fatigue limit (CAFL) is reached which means that the internal stresses are so low that they will never lead to fatigue failure.

Although in theory the S,N-curve may only be used for the crack initiation stage, in practise it is often used for the total fatigue assessment that includes the crack initiation phase and the crack propagation phase. Depending on the material that is used this practice is good enough or bad. Here it will only be used to describe the crack initiation stage. If no load ratio is given for an S,N-curve, then the S,N-curve is given for a fully reversed load ($R = -1$) of an unnotched specimen. This is the basic load ratio to determine a S,N-curve as the S,N-curves for many other load ratio's could be extracted from $R = -1$ based on the Goodman, Gerber or Schütz equation provided by Schijve[12]. These equations are represented respectively in equations 2.6, 2.7 and 2.8.

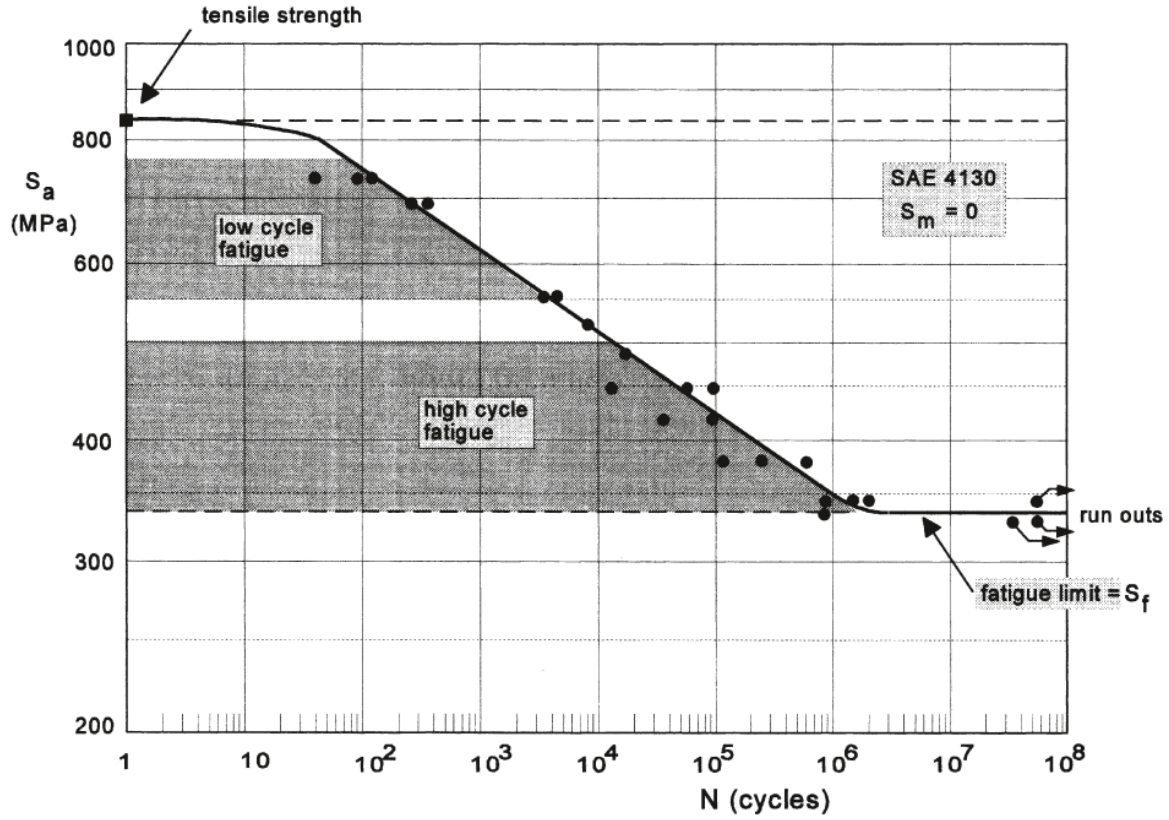


**Figure 2.6:** S,N-curve for an unnotched specimen with $\sigma_m = 0$ for a low-alloy steel (SAE41300). The figure has been retrieved form the book of Schijve[12].

$$\frac{\sigma_N}{\sigma_{N,\sigma_m=0}} = 1 - \frac{\sigma_m}{\sigma_U} \tag{2.6}$$

$$\frac{\sigma_N}{\sigma_{N,\sigma_m=0}} = 1 - \left(\frac{\sigma_m}{\sigma_U}\right)^2 \tag{2.7}$$

$$M = \tan(\phi) = \frac{\sigma_{N,\sigma_m=0} - \sigma_{N,R}}{\sigma_{N,R}} \tag{2.8}$$

In these equations $\sigma_U$ describes the ultimate stress of the specimen during one cycle, hence during a static test. $M$ describes the sensitivity factor for the material to different load ratios. $\sigma_{N,\sigma_m=0}$ equals the stress level for a certain number of cycles $N$ till failure under standard circumstances. $\sigma_N$ equals the stress level for a certain number of cycles $N$ till failure at a certain mean stress which is usually considered as the output of these equations. For the Schütz equation $\sigma_{N,R}$ is considered often as output for the stress level for a certain number of cycles $N$ at a specific load range. Many tests concluded that the material response is between the Goodman relation and the Gerber relation. What is often done is using the Schütz equation to determine if the Goodman equation or the Gerber equation resembles the material better Alderliesten[7] stated. Transforming the original S,N-curve to the S,N-curve adjusted for the load ratio has influence on both the upper and lower limit as the entire stress range is shifted. For stress concentrations the effect of changing the S,N-curve is only on the lower as plastic shake down prevents the effect on the upper limit.

### 2.3.3. Crack propagation propagation phase of a structure

After assessing the crack initiation phase, it is time to assess the crack propagation phase. It is enough for one crack to pass through the cross-section to result in failure. Therefore only the fastest crack has to be investigated. During the assessment of the crack propagation phase, one will encounter three distinct stages of crack propagation rate as is shown in figure 2.7. First of all a slow crack growth occurs which increases in speed until the acceleration levels off and enters the second stage. During the second stage there is a constant increase in crack growth speed until the third stage has entered. In the third and final stage the crack growth accelerates exponentially till failure makes it quite sudden. The second stage is described by the Paris law[9]. The Paris law is given in equation 2.9.

$$\frac{da}{dN} = CS^b \tag{2.9}$$

Here the crack propagation speed $\frac{da}{dN}$ equals a logarithmic function with $a$ the crack length and $N$ the number of cycles. $C$ and $b$ are material constants with units related to the observations made. $S$ is a factor that describes the load severity at the crack tip. More on this will be discussed during the material specific assessment as crack propagation is also material and thickness dependent while crack initiation is geometry and load dominated.

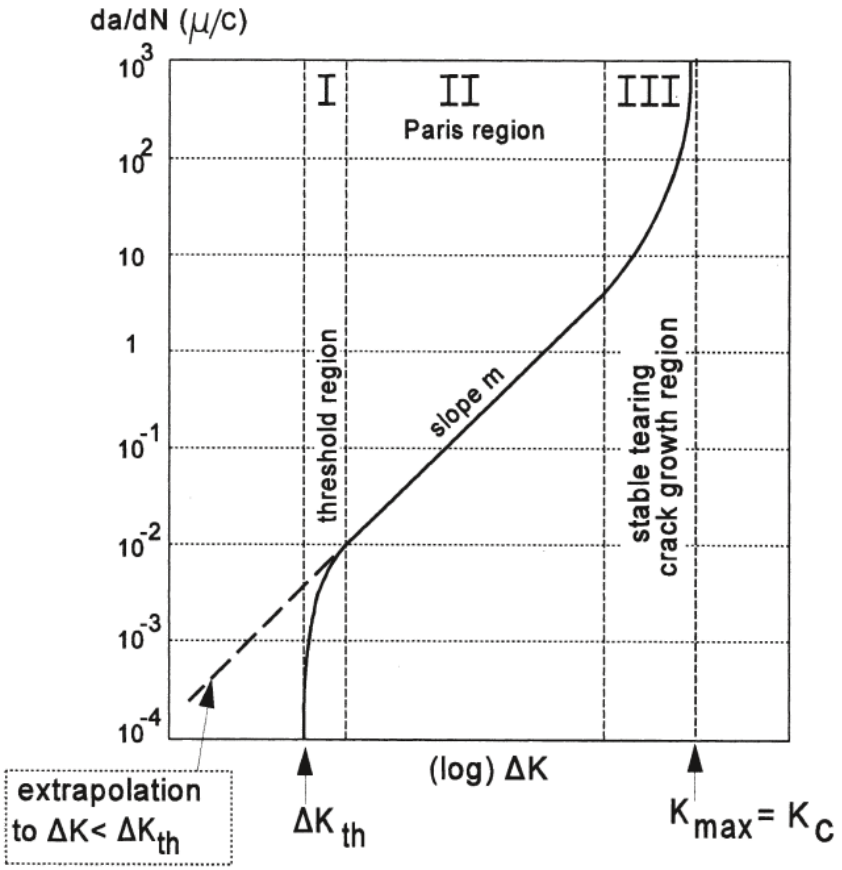


**Figure 2.7:** The general concept op the Paris law describing the crack propagation speed based on the stress intensity at the crack tip. The figure has been retrieved form the book of Schijve[12].

## 2.4. Fatigue assessment for steel

### 2.4.1. Fatigue mechanisms present in steel

As the fatigue assessment is mechanism dependent, the mechanisms related to steel will be discussed. There is actually one main mechanism identified during fatigue assessment with three modes: in-plane tension (mode I), in-plane shear (mode II) and out-of-plane/transverse shear (mode III). A visualisation of each mechanism is provided in figure 2.8. Keep in mind that cracks are always a surface despite drawing them as a line in a two dimensional drawing. In figure 2.9 the three different types of cracks are illustrated that could be encountered. Based on the length and location it is called either a corner crack, surface crack or through crack.

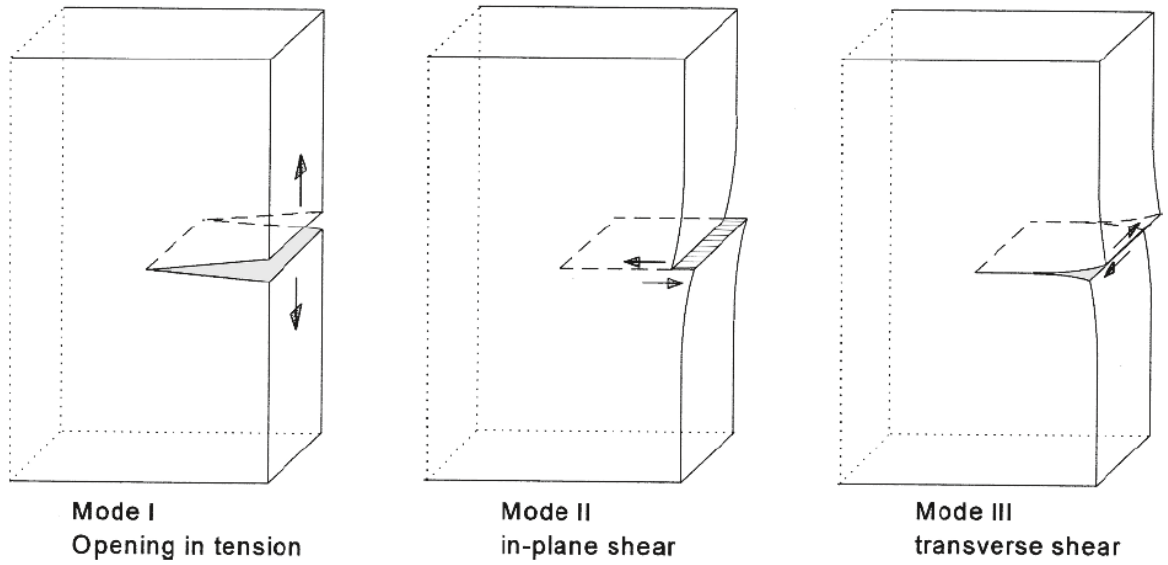


**Figure 2.8:** The three fundamental failure modes in steel caused by fatigue loading. The figures are drawn in top view, thus modes I and II are in-plane and mode III is out-of-plane. The figure has been retrieved form the book of Schijve[12].

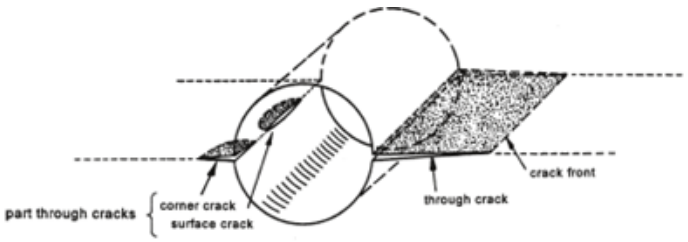


**Figure 2.9:** An illustration of the three types of cracks that could occur. If the crack is entirely through the cross-section of the specimen, than it is called a through crack. If the crack is on the outer surface and only partially through, then it is called a corner crack. If the crack is embedded or at the internal cut-out, then it is called a surface crack. The figure has been retrieved form the book of Schijve[12].

Fatigue cracks in steel start as surface cracks that are governed by shear slip during the crack nucleation stage. As soon as the crack is large enough to propagate perpendicular to the applied local stress, then it is no longer in the initiation stage, but in the propagation stage as is visualised in figure 2.10. Each time a crack makes a change in course, it means a different failure mode is governing. So in an experiment it is possible to first observe mode II as governing failure mode during the crack initiation

phase, then observe mode I as governing failure mode for the main part of the propagation phase and finish with mode III due to instabilities of the system. Do note that the grain boundaries of the steel have influence on the crack growth rate. Especially during the crack initiation phase the grain boundary could temporary slow down the crack growth by a factor 100. Although the grain boundaries at the surface cause faster crack initiation due to being an imperfection, it does help in the long run to slow down the microcrack growth as is shown in figure 2.11.

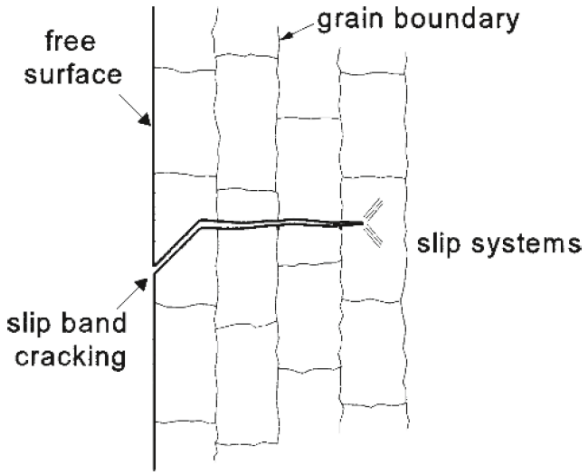


**Figure 2.10:** An illustration of the crack initiation in steel with a surface micro-crack growing in mode II starting from the edge diagonally. The crack continues after the corner in the crack propagation phase as a macro-crack growing in mode I. The figure has been retrieved form the book of Schijve[12].

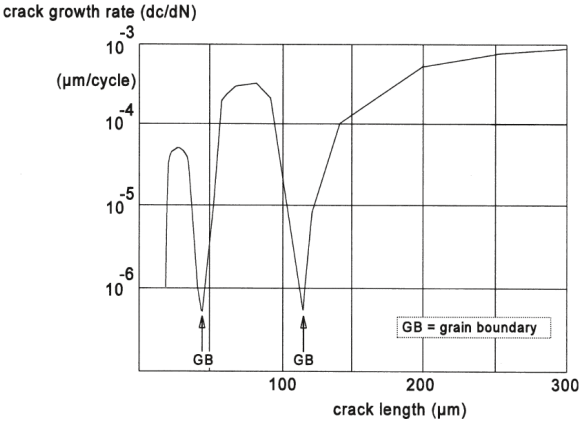


**Figure 2.11:** A crack growth curve on micro-scale for the crack initiation phase visualising the effect of grain boundaries on the crack growth of figure 2.10. The figure has been retrieved form the book of Schijve[12].

### 2.4.2. Crack initiation in steel

Whether the material will have its main life in the crack initiation phase or in the crack propagation phase depends on how easy cracks are formed and how thick the material is. As steel is a metal that is cast or rolled into its final shape, there are not so many imperfections. On the other hand, steel profiles are thin as steel is heavy and rigid compared to its weight and strength. Thus steel profiles have the majority of their fatigue life in the crack initiation phase. This is the reason why the crack propagation phase is often neglected and considered as an extra safety feature during the design process. Only if cracks are

observed in existing structures and the engineers want to know how much fatigue life is remaining in the steel cross-section, then they turn to the fatigue propagation calculations. The fatigue initiation phase could be thoroughly assessed by adding multiple parameters to reduce the fatigue strength next to the Goodman or Gerber equations described in section 2.3.2 of chapter 2. The four main parameters that are used are: the stress concentration factor $K_t$, the notch sensitivity factor $K_f$, the fatigue limit ratio $\alpha_f$ and the surface smoothness factor $\gamma$.

The first and foremost important parameter is the stress concentration factor. The stress concentration factor is a stress multiplier that takes into account the local geometry to obtain the peak stress. The definition of $K_t$ is defined in equation 2.10.

$$K_t = \frac{\sigma_{peak}}{\sigma_{nom}} \tag{2.10}$$

$K_t$ is influenced purely by the geometry and the direction of loading. It has no unit. The stress concentration factors could be any value ranging from about a negative two up to about a positive twenty. For that reason it is very important to design the structure in such a way that the stress concentration factor is as close as possible to zero. A small example would be that of the stress concentration around a circular hole as is given in figure 2.12. For an ellipse with the semi-major axis $a$ and semi-minor axis $b$ it is known that the stress concentration at point A in an infinite plate is equal to what is provided in equation 2.11. For a circle in an infinite plate $K_t$ as a function of the angle of the polar coordinate $\phi$ is known along its entire periphery. This function is defined in equation 2.12.

$$K_t = 1 + \frac{2a}{b} \tag{2.11}$$

$$K_t = 1 + 2cos(\phi) \tag{2.12}$$

In that case the stress concentration factor for a circle would be $+3$ at the point where the diagonal would be perpendicular to the load (point A). A stress concentration factor of $-1$ is found at the points where the diagonal is parallel to the load (point B). It is allowed to use superposition of stress concentration factors. So for a plate with a circular hole loaded in in-plane vertical and in-plane horizontal direction, the stress concentration factor will be $+2$ for all of these four positions. Thus the plate is better in resisting bi-axial loading than uni-axial loading despite applying more total force. Hence for multiple loading the superposition is taken by addition of the stress concentration factors. However, if the circle would have a notch, then that notch would also have an additional stress concentration factor. In that case the superposition will be performed by multiplication of the stress concentration factors as the stress concentration factor for the larger geometric imperfection results already in higher local stresses in the area. This is now further amplified locally by the smaller geometric imperfection of the notch. Whether this last approach is conservative or not depends on making an over- or underestimation of the material presence of the notch as is shown in figure 2.13. An underestimation of the notch size results in conservative results as an underestimation of the notch size leads to overestimation of the present material. While the absence of more material in reality forces the stress to divert earlier. Thus a smoother stress path is created, therefore a lower stress concentration is observed. An overestimation would invert the reasoning, therefore result in observing a higher stress concentration than is predicted. There is always some over estimation made as the stress concentrations follow a gradient based on the distance to the crack tip. In other words, the value of $K_t$ decreases gradually when further from the notch or cut-out. There are many formulae available to estimate the concentration factors of the basic cases.

This is where FEM comes into play as a finite element analysis already calculates the peak stresses due to geometry. Therefore the obtained peak stress in such an analysis no longer needs to be multiplied with a stress concentration factor. Do note that many of these results are mesh dependent, hence a proper way of extraction of data is required to have consistent results. When applying the stress concentration factor to the S,N-curve, then it should only be applied to the lower limit as only the CAFL is affected by it. During the first $100$ cycles the plastic shake down effect causes to have a much larger area to be loaded in plastic response of stress level rather than a smaller area with a steeper gradient.

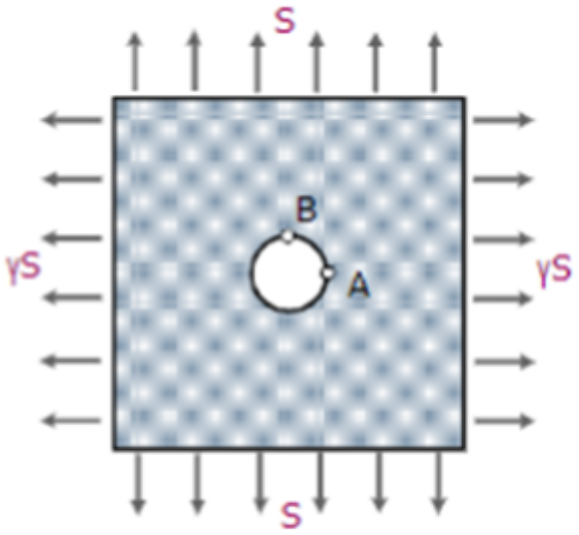


**Figure 2.12:** A visualisation of an example of a plate with a circular cut-out loaded with a stress $S$ in one direction and a stress $S$ multiplied with a factor $\gamma$ in perpendicular direction. Figure is retrieved from the lectures of Alderliesten[7].

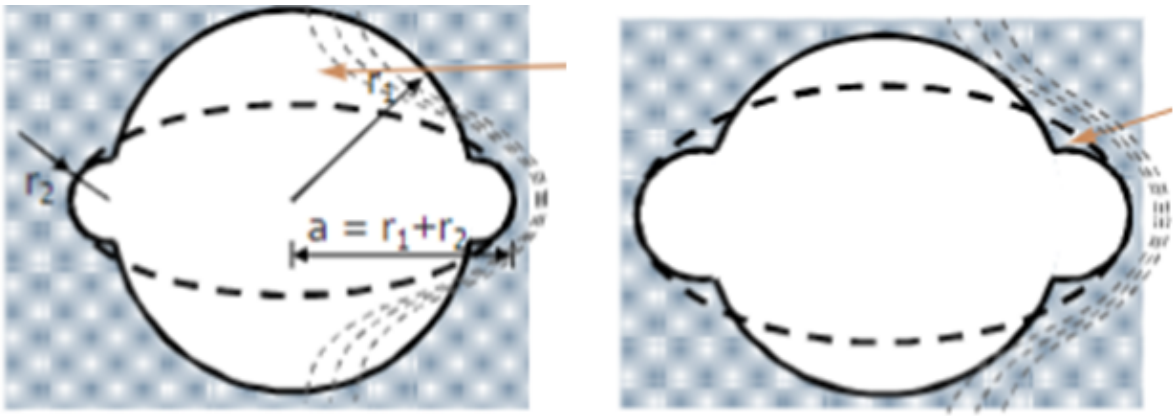


**Figure 2.13:** A representation of the premature or delayed diversion of the stresses surrounding the notch in the cut-out. The left figure shows an underestimation of the material and results in higher calculated $K_t$ than in reality. The right figure illustrates an overestimation of the material resulting in a lower calculated $K_t$ than will be present in reality. The figure is retrieved from the lectures of Alderliesten[7].

The second parameter is the notch sensitivity factor. $K_f$ is related to a material constant $A$ and a notch radius $\rho$. A deterministic equation is given in equation 2.13 which is also a function of the stress concentration factor. If $K_f$ is close to the value $1$, then this correction factor may be omitted. The value of $\sqrt{A}$ is given in figure 2.14 and must be applied without any conversion in equation 2.13.

Hence it is easier to write $\sqrt{A}$ outside of the fraction. As this parameter has the same effect as the stress concentration factor, it is only applied to the lower limit of the S,N-curve.

$$K_f = \frac{K_t \left(1 + \frac{1}{K_t}\sqrt{\frac{A}{\rho}}\right)}{1 + \sqrt{\frac{A}{\rho}}} \tag{2.13}$$

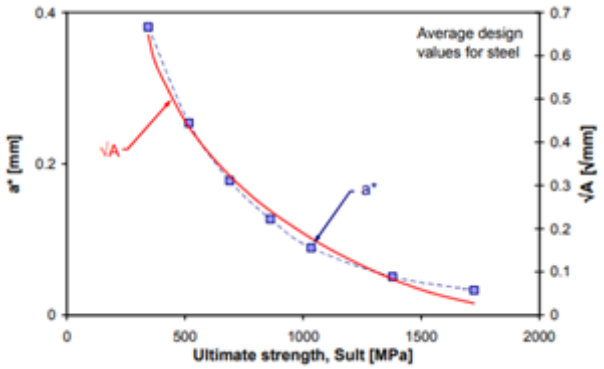


**Figure 2.14:** Graph showing the material constants $A$ and $a*$ dependent on the ultimate stress of the material. These two parameters are equivalent. The figure is retrieved from the lectures of Alderliesten[7].

The third parameter is the ratio that describes the value of the fatigue limit according to the ultimate stress of the steel alloy. Apparently there is a material type dependent relation between the CAFL and the ultimate stress of metals. In general it could be said that the ratio $\alpha_f$ between CAFL and ultimate stress is $\frac{1}{2}$ for steel with an ultimate stress below 1200 [MPa]. For steel with an ultimate stress above 1200 [MPa] it is more suited to have a ratio of $\alpha_f = 0.4$ as is shown in figure 2.15. Each material has its own ratio, for aluminium this value is at about $\alpha_f = 0.3$ and for cast iron it is $\alpha_f = 0.4$ while tin alloys tend to have $\alpha_f = 0.5$ no matter the ultimate strength according to Schijve[12]. Also this parameter only has influence on the lower limit of the S,N-curve as the definition already provides, it is the ratio between CAFL and ultimate stress.

Also the last parameter only has influence on the CAFL as the plastic shake down would help to overcome the imperfections due to the surface roughness. The surface finish factor $\gamma$ is the ratio between the resultant stress caused by the applied surface quality over the resultant stress in case of a high surface quality as is shown in equation 2.14. In that case a worse surface quality would result in a higher stress which increases $\gamma$, hence the CAFL needs to be divided by $\gamma$.

$$\gamma = \frac{\sigma_{1,f,appliedsurfacequality}}{\sigma_{1,f,referencesurfacequality}} \tag{2.14}$$

### 2.4.3. Crack propagation in steel

The steel crack propagation phase is assessed according to the Paris law[9] as given in equation 2.9 in combination with the three failure modes described in paragraph 2.4.1 of chapter 2. In the Paris law[9] one could argue that $\frac{da}{dN}$ is the crack resistance. In that case $S$ would be called the crack driving force or solicitation. For steel the assessment is based on the plasticity around the crack tip. If someone wants to calculate the stress concentration factor $K_t$, then that person will encounter that the stress

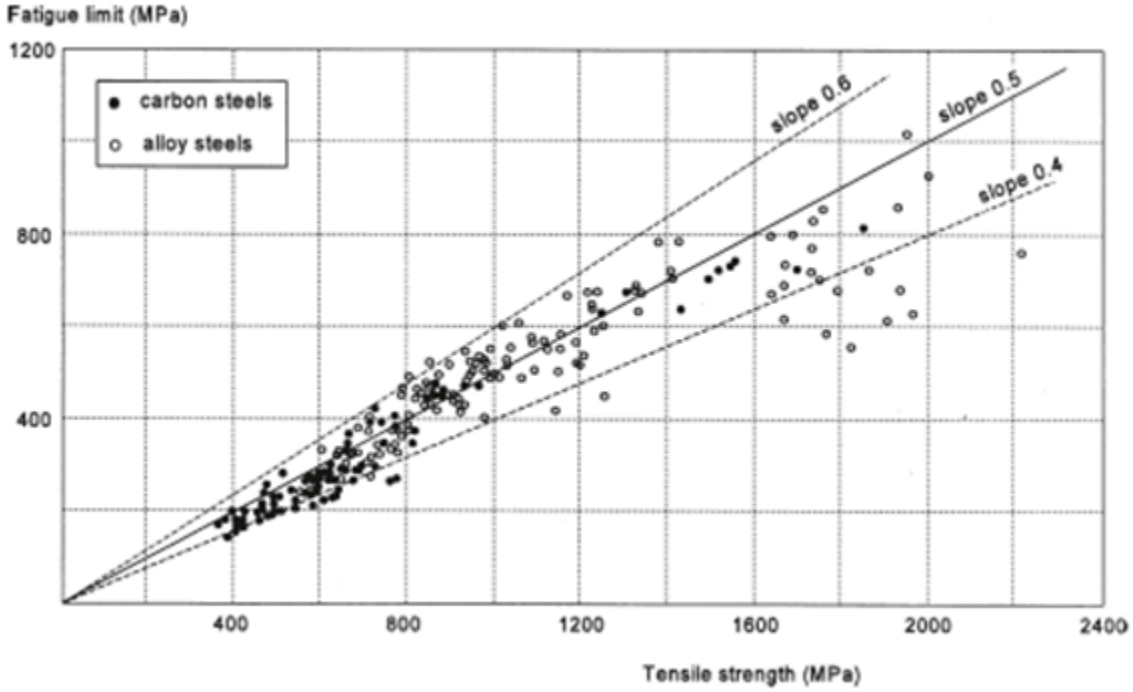


**Figure 2.15:** A graph showing the relation between the constant amplitude fatigue limit of an unnotched specimen (vertical axis) and the ultimate stress (horizontal axis). The figure is retrieved from the lectures of Alderliesten[7].

concentration in the crack tip will be infinite. As it is obvious that in reality a notch does not necessarily lead to failure upon loading for one cycle, there must be more to this. For this there is a stress intensity factor $K$ to calculate that replaces $K_t$. The stress intensity factor describes the stress field around the crack tip, generally there is an increase of stress. Do note that although $K_t$ and $K$ have aspects in common, they are definitely not the same. First of all, $K$ has a unit for example [MPa $\mathrm{m}^{\frac{1}{2}}$] which is dependent on the stress level. Also $K$ is dependent on the meso-scale geometry only, while $K_t$ is dependent on the micro-, meso- and macroscale geometry. On top of that $K$ is dependent on the crack length. Equation 2.15 defines the mathematical formulation of $K$ according to the book of Schijve[12].

$$K = \beta K_t \sigma \sqrt{\pi a} \tag{2.15}$$

$K_t$ is optional to take into the formulation of $K$, many handbooks will separate $K_t$ as a factor to multiply the stress intensity of the macroscale geometry afterwards. $K_t$ has the same function as in the crack initiation phase and describes the influence of cut-outs on the increase of the local stress field and still has no unit. $\beta$ is a geometry factor without unit to describe the mesoscale geometry such as whether the notch is internal or on an edge and considers the crack length in relation to the total width. $\sigma$ is the applied load, if $K$ is addressed in [MPa $\mathrm{m}^{\frac{1}{2}}$] then $\sigma$ must be addressed in [MPa]. Depending whether someone is interested in failure, the crack propagation rate or the crack opening threshold, $\sigma$ becomes respectively $\sigma_{max}$ or $\sigma_{opening}$ for which the definitions of figure 2.19 are applied. $\pi$ is the well known constant without a unit. $a$ describes the crack length in [m] for $K$ in [MPa $\mathrm{m}^{\frac{1}{2}}$]. Is a crack in the centre of the material, then it has a length of $2a$ and if the crack starts at the edge of the material, then it has a length of $a$. If there are any cut-outs from which the crack grows, than these cut-outs have to be taken into account in the length of the crack as the material "feels" this absence of material through the reduced stiffness as is explained by Alderliesten[7].

Notice that $K$ increases with crack length under a constant amplitude force load. At a certain crack length the cross-section fails. Failure during the final cycle either happens due to the direct ultimate limit of the cross-section or due to fatigue cycle having such a great propagation rate that it is able to rupture the remaining cross-section in one cycle. It is assumed the reader knows how to perform the final failure due to static rupture of the gross cross-section. The final failure due to an immense crack propagation rate will be explained. As figure 2.7 already shows, there are three stages in crack propagation rate. The last stage is unstable as the crack growth rate now increases exponentially as the crack becomes larger and the cross-section becomes smaller, which increases $\sigma$ as well. At a certain point the stress intensity factor during maximum loading $K_{max}$ reaches the critical value $K_C$. Depending on which mode the specimen is loaded, this is $K_{I,C}$, $K_{II,C}$ or $K_{III,C}$. For metals $K_{I,C}$ is often governing due to larger thickness of the cross-section. It is possible to calculate a $K_C$ that allows to perform a combined unity check by using weight factors in the addition of each individual unity check. Upon calculating the number of cycles till $K_C$ is reached one would notice that the cross-sections with smaller thickness generally fail earlier than thicker because there is less length to cover. However, it is not proportionally to the thickness. This effect is described in the increase of $K_C$ for the thinner cross-sections as is illustrated in figure 2.16. The thinner cross-sections are dominated by modes II and III instead of mode I. Mode I has generally a lower value for the critical energy release rate than modes II and III. The best designs tend to have multiple thinner layers of material since the thinner layers have a higher critical stress intensity factor before failure. Also the crack arrest phenomenon occurs between each layer which slows down the crack growth rate a lot, because it has to initiate a new crack in the next layer.

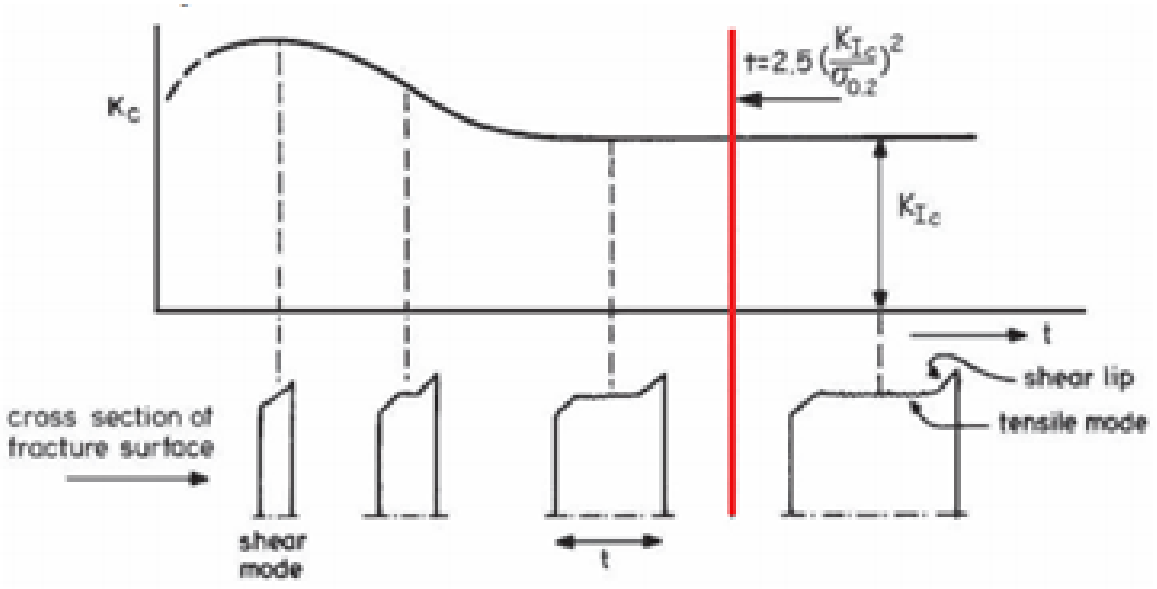


**Figure 2.16:** The critical stress intensity factor $K_C$ for different thicknesses as a result of different governing failure modes between thick and thin cross-sections. This figure is retreived from the lecture of Alderliesten[7].

Upon assessing the fatigue life of a structure, one would notice that the order of cycle amplitudes is important during the assessment of variable amplitude spectra, especially during the second stage of crack propagation where the Paris law[9] is applicable. During the crack initiation phase it is already noticeable that a specimen that is first loaded with a set of cycles with an amplitude that is below the CAFL followed by a set of cycles with an amplitude cycles above the CAFL will allow more cycles till failure than first having the larger amplitude cycles succeeded by cycles with a smaller amplitude. This is caused by the damage generated by the larger cycles such that the lower cycles, which initially would not result in damage if applied to an undamaged specimen, will now propagate the damage as

the material is now weak enough. Numerically this is explained by the fact that now for the low cycles $K$ has to be used instead of $K_t$, because the cycles with a larger amplitude caused a crack initiation. Therefore the cycles with a smaller amplitude only need to propagate the crack. Using the theory of crack propagation with the Paris law[9] equation explains it further.

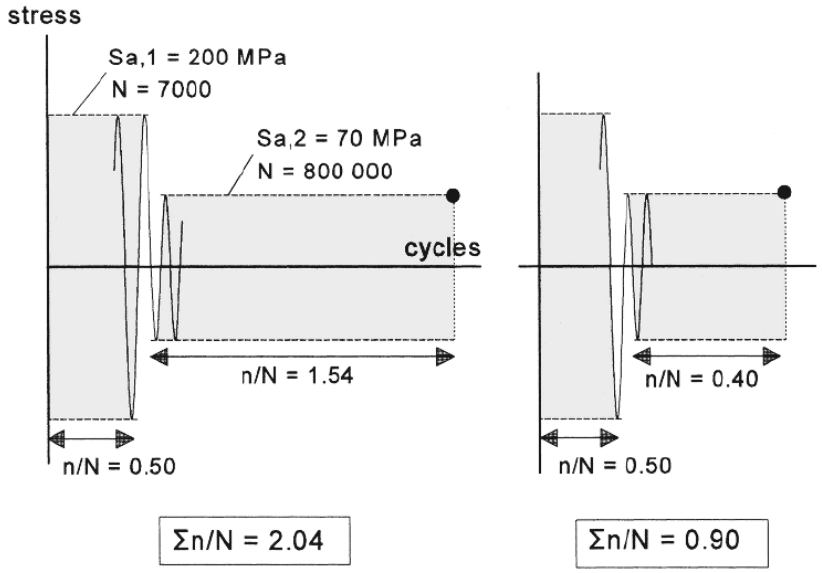


**Figure 2.17:** A visualisation of ending the previous set of cycles with a peak on the left and ending the previous set of cycles with valley on the right. The second set is the remaining amount of cycles with a smaller amplitude till failure. For the right figure this results in a smaller amount of cycles. The difference in results also shows how much total equivalent damage there is at failure using the cumulative Miner's rule. Values above one indicate it could take more cycles than anticipated by the Miner's rule and values below one indicate it could take less cycles than anticipated by the Miner's rule. The figure is retrieved from Schijve[12].

The second reason which is also related to the second stage of the crack propagation: there are two important phenomena related that create this difference. Upon having the set of cycles with larger amplitude first, it makes a difference whether the set ends with the peak or the valley of the cycle. Ending upon the peak as shown on the left in figure 2.17 will result in crack retardation while ending in a valley as is shown on the right in figure 2.17 will result in crack acceleration. The crack retardation effect is caused by the plastic zone in front of the crack tip. During crack opening of the cycle, a part of that plastic zone will reach ultimate stress and break resulting in the propagation of the crack. Also a new part of the previously elastic loaded material will reach yielding stress and will deform plasticly. Hence a crack closure effect is observed as the plastic deformation during tension deforms the crack tip in such a way that the material will be prematurely closed before the material is fully unloaded. It is this deformation that will result in local compressive forces during unloading. If the unloading is unfinished or compressive forces are applied, then these local compressive forces will result in a plastic deformation in the other direction creating a reverse plastic zone. Despite the reverse plastic zone will have plastic compressive stresses instead of tensile stresses as during the creation of the plastic zone, the reverse plastic zone does not undo the plastic deformation of the tensile half cycle. Moreover it creates additional plastic deformation in order to achieve it. This phenomena of the crack closure effect is visualised in figure 2.18.

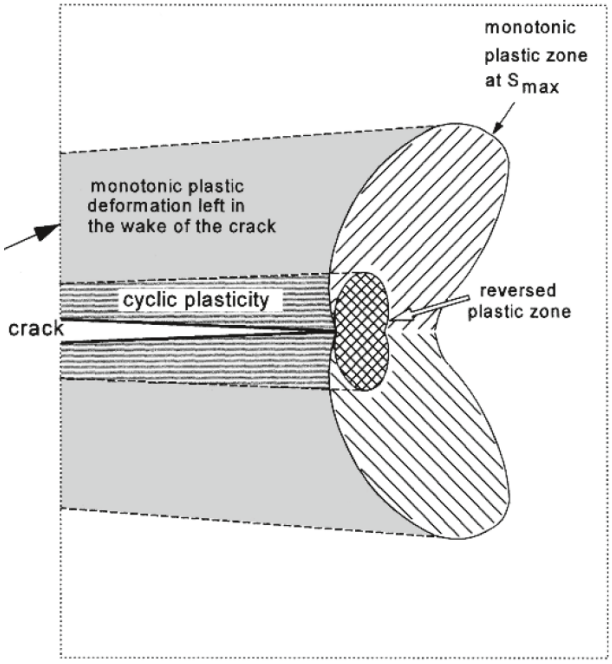


**Figure 2.18:** A visualisation of plastic zone due to tensile loading in metal and the reverse plastic zone due to the deformation causing compressive stresses during unloading. The figure is retrieved from Schijve[12].

If the amplitude of $K$ remains constant, then the size of plastic zone and reverse plastic zone remain constant. Upon "over-closure" of the crack tip during $K_{min}$, the compressive forces become more negative which increases the opening stress intensity factor $K_{opening}$. Upon increasing $K_{opening}$ the crack tip opens again in the next cycle as is drawn in figure 2.19. $K_{opening}$ therefore determines how much effective stress intensity remains as $K_{eff}$ is defined in equation 2.16.

$$K_{eff} = \Delta K - K_{opening} = K_{max} - K_{min} - K_{opening} \tag{2.16}$$

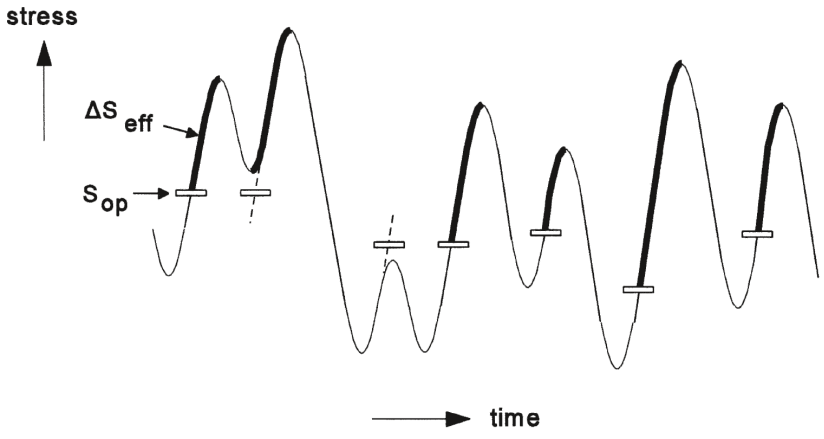


**Figure 2.19:** A visualisation of changing opening stress as a result of a change in opening stress intensity factor $K_{opening}$. The change in $K_{opening}$ depends on the amount of "over-closure" from the previous cycle, The figure is retrieved from Schijve[12].

If more compressive stresses are present around the crack tip due to a change in amplitude and the maximum stress is reduced for the next set of cycles e.g.: an overload cycle or a sequential set of cycles with smaller amplitude after the peak, then the phenomenon of crack retardation occurs. Having one cycle with higher compressive amplitude stress will not help as it will only increase the reverse plastic zone instead of the plastic zone. It is the plastic zone itself that causes the crack growth rate to decrease. It is more difficult to let the crack pass through the plastic deformed material than through virgin material. As the overload cycle caused more plasticity ahead of the crack tip than there would normally be for that lower amplitude, it will take more cycles to propagate the crack for a short period. This increased number of cycles could be so many that it causes the crack growth acceleration due to the overload cycle to have less effect than the crack retardation during the sequential cycles as is illustrated on the left of figure 2.20. The crack retardation effect is described in the crack growth rate, thus the first part of the retardation is the delayed retardation where the crack growth slows down up to the maximum retardation. The maximum retardation is when the lowest crack growth rate is observed during the retardation. When the expected original crack rate is obtained again, which happens at the end of the additional plastic deformation zone, then it is also the end of the retardation. Placing positive overload cycles strategically increases the fatigue life as is illustrated on the right of figure 2.20.

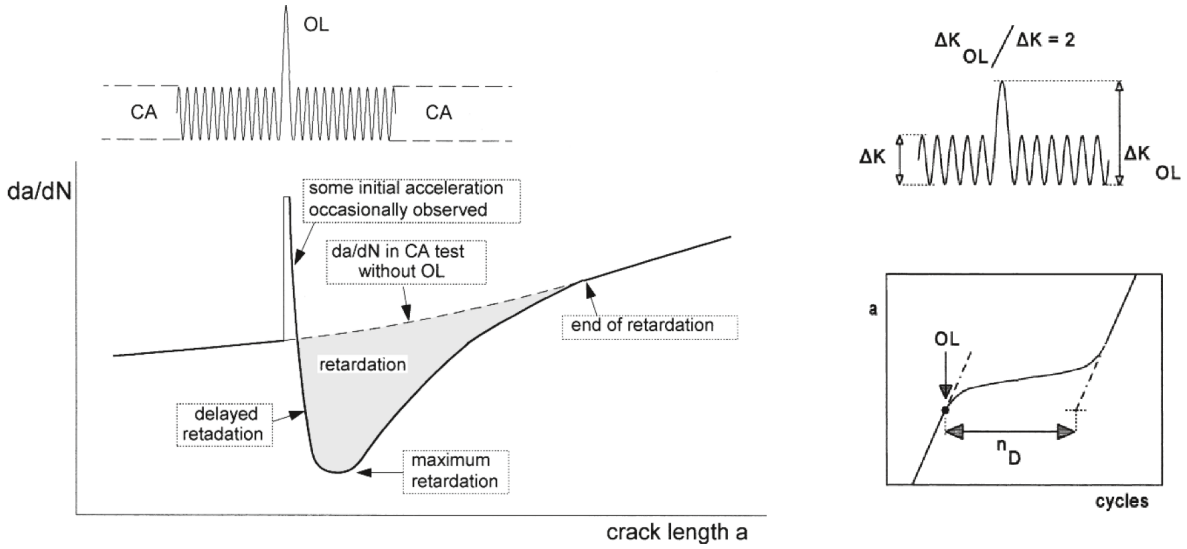


**Figure 2.20:** An illustration of the effect of an overload cycle on the crack propagation rate. On the left the overload initially accelerates the crack growth rate, but due to the extra plasticity created by the overload cycle the crack growth rate decreases till under the normal expected rate causing the retardation effect. This improves fatigue life as is illustrated on the right that the crack length only increase limited during the succeeding set of cycles. Normal crack growth rates resume after the retardation effect is over which is at the end of the extra plastic zone. The figure is retrieved from Schijve[12].

As is already shown in figure 2.7, the first stage is limited by a certain threshold stress intensity value $K_{th}$ which is related to the effective CAFL as is explained by Alderliesten[7]. This threshold value $K_{th}$ needs to be determined empirically and is material dependent. It describes the truncation of crack growth rates to be taken into account since no crack propagation is present below the effective CAFL. Values of $K_{eff}$ below the threshold value $K_{th}$ are below the effective CAFL, therefore they will not be taken into the summation of total crack length as they do not cause any crack propagation. For steel this limit is present as it is for many metals, only the value differs from other metals. If $K_{eff} > K_{th}$ is taken into account, then $K_{th}$ must also be subtracted from $\Delta K$ to obtain $K_{eff}$ which results in equation 2.17 which is reformulated by Alderliesten[7].

$$K_{eff} = \Delta K - K_{opening} = K_{max} - K_{min} - K_{opening} - K_{th} \tag{2.17}$$

## 2.5. Fatigue assessment for composites

### 2.5.1. Fatigue mechanisms present in composites

There are parallels between the principles of fatigue assessment in steel and composites such as monitoring the strength degradation of the material for different load levels. However, there are also differences present. Some differences are subtle such as using the energy release rate instead of stress intensity factor. Other differences are more severe such as the (number of) mechanisms that are involved and the number of cycles of the fatigue life spent in the crack initiation or propagation phase. The reader is suggested to read paragraph 2.4 of chapter 2 as a prerequisite as the focus will be on the differences in assessment compared to steel.

For composites there are advantages of using the residual strength and the residual stiffness curves compared to the S,N-curves and constant life diagrams (CLD). Especially once the relation between the residual strength and the residual stiffness is known and defined on the basis of a damage parameter. This idea is confirmed by the earlier findings of Van Paepegem and De Grieck[8]. In theory the S,N-curves and CLDs are only allowed for crack initiation, but are often used for crack initiation as well as the crack propagation phase. For the crack propagation phase the residual strength and residual stiffness curves are developed. As composites have a limited crack initiation phase, but a long crack propagation phase, those curves are more applicable to the composite fatigue assessment. For metals the relative strength could be easily monitored as it decreases more gradually, but for composites the stiffness could be more easily monitored as the stiffness decreased more gradually. Therefore if the relation between residual stiffness and residual strength is known, then only a limited amount of testing is required. A limited amount of tests are required because stiffness tests are non-destructive. Therefore the same specimen could be measured at multiple occasions during the fatigue tests. This will not only provide less scatter, but also provides more insight about the development of the stiffness degradation of an individual specimen as is mentioned by De Grieck and Van Paepegem[18].

The biggest difference between the steel and composite material are the mechanisms. Whereas steel has one mechanism with three different failure modes, one for each direction of loading, while composites have at least three mechanisms with each its respective coice from the same failure modes as available for steel: inter fibre failure (IFF), delamination (DEL) and fibre fracture (FF). These were the significant mechanisms observed by Brod et al.[1] as is illustrated in figure 2.21. Each of these three mechanisms will be explained in the paragraphs 2.5.2 and 2.5.3 of chapter 2 as these are related to the crack initiation phase and the stages during the crack propagation phase. Some more variants of each of these mechanisms could be distinguished based on the length of the fibre and the direction of the fibre. Within a layer of fibres the different mechanisms that are possible at the crack tip, depending on the fibre direction, are illustrated in figure 2.22. If cracking occurs in the matrix of a layer, then two variants are possible: the fibres tend to pull out or break. If the fibres are short, then it is more likely that fibres will be pulled out during cracking as the amount of shear resistance with the matrix is low. If the fibres are long, than this shear resistance may become larger than the tensile strength of the individual fibre. In that case the fibre breaks. Delamination is always between two fibre layers resulting in a clean(er) cut.

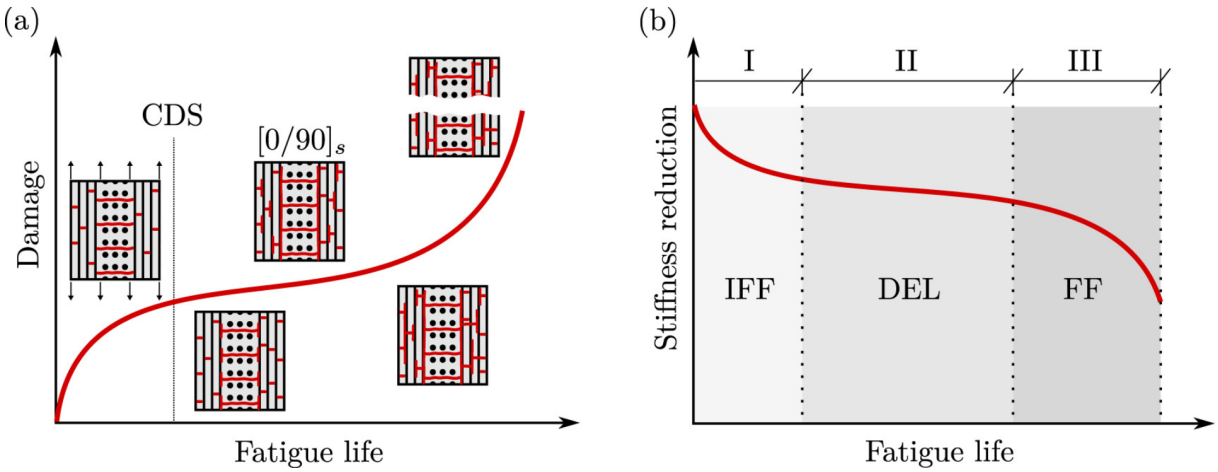


**Figure 2.21:** The damage accumulation by the different mechanisms is illustrated on the left. IFF is the inter fibre failure, DEL is the delamination and FF is the fibre failure. The result in residual stiffness is illustrated on the right. The amount of damage accumulated is related with the reduction in relative stiffness. The illustration was retrieved from Brod et al.[1].

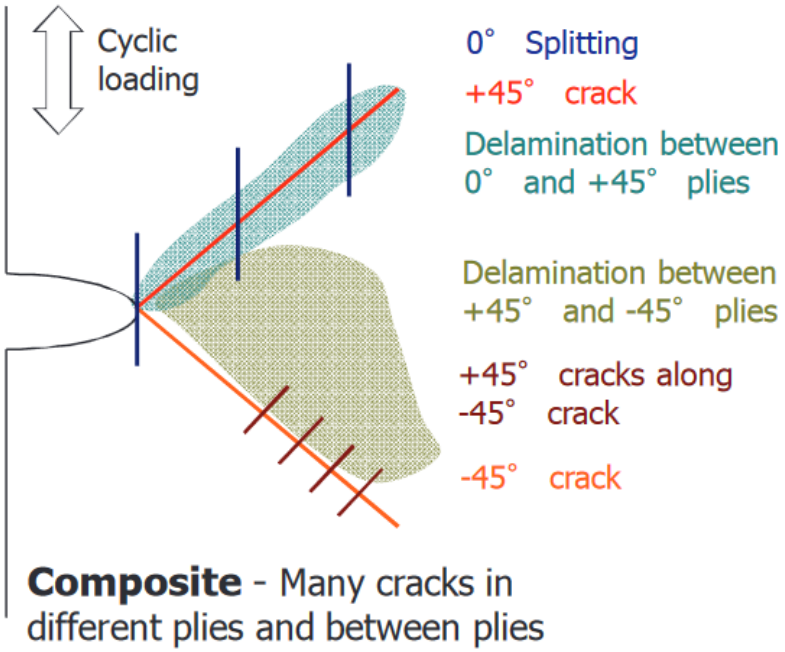


**Figure 2.22:** At the crack tip there is no single possible crack mechanisms within a certain range of angles to the already existing crack as is present in steel. In composites there are several crack mechanisms possible at any given moment. The figure is retrieved from the lectures of Alderliesten[7].

Whether or not all three mechanisms come to expression as an individual stage upon testing, depends on the type of loading that is applied. Since the compact tension specimen (CT specimen) is a sort of in-plane bending test, it is expected to observe only two stages with the three mechanisms. Brod et al.[1] observed these three mechanisms sequentially for an out-of-plane bending fatigue test resulting in three stages. The three mechanisms are sequential as the out-of-plane bending causes a linear stress distribution over the thickness of the specimen. Therefore the outer layer is activated the most. How exactly one mechanisms leads to another mechanism will be explained in section 2.5.3 of chapter 2. These fatigue mechanisms are also observed for in-plane loading by Bartowiak et al. [2]. Despite observing the same three mechanisms, Bartowiak et al.[2] observed that only two stages came

to expression in the in-plane tension-tension loaded fatigue test. If a specimen is loaded in-plane, then all fibre layers are loaded equally with the applied stress, thus an uniform stress distribution is present over the thickness of the specimen. This uniform stress distribution allows each fibre layer to develop a crack due to IFF and FF, instead of one crack for the entire layup. These cracks are then be merged into one larger crack through the delamination mechanism, if the delamination results in less fatigue life than solely on the intraply mechanisms. While out-of-plane bending test has it similarities with the CT specimen with tension stresses on one side and compression stresses on the other side, the in-plane tension-tension loaded fatigue test has similarities with the CT specimen as both are loaded in-plane. Therefore the expected response for the CT specimen will be in-between those two scenarios. As the three failure mechanisms are observed in both the out-of-plane bending fatigue test as well as the in-plane tension-tension fatigue test, it is expected that these three are present in compact tension specimen as well. However, as upon the in-plane tension-tension fatigue test only has two stages that come to expression, it is expected that the in-plane bending of the compact tension specimen will also show two stages. This happens when one of the mechanisms overlaps with (one of) the other two mechanisms. That is what is observed by Bartowiak et al.[2]. The most probable situation would be that the delamination will overlap with the FF in the material (stage III). It does not exclude it might also happen during stage I, however, it is unlikely to initiate delamination if the IFF cracking is not fully through the material layer. The delamination is seen as an auxiliary mechanism that aids to obtain more critical crack patterns during multiple simultaneously initiated in-plane cracks.

Despite that both figures 2.7 and 2.21 have three stages present and both describe a crack propagation behaviour, they are not directly related to each other. Physically the difference is that the Paris law is used to describe the crack propagation rate based on the different critical energy release rates. This is merely based on one mechanism that shows different modes in the Paris law curve: stage I is mode II, stage II is mode I and stage III is mode II. The crack propagation rate in composites is often replaced by the damage propagation rate which is proportional to the crack propagation rate. The damage propagation rate is related to the residual stiffness curve since the residual stiffness is based on a damage parameter as is shown in figure 2.21 where the derivative of $\frac{E}{E_0}$ is proportional to $\frac{dD}{dN}$. Despite that the residual stiffness is based on a damage parameter, the damage propagation rate is not necessarily proportionally related to the stiffness degradation rate. The damage propagation rate is related to the energy release rate which is not necessarily proportional to the fatigue life. This is also observed as the damage propagation rate is decreasing first as is shown in the convex curve of stage I in figure 2.21. The Paris law[9] curve in figure 2.7 on the other hand shows an increasing damage propagation rate for increasing energy release rate. In other words, the fatigue life and the energy release rate are not linearly related.

Also the layup of the composite ply has influence on the type and location of cracking as described by Pakdel and Mohammadi[19]. Figure 2.23 shows their findings for a symmetric ply. In symmetric layup with fibres either close to parallel or perpendicular to the loading, the outer plies are damaged first. If the fibres of the ply are close to $45$ °to loading, then both outer plies are simultaneously damaged first. Only for angles in-between the mid-plies are damaged first.

The second major difference is the response to the different loading regimes. Composites have an excellent resistance against tensile fatigue loading, but are much worse than metals in compressive fatigue loading as is illustrated in figure 2.24. This is caused by the compressive strength being less than the tensile strength and the occurrence of different mechanisms. Therefore it is important to state during a fatigue assessment in which loading regime the material is loaded.

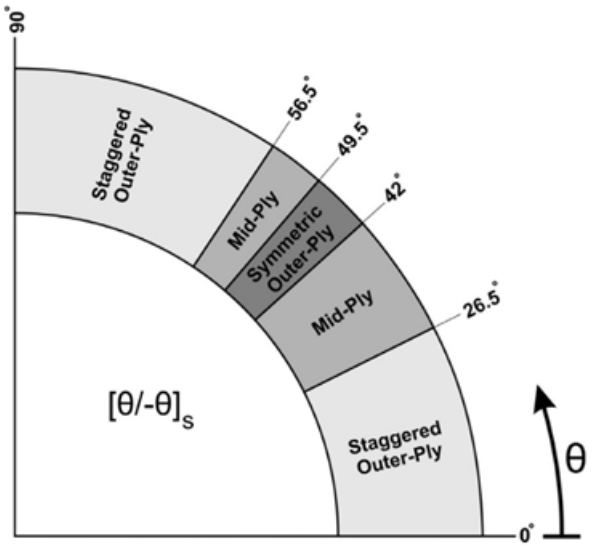


**Figure 2.23:** A diagram showing the influence of the angle of the composite layup on which layer will fail as first during fatigue loading investigated by Pakdel and Mohammadi[19]. The angle $\Theta$ describes the angle between the fibres in the ply and the direction of the applied load. The layup is symmetric with the outer plies having an angle of $+\Theta$ and the inner plies having an angle of $-\Theta$.

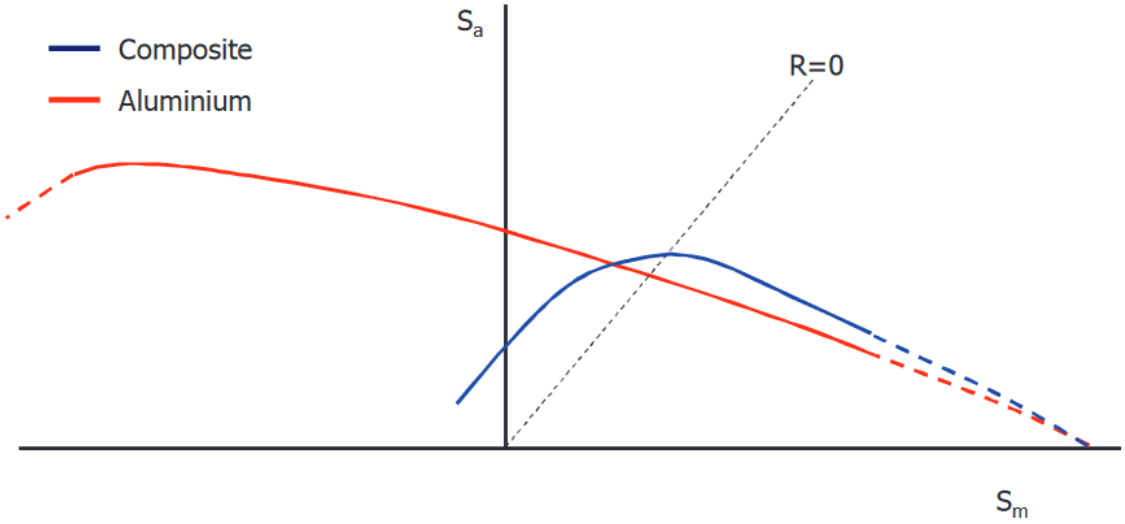


**Figure 2.24:** A diagram with the blue line representing the composite constant life diagram for different combinations of mean stress (horizontal) and amplitude stress (vertical). The red line represents the aluminium. It shows that the composite is much worse in negative loading than metals. The figure is retrieved from the lectures of Alderliesten[7].

### 2.5.2. Crack initiation in composites

The crack initiation is considered to be a damage accumulation on structural level due to having many possible damage mechanisms at different locations that depend on the fibre orientation, the load ratio, the crack length, the number of cycles, the fibre properties and the matrix properties. Hence the crack initiation stage is often not considered in composite structures. Ovalisation of the fibre voids in the matrix could be considered as crack initiation as no distinctive crack surface is present at first. However, it is more suited to address it during crack propagation as the matrix needs to become damaged to link the ovalisation of different voids.

### 2.5.3. Crack propagation in composites

Although the stages of figure 2.7 are present during a long duration of cycles for example during delamination, they are not that clear for composites as for steel. The first subtle difference is the fact that composites do not have a well-defined threshold value $K_{th}$ or for composites rather a threshold energy release rate $G_{th}$. As already discussed, composites have a limited crack initiation phase and directly continue to the crack propagation phase due to the brittleness of the material. There is actually no CAFL present in composites. Therefore no truncation is allowed, thus all the crack growths have to be taken into account. Therefore it is more useful to look at the propagation stage in terms of mechanisms instead of modes. Each time a new mechanism became governing, a new stage in stiffness degradation in the out-of-plane bending was observed by Brod et al.[1]. This was illustrated in figure 2.21.

Initially composites will have inter fibre failure (IFF) straight from the start. During IFF the crack formation starts with ovalisation of the holes in the matrix material created by the fibres during lamination as is shown in the left drawing of figure 2.25. This is similar to a bolt in a lug with not enough embedment resistance. Once a couple of ovalised holes link up, a micro-crack is created as is shown in the centre left drawing of figure 2.25. Within a couple of cycles the micro cracks link up to macro cracks as shown in the centre right drawing and the right picture of figure 2.25. This means that composites have a negligible crack initiation stage and the fatigue life has to come from the crack propagation phase. This is the third major difference with steel where the crack initiation stage is the most important. It degrades the stiffness quickly, but without a significant decrease in strength. The mechanism is stabilised quickly as the crack is arrested at the interface between two layers of fibres. The second ply with the fibres in the other direction causing the crack growth rate to slow down and start to move sideways between the plies as is shown in figure 2.26. Locally there is a stress drop in the ply since the forces cannot be transferred through the crack similar to what is observed in the cracking of a reinforced concrete beam loaded in tension. The stresses that were supposed to go through the crack are now deviated to the adjacent plies.

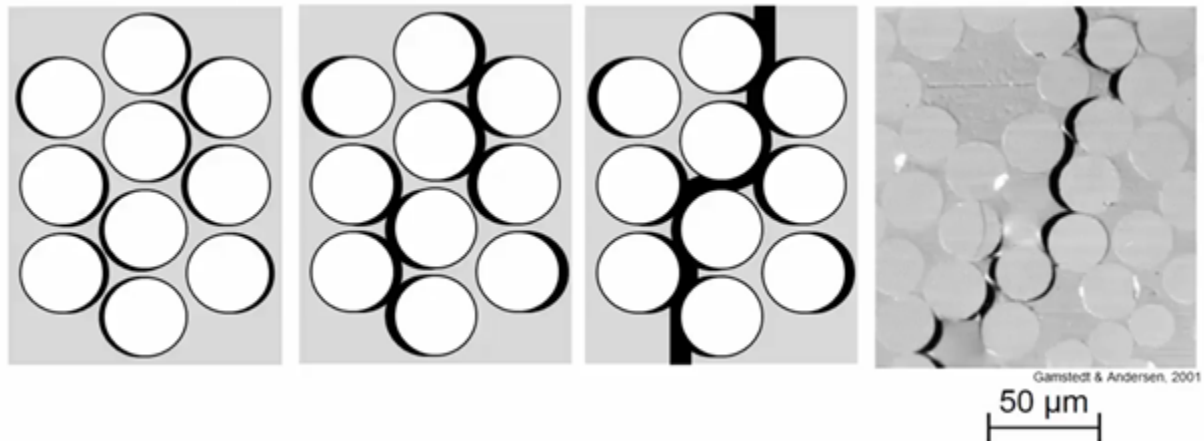


**Figure 2.25:** A visualisation of the ovalisation of the matrix around the fibres of the composite on the left. Linking the ovalised holes to create micro-cracks is shown on the centre left. Linking all the micro-cracks to create a macro-crack through the layer is shown on the centre right. An electron microscope photo of a composite ply with a crack through the layer is shown on the right. The illustrations on the left are retrieved from the lectures by Alderliesten[7] and the picture on the right is from Gamstedt and Andersen[20].

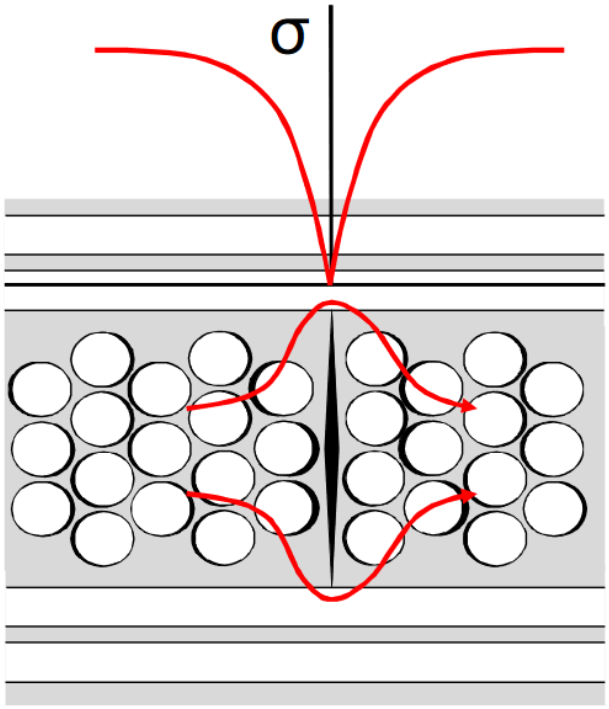


**Figure 2.26:** After linking up the ovalisation to create a macro crack through the ply, the stresses in the ply need to be diverted around the crack to the adjacent plies. Hence locally there are no stresses in the ply. The figure is retrieved from the lectures of Alderliesten[7].

During the second stage of figure 2.21 delamination is the main mechanism. It is also a relatively stable mechanism that could be described by the Paris law. Instead of calculating the stress intensity factors around the crack tip, it is more common to define the energy release rate in composites since the composite failure mechanisms are often described in energy values. Although preferably using energy values for composites, the energies could be translated into stress intensity factors using equation 2.18 provided by Alderliesten[7].

$$G = \frac{K^2}{E} \tag{2.18}$$

With $G$ the energy release rate which has in general the units [MPA m], $K$ the stress intensity factor in [MPa $\mathrm{m}^{\frac{1}{2}}$] and $E$ the Young's modulus of the material in [MPa]. The energy release rates $G_I$, $G_{II}$ and $G_{III}$ are respectively related to $K_I$, $K_{II}$ and $K_{III}$. Hence $G_{I,C}$ is used to describe the amount of energy required to break a piece of (composite) material in plane using the in-plane normal stress (mode I). $G_{II,C}$ is used to describe the amount of energy required to break a piece of (composite) material in plane using the in-plane shear stress (mode II). Finally $G_{III,C}$ does this for the amount of energy required using the out-of-plane shear stress (mode III). Again it is possible to formulate a $G_C$ that takes into account the combined unity check with a certain weight ratio. The Paris law[9] for composites is changed with the effective energy release rate replacing the effective stress intensity as provided in equation 2.19. $\Delta G_{eff}$ has to be calculated identically as $\Delta K_{eff}$ in equation 2.17.

$$\frac{da}{dN} = C\left(\frac{\Delta G_{eff}}{\Delta G_C - G_{max}}\right)^m \tag{2.19}$$

$\frac{da}{dN}$ is the crack growth rate in [m/cycle], $C$ and $m$ are material constants, $G_{eff}$ is the effective energy release rate in [MPa m], $\Delta G_c$ is the equivalent critical energy release rate in [MPa m] and $G_{max}$ the maximum energy release rate during a cycle in [MPa m]. The delamination occurs when the micro-cracks due to the IFF reach the edge of the thickness of the ply. As the stress is transferred through the matrix between the plies to bypass the crack, the bonding between the plies could delaminate due to an increase in transfer stress as is illustrated in figure 2.27. This delamination is in shear for the plies despite being in the same direction as the loading, hence it is mode II failure of the matrix.

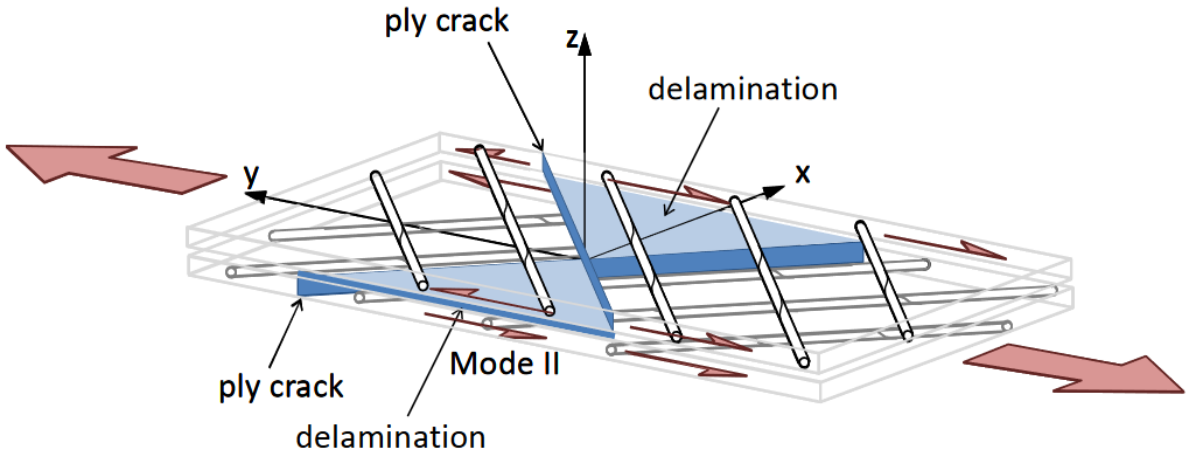


**Figure 2.27:** An illustration of the delamination between the plies caused by shear failure after the initial crack is through the ply. The figure is retrieved from the lectures by Alderliesten[7].

At a certain point the matrix is damaged in such a way that the fibres have to take all the load. When that is locally possible, stage III of figure 2.21 takes place. Now fibre failure (FF) will occur. In the fibre it is possible to observe single cycles in the form of rivermarkings as shown in figure 2.28. One could define this as a crack initiation phase on a structural level if the crack propagation phase is defined to start as soon as the first fibre has fully failed. This will in its turn cause the adjacent fibres to fail. This mechanism is unstable and has exponential growth. It is also the last mechanism before final failure.

As mentioned earlier, the composite material is rather assessed by tracking the damage accumulation than the stress intensity. Many of the failure mechanisms will have a specific damage parameter which will count the amount of damage in the material for a certain failure mode over the different cycles. This is due to the final large difference between the steel and the composite material. In steel the residual strength tends to decrease quickly during testing, but maintains its stiffness for a long time. On the other hand composite tends to reduce in stiffness from the start, but keeps its residual strength for a long time as is illustrated in figure 2.21. In figure 2.21 three stages are identified: stage I with a small rapid decrease in stiffness, stage II with long gradual decrease and stage III with a sudden extreme decrease in stiffness as has been reported by Brod et al.[1].

These regions are better related to the different failure mechanisms IFF, delamination and FF for the stages I, II and III respectively. It is better in representing the fatigue life using residual stiffness in composites than the crack length using figure 2.7. For that reason in composites often the damage parameter is related to the residual stiffness of the component. The residual stiffness could be related to the residual strength if an appropriate damage model is used. The residual strength model in its turn could be used to create S,N-curves as is shown in figure 2.29 by Hashin[22].

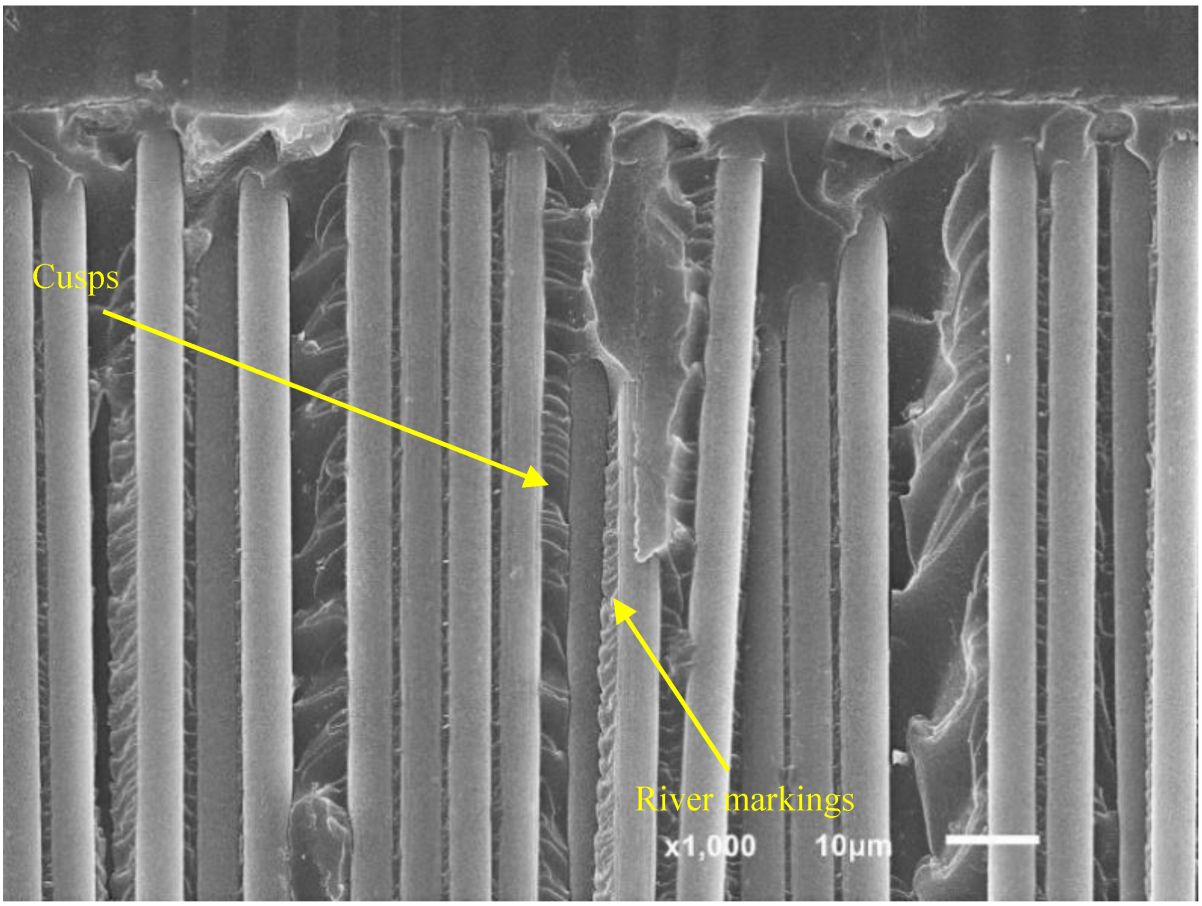


**Figure 2.28:** A picture from an electron microscope showing the fibre failing due to fatigue loading. It shows the river markings of mode I failure for the in-plane normal stress and the cusps for the mode II failure for the in-plane stress. Every cycle produces either a cusp or a river marking in a fibre that is tearing apart. Source of the figure is from the research performed by Argüelles et al. [21].

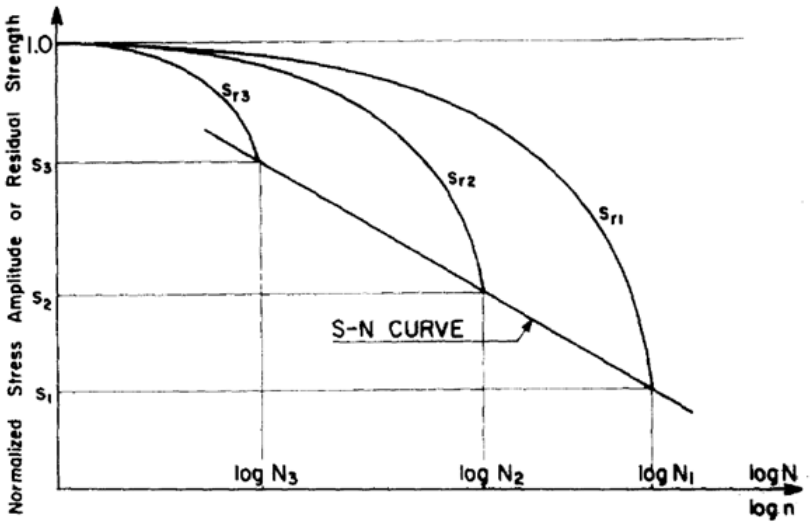


**Figure 2.29:** A graph showing the decrease in the residual strength until failure occurs due to the damage accumulation. Whereas the S,N-curve describes final failure for many stress levels, the residual strength curves $S_{r,i}$ describe the remaining strength in the material after loading it for a certain amount of cycles at a certain amount of stress. Only at failure the S,N-curve and the residual strength model describe the same observation. Hence an S,N-curve could be obtained by running residual strength models at multiple stress levels till final failure. The figure has been retrieved from the research performed by Hashin[22].

However there is one major drawback to this method. In order to succeed, the crack has to occur within the points of measurement. Otherwise the stiffness degradation will not be observed as is illustrated in line 4 of figure 2.30. As the observer wants to be sure to capture the cracks and not have to guess upon the future crack, line 5 would not be suited as well. Even if the crack is observed, the measurement of the residual stiffness is still biased based on the location of measuring as shown in lines 1, 2 and 3 of figure 2.30. Since especially in composites there is little plastic zone around the crack tip, the stiffness reduction mainly has to come from the crack opening displacement as the crack propagates through the two measurement points. As the fatigue damage assessment is for the entire cross-section, the strain must be measured over the entire height of the cross-section. This gives the best representation of the total amount of damage that is accumulated during a cycle as is shown in figure 2.21. The configuration of line 1 allows to have accurate measurement of the initial stiffness degradation in stage I due to IFF as it is able to measure it. Lines 2 and 3 do even a slightly better job at capturing the stiffness degradation due to a crack running through their measurement points, but these methods are so sensitive that those configurations will miss out when stage II starts. Stiffness degradation due to delamination in stage II is also captured in configuration line 1 and final stage III due to FF as well. For the final stage it is important not to have too sensitive measurements as it is unpredictable and large sudden movements are present. This makes it difficult to create a regression of the overall movement when measuring only locally such as configurations lines 3 and 5.

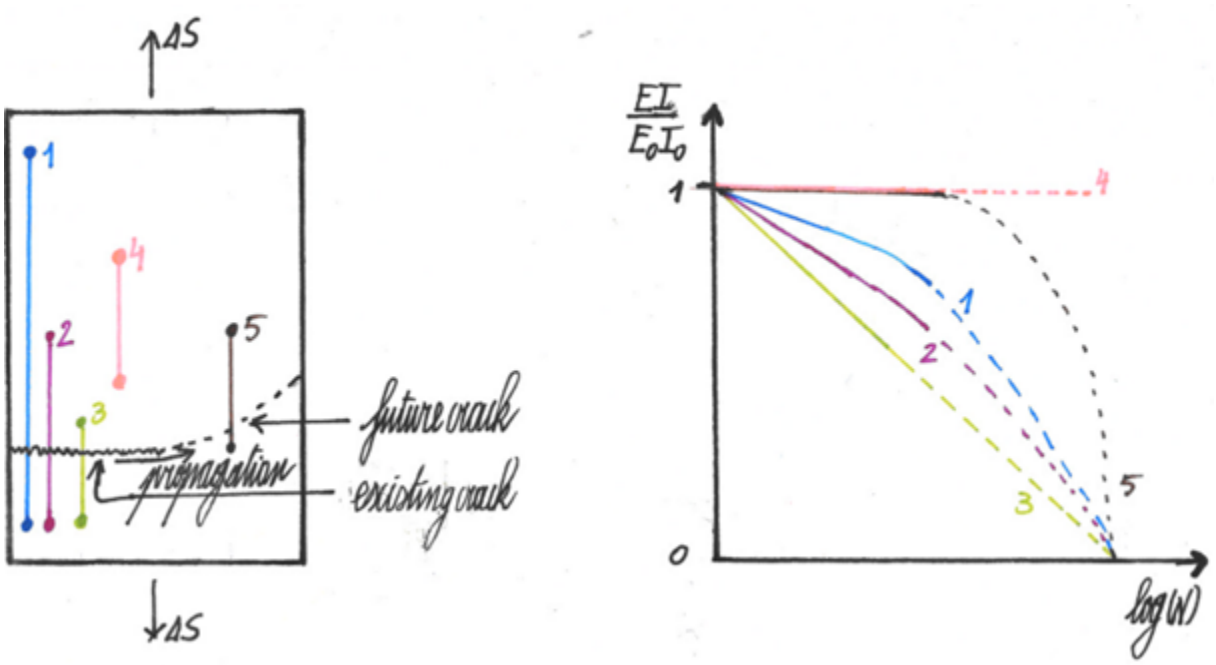


**Figure 2.30:** An illustration of the different possible locations to measure the stiffness degradation in a specimen with an edge crack loaded vertically with a stress range $\Delta\sigma$. Each configuration is labeled from 1 to 5 on the left. Each different location of measurement has a different regression of the residual relative stiffness drawn on the right, thus making a different prediction about the future crack propagation. The existing crack is drawn with a solid line and the future crack with a dashed line.

## 2.6. Hypotheses review chapter 2

### 2.6.1. Three newly posed hypotheses as result of chapter 2

There are three hypotheses based on the theory of composites. The second hypothesis is related to the first hypothesis. If the first hypothesis is false, then the second one is probably false as well and vice versa. If the third hypothesis is false, then hypothesis 1 and 2 could still be true.

**Hypothesis 1: A compact tension specimen loaded with a fatigue load in the pins will have two stiffness degradation stages.** It is posed based on the theory given in section 2.5.1 of chapter 2. Since for both the out-of-plane bending fatigue and in-plane tension-tension fatigue similar mechanisms are observed, it is expected that the compact tension specimen will also have those three mechanisms (IFF, DEL and FF). Future test results should point out if that is true, for now this is an assumption that has been made. It cannot be investigated with modelling as the user defines how many mechanisms will be included. However, what could be investigated is the number of stages observed due to those three mechanisms. Since the in-plane tension-tension fatigue loaded tests has two stages, it is expected that the compact tension specimen will have two stages as well due to the in-plane loading. *This hypothesis can not be proven yet as it requires tests results in order to do that. For now it is assumed the only three significant failure mechanisms are IFF, DEL and FF.*

**Hypothesis 2: In a compact tension specimen loaded with a fatigue load in the pins the delamination will overlap with the inter fibre failure or the fibre failure.** From hypothesis 1 it will be known if the compact tension specimen will only have two stages or more. In the case that it has only two stages, one of the mechanisms will have to overlap with at least one of the other mechanisms. Since the two in-plane mechanism are unlikely to occur together, the delamination has to overlap with at least one of the two mechanisms as is pointed out in section 2.5.1 of chapter 2. *This hypothesis can not be proven yet as it requires tests results in order to do that. For now the delamination will be assumed to overlap with the IFF and FF.*

**Hypothesis 3: The three significant fatigue failure mechanisms present in a compact tension specimen are best simulated by a combination of three individual models.** From the master Structural Engineering the philosophy is to first recognise all possible (significant) failure mechanisms. If all mechanisms are taken into account and taken into account correctly, then generally the structure is designed safely. One of the safe manners to implement all failure mechanisms correctly is to assign a failure criterion to each of those. Each criterion could be described by a certain modelling technique, for instance a damage model. Lumping mechanisms into one criterion may lead to a loss of overview and mixing up the underlying assumptions. Therefore it is stated that modelling the three mechanisms with three individual models will lead to the most accurate result. Section 3.9.1 of chapter 3 will provide a proof.

## 2.7. Conclusion chapter 2

In composites the crack initiation phase is negligible, only a hand full of cycles of high-cycle fatigue are part of the crack initiation phase. Thus at most $1\%$ of the fatigue life of composites is considered the crack initiation phase as cracks in composites emerge very quickly due to the brittleness of the material. On the other hand, the crack propagation phase is relatively long which is the remaining part of the fatigue life, generally over $99\%$ of fatigue life. During the crack propagation phase the

stiffness of the material could be observed on multiple occasions during a fatigue test. The strength could be observed as well, but that requires multiple specimen as it will need destructive testing.

The relative residual stiffness shows three distinct phases for out-of-plane bending: a small but rapid decreasing stiffness at the start due to inter fibre failure cracking, followed by a steady decreasing stiffness caused by delamination and a progressively decreasing stiffness at the end due to fibre failure. During the first two stages the strength decreases only slightly which is barely noticeable, but during the last stage it degrades progressively just as the stiffness. This behaviour is related to the damage done to the fibres and is similar to the Paris law curve using the damage propagation rate to replace the crack propagation rate. Only the general failure mechanisms of composites are assessed whereas the mechanisms related to unidirectional, woven fabric or chopped strand mat layers are of lesser influence in terms of fatigue life mechanisms. Hence only the inter fibre failure, the delamination and the fibre failure mechanisms will be considered in the models.

During the out-of-plane bending these three mechanisms occur sequentially, but during in-plane bending the delamination overlaps with stages I and III. Therefore only two distinct phases will be observed: stage I and stage III. The delamination only provides extra possibilities to find more critical crack patterns by interlinking multiple separate cracks starting at different positions. Only then a more critical crack pattern is obtained that results in a structural mechanism that has less fatigue life than each individual ply separately. Notice that this will only happen if the interply interaction is relatively weak to the intraply properties, otherwise it will slow down the cracking behaviour. The delamination could be metaphorically seen as a spring support. A spring support has an effect that is between a hinged and a clamped support. The hinged support is obtained by simulating layers separately and the clamped support is obtained if the layers are glued with infinitely strong glue. As this interaction becomes too complicated to be calculated by hand accurately, it is required to simulate it using computer software. One of the options is to use a finite element model (FEM) in Abaqus[3]. Using a FEM also has the advantage of predicting residual strength at any given point by adding an additional static load step after the cyclic analysis.

# Chapter 3: The ideal model

## 3.1. Introduction

As stated in the theory, three failure mechanisms (inter fibre failure, delamination and fibre failure) are expected during the fatigue failure of composites. As the delamination (DEL) mechanism overlaps with the inter fibre failure (IFF) and the fibre failure (FF), it is complicated to predict the fatigue life by hand. From the master structural engineering the standard procedure is to model each mechanism with a separate formulation, but do the three mechanisms necessarily require three formulations for the model of a wrapped joint? If so, how does the model take care of these failure mechanisms? The main goal is that the ideal model should be able to predict the residual fatigue life accurately with the correct cracking pattern. So what are the advantages of modelling the composite fatigue failure with failure mechanisms in the first place? All the questions will be answered in section 3.3.

In the section 3.4 candidate models will be selected based on how well they represent the failure mechanism on a meso-scale level. Thus for each mechanism there will be a formulation discussed that fits the mechanism with its initiation and propagation criteria.

After the trade-off of the model, it will be continued with some side notes to be considered when using the direct cyclic analysis in Abaqus[3]. Abaqus allows to take measures to reduce computational effort in the fatigue analysis. Let it be trivial that an elastic model on its own will not do the job as in that case the material would have infinite strength since it does not take into account failure mechanisms. The linear elastic analysis is only good in determining stress distributions in the elastic regime of the material. Therefore it is good in determining the stress distribution till the onset of non-elastic response.

Each mechanism has a certain initiation requirement and a propagation definition to determine when the damage, the crack or the plastic strain increases and by how much. What are these initiation requirements and propagation definitions for the used models? What underlying assumptions are made to comply with these requirements? All of these questions will be answered in sections 3.6, 3.7 and 3.8 for the plasticity model, ductile damage model and VCCT model respectively. The focus of the report will be on how the models implement the numerical mechanism with regard to the physical mechanism and why they are suitable for the analysis. Only the general theory of each model and every possible suboption will be discussed in this chapter. The precise input will be discussed in chapter 4.

## 3.2. One hypothesis that will be proven in chapter 3

Chapter 3 will give answer to one hypothesis. The answer will be formulated in section 3.9.1 of chapter 3.

**Hypothesis 3: The three significant fatigue failure mechanisms present in a compact tension specimen are best simulated by a combination of three individual models.**

## 3.3. Advantages of using multiple mechanisms on mesoscale to model fatigue behaviour

In order to predict the residual strength and to obtain the S,N-curves accurately, the model will be calibrated on the residual stiffness test results. In the end, the S,N-curve is nothing more than showing the residual strength of the final cycle after a certain amount of cycles with a constant amplitude as is illustrated in figure 2.29 by Hashin[22]. The advantage of the residual stiffness is that the relative residual stiffness is decreasing more gradually than the relative residual strength as is shown in figure 3.1. Therefore it is more accurate and reliable to calibrate a model on the relative residual stiffness.

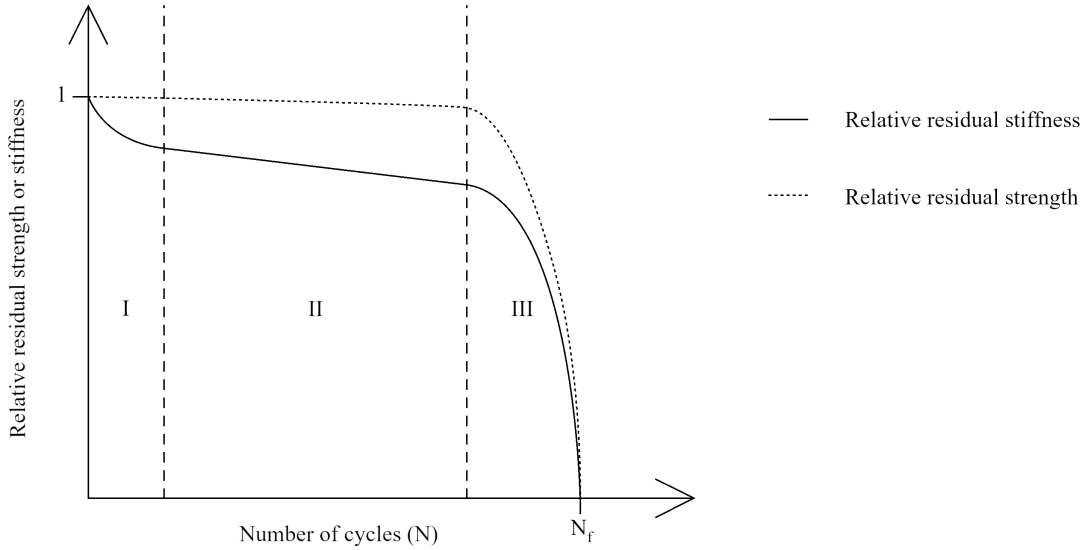


**Figure 3.1:** A qualitative illustration of the residual stiffness (full line) and residual strength (dotted line). Both parameters are normalised by their respective initial stiffness or strength to obtain the relative residual values. The residual stiffness has an initial decrease due to the inter fibre failure (stage I), then it settles to a gradual constant decrease due to the delamination (stage II) and exponentially decays to 0 at final cycle $N_f$ due to the fibre failure (stage III). The residual strength decreases very slightly during due to the IFF (stage I), but start to degrade more due to the delamination (stage II) until it reaches a critical damage point on which the fibres start to fail due to the FF (stage III) that creates a rapid decrease to 0 at final cycle $N_f$.

The model needs to include the mechanisms occurring during the fatigue degradation correctly to be able to predict the relation between the residual stiffness and the residual strength, preferable a model is used that is not limited by a specific material or with that specific geometry. If the physical mechanisms are modelled with an accurate numerical mechanism, then calibrating once is sufficient. If a single mechanism in the model is mimicking multiple real mechanisms, then a calibration is needed every time the material or the geometry changes. If each real mechanism is modelled with separate numerical formulations, then the model has to be calibrated only once per material. So little to no calibration should be required in modelling different geometries. This is why the model that will be proposed is desirable.

As there are three stages observed in the stiffness degradation diagram of Brod et al.[1], at least three sets of constitutive relations are needed. It is assumed that these three major failure mechanisms are currently the only three mechanisms that have influence on the fatigue behaviour of the composites. After calibration on the residual stiffness, some destructive strength test are still required in order to check the model on the relation between residual strength and residual stiffness. This is especially required if different failure mechanisms are expected upon modelling different materials.

A micro-scale model, despite simulating the fibre-matrix interaction more accurately and for that reason probably the structural behaviour as well, will be excluded in order to prevent extreme computational time. The meso-scale level model will be looking at the layer as if it is one piece, therefore limited calibration from tests and limited computational time is needed. This is desired since the fatigue simulations already take a lot of time to simulate all the cycles.

## 3.4. Selecting models to describe the fatigue behaviour in composites

### 3.4.1. Limitations on the considered models in the trade-offs

The investigation limits itself to the models that are readily available in Abaqus[3]. Readily available models are models that are accessible in Abaqus[3] by dialog boxes. In a general sense there are three types of readily available mechanical models present in Abaqus[3] Standard/Explicit that define the material beyond its elastic regime: the plasticity models, the dynamic models and the smeared/discrete crack damage models. The dynamic models are excluded from further considerations; it is assumed that the dynamic influences are negligible. This will limit the frequency of testing to a maximum of about $4$ [Hz] according to the ISO-norm 15850[4]. There is an option to do fast testing that includes the dynamic effects, but it will require that the temperature changes have to be considered. The dynamics models are the plasticity-viscous model, the damping model, the eos model and the viscosity model. Furthermore, after some eliminations of certain models in certain group of models, only the advantages and disadvantages of each group are discussed. Detailed trade-off is provided in sections 3.6, 3.7 and 3.8 of chapter 3.

### 3.4.2. Readily available elasticity models

As a basic first step, the elasticity regime of the material is simulated using the (linear) elastic model. The other elastic formulations are more suited for other materials such as foam (the hyperfoam model, the low density foam model), rubber (the hyperelastic model and the hypoelastic model) or other materials (the porous elastic model and the viscoelastic model). It is not required to make the elastic model more difficult than the standard elastic model, because the elastic model allows to describe the orthotropic stiffness of the composite already. Within the elastic model it is possible to define the stiffness of the composite either as an equivalent isotropic stress, as a lamina, with engineering constants, with an orthotropic formulation or with an anisotropic formulation. All of these options are valid for composites keeping in mind that the isotropic model has its limitation. Further down the list it allows to enter more values, therefore create more complex stiffness matrices (less symmetry assumptions or other material assumptions). First investigations will be performed using the isotropic model due to its simplicity, later the orthotropic stiffness properties of the laminate will be given using engineering constants although it will be mentioned as orthotropic. The suboption fail stress or fail strain allows to set a limit on the elastic regime which is useful if only a linear elastic model is run. This is not applicable to the case of fatigue. The traction and coupled traction options are discarded since those describe cohesive elements. The shear model is discarded since the composite material will have mainly longitudinal stiffness.

As long as the physical structure does no exceed the yield stress, neither damage initiation, then an elasticity model is sufficient. For static analysis this is sufficient. For fatigue analysis in steel with the applied stress below the level of the CAFL as well. However, for fatigue in composites this is not sufficient as composites do not have a CAFL. Hence damage is initiated. Thus the elasticity model is only a partial solution and cannot model the entire observed fatigue behaviour that includes damage.

### 3.4.3. Readily available smeared crack models

The smeared crack damage models for ductile metals are: the ductile damage model, the Johnson-Cook damage model, the shear damage model, the FLD, the FLSD, the MK model and the MSFLD. Only the ductile damage, the Johnson-Cook damage models and the shear damage model are interesting since the others are forming models. The Johnson-Cook damage model is a special version of the ductile damage model, but is only available to Abaqus/Explicit according to the MIT manual[23]. The direct cyclic analysis is used in fatigue loaded models for analysing the fatigue behaviour which implies the models that will be create are implicit models. Thus the Johnson-Cook damage model is unavailable. The shear damage model is for shear band localisation as explained by the MIT manual[23]. Since this effect is not observed either by Brod et al.[1] or Bartowiak et al.[2], it will be excluded. There are other possibilities for damage models, one is a general traction-separation law which has a list of possibilities of taking into account the damage: the quadratic strain, the quadratic stress, the maximum strain, the maximum stress, the maximum principal strain and the maximum principal stress. These six options are similar in behaviour, only a slight difference is present in the definition of when damage starts and when final failure happens. These will be considered as one group of traction-separation laws during the trade-off. Then there are three more damage models for specific applications: the Hashin damage model for composites, the Mullins effect for elastomers and the brittle cracking model for concrete. Elastomers are rubberlike materials that have large ductility. This option is discarded since composites are brittle. Brittle cracking is a valid option during crushing of the material. In the end a compact tension specimen (CT specimen) is modelled that is not pressure dependent, thus a brittle cracking model would make it unnecessarily difficult. The Hashin damage model should be a valid option, however it is not yet available in combination with the direct cyclic analysis[1]. Thus the Hashin damage model can not be used. In short the damage models that could be used are the ductile damage model and the traction-separation laws.

### 3.4.4. Readily available discrete crack models

There are also damage models available that describe discrete crack damages along interfaces, these are: the cohesive zone model (CZM), the extended finite element method (XFEM) and the virtual crack closure technique (VCCT). The VCCT and the XFEM models require an extra step by defining the crack medium. This tells Abaqus[3] where a crack propagation is allowed for that model[2]. The XFEM also requires a damage model to define when failure has to occur as the XFEM only enriches an element. If a fatigue analysis has to be performed, then the discrete damage models require an extra step that involves implementing keywords[3]. Therefore these models are actually exceptions to the criterion of being a readily available tool. The required keywords templates are described in table 3.1 for the fatigue

[1] This needs to be double checked

[2] This step is either performed by copying keywords templates from lines 1 and 5 of table 3.1 or by finding a dialog box in the interaction module of Abaqus[3]. The dialog box is found by going through "Special" → "Crack" → "Manager" → "Create". The rest of the dialog box is self-explanatory.

[3] The keywords-file is accessed by a right-click on the model followed by selecting the option "edit keywords".

VCCT, the fatigue XFEM and fatigue CZM. For the fatigue VCCT criterion it is required to define the interaction properties in the interaction properties section of the keywords. These have to be assigned to each interface according to lines 3 and 4 of table 3.1. Line 3 is required once per property and line 4 once per interaction. Similarly, for each interface a contact pair needs to be assigned in the interaction section according to line 5 of table 3.1 as is stated by the tutorial of Ramsaier[24]. For the XFEM it is only required to implement one of the options of the Line 2 templates since the rest is defined in a dialog box. These keywords are entered for the surface properties in the interaction properties according to Simutech[25]. For the CZM model it is again only required to implement one of the Line 2 templates since the rest is defined in the interaction as mentioned in the MIT manual[26][27]. Anyway, all of these models have the opportunity to be compatible with the direct cyclic analysis as long as they describe the interface between two layers.

**Table 3.1:** Template for the input data line to complete a VCCT interface for the fatigue analysis. The XFEM method has all of its medium defined in a dialog box and the CZM does not require additional information. However, both still lack of a fracture criterion definition for the fatigue that uses one of the "Line 2" methods (BK law[28], power law[29] or Reeder law[30]). It is required to change the values between "<" and ">" with the intended value for the analysis or make it blank if not taken into account.

| | |
|---|---|
| Line 1 | *Debond, slave="<name of slave surface>", master="<name of master surface>", debonding force=STEP, frequency=1 |
| Line 2 BK | *FRACTURE CRITERION, TYPE=fatigue, MIXED MODE=BK, TOLERANCE=<tolerance><br><$c_1$>,<$c_2$>,<$c_3$>,<$c_4$>,<$\frac{G_{th}}{G_c}$>,<$\frac{G_p}{G_c}$>,<$G_{I,c}$>,<$G_{II,c}$><br><$G_{III,c}$>,<$\eta$>,<$T$> |
| Line 2 Power | *FRACTURE CRITERION, TYPE=fatigue, MIXED MODE=POWER, TOLERANCE=<tolerance><br><$c_1$>,<$c_2$>,<$c_3$>,<$c_4$>,<$\frac{G_{th}}{G_c}$>,<$\frac{G_p}{G_c}$>,<$G_{I,c}$>,<$G_{II,c}$><br><$G_{III,c}$>,<$T$>,<$a_m$>,<$a_n$>,<$a_o$>,<$T$> |
| Line 2 Reeder | *FRACTURE CRITERION, TYPE=fatigue, MIXED MODE=REEDER, TOLERANCE=<tolerance><br><$c_1$>,<$c_2$>,<$c_3$>,<$c_4$>,<$\frac{G_{th}}{G_c}$>,<$\frac{G_p}{G_c}$>,<$G_{I,c}$>,<$G_{II,c}$><br><$G_{III,c}$>,<$\eta$>,<$T$> |
| Line 3 Interaction property | *Surface Interaction, name=<name of interaction><br>1., |
| Line 4 Property assignment | *Clearance, master="<name of master surface>", slave="<name of slave surface>", value=<value of the clearance><br>**Interaction: <name of interaction> |
| Line 5 Interactions | *Contact pair, interaction=<name of interaction>, small sliding<br><name of slave surface>,<name of master surface>,<name of bonded nodes set> |

### 3.4.5. Readily available plasticity crack models

The plasticity models are available in many different variants to describe the stress-strain relation beyond the yield stress. The strength of composites is not significantly influenced by pressure, hence the Mohr-Coulomb and Drucker-Prager models are discarded since they are more complex than required without any additional advantage. Since the composites are not dominated by an internal friction angle, neither a dilation angle, it is assumed that composites have an associated flow. Hence the following list of plasticity models are excluded: the cap plasticity model, the concrete damage plasticity model and the soft rock plasticity model. The cast iron plasticity model only allows to change the Poisson's ratio, hence no degradation in stiffness is possible which is required. Since the composite material behaves vastly different than clay and foam; the clay plasticity model and the crushable foam model are excluded. The concrete smeared cracking model focuses on compressive loading instead of tensile, thus will be excluded for the same reasons as the brittle cracking damage model. Although the fatigue analysis will describe a process that takes a long time, it will not be the application of one constant load since it is a cyclic load. Thus the creep model will not help to describe the problem. Since the combined material is modelled and not only the matrix or the fibres, the porous metal plasticity model will not be suited. Finally, there is also not much swelling present thus the swelling model is discarded. That leaves the standard plasticity model being the only model available for this application.

The (standard) plasticity model has many variants to choose from. First of all a choice is made between the isotropic hardening, the kinematic hardening, the multilinear-kinematic hardening or the Johnson-Cook hardening. The Johnson-Cook hardening is a special isotropic hardening for high strain rate dependent problems as is written in the MIT manual[31]. This thesis excludes rate dependent behaviour since the dynamic effects are neglected, thus it is a quasi-static problem. Also with composites there are relatively small strains till failure, thus it will not be strain rate dependent according to Zmudzski[32]. The multilinear kinematic hardening is similar to the standard kinematic hardening such as the Johnson-Cook hardening is similar for isotropic hardening. Therefore is will not be considered. There is also an option to combine the isotropic hardening with the kinematic hardening (combined hardening). Although it is expected that the combination of isotropic and kinematic hardening will be required, it is best to limit the hardening first to a single hardening rule that describes the test results best. For the same reason it is also momentarily best to keep the number of backstresses for the kinematic hardening to one and extend it only if it is required to obtain higher accuracy.

The (standard) plasticity model also has several suboptions: rate dependent, potential, cyclic hardening, ORNL, cycled plastic and anneal temperature. As mentioned earlier the CT specimen is not strain rate dependent due to the low stains, thus the rate dependent hardening is excluded. ORNL is the Oak Ridge National Laboratory constitutive model for components in nuclear systems at elevated temperatures as explained by the MIT manual[33]. This is not close to the application on which the wrapped joint is focused. The cycled plastic suboption is required to complete the ORNL suboption. The anneal temperature suboption is to tell Abaqus[3] at which temperature the material loses its memory about the hardening it has experienced, the MIT manual stated[34]. That means it no longer makes a difference between deformation caused by loading or by creating the geometry straight away. Since the temperature elevations are not considered, this option is discarded. That leaves only the suboptions potential and cyclic hardening. The potential suboption is to describe anisotropic hardening or creep according to the Hill criterion[35] and the cyclic hardening is to describe an isotropic hardening for cyclic loading provided in the MIT manual[36]. Both of these options could be used (simultaneously) in addition to the already described kinematic or isotropic hardening in the plasticity model.

Since there are a couple of combinations of suboptions with options possible, each combination will be briefly explained. If both suboptions (potential en cyclic) are used, then the potential suboption describes (mainly) the change in shape of the yield contour, the cyclic hardening suboption (actually an isotropic hardening) defines the size of the yield contour and the kinematic hardening defines the location of the yield contour. If only the suboption potential hardening is used, then the potential hardening describes the change in shape and size of the yield contour and the kinematic hardening the location. Unless the potential hardening is used in combination with isotropic hardening, then the potential hardening describes mainly the shape and the isotropic hardening the size. If only the suboption cyclic hardening (an isotropic hardening) is used, then the cyclic hardening describes the size of the yield contour and the kinematic hardening the location of that yield contour. The combination of the suboption cyclic hardening with the option isotropic hardening has not been tried, but it would be expected to result in an error or one of the hardening formulations is redundant. Without any suboptions the kinematic hardening will describe a change in location of the yield contour and in case of isotropic hardening the plastic model will describe a change in size. A more detailed explanation of kinematic and isotropic hardening is illustrated in section 3.6.4 of chapter 3. For the trade-off, each of these models will be compared for their specialised description since every combination is possible as long as not twice the same option is chosen. It compares the change in shape of the yield contour for the anisotropic hardening described by the Hill criterion in the potential suboption, the change in size of the yield contour by the isotropic hardening and the change in location of the yield contour by the kinematic hardening.

### 3.4.6. Trade-off of non-linear model types

The elasticity model is not considered in the trade-off as it definitely included in the model to describe the non-damaged state of the material. Therefore only the non-elastic model groups are considered: plasticity models, smeared crack damage models and discrete crack damage models.

All of these groups of non-elastic models have certain advantages and disadvantages. The groups are compared in table 3.2 for certain criteria related to modelling fatigue in composites. First of all the models have to be compatible with the direct cyclic analysis in order to simulate long sequences of cycles easily. If it is able to do so, then it deserves a '-'. If it also allows cycle jumping then, it will be awarded '+'. If it also includes a Paris law[9] as input, then it will be awarded with an '++'. The second criterion is whether it shows a crack or not. The cracking type will be mentioned and a grade will be given based on it. The freedom of the crack type will be graded on if it requires a precrack, if it requires a predefined crack interface and if it is element size dependent. Based on this information it is determined how well these models will simulate one of the failure mechanisms. Also a range on the number of input parameters will be given. The more parameters that are needed, the more tests that are required. This is a disadvantage as a fatigue test takes a long time to perform $\left(\frac{1000000[\text{cycles}]}{4[\text{Hz}]} = 250000[\text{s}] = 70[\text{hours}]\right)$. The Paris law[9] is currently considered to be the most accurate representation of a fatigue crack growth. The higher the guarantee on a Paris law[9] relation, the more positive the model is graded. Finally a note is given whether the crack is completely described on empirical fatigue formulations or whether the model is based on static understanding of the material.

**Table 3.2:** Trade-off table of the three different types models on describing the cracks in a fatigue analysis. The comparison is done qualitatively unless an indisputable value is present. The range is defined as "–" for impossible, "-" for impractical, "0" for not preferred, "+" for good alternative and "++" for preferred option. The assessment has been performed for the different category of mechanisms first. After that it has been further defined per individual mechanism. The delamination is the only interply mechanisms and the inter fibre failure and fibre failure together are the intraply mechanisms. For the intraply the maximum of the individual mechanisms is chosen.

| Criterion | Smeared crack damage | Plasticity | Discrete crack damage |
|---|---|---|---|
| Compatibility with direct cyclic analysis | + | - | ++ |
| Cracking | Smeared | No cracking | Discrete |
| Precrack required | No | Not applicable | Yes |
| Predefined crack path | No | Not applicable | Yes, except XFEM |
| Mesh dependency | Limited for convergence | Not applicable | No |
| Inter fibre failure | 0 | + | -, XFEM 0 |
| Delamination | - | – | ++, XFEM - |
| Fibre failure | ++ | 0 | –, XFEM ++ |
| Number of input parameters | 4 | 3 to 12 parameters | Static 4 to 7, fatigue 9 to 13 |
| Accuracy | 0 | 0 | ++ |
| Underlying mechanism related to fatigue | Static | Static | Fatigue empirical |

Three of the possible constitutive models groups are compared in table 3.2 as an overview of their advantages and disadvantages that will be elaborated here. The VCCT model and XFEM were developed to be compatible with the direct cyclic analysis as the fatigue formulation has additional parameters to define a Paris law[9] and it allows cycle jumping, so it is graded with a "++". The CZM is not tested, but in theory it should work as well. The smeared crack damage models and plasticity models on the other hand are still possible in combination with direct cyclic analysis, but no Paris law[9] could

be defined. Thus the smeared crack models are graded with a "+". The plasticity models are currently not compatible with the cycle jumping algorithm, thus they are graded with a "-". Let it be clear that the plasticity models do not provide any crack visualisation, while the smeared crack damage models show a crack by deleting the elements of which an integration point has reached full degradation. This is a smeared crack visualisation. The smeared crack models have the major advantage of not requiring a predefined crack path nor a precrack. That provides a lot of freedom which omits the need of modelling every possible crack initiation position. The discrete crack models have a discrete crack visualisation by defining the interfaces as possible crack paths. Those interfaces have no geometrical thickness, thus provide a clear cut at the cost of explicitly modelling the propagation of every possible precrack in different analyses. The smeared crack damage model and the plasticity model are both able to model the effects of crack formation within a layer. The smeared crack damage model is better at it as it also visualises the crack, therefore it is graded with a "++" for fibre failure, but with a "0" for inter fibre failure. The plasticity model graded with a "0" for fibre failure as no crack visualisation is present since it only shows the effect of stiffness degradation. For the inter fibre failure it is graded slightly higher with a "+", because it has the advantage of being first after the elastic model. Therefore if a damage and a plasticity model are implemented, it always occurs between the elasticity model and the damage model. The discrete crack damage models are impractical in modelling and computing in-plane failure as is shown with the VCCT slicing model in appendix B, thus graded as "-" for both the inter fibre failure and the fibre failure. For the interply failure it is the other way around, here the discrete crack damage models are the preferred option as the delamination is an interaction failure, therefore it is graded with a "++". If someone is creative with the smeared crack damage model or the plasticity model, then that person will probably find a manner to mimic the interply failure by modelling the adhesive with solid elements. However, this is highly unlikely, therefore it is graded with a "-". With relation to the intraply and interply failure, a more precise distinction is provided per failure mechanism. For inter fibre failure on meso-scale the plasticity model is the preferred option as it does not a crack in the elements, therefore graded with a "+". The ductile damage model is possible, but not is not the preferred option thus is graded with a "0". This will be explained in more detail in section 3.6.2 of chapter 3. The discrete crack damage models are not suited for the inter fibre failure. Probably there is a possibility somehow for a VCCT slicing model with many elements over the thickness of the ply. Thus it is graded with a "-". The XFEM is an exception as the free crack path allows easier modelling of any intraply failure, therefore XFEM is rated as "+" for IFF and FF. For the delamination the discrete crack damage models, with exception to the XFEM, are clearly the most suitable model developed to date for fatigue, therefore it is graded with a "++". The XFEM is better at modelling intraply mechanisms as it splits elements. Generally interfaces are not modelled with regular elements in Abaqus[3], but with interface elements. These interfaces could be modelled explicitly using elements (not interface elements), it that case cohesive elements have to be used. Therefore the XFEM is rated as "-". The smeared crack damage models do work to model delamination if the interaction is modelled with elements just as for the XFEM, but it is impractical thus it is graded with a "-". Similar reasoning is applied for the plasticity models, but as the plasticity model on its own would not crack it is graded with a "–". The number of input parameters for the ductile damage model is always $4$, while for the plasticity models it depends on the number of backstresses that are included and if anisotropic hardening is included. The discrete damage models take $4$ to $7$ parameters for the static formulation and $9$ up to $13$ parameters for fatigue formulation depending on which mixed mode behaviour is chosen and whether to include an additional crack initiation criterion. The discrete crack damage models are completely empirical based on the Paris law[9] that has to be calibrated for each material on fatigue tests. The plasticity model and ductile damage model would in theory link the static coupon test to the fatigue behaviour of any geometry. Therefore it is graded to be static in theory although additional fatigue tests are advised.

In short, use a discrete crack model such as VCCT or CZM if the crack surface is already known in advance. This is the case for interply failure as the interface between the plies acts as a predefined crack surface for the delamination. Use the smeared crack model or XFEM if the crack surface is not known in advance. This would be in the case of intraply failure. However, if the crack formation and damage accumulation are not that important, but is important to simulate a stiffness degradation while allowing a strength increase, then consider to use an (anisotropic) plasticity model instead.

## 3.5. Direct cyclic analysis as speed up of fatigue simulations

If no computational accelerations are applied, then a fatigue analysis needs to calculate for every increment of every cycle the displacement field with the according stresses. For the high-cycle fatigue analysis with a million cycles this will take years. The direct cyclic analysis is an analysis method that is able to reduce the large required computational effort for a fatigue analysis. It stores only the final iteration of the calculated cycle. The major reduction in computational time is thanks to forward damage extrapolation that enables this so-called "cycle jumping".

The direct cyclic analysis iteratively calculates the next state of the material in the fatigue analysis at $N = n$ by extrapolating the damage at $N = n - x$ over the cycles that are not simulated. As such it is required to have an accurate prediction of the damage in the cycle that is simulated. For this Abaqus[3] implicitly calculates the state of deformation based on the material model and boundary conditions. Therefore iterations are required to obtain results with an equilibrium between the internal forces and the external forces. Abaqus[3] uses the Fourier series as an estimate of the real displacement field to find a stable solution according to the MIT manual[37]. This also speeds up the analysis as the displacement field will always be continuous, hence managing the number of Fourier terms helps to improve the accuracy of the results or the speed of the calculations. The direct cyclic analysis will be further discussed in section 4.4 of chapter 4.

## 3.6. Applying the plasticity model for inter fibre failure

### 3.6.1. General concept of the plasticity model

If the elastic formulation of the material is no longer sufficient, one of the first solutions to consider is to include the plastic property of the material. Originally the plasticity model is designed for ductile materials such as steel during a static analysis. It defines the stress-strain relation beyond the yield stress until the ultimate stress has been reached. In the theory of plasticity the cross-section would fail if a plastic hinge would occur in the structure that leads to a mechanism. In order for a plastic hinge to occur, it requires that the entire cross-section needs to have plastic (ultimate) stress as is illustrated in figure 3.2 according to the lectures of Hoogenboom[38] . On the contrary the elastic failure happens when the first part in one cross-section reaches yield stress.

Note that finite element models (FEM) generally do not consider reaching the elastic limit as failure during the static linear elastic analysis unless the user defines it by means of plasticity or damage. Another option would be to manually check during the elastic analysis if the elastic limit is reached. The yielding and the hardening or the softening of the material is physically rearranging the dislocations of the crystalline structure of the material. For a metal it results in hardening as the dislocations are moved

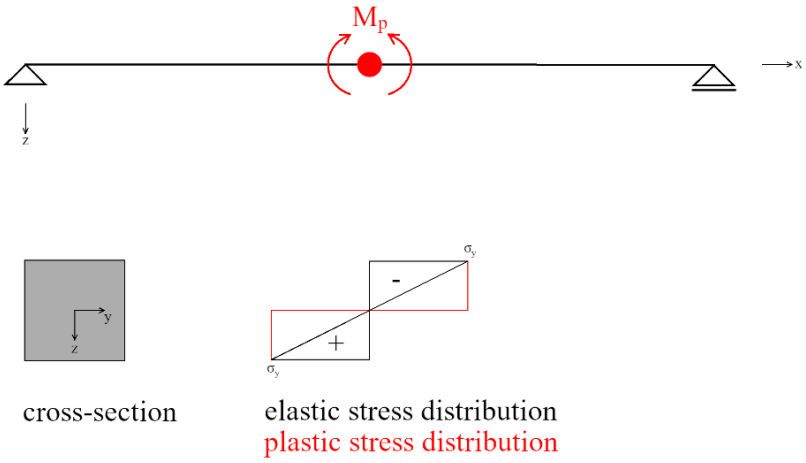


**Figure 3.2:** Cross-sectional stress distribution on a simple supported beam that is first loaded until yield stress in the centre cross-section (black) and then loaded plasticly until ultimate stress of the cross-section (red).

to the grain boundaries, therefore the dislocations are removed from within the grain. This improves the number of bonds between the atoms in the grain as is shown in figure 3.3. Thus the strength of the material increases. Upon elongating in the plastic regime, it becomes visible that the material also starts to contract sideways in a phenomenon called necking as is shown in figure 3.4. Be aware of the fact that the true stress-strain diagram always has a positive rate of hardening as less faults are present in the remaining cross-section, even if the ultimate stress in the engineering stress-strain diagram has been surpassed as is illustrated in figure 3.5 for steel. This is because the engineering stress and strain still assumes that the original cross-section size is still in place during the necking. Of course there is a limit to it as at a certain point the atomic bonding strength is reached due to having a cross-section with almost no size and little dislocations as stated by Copuruglo and Jonkers[39]. For the true stress-strain relation it still results in a positive rate as the reduction in the cross-section overcomes the reduction in the applied force. However, for the engineering stress-strain relation there is no reduction in the cross-section assumed, thus a negative rate at the last part to failure is obtained.

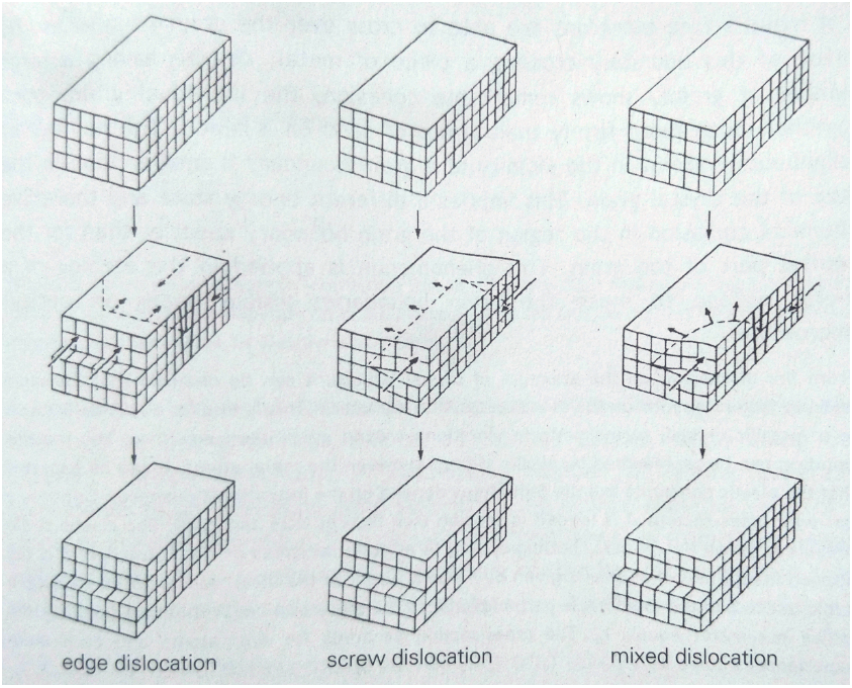


**Figure 3.3:** A visualisation of the three atomic mechanisms in metallic crystalline structures that remove dislocations upon yielding the metal. If the dislocations are removed, then more bonds are present that cause to increase the strength of the material. The figure is retrieved from the book written by Mourik et al.[40].

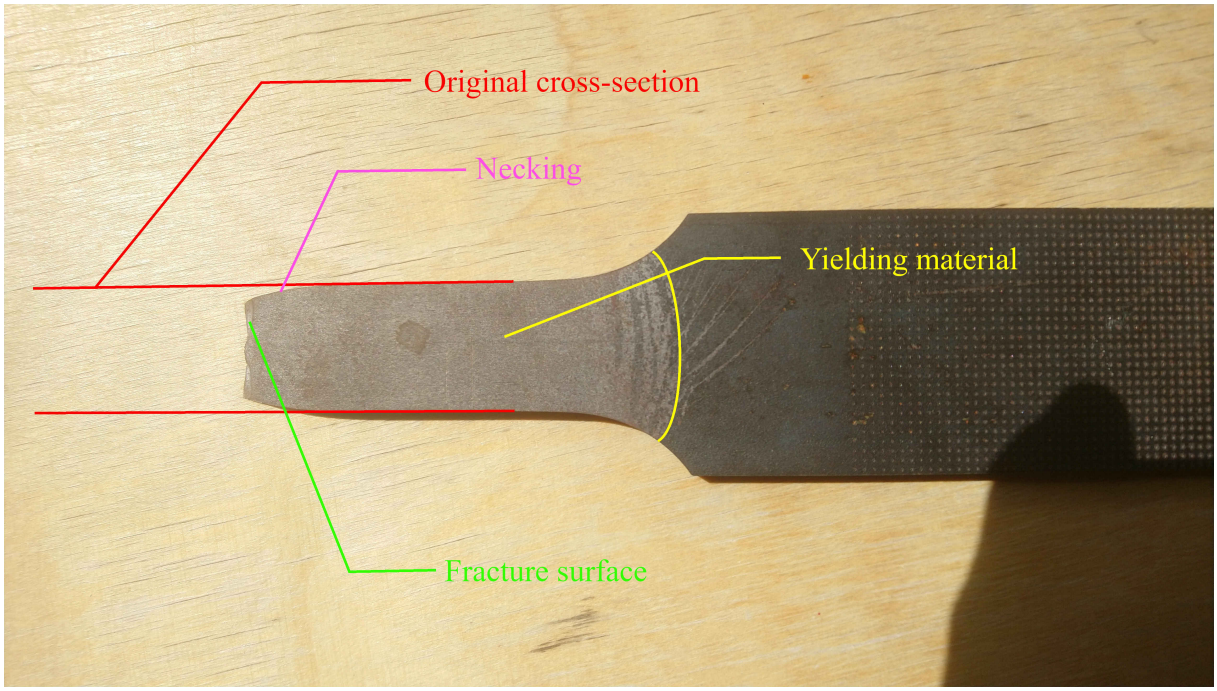


**Figure 3.4:** A picture of a tensile tested steel coupon showing the fracture surface annotated in green, the yielded material annotated within yellow boundary and the necking annotated in pink where cross-section starts to deviate from the original cross-section which is annotated in red.

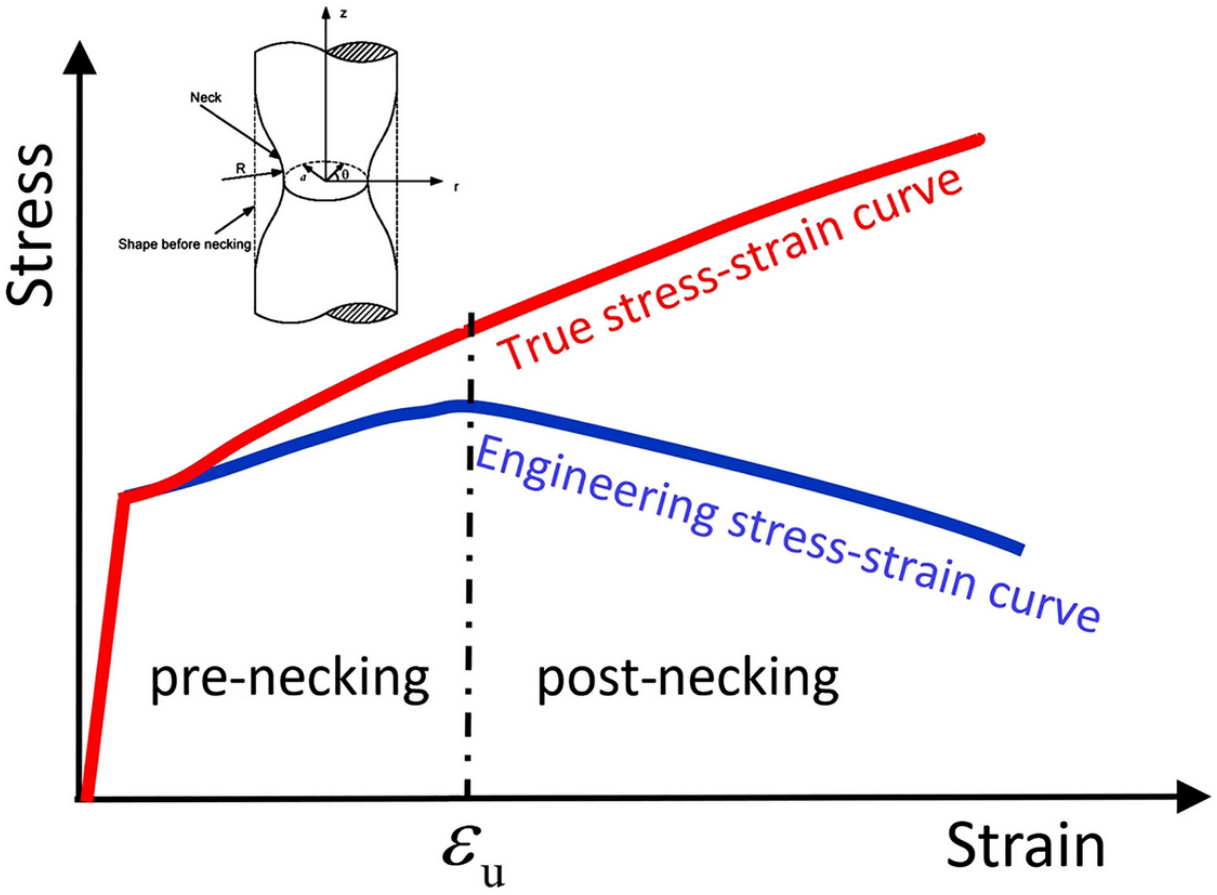


**Figure 3.5:** A diagram showing the true stress-strain curve in blue and the engineering stress-strain curve in red. As soon as yielding starts, the engineering stress-strain relation and the true stress-strain relation deviate as the side ways contraction due to tensile pulling of the coupon result in a cross-section reduction. This difference is even more pronounced at the point of reaching the ultimate stress in the engineering curve at which necking starts. This figure is from Tu et al.[41].

### 3.6.2. Applicability of the plasticity model for inter fibre failure

In composites the inter fibre fatigue failure (IFF) may have a different origin than plasticity as IFF is caused by damage, but it has a similar effect on the layer at meso-scale as the plastic response of metals. In composites the failure mechanism is an embedment failure around the fibre that causes this effect on meso-scale. Upon pulling and unloading the layer, the matrix around the fibre deforms differently due to the different stiffness of the matrix and fibre. This causes embedment failure which looks like a bolt ovalising a hole in a metal lug. By moving back and forth under the cyclic loading the ovalisation increases until the holes link up forming a micro crack, as is described already in figure 2.25. As this cracking is within the ply it will be "invisible" at meso-scale. The effect is that the material is able to reach higher stress levels, but at a different stiffness than the initial stiffness. In spite of the increase of the strength, the stiffness decreases. That effect is visible in the static coupon test results in figure 3.6. So a model, such as the plasticity model, that allows stiffness degradation without having cracks is suited for this failure mechanism. The underlying assumption is that the static coupon test initially loses its stiffness due to static IFF that would be the cause of embedment failure. At least what could be observed is that during the fatigue tests the IFF does not lead to a reduction in strength. The choice whether the isotropic or the kinematic hardening mimics the mechanisms better has to be determined from the fatigue tests with fully reversed load cycles $R = -1$. During the static tests both hardening formulations allow

to mimic the mechanism identically. All in all, although the plasticity model is developed for the static analysis, it is allowed to be applied in direct cyclic analysis as a combined cyclic hardening without any adaptations to the formulation as is stated in the MIT manual[42].

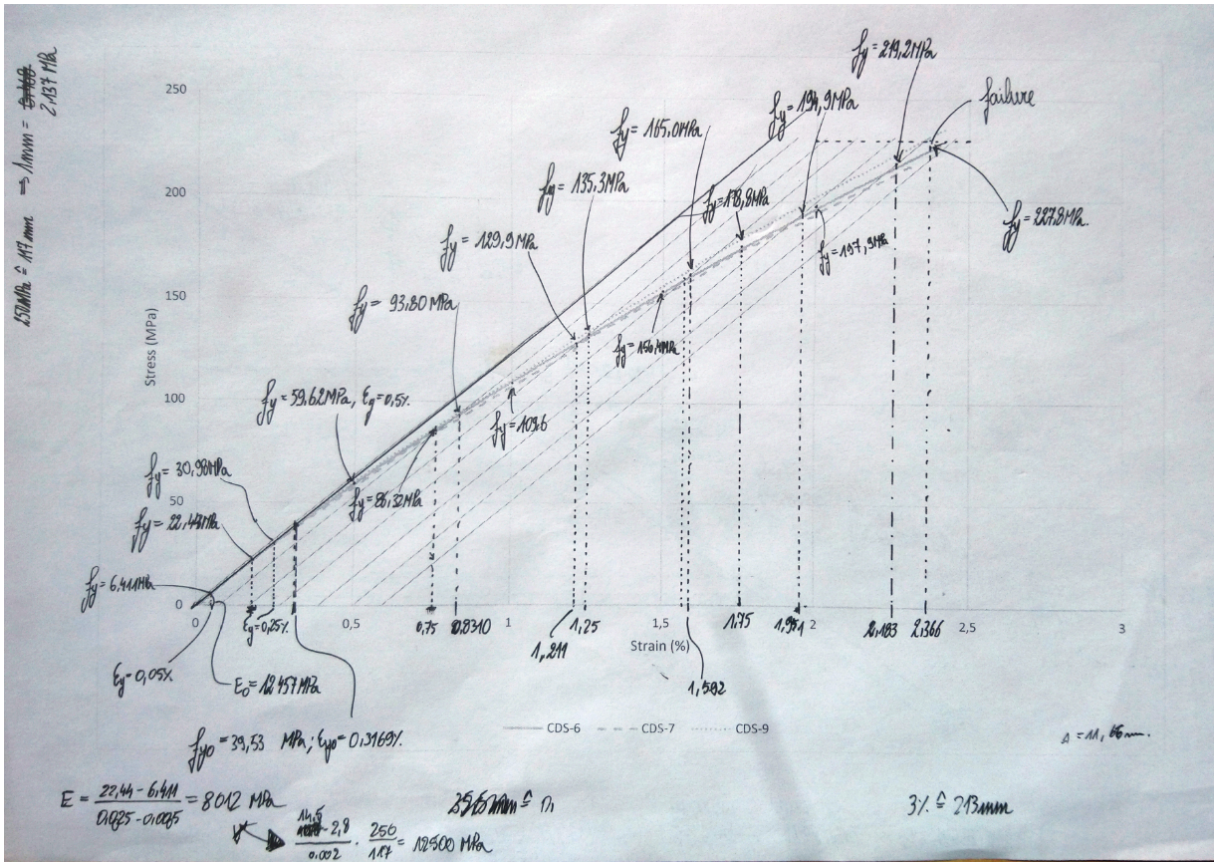


**Figure 3.6:** The output stress-strain diagram of the static loading test results of material testing performed by the composite research group of civil engineering at the TU Delft[43]. Further material details are classified . The solid black line is the initial tangent line representing the Young's modulus of the material at $E = 12285$ [MPa]. The material model will take the average stress-strain relation of the three test specimen CDS-6, CDS-7 and CDS-9. The coordinates for this average curve are given in the graph as a coordinate for the strain and a coordinate for the according stress.

The plasticity model is chosen over the option of a damage model. Compared to the VCCT and the CZM it might be obvious that the plasticity model is preferred due to its freedom to initiate the non-linear behaviour everywhere, but compared to the XFEM and the smeared crack models it is not that clear. As already mentioned earlier, the IFF does not degrade the strength while the stiffness is degraded. In literature only one damage model was formulated by Lemaitre[44] that increases the stresses in the element as the damage parameter $D$ increases. This is defined as a damage hardening model. $D$ is defined on the range $[0, 1)$ with $0$ meaning no damage and $1$ meaning completely damaged. This formulation is described in equation 3.1. Ultimately an infinite stress would be obtained if $D$ increases toward $1$. Therefore in practice $D$ often has an upper bound value of $0.2$ to $0.5$ as provided by Lemaitre[44]. However, this formulation or other possibly existing damage hardening models are not available in one of the smeared or discrete damage models readily available in Abaqus[3]. Another option would be to define an evolution stage as is described in figure 3.7 that includes the IFF and FF in one damage model. This would still separate the IFF and the FF stage in one element. It is required that the stress resistance initially increases after crack initiation. Unfortunately all damage models only allow a monotonically decreasing evolution stage since the tabular form is not an option for a definition based on the fracture energy. That means this initial increasing stress resistance is not possible, even not a constant stress as is

illustrated in figure 3.7. For that reason, the only option left would be a damage mechanism separately for the IFF. That damage mechanism needs to have a shallow degradation in order to best preserve the strength. This would make IFF a competing mechanism with the FF. This is because after degradation due to IFF the strength still decreases. That requires either the FF to be defined on a certain strain instead of stress. This is not possible as well within the readily available models in Abaqus[3], thus it is more convenient to model the IFF based on a plasticity model.

$$\sigma_{eff} = \frac{\sigma_{nom}}{1 - D} \tag{3.1}$$

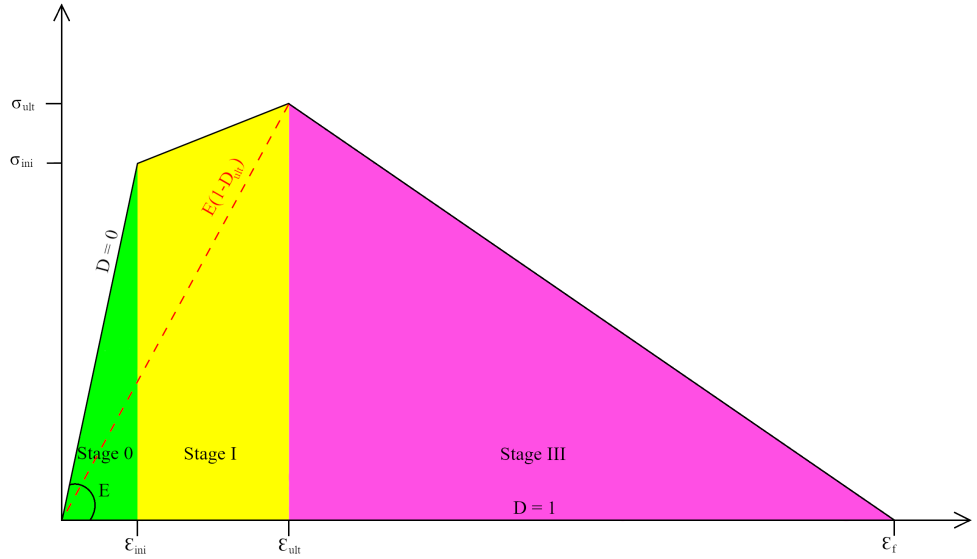


**Figure 3.7:** An illustration of modelling the intraply mechanisms using a bi-linear degradation of a damage model. Stage 0 represents the undamaged stage. On element level the ultimate stress is not surpassed until $\varepsilon_{ini}$ is reached that describes the onset of matrix cracking with the corresponding stress for damage initiation $\sigma_{ini}$. Stage I describes the inter fibre failure with the strain $\varepsilon_{ult}$ describing when stage I ends and stage III starts with the fibre failure. At that strain the maximum stress $\sigma_{ult}$ is reached.

One might argue that modelling IFF is unnecessary and for that reason bypass the problem of requiring a damage hardening model. From a design standpoint of view it is interesting to know when the strength starts to degrade. In that perspective the stiffness degradation due to the IFF plays a major role. If the IFF is not modelled, then it would lead to discrepancies in predicting the stiffness degradation. Moreover, it would make the stiffness degradation just as sudden as the strength degradation. Thus less accuracy is present in the predictions. This nullifies the advantages of having a much simpler model with only damage models included.

In short, the plasticity model is the only way with the readily available models in Abaqus[3] to reduce the stiffness of an element without initiating the (progressive) degradation of the strength. One major drawback has to be kept in mind. The deformation caused by the plastic tensile response of plasticity model will result in an overclosure of the crack that will lead to additional compressive forces as is described in section 2.4.3 of chapter 2. In metals it makes it more accurate as there is a plastic wake present in front of the crack tip. In composites this plastic wake is not present as the composites in the first place do not have significant plastic deformation, but rather a crack due to a tensile load. Secondly, composites are more likely to crush in compression instead of deforming plasticly.

### 3.6.3. Initiation of plasticity by yield stress

Plasticity starts where the elasticity ends. This is on the moment that the yield stress is reached. Initially this will be at the initial yield stress provided as input for modelling. In reality the yielding in metals is defined as the stress level at which the material starts to gain more elongation for a moment while the stresses do not increase in an engineering stress-strain diagram. In composites the yield stress will not be so clear as is shown in figure 3.6. One could argue that the composite material starts its plastic regime immediately at the start of loading as from thereon the stiffness degrades. Someone else could state the elastic regime of a composite is large as with a bi-linear model it is still a good representation of the reality with one part of the line representing the elastic part and the other part of the line the plastic part. Fortunately an ISO-norm 527[45] has been set up to counter this dispute. The yield stress is defined at the stress level for which the tangent of the stress-strain relation deviates too much from the stiffness between $\varepsilon = 0.05\%$ and $\varepsilon = 0.25\%$.

If the material has been unloaded, then the plasticity will be initiated again only on the updated value of the yield stress. This will be above the initial plasticity if hardening occurs and below the initial plasticity if softening occurs. Abaqus[3] does the assessment in this way as during the unloading the material deforms elastically first until the yield stress has been reached again. In chapter 4 section 4.5 this will be explained more thoroughly. This manner is in line with the hypothesis of the course on plasticity as explained in the lectures of Hoogenboom[38] and later it will be proven that Abaqus[3] assesses the plasticity in this manner for cyclic loading.

### 3.6.4. Evolution of plasticity by hardening

After initiating the plasticity, the plasticity evolves causing numerical hardening or softening to mimic the physical hardening or softening. Numerically this evolution changes the yield stress of the material. During the hardening the yield stress will increase and during softening it will decrease [42]. There are two manners of hardening (isotropic and kinematic) and there is one option for softening (isotropic). The isotropic hardening or softening will reshape or resize the yield contour of the material as stated by Borst and Sluys[46] such that the yield stress increases or decreases in that direction of loading respectively for hardening or softening. The yield contour is a line in a two dimensional representation or a surface in a three dimensional representation that indicates the combinations of local normal and local shear stresses in the material that lead to yielding. The yield contours are also drawn for structures based on the displacements and forces. These are generally called failure criteria, but in principle they are the same according to Hoogenboom [38]. Upon yielding it is almost inevitable to move along the yield contour as well, because the material hardens according to the plastic potential function and not the hardening function to find equilibrium. The associated flow rule states that a material is ideally plastic only if the vector **m** of the plastic flow is a multiplication of the gradient vector **n** for the yield contour as is explained by Borst and Sluys[46]. So only the ideal plastic materials that follow the associated flow rule will have equilibrium along the same vector as the hardening. In case a material does not follow the associated flow rule, than the yielding moves relatively along the yield contour as is illustrated in figure 3.8a for isotropic hardening. Kinematic hardening also works with plastic flow and gradient vectors. Despite it is theoretically possible to have kinematic softening, in practice only kinematic hardening is applied as kinematic hardening translates the yield contour without reshaping or resizing as is illustrated in figure 3.8b. Kinematic softening will therefore be applied by applying the hardening vectors in opposite direction. Abaqus[3] only accepts hardening vectors for kinematic hardening.

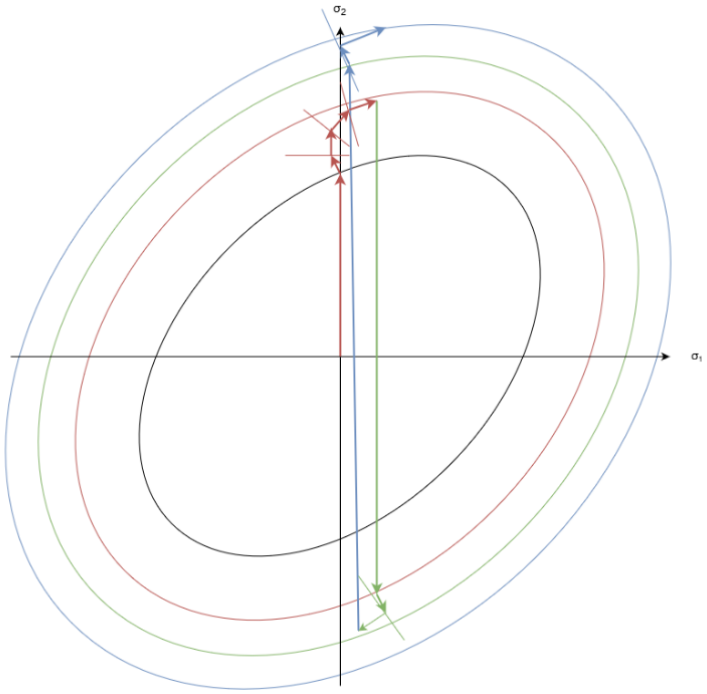


**(a)** An visualisation of the change in yield contour due to isotropic hardening.

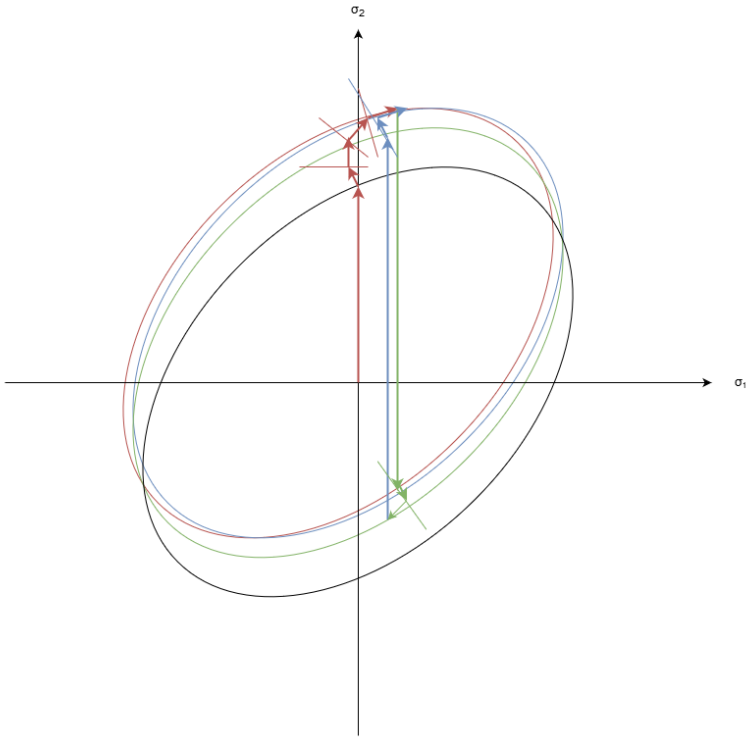


**(b)** An visualisation of the change in yield contour due to kinematic hardening.

**Figure 3.8:** An visualisation of a material with isotropic hardening fatigue loaded only in principal stress $\sigma_2$ direction without lateral constraints, therefore only moving vertically. Initially the red arrow shows this along the y-axis for the elastic regime. When it reaches the yield contour (black ellipse), the yielding starts according to the plastic flow vector $m$ (smaller red arrows) which are perpendicular to the lines of equal plastic potential of the plastic potential function $g$ (small thin red lines). Upon yielding the yield contour increases in size due to its isotropic hardening definition where it is to keep position and shape and only enlarges in all directions with the gradient $n$ of the yield function $f$ as shown on the left in figure 3.8a. For the kinematic hardening the yield contour moves while keeping the size and shape. It will move with the gradient $n$ of the yield function $f$ as is shown on the right in figure 3.8b. As $m$ and $n$ are different, the yield point no longer is on the y-axis, but it moves along the yield contour. During unloading the material first deforms elastically first.

Depending on the mechanism that has to be described either kinematic or isotropic plasticity is more suited based on observations in test results. Inter fibre failure is due to enlarging of the holes around the fibres. Therefore the underlying mechanism is an embedment failure of the matrix material that leads to more easy deformations and slight strength decrease. For now it will be modelled as an isotropic hardening as is assumed that the increased movement also affects the yield contour on the opposite side in the same manner. In other words the hardening on the tension side also creates hardening on the compression side and vice versa. Also the stresses in perpendicular direction of the main loading will be somewhat affected by the increased movement. It will be shown this will allow to obtain accurate results with a model that is simple to understand. At this moment realise that isotropic hardening will result in the relaxation of the mean stress for displacement controlled analysis as is shown in figure 3.9. For unidirectional plies this will be the only mechanism. The additional mechanisms present in woven fabrics are best described using kinematic hardening. The first mechanism is a matrix crack parallel to the fibre [47] and the second mechanism is a crack propagating along the yarn periphery as was observed by Montesano et al.[48]. The yarn is the bundle of individual fibres that form a strand of fibre. It are these strands that are woven into a woven fabric by alternating above or below the crossing yarns. The yarn mechanism occurs around the outer fibres of the yarn. Both mechanisms are drawn in figure 3.10. These two mechanisms are modelled best as kinematic hardening as no stiffness or strength degradation is observed. Only a mere shift in strains is observed. Notice that the idea is to replicate a stiffness degradation model where the stiffness is defined as the stress difference over the applied displacement for the fatigue cycle. Therefore if the ratchet strain (the difference between the final strain of cycle $n$ and cycle $n + 1$) is constant than it will not show degradation in stiffness. In other words the ratcheting is desired for these mechanisms as is shown figure 3.11. Due to complexity the focus will be on the inter fibre failure mechanism, hence these latter two mechanisms will not be addressed now, but might have to be included in future analysis to improve accuracy.

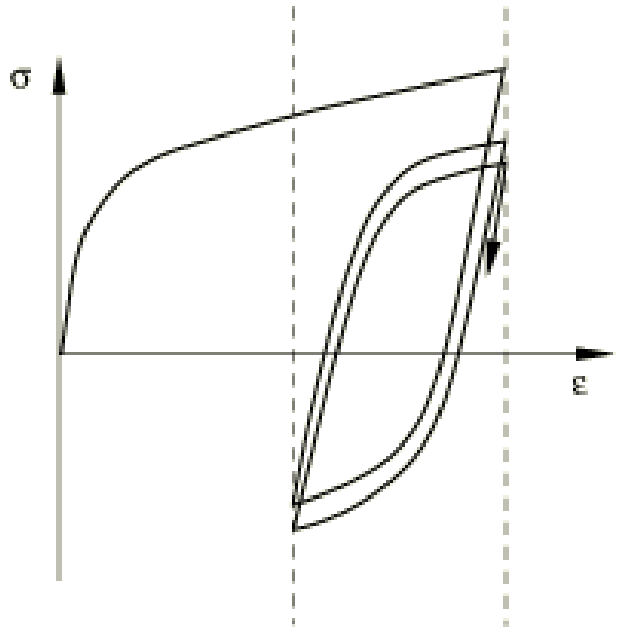


**Figure 3.9:** An illustration of a displacement controlled fatigue analysis with isotropic softening material parameters showing a decrease of stresses over each cycle. As the elongations are kept the same due to the displacement controlled analysis, the stiffness decreases due to a decreasing stress as response. Source of figure: MIT Abaqus manual[36]

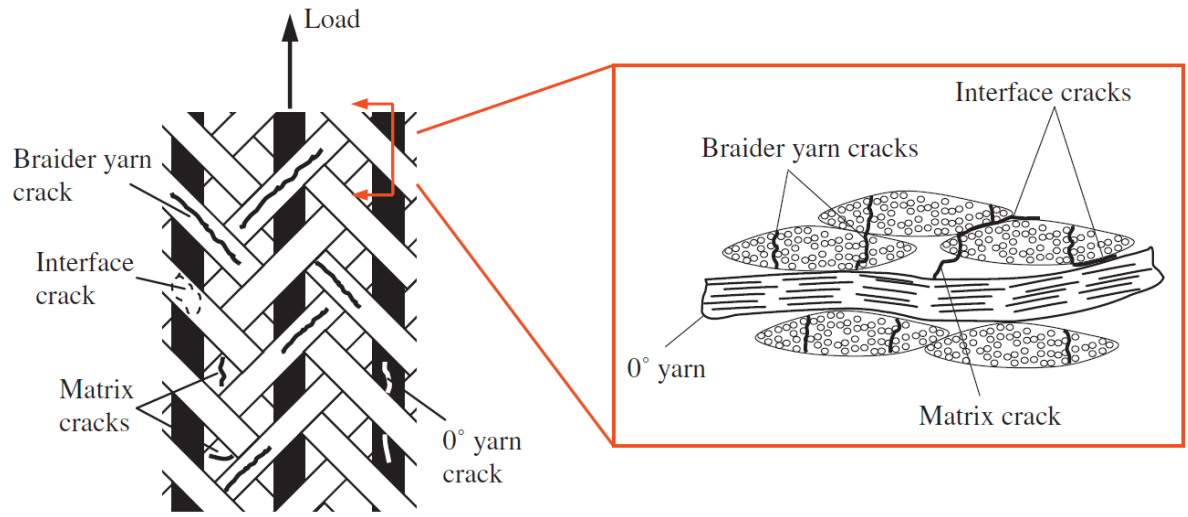


**Figure 3.10:** A drawing of multiple microscopic failure mechanisms specific for woven fabrics. In top view on the left the (braider) yarn crack, interface crack (between two yarns) and matrix crack (in the empty space of the yarns) are drawn. A cross-sectional view is given on the right. Source of figure: Montesano et al.[48].

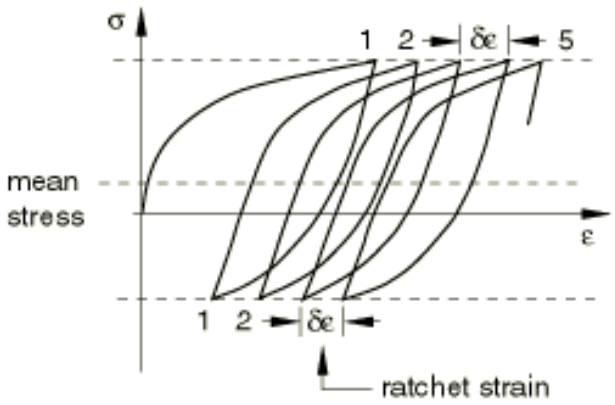


**Figure 3.11:** An illustration of a force controlled fatigue analysis with kinematic hardening material parameters showing a constant ratchet strain over each cycle. As the elongations are kept the same due to the displacement controlled analysis, the stiffness will not decrease due to ratcheting as the stresses do not change. Source of figure: MIT Abaqus manual[36]

Although the damage mechanisms could not be implemented in the desired manner, an option that would at least improve the accuracy of the plasticity model is to include the Hill criterion for anisotropic hardening by adding a potential function. It does so by providing different hardening rates in different material directions. It therefore is the strength equivalent of the orthotropic stiffness defined in the elasticity model. That would mean there is an opportunity to model different strengths in different directions similar to the Hashin damage model[10]. The Hill criterion[49] achieves this by having six weight functions that relate the yield stress in each direction to the equivalent initial yield stress $\sigma_{y,0}$. The higher the weight function, the lower the allowed stress is in that direction since the higher weight function lets the applied stresses in that direction reach the equivalent yield stress faster. The weight functions are provided in equation 3.3 and the relative parametric ratios $R_{ij}$ that describe the ratio of the allowable stress if only loaded in that direction over $\sigma_{y,0}$ in equation 3.2. The Hill criterion[49] itself is provided in equation 3.4[35]. Do notice that the Hill criterion[49] does not make a difference between the tensile and compressive strength. For that the Hashin damage model[10] would be superior (in a static analysis). One might come up with the idea to use the kinematic hardening to shift the yield contour and make a difference between the tensile and compressive strength in that manner. However, there is a problem to be identified that discourages this idea. Despite the kinematic hardening only allowing

hardening (no softening) and being defined in a tensile direction, it does act in the compressive direction as well as is reported by Mavrodontis[50]. In other words, a lower compressive stress will not be achieved. For a compact tension specimen that should not be dramatic. This boils down to the decision whether it is worth it to investigate the six parameters in tests to describe the increase in accuracy due to the anisotropic hardening. It would also complicate the models, which is not desired in order to relate the effect in each outcome to the modelling technique that has been used. For that reason the anisotropic hardening is for now set aside as it could always be implemented as an extension of the kinematic and/or isotropic hardening.

$$\begin{cases} R_{11} = \frac{\sigma_{11}}{\sigma_{y,0}} \\ R_{22} = \frac{\sigma_{22}}{\sigma_{y,0}} \\ R_{33} = \frac{\sigma_{33}}{\sigma_{y,0}} \\ R_{12} = \frac{\sigma_{12}}{\tau_{y,0}} \\ R_{13} = \frac{\sigma_{13}}{\tau_{y,0}} \\ R_{23} = \frac{\sigma_{23}}{\tau_{y,0}} \\ \tau_{y,0} = \frac{\sigma_{y,0}\sqrt{3}}{3} \end{cases} \tag{3.2}$$

$$\begin{cases} F = \frac{1}{2}\left(\frac{-1}{(R_{11})^2} + \frac{1}{(R_{22})^2} + \frac{1}{(R_{33})^2}\right) \\ G = \frac{1}{2}\left(\frac{1}{(R_{11})^2} + \frac{-1}{(R_{22})^2} + \frac{1}{(R_{33})^2}\right) \\ H = \frac{1}{2}\left(\frac{1}{(R_{11})^2} + \frac{1}{(R_{22})^2} + \frac{-1}{(R_{33})^2}\right) \\ L = \frac{\sigma_3}{2(R_{23})^2} \\ M = \frac{\sigma_3}{2(R_{13})^2} \\ N = \frac{\sigma_3}{2(R_{12})^2} \end{cases} \tag{3.3}$$

$$f_{(\sigma)} = \sqrt{F(\sigma_{22} - \sigma_{33})^2 + G(\sigma_{33} - \sigma_{22})^2 + H(\sigma_{11} - \sigma_{22})^2 + 2L(\sigma_{23})^2 + 2M(\sigma_{31})^2 + 2N(\sigma_{12})^2} \tag{3.4}$$

Let it be clear that composite material will be formulated much more brittle than mild steel. Since the plasticity model is initially developed to handle ductile materials, therefore on the bottom line the question is: is it possible to model the composite material as a brittle steel? At least the stress-strain curve will need to have smaller intervals than steel to maintain accuracy for the definition of stress-strain.

## 3.7. Applying the ductile damage model for fibre failure

### 3.7.1. General concept of the ductile damage model

The ductile damage model describes the mesoscopic cracks in the material. These cracks are visible on ply level, hence the reason to use the term mesoscopic. The ductile damage model is originally developed for ductile materials such as steel in a static analysis as a smeared crack model. Although it is developed for the static analysis, it has proven itself also to be applicable in the direct cyclic analysis. It accounts for the crack within an element by keeping track by a so called stiffness penalty parameter

$K$ or damage parameter $D$. The definition of both is similar to another and is even identical if there is a proportional relation between the damage and the stiffness degradation. To avoid confusion with $K$ as stress intensity factor, the damage parameter $D$ will be used from now on for the damage. If the damage parameter reaches $1$, then the element is considered to have no more stiffness or strength, hence it is broken. The broken elements could be deleted by Abaqus[3] if element deletion is enabled. For numerical reasons the element will be deleted by default if the damage parameter exceeds a damage value of $0.99$, but that value could be changed to the user's preference. Only a value of exactly $1$ or higher will not be tolerated as $1$ would lead to numerical difficulties and above $1$ is physically not possible.

### 3.7.2. Applicability of the ductile damage model for fibre failure

It is applicable to composites as composites do not have infinite strength, not even a constant strength over time. In other words, if enough cycles are applied, then it will always be torn apart. Therefore some sort of degradation criterion is needed that also allows the visualisation of cracking. A layer has many yarns, as such each an element with a size of about 2 [mm] represents many yarns in a meso-scale model. Every time a load leads to damage in the sense it breaks a fibre in a yarn, both the strength and the stiffness reduces. This failure is progressive for fatigue loading meaning that it will damage more fibres each cycle until final failure is reached where the last fibres break at once as is illustrated in figure 3.12.

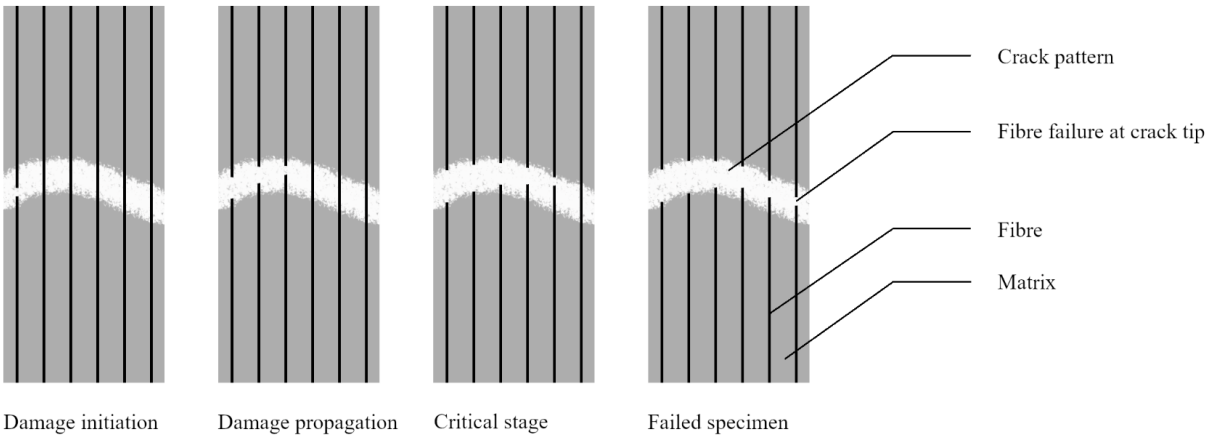


**Figure 3.12:** An illustration of the progressive fibre failure mechanism in the material. The drawn area could be seen as an element of a finite element model. The fibre fracture happens after the matrix has cracked already. Upon failure of the fibres the crack propagates and gets wider till the critical stage before the final cycle. During the final cycle the last fibre(s) crack causing the material to fail and no longer be able to endure the fatigue loading.

This progressive failure happens only at last stage (stage III) of the fatigue. The failure happens in final stage not only because it is purposefully initiated there, but also the matrix is much weaker than the fibre. After the matrix has cracked first, a chord action will occur where the fibre is not broken yet and the matrix around has been chipped of the fibre, since the matrix mainly provided compressive strength, shear strength and stiffness and the fibres tensile strength. In that case it has lost much of its stiffness but not much of its strength during tension as the fibres are much stronger. During compression the structure is mainly dependent on the matrix for strength, therefore composite structures are much worse in resisting fatigue loading with $\sigma_{min} < 0$ than with $\sigma_{min} \geq 0$ as is shown in figure 2.24. In order to let the fibre fail, the fatigue loading will cause striations in the fibre during stages I and II. The fibres will be showing cusps and river markings as illustrated in figure 2.28. This takes a long time, which is the second reason why strength degradation happens in the last stage. When the one fibre completely

fails, then the force has to be transferred to the surrounding fibres, therefore increasing the stresses on the remaining fibres. This will result in more fibres breaking each cycle like an expanding domino effect.

Again the VCCT and the CZM are inferior solutions to the ductile damage model to simulate FF for the reasons given in section 3.4 of chapter 3. In short, the limitation of requiring to predefine crack paths makes the VCCT and CZM unattractive for FF as is illustrated in the VCCT slicing model of appendix B.

It is possible to use a plasticity model to describe the effect, just as the IFF will be described by the plasticity model. It could be achieved by decreasing the equivalent stress ($\sigma_{eq}$) after exceeding a certain equivalent plastic strain ($\varepsilon^{p}_{eq}$). Final failure would in that case be described by a close to zero stress state after exceeding the ultimate stress. However, since the ductile damage model is capable of reducing the stress and the stiffness just as it is caused in reality by FF. There is no need any more to model a damage mechanism with a plasticity model. In this case the damage model will be a more accurate representation of degradation due to the mechanism. Additionally, the ductile damage model will always be an augmentation to the plasticity model.

It could be useful in this case to use the XFEM instead of the ductile damage model. The XFEM is even compatible with the VCCT if the VCCT is used for the interply behaviour according to the MIT manual[51]. Also the XFEM is based on the Paris law[9] for fatigue. Additionally, it requires a traction separation law to complete the definition which implies that the XFEM is able to take into account the different strengths for different modes. However, there is one major drawback, it requires a precrack. This makes the entire the XFEM approach unattractive for the wrapped composite joint since simulating many different variations of initial cracking is undesired. The smeared crack models do not suffer from this.

Then there is only one more option to discuss: a traction-separation law or a ductile damage model. There is no fundamental argument to choose one or the other. For convenience the ductile damage model has been chosen since He[52] already used it in his models. Thus for the ductile damage model the parametric input was already known for the wrapped composite joint.

### 3.7.3. Damage initiation criterion

Damage initiates once a certain stress level $\sigma_i$ has been reached in the material. Depending on the direction of the applied stress and the formulation of the material it is determined which (combinations of) traction-separation law(s) will be used (mode I, II or III). As it is not on an interface such as VCCT, but in the material to describe a smeared crack, it will be a stress-strain relation. A smeared crack model will not provide an exact representation of the crack in terms a clear cut. The crack could be anywhere in the broken elements. This fracture of fibres is well modelled using the ductile damage model where the failure of a fibre would result in a slight increase of the damage parameter. Hence the ultimate strength of the damage model has to be related to that of the single fibre in the material.

The damage initiation criterion describes the moment when the ultimate material strength is reached and starts to tear apart in order to allow more deformation. In the new deformed state equilibrium will be reached if the structure is able to redistribute the stresses in a better way such that is capable of handling the forces and stresses in the new configuration as a result of the tearing apart.

What if the FF was not taken into account? It would certainly make the model simpler with less parameters to calibrate with test results. However, excluding the FF will also eliminate the opportunity

to determine when strength degradation starts in stage III. Since it is important to simulate that, the FF must be taken into account.

### 3.7.4. Damage evolution criterion

The damage evolution describes how fast the strength decays over the elongation imposed by the prescribed displacement. Once the damage is initiated the damage parameter $D$ increases slightly. This should be accordingly to the amount of damage that is observed during tests caused by the mechanism. Abaqus[3] uses this damage parameter to degrade the initial stiffness to the supposed stiffness related to the amount of damage. Although this is often a linear relation between the residual stiffness and the damage parameter, it does not necessarily have to be so. For example if an entire I-profile cross-section is modelled with one beam element, then it is better to adjust the relation. Abaqus[3] uses a linear relation by default in the ductile damage model and that is sufficient for the application on composites modelled with a mesh of elements assigned to each layer. The composite will be modelled per layer, therefore having rectangular cross-sections. In that case the stiffness cross-section will not be that much more affected than by having only a linear relation between the damage parameter and the residual stiffness between the elements. The damage that is done to the element can not be restored, just as it would be in the physical world for the fibre failure. The stiffness and the strength are kept with their original values unless damage has been done to the fibres which is also expected from the physical behaviour of the mechanism. Since with the ductile damage model it is possible to create a brittle material that could still be run using the direct cyclic analysis, it has a large potential in predicting the fibre failure in composites during fatigue loading. All these arguments favour the choice of using the ductile damage model for the fibre failure mechanism.

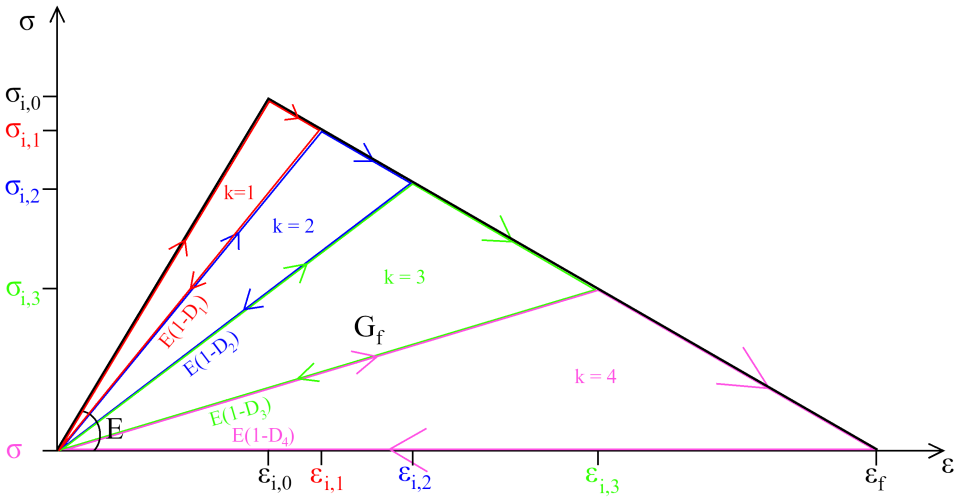


**Figure 3.13:** The stress-strain relation of the material properties describing the smeared crack model. The black contour is the input given for the smeared crack model where $E$ is the Young's modulus of the material and the initial stiffness of the model, $\sigma_{i,0}$ is the first initial stress for crack/damage initiation. The degradation is given for each fatigue cycle, in this case four cycles lead to failure of the element. Notice that the once over the top, the stiffness degrades according to the increased damage. In this case it is a linear relation between damage and stiffness degradation. Unloading and reloading is along this adjusted stiffness. The succeeding $\sigma_{i,k}$ indicate the stress levels when the damage propagates further for the cycles $k = 1$ through $k = 4$. For each initial stress a corresponding initial strain is given on the horizontal axis. The failure strain $\varepsilon_f$ is the given input dictating when the element is considered to be failed. Here is a linear strength degradation shown, an exponential or a multi-linear could be opted as well. The energy dissipated in a cycle is the area enclosed by the arrows, the sum of the dissipated energy is equal to the fracture energy $G_f$.

The damage evolution addresses the damage indeed by increasing a damage parameter that reduces the stiffness. However, this alone is not sufficient to let a specimen fail. First to notice is that the stress-strain curve shows a decrease in stress after the damage initiation strain $\varepsilon_{i,0}$ has been reached and passed. Note that the stress-strain curve has the same features as the traction-separation law with the largest difference in formulation using strains and stresses as input instead of stresses and displacements, as the ductile damage model is a smeared crack model to describe a crack in an element (not between elements using interaction elements). See the stress-strain relation as an amount of resistance the element will provide for a specific amount of elongation. $\sigma_{i,0}$ could be seen as the maximum strength resistance the element will provide. In contrast to the plasticity model where the initial yield stress could be passed multiple times based on the type of hardening, in the damage model $\sigma_{i,0}$ could only be reached once. So when the damage starts, it has an immediate effect on the strength. The new stress limit for a continuation of the damage evolution in the next cycle is set at the intersection of the degraded stiffness line with the decreasing branch of the stress-strain curve. If the resistance stress $\varepsilon_{i,k}$ is not enough then the new $\varepsilon_{i,k}$ will be exceeded and damage will be added to obtain a new equilibrium with a new damage stage. Abaqus[3] sees no difference in stiffness between an element with an initial stiffness that is reduced by a damage parameter or an undamaged element that has the reduced stiffness from the start. The element has failed when the damage reaches the value of 1 as that results in the element to have no more stiffness. For the (multi-)linear degradation the final strength is theoretically 0 while on the other hand for the exponential degradation it would in theory never reach exactly 0. For both cases the element is numerically still present with a very small resistance, but is visually deleted in the results as a visualisation of the crack. This small resistance has no significant effect on the analysis. When it reaches its no-resistance state, it is said it has reached its failure strain $\varepsilon_f$. This stress-strain relation encloses a triangular shape for a linear degradation. Upon integrating the triangle the failure energy or energy release rate $G_f$ is obtained. Abaqus[3] integrates it numerically. All these features are visualised in figure 3.13. As the ductile damage model is complementary to the plasticity model, the ductile damage model is the continuation of the plasticity model if correctly defined as is illustrated in figure 3.14. Despite the change from the traction-separation law to an augmentation of the plasticity model, the principles of figure 3.13 do still apply.

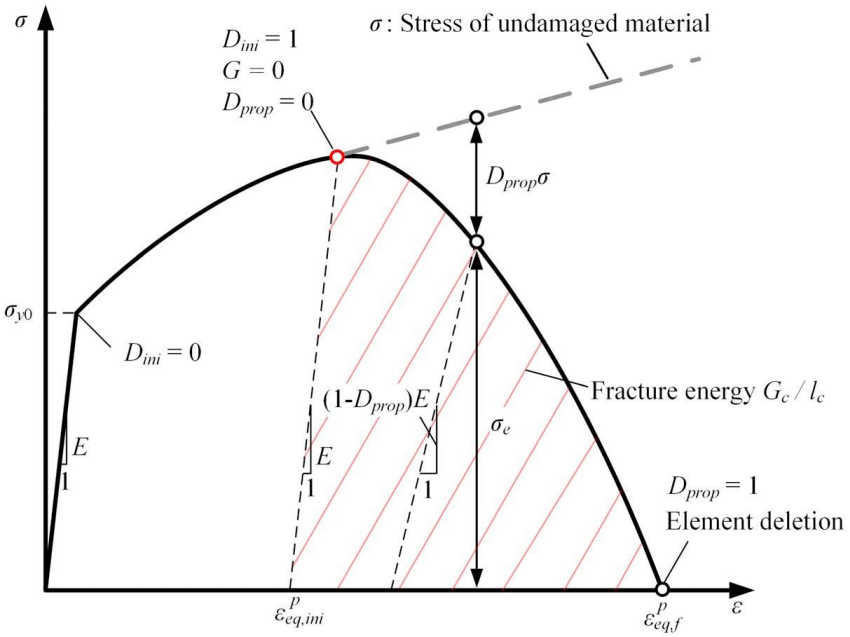


**Figure 3.14:** An illustration of the effect of the ductile damage model in combination with the plasticity model on the true stress-strain relation of the material. Source of figure: Jia et al. [53].

## 3.8. Applying the virtual crack closure technique for delamination

### 3.8.1. General concept of the virtual crack closure technique

The Virtual Crack Closure Technique (VCCT) is able to determine which part of the interface is still bonded, therefore it is also able to determine which part has been debonded. The VCCT is a discrete crack model. It models the crack by predicting the crack length based on a force required to close the crack opening displacement (COD) along a predefined interface. It has a crack initiation criterion and a crack propagation criterion that is slightly different for static loading versus fatigue loading. The crack initiation criterion defines if nodes have to be released from another to achieve energy equilibrium or not. The propagation criterion determines how many nodes have to be released at once.

### 3.8.2. Applicability of the virtual crack closure technique

The small resin layer between the fibres are the interfaces that could delaminate. Delamination is the failure mechanism where the adhesion failed due to local splitting of the layers as is shown in figure 3.15. It is a progressive failure mechanism that is relatively stable. The term progressive is used here as: once the delamination starts, it is unlikely to stop by itself if there is no change in loading or geometry. The VCCT model is developed to handle cracks at interfaces as it uses the principles of the linear elastic fracture mechanics (LEFM). Also the VCCT model is compliant with the direct cyclic analysis. It is actually a regularly used technique to describe fatigue failure, not only in Abaqus[3] but also in other finite element software.

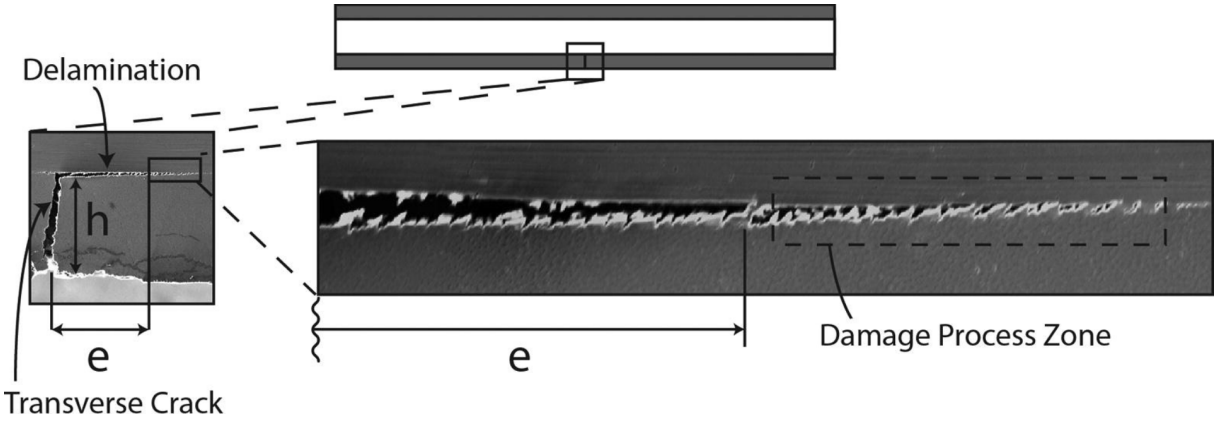


**Figure 3.15:** A microscopic picture of delamination in a composite laminated material. Initially there is a transverse crack in the outer edge that changes direction from moving inwards through the outer layer to along the fibre causing the outer fibres to delaminate from the rest. The second enlarged figure shows the difference between the zone that is fully delaminated ($e$) and a zone that still formed by micro-defects (the damage process zone) according to Zou et al.[54]. Figure is retreived from Reiner et al.[55].

The delamination could be excluded from the analysis by modelling all the plies together in one continuum shell element with composite layup or by connecting all the layers with tie constraints. The latter has been performed as an intermediate step before introducing the VCCT interactions. The influences of the tie constraints and the VCCT interactions on the final model will be discussed in section 5.5.1 chapter 5. For a CT specimen it is sufficient not to include the delamination since it is assumed that there is no separate second stage for the in-plane loading. Hence if there is any delamination effect present, it could be included in the IFF model or the FF model.

A discrete crack model has been chosen over the smeared crack models and plasticity models for the reasons provided in section 3.4 of chapter 3. The choice of the XFEM is inferior to the VCCT since the VCCT could be given a small precrack at multiple possible crack initiation locations at once. In this case it is advised to use a small local mesh in order to have the precracks as small as possible. The advantage remains in allowing to simulate multiple crack initiation points simultaneously.

Despite a CZM would not need any precrack at all, the VCCT model was preferred. The VCCT model was preferred since there was much more information available about the VCCT model in combination with the direct cyclic analysis as there was a complete tutorial available by Ramsaier[24]. It has not been tested yet if CZM would be able to fulfil the same job. Theoretically it is expected it would since the required input would be similar to the VCCT. It might be interesting to do so for future investigation.

### 3.8.3. Crack initiation criterion for equivalent energy release rates

The crack initiation criterion in the static analysis determines whether a node should be released or not by calculating the force required to close the crack for that element of the interface as is shown in the left drawing of figure 3.16. Let it be clear that at least two elements are required to have an interface between them. If the required force is large enough such that the work performed by the required closing force is larger than the energy stored between the elements for that direction, then the interaction is considered to be failed according to the MIT manual[56]. The right drawing of figure 3.16 shows the correlation between the critical energy release rate for a certain mode and the work performed by the closing force. This is visualised by the release/separation of the two nodes that were initially bonded.

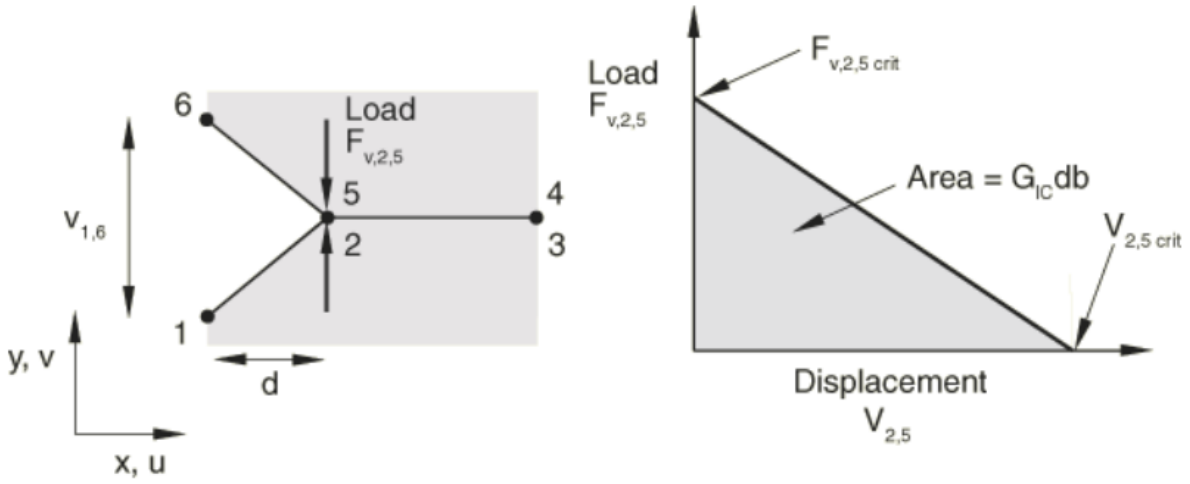


**Figure 3.16:** The left drawing shows the derivation of the principle of VCCT for static loading. Consider the interface of two geometries where node 2 of the bottom surface is about to be separated from node 5 of the top surface by the propagating crack already present between nodes 1 and 6. The force $F_{v,2,5}$ represents the local force required to keep the crack closed. The right shows the relation between the local external work performed by the required closing force and the critical energy release rate (illustrated for mode I). The displacement $V_{2,5,crit}$ is the crack opening displacement that will be present if no closure force would be present. This displacement is based on the stiffness of the parent material, as such the required force will also be determined on the stiffness of the parent material. $d$ and $b$ are the dimensions of the surface of the element that is about to get released. $d$ is in length direction of the crack and $b$ in depth direction of the crack. The critical energy release rate has therefore to be given in [Nmm/mm$^2$] so is independent of the mesh size. Source of figure: MIT Abaqus manual[56].

For the static analysis the VCCT criteria are useful as only the energy is needed as extra input; the crack growth resistance of the interface is based on: the critical energy release rate, the element size and the stiffness of the parent material. The stiffness properties of the parent material are involved in determining how much local force is required to close the crack since there is a difference in displacement field before and after releasing a node. Therefore a different energy equilibrium with the external applied global forces is obtained as provided in equation 3.5. For this energy balance it is assumed the material only deforms in shear and the displacement of $v_{1,6,i+1} = 2v_{1,6,i}$ as is illustrated in figure 3.17. In this case the dependency on $G$, which is a material stiffness parameter for shear, is eliminated as much as possible. Equation 3.5 shows that the stiffness of the parent material does not cancel out. Hence the solution is dependent on the material stiffness of the element. Therefore a different displacement field between released and unreleased will thus result in different stress fields. This will be analogous for bending and axial deformation.

$$\begin{cases} F(v_{1,6,i+1} - v_{1,6,i}) = G_{I,c} + \frac{\tau\gamma}{2} \\ \tau = \gamma G \\ \gamma = \frac{v_{2,5,i+1} - v_{2,5,i}}{h} \\ v_{2,5,i} = 0 \\ v_{2,5,i+1} = v_{1,6,i} = \frac{v_{1,6,i+1}}{2} \end{cases} \implies v_{1,6,i+1} = \frac{Fh^2 + \sqrt{-h(G_{I,c}G^2t - F^2h^3)}}{2G} \tag{3.5}$$

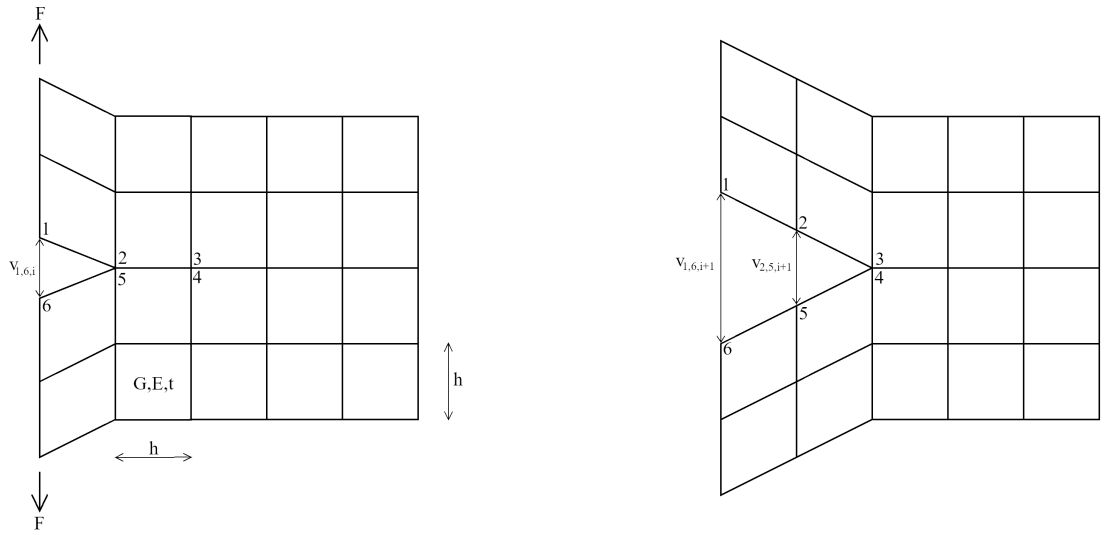


**Figure 3.17:** An illustration of the difference between the deformed state before releasing node 2 from 5 on the left versus after releasing node 2 from 5 on the right. The certain displacement needed is based on the element stiffness ($E$ [MPa] and $G$ [MPa]), its geometry ($h$ [mm] and thickness $t$ [mm]) and the applied force. It is assumed there is a pure shear deformation active and a critical energy release rate of $G_{I,c}$ [J/mm$^2$].

The direct cyclic analysis will have a crack initiation criterion based on the Paris law. For this criterion different material parameters are used than for the propagation. The crack initiation criterion determines how many cycles are needed to have critical energy release rate at crack tip high enough such that the interface at the crack tip fails according to the MIT manual[56]. Failure at the crack tip leads to propagation of the crack tip. An exact formulation will be provided in chapter 4 section 4.7.2.

### 3.8.4. Crack propagation criterion for equivalent energy release rates

The crack evolution determines how fast the crack propagates through the enriched interface. For the static analysis it determines the local stress state for the prescribed displacement. If the crack initiation criterion determines that propagation has to occur, then by iterations it is determined how many nodes should be released per increment to allow the necessary deformation. In other words, another node is released in an increment if an equilibrium solution was not obtained by releasing the previous node. This will be done node by node and checking the initiation criterion after each node that has been released. As the interface is relatively thin compared to the global structure and only the most critical interface determines the final failure, the properties of the parent material are a good approximation of the stiffness of that interface. The advantage of using the VCCT is the fact that only the critical energy release rates are needed as additional properties which makes it elegant. These energy release rates could be experimentally determined and are even standardised in the ISO-norm 15850[4] for the tests of the different modes.

For the direct cyclic analysis the Paris law is used to determine how far the crack propagates. The simple version of the Paris law that was given in equation 2.9 is used with the critical energy release rate as the load severity $S$. Actually the range of the critical energy release rate $\Delta G = G_{max} - G_{min}$ is used based on the mixed mode formulation for $G_{max}$ and $G_{min}$. The two material constants $c_3$ and $c_4$ will remain constant, but $\Delta G$ will progressively increase with the increase in crack length. Hence the crack will exponentially grow as the rate of crack growth is dependent on $\Delta G$, which makes it a vicious circle with a positive feedback loop as is shown in equation 3.6.

$$\begin{cases} \frac{da}{dN} = CG^b \\ G = \frac{K^2}{E} \implies G = \zeta a \\ K = \varepsilon\sqrt{a} \end{cases} \tag{3.6}$$
$$\implies N_f = \frac{a_f^{-b+1} - a_i^{-b+1}}{(-b+1)C\zeta^b} + N_i$$

Here $b$ and $C$ are the material constants according to equation 2.9 and $G$ is the critical energy release rate in [J/mm$^2$]. $a$ is the crack length in [mm] and $N$ the number of cycles. The subscripts $i$ and $f$ indicate initial and final cycle respectively. As $i$ and $f$ are true for any interval, the crack length per number of cycles could be calculated. Figure 3.18 is obtained by keeping the initial length constant at $a_i = 10$ [mm] and increasing $a_f$ with a logarithmic progression. The material constants are set to $b = 2$ and $C = 10^{-9}$ for this example. These are arbitrary values to show the progressive behaviour of the Paris law. Additionally the simplification of using an arbitrary $\zeta$ with $\zeta = 100$ which includes all types of stress concentrations and stresses ranges.

The Paris law[9] curve is observed numerous times in experiments, not only in metals, but also in composites. It might not be a law that gives a casual relation, but it is a good method for an empirical approximation. At least two tests are required in order to determine material factors $C$ and $b$. The threshold and the critical values could be extracted by these two experiments as well if carried out carefully.

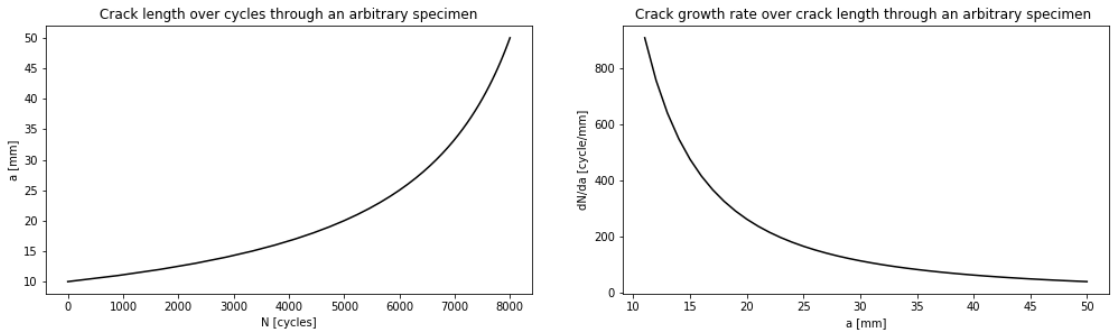


**Figure 3.18:** The left plot shows the crack length through an arbitrary specimen for certain applied amount of cycles with material constants $C = 10^{-9}$ and $b = 2$. There is an initial crack present of 10 [mm] and a combined factor $\zeta = 100$ [N/mm$^3$] that includes the stress concentrations and the load itself. The right figure shows the crack propagation rate of the crack propagation in the left figure. Here the decreasing amount of cycles needed to propagate the crack 1 [mm] further is clearly visible.

## 3.9. Hypotheses review chapter 3

### 3.9.1. Proof to one hypothesis listed in section 3.2 of chapter 3

**Proof of hypothesis 3: The three significant fatigue failure mechanisms present in a compact tension specimen are best simulated by a combination of three individual models.** In section 3.3 of chapter 3 it was stated that fatigue in composites is best assessed based on their failure mechanisms which are traceable in a residual stiffness degradation curve. The residual stiffness degradation has three different stages for an out-of-plane loading implying that each mechanism leads to a vastly different response. To mimic this degradation accurately it is best to use one model for each mechanism as is explained in section 3.3 of chapter 3. That allows to isolate the behaviour per mechanism which in the end results in more accurate models.

### 3.9.2. Seventeen newly posed hypotheses as result of chapter 3

Based on the options available in the different modules, a list of new hypotheses are set up.

**Hypothesis 4: If 10 iterations are used per load cycle for a force controlled analysis on a one element model, then equilibrium is reached for each load cycle.** The number of iterations is important in an analysis. The direct cyclic analysis is an implicit solver for non-linear problems. Therefore there are some discrepancies in estimating the results. Especially if it is not a bi-linear relation. For the force controlled analysis more iterations help to obtain force equilibrium. The number 10 is expected to be sufficient for a one element model. This value will be discussed in section 4.8.1 of chapter 4.

**Hypothesis 5: Using 2 iterations per load cycle for a displacement controlled analysis on a one element model will result in an element response that is closest related to the input parameters of the plasticity model.** For the same reason as the force controlled analysis, running more iterations helps to make corrections on the control sequence. The displacement analysis needs less iterations to obtain an accurate solution since Abaqus[3] tries to find a solution based on an imposed displacement

field that is compliant with the boundary conditions and the stiffness of the material. Therefore a displacement controlled analysis is inherently more accurate than a force controlled analysis with the same amount of iterations. The value of 2 will be discussed further in section 4.8.1 of chapter 4.

**Hypothesis 6: The direct cyclic analysis without cycle jumping with a displacement controlled fatigue loading will result in a sequence of half cycles with static loading for each half cycle.** Without cycle jumping every load cycle will be calculated. Since the load is a prescribed displacement it will explicitly impose that displacement on certain intervals and observe the required force due to the displacement field. Since Abaqus[3] does not make a difference between a material that has reached a certain yield stress due to hardening or as initial input, it does not matter if a cycle has already been passed. Therefore each cycle could be seen individually. Moreover, Abaqus[3] does not make a difference between a user-defined a deformation field from the start or a deformation field caused by plastic deformation to reach equilibrium. Hence each load cycle could be seen as two individual half cycles with a displacement controlled analysis. This will be checked in chapter 4.

**Hypothesis 7: If the direct cyclic analysis is applied on a one element model with isotropic hardening for plasticity, which has a displacement controlled load with $R = 0$, 2 iterations per load cycle and no cycle jumping ($dN = 1$), then the stress-strain response will follow the loading-unloading-reloading principles of the plasticity theorem.** From hypothesis 6 it is known that the direct cyclic analysis is a series of static half cycles under certain conditions. The one element model will have its loading mainly in the plastic response. Therefore it should also follow those principles. This will be investigated in chapter 4.

**Hypothesis 8: If the direct cyclic analysis is applied on a one element model with the ductile damage included, which is loaded with a force causing a stress larger than the ultimate stress, then no equilibrium will be found in the degraded state leading immediately to full failure.** If the direct cyclic analysis is merely a sequence of static loading (hypothesis 6), then the effects on the material could be superpositioned. Once the ultimate stress is reached, a force controlled analysis will no longer find equilibrium, thus will result in complete failure. This will be investigated in chapter 4.

**Hypothesis 9: If the direct cyclic analysis is applied on a one element model with the ductile damage included, which loaded with a displacement causing a strain larger than the crack initiation strain $\varepsilon_{ini}$ but smaller than the fracture strain $\varepsilon_f$, then a single equilibrium point will be found with a degraded stiffness.** If the direct cyclic analysis is merely a sequence of static loading (hypothesis 6), then the effects on the material could be superpositioned. A displacement controlled analysis is able to continue beyond the ultimate stress and to find an equilibrium solution in the branch of the decreasing stress-strain relation as long as the fracture strain is not surpassed. If multiple cycles are imposed, it is expected that it will repeat itself to that point of damaged deformation. This will be investigated in section 4.8.1 of chapter 4.

**Hypothesis 10: If the direct cyclic analysis is applied on a one element model with the plasticity model, then no plasticity will be extrapolated during the cycle jumping.** The direct cyclic analysis is able to extrapolate damage. It is explicitly stated "forward damage extrapolation", but no additional information was found in manuals if it could also extrapolate plastic deformation. For that reason it is checked if the damage extrapolation also extrapolates the plasticity. This hypothesis will have a circumstantial proof in section 5.8.1 of chapter 5.

**Hypothesis 11: If the direct cyclic analysis is applied on a compact tension specimen with the ductile damage included, which is loaded with a displacement or force causing the stress in an element to be larger than the ultimate stress, then it transfers its burden of load to its surrounding**

**elements in order to find equilibrium.** This will be proven with a proof by contradiction. If an element would not be able to transfer the burden of load to its neighbouring elements, then the entire structure would fail at once when the ultimate stress in one of the elements has been reached. For a model where all the elements are placed in sequence (obtainable by dividing the one element model into multiple elements only along the vertical axis), this will be true. If this is true, then the compact tension specimen will fail once the first element has reached its ultimate stress. However, the compact tension specimen has multiple elements in parallel. Each element along the critical path could be seen as a spring. Even with a certain imposed force, the springs will react as if it is an imposed displacement, which will be a combination of a translation and rotation. This is caused by the compact tension specimen being loaded in the pins instead of directly on the nodes of the elements along the critical path. Seeing the critical path as a set of springs also provides the insight that the ultimate force of the structure will be reached only if the first element has reached the fracture strain $\varepsilon_f$ instead of $\varepsilon_{ini}$ at the ultimate stress. This will be shown in chapter 5.

**Hypothesis 12: If only the VCCT model in Abaqus[3] is used to describe both the inter-ply and intraply interactions with a delamination mechanism, then the compact tension specimen model with fatigue loading will become computational too heavy to execute.** This was the initial model made to investigate the compact tension specimen. The model is found in appendix B. For the static loading the VCCT slicing model was successful despite being computationally heavy. A proof for VCCT slicing model with the fatigue loading is provided in appendix B.

**Hypothesis 13: Using the plasticity model for the inter fibre fracture will result in an overclosure of the crack due to the plastic deformation which is not present in reality.** In steel it is known that the plastic deformation results in overclosure of the crack. This is illustrated in section 2.4.3 of chapter 2. The plastic model is able to recreate that overclosure effect due to the plastic deformation. In reality composites will fracture instead of plasticly deform due to their brittleness. However, the plasticity model is used for the inter fibre failure to describe the material response from its yield stress to its ultimate stress. With it, the plasticity model still creates an overclosure due to plastic deformation, because the plasticity model will not make a distinction between modelling steel or composites. This effect will be investigated in chapter 5 where the compact tension specimen is able to show a crack.

**Hypothesis 14: If $\frac{C_n}{\gamma_n} = Q_\infty$ and $\gamma_n = b$, then isotropic hardening and kinematic hardening will result in the same response for the static loading on a one element model.** Moving only in a single direction of the yield contour will not indicate a difference whether the yield contour is moving or increasing in size. In other words, if only one load direction is investigated, it is always possible to describe the hardening with kinematic or isotropic hardening. Even anisotropic hardening will not be observed if the ultimate stress and ultimate strain are not known. It is impossible to distinguish if the material fails due to reaching the ultimate stress or the reduced value of the ultimate stress based on the hardening functions. Section 4.8.1 of chapter 4 will provide a proof to this hypothesis.

**Hypothesis 15: Increasing $\sigma_{y,0}$ will result in a longer fatigue life in a one element model with force and displacement controlled fatigue with $R = 0$.** If the plasticity model follows the plasticity theorem during the direct cyclic analysis (hypothesis 7), then increasing $\sigma_{y,0}$ will make the elastic stage persist longer. More elasticity means less accumulation of plastic deformation, thus it will take longer to reach the ultimate stress. A proof will be provided in section 4.8.1 of chapter 4.

**Hypothesis 16: Increasing $E$ will result in shorter fatigue life in a one element model with displacement controlled fatigue with $R = 0$.** If the plasticity model follows the plasticity theorem during the direct cyclic analysis (hypothesis 7), then increasing $E$ will make the elastic stage shorter since the yield strain is reached earlier. Less elasticity means more accumulation of plastic deformation,

thus it will take less cycles to reach the ultimate stress. A proof will be provided in section 4.8.1 of chapter 4.

**Hypothesis 17: Increasing $\nu$ will result in an equally long fatigue life in the one element model, with displacement controlled fatigue and $R = 0$, that has no redundant boundary conditions .** If the plasticity model follows the plasticity theorem during the direct cyclic analysis (hypothesis 7), then increasing $\nu$ will not change the analysis due to the boundary conditions allowing free contraction. A circumstantial proof will be provided in section 4.8.1 of chapter 4.

**Hypothesis 18: Increasing $Q_\infty$ will result in longer fatigue life in a one element model with a force or displacement controlled fatigue with $R = 0$.** If the plasticity model follows the plasticity theorem during the direct cyclic analysis (hypothesis 7), then increasing $Q_\infty$ will increase the ultimate stress. If more stress is allowed before failure, then it will have a longer fatigue life. A proof will be provided in section 4.8.1 of chapter 4.

**Hypothesis 19: Increasing $b$ will result in shorter fatigue life in a one element model with displacement controlled fatigue with $R = 0$.** If the plasticity model follows the plasticity theorem during the direct cyclic analysis (hypothesis 7), then increasing $b$ will make the plastic stage shorter since the ultimate stress will be reached with less plastic deformation. Reaching ultimate stress faster means a shorter fatigue life. A proof will be provided in section 4.8.1 of chapter 4.

**Hypothesis 20: Increasing $\eta$ or $\dot{\varepsilon}$ will not alter the results in the one element model or the compact tension specimen model with a force or displacement controlled fatigue analysis.** The model is strain independent due to the small strains applied and low frequency of loading. Also is the model pressure independent since no Mohr-Coulomb, Drucker-Prager or similar criteria is used. A circumstantial proof will be provided in section 4.8.1 of chapter 4 for the one element model. If it does not have influence on one element, then it will not have influence on a model with multiple elements as well. Therefore it will not have influence on the compact tension specimen model.

## 3.10. Conclusion chapter 3

None of the individual models that are proposed would individually be able to fully mimic the fatigue behaviour of the composite that has multiple mechanisms. Each model has it strengths and weaknesses. The best proposal is by combining the models such that each model simulates the mechanism that the model is best suited for. For the inter fibre failure that will be the plasticity model, for the delamination the best model is the VCCT model and for the fibre fracture that will be the ductile damage model. The plasticity model and ductile damage model have the advantage of being compatible and sequential, therefore within an element, stages I and III will always be separated. How the residual relative stiffness is controlled will be shown in the chapter 4. Also the smeared crack model requires to simulate one initial crack pattern instead of every possible initial crack position as the smeared model does not need initial cracks. Additionally, modelling the meso-scale effects instead of the micro-scale mechanisms speeds up the analysis. Furthermore, if the VCCT was used for in-plane cracking then it would be computationally heavy due to the large number of interfaces that are defined. On top op that, the direct cyclic analysis provides a usefull tool to speed up the calculations while maintaining the accuracy. With the choice of models presented in this paragraph the visualisation of cracking of the elements with composite properties is reserved for the ductile damage model and the crack as result of separation of the plies for the VCCT. Two major assumptions were made to propose this model: only the three mentioned mechanisms are important and the inter fibre failure does not lead to large cracking.

The development of the fatigue life of composites starts with the plasticity model. The plasticity model initiates the plastic strain when the yield stress is reached and evolves the yield stress according to the hardening of the yield contour.

The ductile damage model has its initiation when the ultimate stress of the plasticity model is reached. Sometimes that value is dependent on the fracture energy and fracture strain. The propagation is dependent on the amount of energy released to allow larger deformations. Only if the analysis is displacement controlled, then it is possible to show a degradation instead of sudden collapse of an element.

The cracks in the VCCT model are initiated by the bonded node set and the propagation is initiated once the threshold energy release rate is exceeded. For static loading the initiation is based on the local work required to close the crack. If the energy to do the work is higher than the energy stored between the two elements, then the crack propagates by releasing a pair of nodes. The cracks in the VCCT propagate during static loading until the initiation criterion is no longer satisfied. For fatigue loading the crack initiation is based on the energy threshold value $G_{th}$. The crack propagation in the VCCT model for fatigue loading is given by a Paris law[9] curve that defines the crack propagation rate.

# Chapter 4: The model implementation

## 4.1. Introduction

During the model implementation it will be shown how the ideal model that is proposed in chapter 3 is put into practice for the simulating the mechanisms. First the ideal model is implemented in a one element model. A one element model has a mesh with a single element to show how the residual relative stiffness is controlled. The one element model is the simplest form of modelling a compact tension specimen for fatigue. The software program Abaqus[3] is used to model the fatigue behaviour of the element. This chapter could be read as a concise tutorial as the input and output of the one element model will be explained step-by-step. Some basic understanding of Abaqus[3] is required; it is expected that the reader knows how to create a model that performs a linear elastic analysis for an isotropic homogeneous material.

The chapter is based on four modules included in the model as addition to the static linear elastic model. Three of these modules are included as material property and one of them as step. A module is here considered as an extra part compared to the ordinary linear elastic analysis. In the earlier chapters these were referred to as models, but to avoid confusion for example between the one element model and the plasticity model, the plasticity model is named as the plasticity module. As such it will also be called the VCCT module and the ductile damage module from now on. The fatigue analysis is included as a step module and is considered to be non-default compared to static analysis. Also there are some considerations to be taken into account using the direct cyclic analysis of Abaqus[3]. Since the direct cyclic analysis is an augmentation of the static analysis, it will be used in all possible combinations of property modules that are included in the model. Here a property module is considered to be a constitutive relation that describes a failure mechanism. That could either be defined in the material properties or in the interaction properties. It will be stated in the corresponding section in which of the two it is applied.

For each of the modules three steps will be discussed: the implementation from theory to modelling, the required input into Abaqus[3] and the obtained output from Abaqus[3]. For the input of the one element model a critical look is given at the values of the parameters that are used for a test material and at the values of the parameters that are suggested for the compact tension specimen with glass fibre material. On the output some critical questions are directed e.g.: when is the model considered to have entered a new stage? Also how do the parameters relate to the fatigue life of the model. Since the model is related to the fatigue cracking, it is expected to follow some sort of Paris law. So how does this model relate to the Paris law?

First the build-up of the one element model will be explained. It will show the geometry and the boundary conditions that are used in the model. It is followed by the implementation of the direct cyclic analysis including the number of iterations that are required and the number of cycles that could be jumped. After that for each mechanism the input values will be given with reasons and the output will be discussed.

## 4.2. Thirteen hypotheses that will be answered in chapter 4

Chapter 4 will give answer to thirteen hypotheses originating from chapter 3. These hypotheses will be answered in section 4.8.1 of chapter 4.

**Hypothesis 4: If 10 iterations are used per load cycle for a force controlled analysis on a one element model, then equilibrium is reached for each load cycle.**

**Hypothesis 5: Using 2 iterations per load cycle for a displacement controlled analysis on a one element model will result in an element response that is closest related to the input parameters of the plasticity model.**

**Hypothesis 6: The direct cyclic analysis without cycle jumping with a displacement controlled fatigue loading will result in a sequence of half cycles with static loading for each half cycle.**

**Hypothesis 7: If the direct cyclic analysis is applied on a one element model with isotropic hardening for plasticity, which has a displacement controlled load with $R = 0$, 2 iterations per load cycle and no cycle jumping ($dN = 1$), then the stress-strain response will follow the loading-unloading-reloading principles of the plasticity theorem.**

**Hypothesis 8: If the direct cyclic analysis is applied on a one element model with the ductile damage included, which is loaded with a force causing a stress larger than the ultimate stress, then no equilibrium will be found in the degraded state leading immediately to full failure.**

**Hypothesis 9: If the direct cyclic analysis is applied on a one element model with the ductile damage included, which is loaded with a displacement causing a strain larger than the crack initiation strain $\varepsilon_{ini}$ but smaller than the fracture strain $\varepsilon_f$, then a single equilibrium point will be found with a degraded stiffness.**

**Hypothesis 14: If $\frac{C_n}{\gamma_n} = Q_\infty$ and $\gamma_n = b$, then isotropic hardening and kinematic hardening will results in the same response for the static loading on a one element model.**

**Hypothesis 15: Increasing $\sigma_{y,0}$ will result in a longer fatigue life in a one element model with force and displacement controlled fatigue with $R = 0$.**

**Hypothesis 16: Increasing $E$ will result in shorter fatigue life in a one element model with displacement controlled fatigue with $R = 0$. Hypothesis 17: Increasing $\nu$ will result in an equal long fatigue life in the one element model, with displacement controlled fatigue and $R = 0$, that has no redundant boundary conditions .**

**Hypothesis 18: Increasing $Q_\infty$ will result in longer fatigue life in a one element model with a force or displacement controlled fatigue with $R = 0$.**

**Hypothesis 19: Increasing $b$ will result in shorter fatigue life in a one element model with displacement controlled fatigue with $R = 0$.**

**Hypothesis 20: Increasing $\eta$ or $\dot{\varepsilon}$ will not alter the results in the one element model or the compact tension specimen model with a force or displacement controlled fatigue analysis.**

## 4.3. One element model as preliminary model

The one element model that consists of one cubic solid element with unit size (1 [mm] in all three directions) is used with the plasticity model and ductile damage model included. As Abaqus[3] is independent of units, all units may be applied as long as there is consistency. In order to provide a better sense of the effect of a value, the unit will be included according to the scheme that describes forces in Newtons [N], sizes in millimetres [mm] and time in [s]. One unit time equals one cycle creating a frequency of 1 [Hz]. A unit sized cube is chosen as the forces and stresses have equal magnitude except for the difference caused by the difference between the engineering stresses and strains and the true stresses and strains. The resultant forces from the output will act as engineering stresses and the stresses from the output are the true stresses. This makes matters easier to explain as the force-displacement diagram is directly related to the engineering stress-strain diagram.

The boundary conditions of the one element model are chosen to keep the model simple to understand. Therefore the bottom surface is fixed in vertical direction as the main motion will be vertically. The forces or prescribed displacements are applied in the four top corners of the element simulating a tensile coupon test with cyclic loading. These forces are explicitly modelled as a group consisting of individual forces instead of a coupled constrained to avoid shear stresses along the top surface due to constraints. The exact input of the applied forces will be discussed later in this section. In order to avoid the element becoming an unguided projectile, it has to be pinned down in the horizontal direction as well. This is done in the most minimalistic way possible to avoid over-constraining since over-constraining could lead to stresses that obscure the relation between the input and the output. Therefore the element is constrained in z-direction (translation degree of freedom 1 equals 0) along the x-axis and constrained in x-direction (translation degree of freedom 3 equals 0) along the z-axis. On the one hand the element is still able to contract and dilate freely during a non-zero Poisson's ratio. On the other hand it has been constrained to avoid wiggling back an forth as a rotation around the z-axis. This prevents unnecessary noise in the output. All this information is condensed into figure 4.1.

The single element will be a 3Dstress element with reduced integration. The solid elements are capable of including the three dimensional effects without bending in the nodes. This is sufficient as the focus is on understanding the properties to be included for the failure mechanisms. That means it only has translational degrees of freedom in the first, second and third dimension in each node. Hence there are no rotational degrees of freedom. This is the simplest formulation of a three dimensional element. This element type is chosen as these types of elements allow the extended finite element method (XFEM) to enrich them and split them if necessary. Do keep in mind that the lack of rotational degrees of freedom require the CT specimen to have multiple elements in thickness directions to take into account the out-of-plane (second order) bending. In case multiple layers are modelled and each layer has one element in thickness direction, then this problem is already solved. If the XFEM is not used, then it is advised to check the solution with continuum shell elements. These take into account out-of-plane bending due to their bending degrees of freedom present in each node. Shell elements could and probably should be introduced once the model is up-scaled to a full compact tension specimen to obtain more accurate results.

The applied load is a cyclic load with a frequency of 1 [Hz], hence it has a cycle time of 1 [s]. This means that the number of cycles equals the amount of time that has passed. The cyclic load starts at 0 load and will be the minimum load in the sequential cycles. The maximum load will be reached every time half-way the cycle. The value of the maximum load will be equal to the value given to the load as the load cycle will be a jigsaw function with an amplitude of 1. In Abaqus[3] the applied load will be either equal to the total amount of force or the average displacement applied in the top corners of the element.

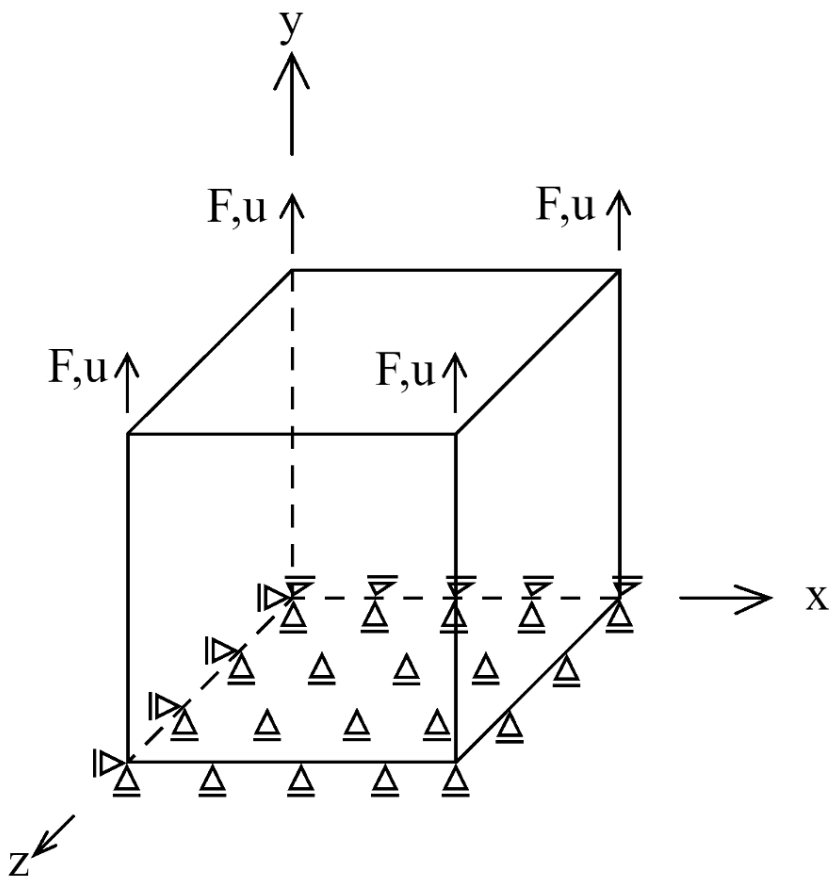


**Figure 4.1:** A visualisation of the one element model. The size of the element is 1 [mm] in all directions. The boundary conditions are given with three dimensional roll supports with hinge. This hinge support will roll in two directions even if only one direction is drawn in the two dimensional drawing. The second direction is in z-direction except for the roll hinges on the x-axis, there the second direction in y-direction. The translation forces or prescribed displacements are applied in y-direction on the top four corners of element.

It will be a linear interpolation of the load in between the minimum and maximum value of the load in the cycle, hence the name jigsaw function. This jigsaw function will be called the amplitude function in Abaqus[3]. The unit function is plotted in figure 4.2. The exact amount of maximum applied load will only be given at specific examples as the type of load changes from force controlled to displacement controlled and from one element to the up-scaled CT geometry. This jigsaw function is chosen for its simplicity. A sinusoidal function would be preferred in the up-scaled model as during the testing the applied load will not have a jigsaw function. The sinusoidal load also gives larger models the opportunity to obtain a more accurate prediction of the behaviour around the extreme values of the function due to the smoothness. In the jigsaw function there is no derivative available in the extreme values, hence some inaccuracies are expected when using automatic incrementation. However, in the one element model a fixed incrementation is used that captures precisely the extreme values. In section 4.5 of chapter 4 it will be shown that predicting the response to plastic behaviour is easier done with jigsaw amplitude function than the sinusoidal function.

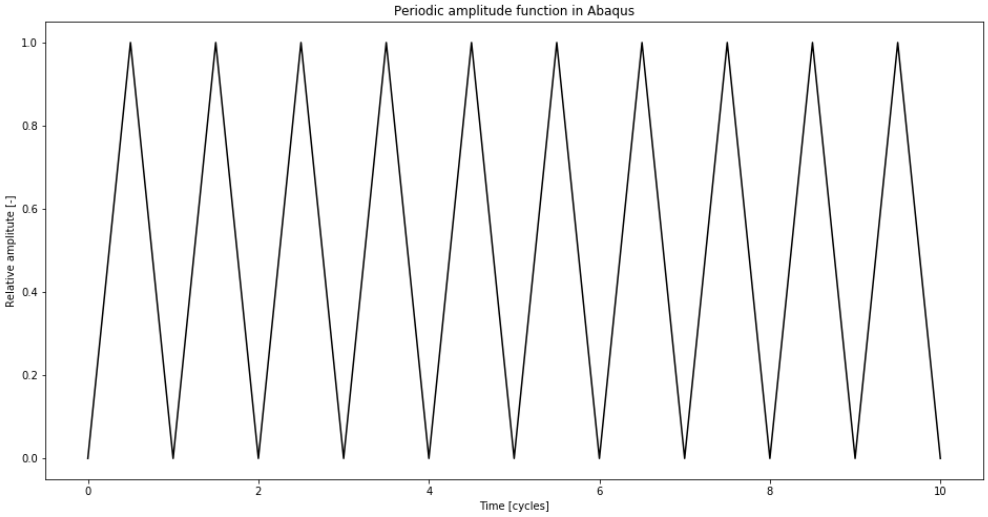


**Figure 4.2:** A plot of the amplitude function defined by using the periodic formulation. The periodic formulation of the amplitude function repeats indefinitely the amplitude function that is defined in the first cycle until the maximum number of applied load cycles or failure has been reached. This first cycle was defined in a tabular form with $0$ at initial time $0$, $1$ at time equals $\frac{1}{2}$ and again $0$ at time equals $1$. From here linear interpolation is used to obtain the amplitude for each increment. The applied amplitude to the element will be this function times the magnitude of the applied load.

## 4.4. Application of the direct cyclic analysis

### 4.4.1. Implementation direct cyclic step

The direct cyclic analysis is a type of analysis that allows to simulate fatigue loading in a more efficient manner than with a static analysis. The static analysis is not made for repetitive loading. Generally the static analysis results in longer computational effort, but sometimes it results in numerical instabilities due to a lack of convergence. The latter was found in the earlier attempts to create a simple model with $20$ elements that included the plasticity and the ductile damage modules. The result was that Abaqus[3] was not able to find a converged solution after the maximum load had been applied. In other words, no equilibrium solution was found. This is the main reason why direct cyclic analysis has to be applied at least as a continuation of the static loading after the maximum load level has been reached. Moreover, if the analysis is force controlled, then the output of the one element model showed during development that it was required to use the static analysis up to maximum load level before starting the direct cyclic analysis. The underlying reason for it being that Abaqus only shows the results of the final iteration while multiple iterations were required to obtain an equilibrium solution for the force controlled analysis. Therefore it meant that the approach up to the unloading will not be displayed.

In order to include the direct cyclic analysis into Abaqus[3], the direct cyclic analysis must be augmented to the static analysis. To augment the static analysis with a direct cyclic analysis, the user has to create a new step and chose to continue from the previous static analysis. The second reason why the direct cyclic analysis is chosen, is for its efficiency in calculating repetitive cycles. As it only stores the final equilibrium state of that load cycle, it is able to calculate a cycle quicker than using the static analysis. In order to obtain sufficient level of accuracy, a correct number of iterations has to be chosen will be discussed in section 4.4.2 of chapter 4. If that is the case, then the direct cyclic analysis is also

able to skip the calculation for a certain number of cycles by extrapolating the damage from the previous step. These measures make the direct cyclic analysis more efficient for fatigue analysis, especially for the composite fatigue analysis where a long stable crack growth period is observed.

### 4.4.2. Input for the direct cyclic analysis

In the end it boils down to taking enough measures to speed up calculations while maintaining sufficient accuracy. The direct cyclic analysis has a lot of input parameters to play with to increase accuracy of the simulation. However, as accuracy increases genuinely the computational time increases as well.

The first and foremost technique to speed up the calculations is the damage extrapolation for (low-cycle) fatigue. This damage extrapolation allows to calculate the damage state at $N = n$ based on the damage state at $N = n-x$ and the damage increment between $N = n-x-1$ and $N = n-x$. It makes a linear extrapolation of the damage increment over the forwarded load time $x$. It gives an estimation of the damage state at $N = n$ according to equation 4.1. Discrepancies between the model and reality may occur as the damage in the model will be piece-wise linear due to the damage extrapolation while in reality it will be exponential. Also the second trouble with the damage extrapolation algorithm is that plasticity is not counted as damage. Hence the damage extrapolation could only be accounted correctly for the ductile damage module and the VCCT module. Therefore during the one element model that includes both the plasticity module and the ductile damage module the cycle jumping can not be used, because as soon as plasticity is extrapolated the models are cycle jumping dependent. Additionally, since it is only one element the stress can not be passed on to the surrounding elements, thus must $\Delta N = 1$. For the full scale model of the compact tension specimen cycle jumping could be applied for the VCCT module if the interface lags behind during stage I as then there will be a stable tearing apart governed by delamination. Stage III during the fibre failure could also be sped up using damage extrapolation when there is little inter fibre failure present in the neighbouring elements. Damage extrapolation will be applied to the ductile damage module if the ply itself lags behind. This will be performed in much smaller steps as there is no linear scaling algorithm activated as for the VCCT.

$$D_{N=n} = D_{N=n-x} + x\Delta D_{N=n-x} \tag{4.1}$$

Cycle jumping also has an effect on how the output will be displayed. Instead of a continuous line, along the different cycles in time, now the line is discontinuous after each cycle that has been calculated. It will resume in the next calculated cycle at the value that would be expected if damage of cycle $N - x$ is extrapolated forward. That means that the intermediate values are kept $0$ or better to say non-existing in the output. Thus the difference is that the response becomes more spiky for $\Delta N > 1$ as is illustrated in figure 4.3.

The second most time influencing method is to play with the amount of iterations performed. Already some notes were made on the amount of iterations. If the fatigue analysis is force controlled, then applying more iterations improves accuracy at the cost of computational time. For the one element model it is clear that $10$ iterations are sufficient to have a converged solution as is shown in figure 4.4. However, what does Abaqus[3] do to obtain a converged solution? That becomes more clear during the displacement controlled analysis. If too many iterations are applied during a displacement controlled analysis, then the output results in a zero-response. That is not what is desired. This is explained by the fact that Abaqus [3] predicts the outcome of the next iteration based on the outcome of the previous iteration instead of the outcome of the first iteration with an improved prediction. For inherent stable

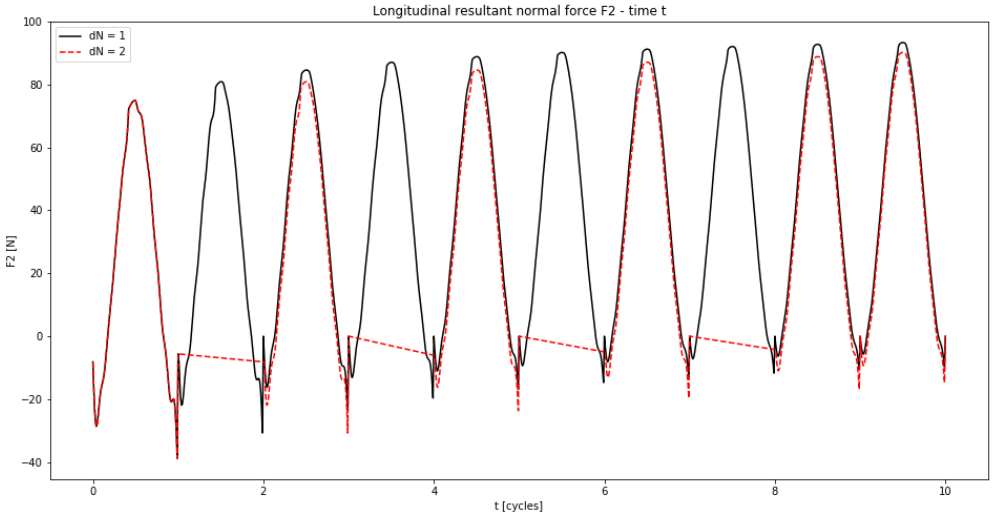


**Figure 4.3:** A time line showing the difference in effective loading applied on the structure due to cycle jumping. Without cycle jumping ($dN = 1$) results in all the load cycles being applied and with cycle jumping ($dN = 2$) only half of the load cycles are applied and the other half are obtained by copying the difference in response of the previous cycle the cycle before that. This results in approximately the same response, but could only be seen at the calculated cycle, therefore it looks less regular with the straight lines going through the even cycles.

converging solutions as a force controlled analysis this works fine with a force equilibrium and a hardening parameter. On the contrary, changing to a softening parameter would result in never reaching force equilibrium once the maximum force resistance at the yield stress is reached. It will also result in a zero-response. When changing to a displacement controlled analysis the force equilibrium requirement is still there. Despite that the requirement is still in place, the displacement controlled analysis will continue beyond the yield stress. In a hardening model the stresses will be increased with increasing strains to obtain a converged solution. As stresses will increase and the iteration is based on the previous outcome where plasticity has already occurred, the next iteration will add on more plasticity. If there is hardening, there will be a converging stability point (unless the ductile damage parameter kicks in as is illustrated in figure 4.4), but during softening a stability point will not be reached until it has decayed to its final stress state. If that final defined stress is (close to) zero, then a zero-response will be observed.

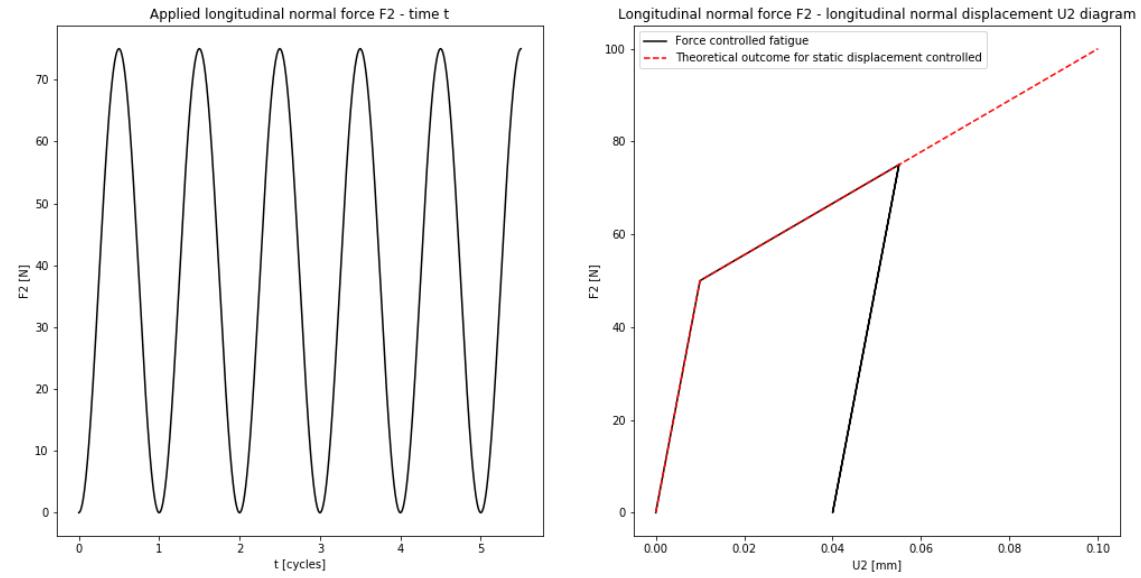


**Figure 4.4:** On the left plot the applied force controlled load cycle is given as a sum of the four top corners of the element. On the right plot the response of the element after ten iterations given in black. The red dotted line shows the material input given. This proves that the model output follows the model input, but with elastic unloading and reloading once equilibrium is reached.

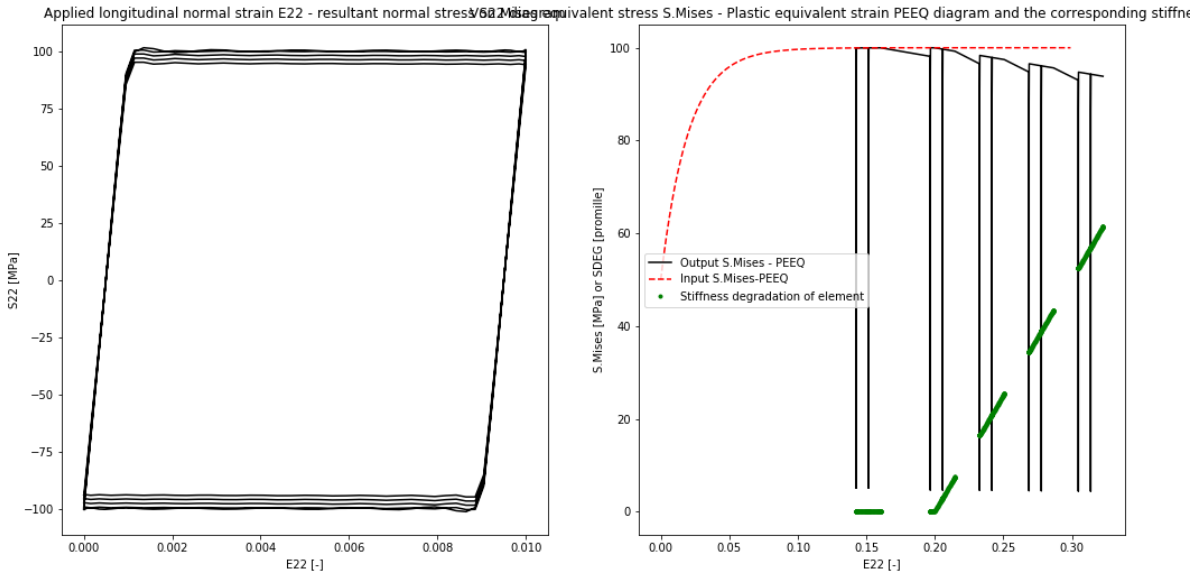


**Figure 4.5:** On the left plot the longitudinal normal stresses are retrieved from the element as response to the prescribed amplitude displacement of $0.01$ [mm]. Clearly the response of the element gets less every cycle or iteration. This degradation of the stresses (black) is more clear in the right plot where the degradation clearly starts together with the rise in stiffness degradation (green) due to the ductile damage module. Thus no longer follows the input (red).

One might argue: is material softening really required? For now this question will be answered simply with a "yes". The short explanation is: this is what is required to let a single element mimic the behaviour of the entire CT specimen. The full explanation for the plasticity module will be given in section 4.5 of chapter 4 and for the CT specimen in chapter 5. For the softening material model the most optimal amount of iterations is found to be two as one iteration still leads to jumps in the solution and more iterations leads to zero-response. For hardening with a displacement controlled analysis, again, at most ten iterations are enough as more is not needed for a displacement controlled analysis. This predicament would be obsolete if the iterations would not only be dependent on the previous iteration, but are rather based on the first iteration with improved predictions for each sequential iteration. Iterating based on the first iteration is straight forward, but what would the improved prediction be? The improved prediction would have to look at the equilibrium between the internal and external forces. If the internal forces are higher, then either a lower yield stress and/or lower stiffness in the plastic branch must be used during the next iteration. If the internal forces are lower than the external forces, then the prediction needs higher yield stress and/or stiffness in the plastic branch. This decision diagram is illustrated in figure 4.6.

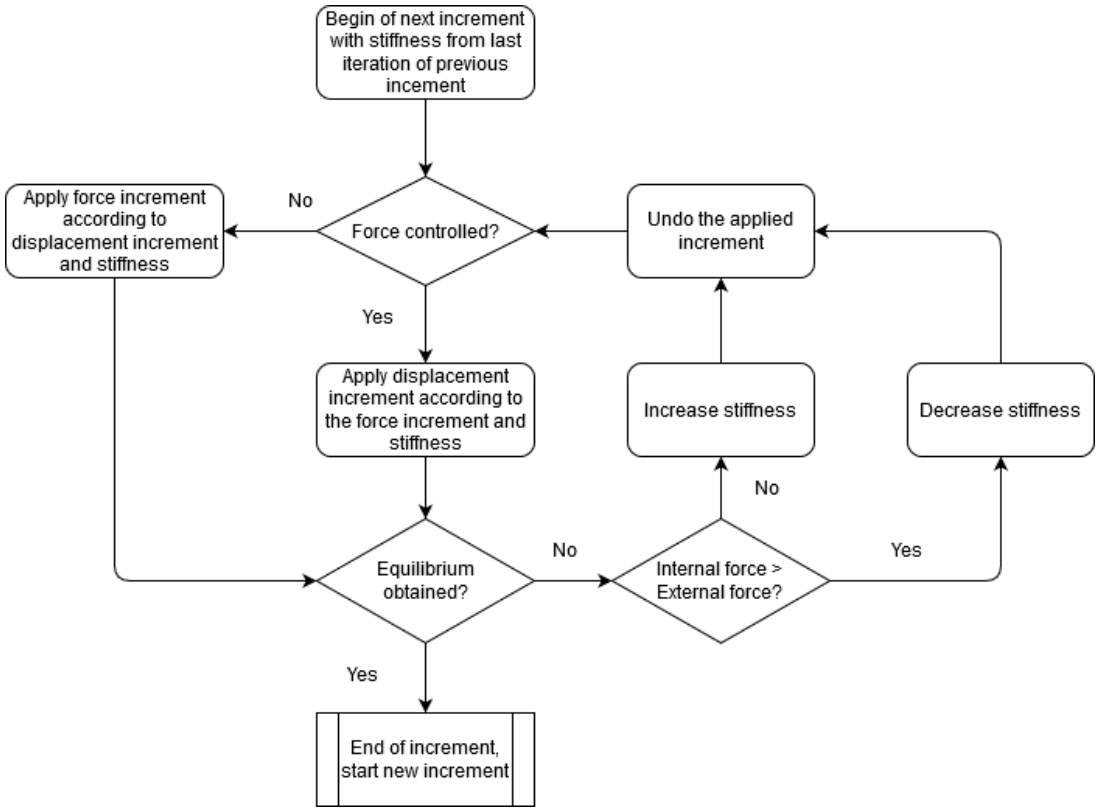


**Figure 4.6:** The qualitative assessment of the proposed iteration scheme. It improves the iteration scheme by starting each iteration from the initial state at that increment instead of the final state after the previous iteration. This scheme could also be applied for displacement controlled analysis while the default scheme only works for force controlled analysis. Start at the top and keep cycling through until equilibrium is reached which allows to start the next increment.

The last decision that has large effect on the calculation speed is the number of increments per cycle, hence the total number of calculations that are performed. This is the baseline of how much calculation effort needs to be fulfilled as the iterations and cycle jumps also directly influence the number of increments that have to be calculated. Therefore it is trivial that more increments may lead to higher accuracy but definitely leads to more calculation time. Hence the most optimal solution would be to decrease the size of the increments around the changes in load direction and abrupt different structural response. With fixed increments not much could be done. To make sure that the most extreme values

of the load are captured as those are the most important points during the fatigue analysis, somewhere around $100$ increments for a jigsaw amplitude function is advised and $20$ increments for the cosine amplitude function. However, if the automatic incrementation of Abaqus[3] is used, then the program will sort itself out if an appropriate initial increment is given. The automatic incrementation is especially valuable in models containing stress concentrations such as the compact tension specimen (CT specimen). The maximum number of increments could be set at the same value as the fixed incrementation or the tenfold of it could be used. The maximum number of increments acts as an upper limit of the number of increments that could be used during a cycle. If more than tenfold is needed, then a different approach would be more useful than wasting time on smaller increments. The initial size of the increment is best set at the same increment size as is advised for the fixed incrementation since it is better to start rather slow and not to leap over certain important changes of the structural response. The minimum size of increments could theoretically be set at $10^{-39}$, but that is useless. It is better to set it ten or hundred times smaller than the maximum number of increments allowed. If a certain part of the load needs more increments, then it is likely that Abaqus needs to make a decision between two possible solutions (bifurcation). It is best to push through this point in a different manner rather than calculating small increments. It is more useful to model the other possible failure mechanisms later in a separate simulation by modifying the model a little to push it into the other direction. The maximum size of increment could be set at $1$, but better to set it at a value smaller or equal to $0.1$ to avoid too large steps being taken. Consider what effect it would have if the maximum load would be exactly in the middle of two increments. How Abaqus[3] decides the size of the next increment during automatic incrementation depends on the amount of iterations that were needed in the previous increment. If only one iteration was sufficient, then the increment size doubles until it reaches the maximum allowed. If all iterations were needed, than it will decrease the increment size with a factor two from its most recent iteration until the lower bound value is reached. If an increment leads to a number of iterations in-between those limits, then the size of the next increment is determined by the amount of iterations that was needed in the previous increment.

A medium time influencing method is the number of elements. The number of elements used does influence the calculation effort, however it is not proportionally to the number of elements. It is less than proportionally, therefore less effective than changing the cycle jump size, the number of iterations or the number of increments. Hence for maintaining an accurate result, it is better to keep the number of elements high enough to have a high level of quality mesh. Do note that more elements not necessarily result in a higher quality mesh as the shape of a single element might be more important. Still the element size is often related to accuracy. Also a smaller element size lead to higher stresses in singularities, therefore faulty stresses may occur. These are called singularities. Singularities might occur at the crack tip even with the plasticity and the ductile damage module engaged to counter this. Therefore take an appropriate amount of elements such that quality is not jeopardised.

It is also possible to change the number of Fourier terms that are used. Although some change is expected, none or too little change in computational time was observed. In theory more Fourier terms should generally make the output field more accurate, but would take more time. However, using more Fourier terms in amplitude functions that are not smooth, may result in large local inaccuracies. In figure 4.7 this effect is shown for a block function. Recommended values for Fourier terms vary between $10$ and $50$ for the minimum and $20$ and $100$ for maximum. The increment of increasing the number of Fourier terms is often set at $5$.

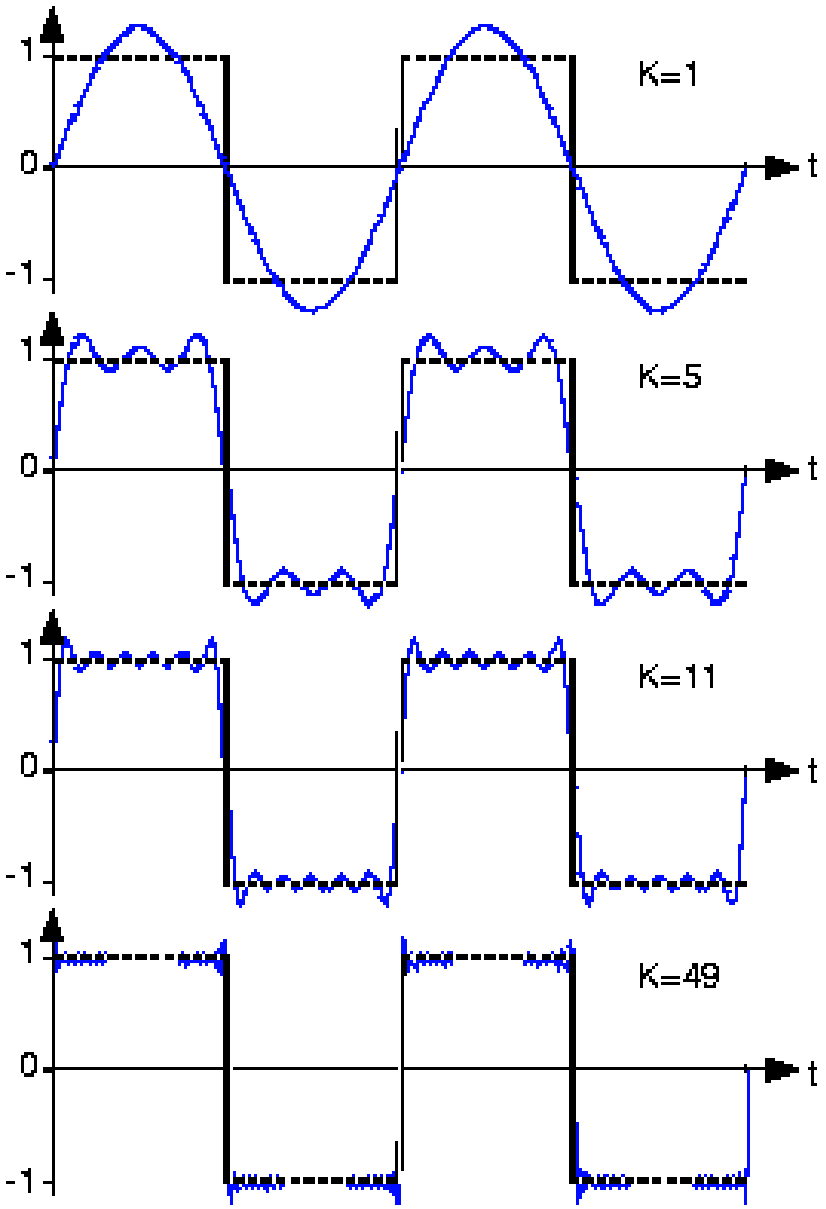


**Figure 4.7:** An illustration showing that increasing the number of Fourier terms (blue) may improve the global approximation of a block function (black). However, at certain amount of terms the Fourrier approximation may lead to large deviations locally as shown at the bottom. The figure is taken from Stackexchange[57].

## 4.5. Application of plasticity model

### 4.5.1. Implementation of plastic material parameters

The plasticity module allows to proceed calculations beyond the yield stress by providing a continued stress-strain relation instead of merely a constant initial stiffness. The plasticity could be seen as a degradation of stiffness after yielding up to where the damage starts (red striped area) as is shown in figure 3.14. For the most materials such as metals this is true, only a select group of special materials will show an increased stiffness. For composites the hardening is included to prescribe the inter fibre failure. Actually the inter fibre failure is a damage mechanism and should be considered as such for micro-scale

models. However, as a meso-scale model is developed for computational speed, the micro-mechanics may be described in a phenomenological model. The result of the inter fibre failure is a reduction of the overall stiffness of the element, not necessarily the strength during tension. This stiffness reduction is shown in the test results of the coupon test illustrated in figure 3.6. Hence the plasticity model is capable of describing the effects of the inter fibre failure.

The stiffness degradation could be modelled with different hardening formulations. First of all, a decision has to be made whether to include the isotropic, the kinematic hardening or a combination of both. There are other hardening options available in Abaqus[3], but these could be boiled down to (different variants of) isotropic or kinematic hardening. To be more precise, the isotropic hardening will be added as a suboption of the combined hardening called cyclic hardening. It is done in this manner as the suboption cyclic hardening is specifically designed to be used in the direct cyclic analysis according to the MIT manual[36]. The kinematic hardening is added due to its nature to recreate the well known ratcheting behaviour during the fatigue loading where stresses remain equal and the strains increase, thus a stiffness decrease occurs. Both the isotropic and the kinematic hardening would be able to reproduce the same outcome during a static (tensile) test, but will lead to different outcome during fatigue loading. This difference is related to the discussion in section 3.6 of chapter 3. In short, the isotropic hardening changes the size of the yield contour and the kinematic hardening the location of the yield contour. Therefore it is required to look at the compressive limit of the material during tensile loading to distinguish a difference between the isotropic and the kinematic hardening to decide which (combination of) hardening is suited. It has to be determined by experiments with fully reversed loading $R = -1$. To obtain a reasonable accurate solution five tests are required. These are first loaded in tension to a certain force and then compressed. The number of five is determined by the fact that three tests are required to estimate the tensile hardening parameters of the first hardening formulation if the parametric formulation is used. At least an equal number of test is required for the other formulations. In order to obtain and check the evolution on the compression side at least two more tests are required to determine the evolution. In other words, one test was already required to obtain the initial yield stress. Additionally, for every hardening formulation two extra tests are required, hence for a model containing one isotropic and one kinematic hardening formulation requires a minimum of five tests to calibrate.

### 4.5.2. Input for plasticity model

Notice that the number of required parameters equals the number of minimum tests required. Both the kinematic hardening and the isotropic hardening could be defined using parameters or tabular input. For each parametric input it is required to give three parameters. The first parameter is the initial yield stress $\sigma_{y,0}$ in [MPa] describing the stress level at which the yield contour is reached for the first time and must be equal among all other hardening formulations. The second parameter describes the amount of stress change between yielding and ultimate stress. The third parameter describes the speed of this stress change. For the isotropic hardening these last two parameters are respectively $Q_\infty$ and $b$ and for the kinematic hardening these parameters are respectively $\frac{C_n}{\gamma_n}$ and $\gamma_n$ with index $n$ indicating the number of the kinematic hardening formulations that are used. Note that the first parameter for the kinematic hardening is dependent on the speed $\gamma$. There is no physical purpose of this normalisation, it is merely a numerical trick as is shown by equation 4.2. The stress in the plastic regime of the material is described by an inverted power law equation starting from the onset of yielding. Hence the initial yield stress is the yield stress at zero plastic equivalent strain ($\varepsilon^p_{eq}$). Since the initial yield stress is equal for all hardening formulations, this means that once the yield stress is reached, all the hardening formulations will act. Only the speed in the formulations will decide how the structure will respond under increased loading, thus which hardening formulations will have the most effect at a specific point in time. From

the yield point on, equation 4.2 will hold as relation between stress and the plastic equivalent strain for the parametric input.

$$\sigma_{y,\varepsilon^p_{eq}} = \sigma_{y,0} + Q_\infty(1 - e^{-b\varepsilon^p_{eq}}) + \sum_{n=1}^{k} \frac{C_n}{\gamma_n}(1 - e^{-\gamma_n \varepsilon^p_{eq}}) \tag{4.2}$$

The kinematic hardening formulations are also known as backstresses. As the second and third term of equation 4.2 are similar, it is possible to create equivalent hardening. This is true for the tensile static loading as is illustrated in figure 4.8, but it is not true for cyclic loading as the compression resistance will change differently between the two types of hardening.

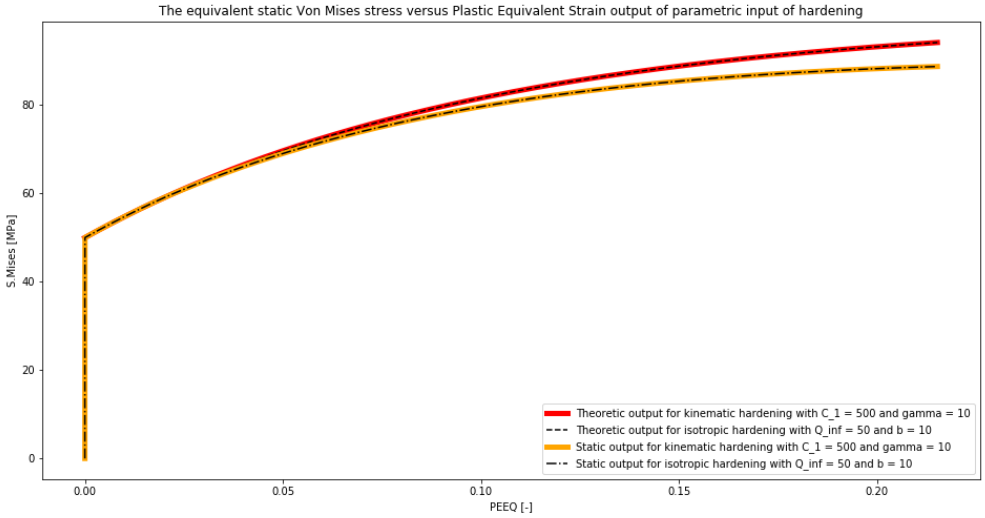


**Figure 4.8:** The top two lines are the input given for the plasticity model for the two equivalent hardening for the static tensile loading. These two lines also represent the desired theoretic output with the red line for the kinematic hardening and the striped black line for the isotropic hardening. As is expected from equation 4.2, these result in the same response. The bottom two lines are the static output for tensile loading with the same hardening parameters as their theoretic output. The orange line is for the static output of the kinematic hardening and the black stripe-dot line for the isotropic hardening. Again an identical output is observed for the static tensile loading. The difference in the output is generated by the definition of plastic strain in Abaqus[3].

Observe there is a small discrepancy between the theoretical output (the input of the static analysis) and the static output. This difference is caused by the formulation of plastic equivalent stresses versus the stresses. The conversion will be explained for a bi-linear plasticity model with kinematic hardening. This bi-linear model is used in the one element model as it is much simpler to check the difference caused by the conversion. According to the MIT manual of Abaqus[42] it calculates the true plastic strain in a slightly different manner than based on intuition. Intuition will define the true plastic strain as the elastic strain subtracted from the true total strain with the elastic strain as the strain at the initial yield stress. That will keep the elastic strain subtracted from the total strain as a constant as is shown in equation 4.3.

$$\varepsilon_{p,true} = \varepsilon_{total,observed} - \varepsilon_{y,input} = \varepsilon_{total,observed} - \frac{f_{y,0}}{E} \tag{4.3}$$

Here $\varepsilon_{total,observed}$ is the total observed strain from the output, $\varepsilon_{p,observed}$ is the plastic strain observed from the output and $\varepsilon_{y,0}$ is the elastic strain provided as input. The elastic input strain is here related to the initial yield stress $f_{y,input}$ and the initial Young's modulus $E$. On the contrary, the yield strain in Abaqus[3] is not kept constant, but is a function of the stress at that point. It observes the new stress as the yield stress from hardening at a certain plastic strain until hardening occurs again. This idea is formulated in equation 4.4

$$\varepsilon_{p,true} = \varepsilon_{total,observed} - \varepsilon_{y,f_y} = \varepsilon_{total} - \frac{f_{y,observed}}{E} \tag{4.4}$$

Here $\varepsilon_{total,observed}$ is the total strain observed in the output, $\varepsilon_{p,observed}$ is the plastic strain observed in the output and $\varepsilon_{y,observed}$ is the elastic strain observed in the output. The elastic strain is related to the yield stress $f_{y,observed}$ at an applied plastic strain and the initial Young's modulus $E$. This is coherent with the dotted line just before the red marked area in figure 3.14. Genuinely FEM tends to estimate the observed yield stress from the applied plastic strain subtracted from the total strain by flipping around equation 4.4 since FEM is a displacement field driven analysis. Force equilibrium check will point out if enough, too little or too much strain has been applied during such an analysis. In other words, as this conversion leads to higher elastic strains during hardening due to the higher yield stresses, the plastic strains will be lower for the same amount of total strain. Vice versa, if the plastic strains are lower, then the stresses will be lower for the same total strain applied. This is what is observed in figure 4.8. During the investigation of the one element model a simple bi-linear relation will be used on which the effect of this behaviour will be visualised. The bi-linear model consists of an initial yield stress of $50$ [MPa] and an ultimate stress of $100$ [MPa] at an intended ultimate strain of $0.1$ [-] with a Young's modulus of $E = 5000$ [MPa]. This line is shown in the figure 4.9 as the blue line. If this would be directly used as input, then Abaqus[3] gives a static response of the orange line in figure 4.9 as $\frac{100[\text{MPa}]}{5000[\text{MPa}} = 0.02$ [-]. This will give an ultimate strain of $0.1 + 0.02 = 0.12$. If a correction was taken already according to the intuitive method in equation 4.3, one would enter an input value of $0.09$ as the ultimate strain as illustrated with the purple line of figure 4.9. This would result in a ultimate strain of $0.09 + 0.02 = 0.11$ as is illustrated by the green line in figure 4.9. In order to correctly apply the definition in equation 4.4, then it is needed to put in $0.08$ as the ultimate strain since $0.10 - \frac{100[\text{MPa}]}{5000[\text{MPa}]} = 0.08$. This input is plotted as the red line in figure 4.9 but will obtain the blue line as output.

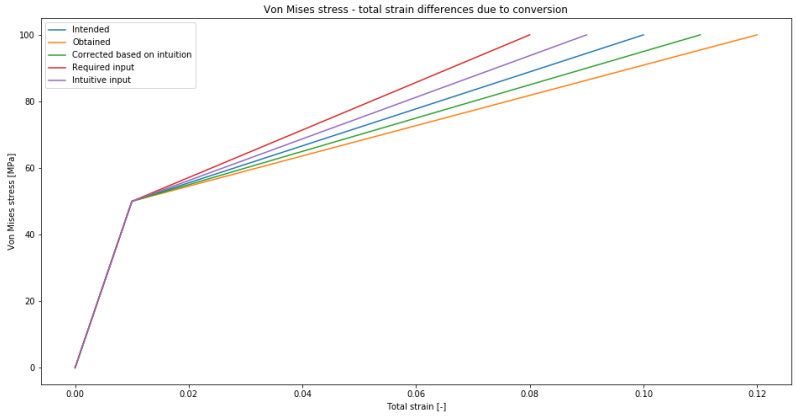


**Figure 4.9:** An visualisation of the effect of different input on the ultimate strain for the plasticity model and the effect of the conversion on the input for an ultimate stress of $100$ [MPa], a Young's modulus of $5000$ [MPa] and a yield strength of $50$ [MPa]. The difference caused by the conversion is $0.02$ strain.

Later the plastic input parameters will be changed to resemble the composite material response according to the static test result. Figure 4.10 shows the calibration of such model. This will be done using the parametric values for four reasons:

1. If there is no proper continuation of the plasticity module with the ductile damage module prescribed, then Abaqus will result it in fatal error that will stop the analysis. This may occur if the fracture energy is not in correspondence with the fracture strain such that the shape of the ductile failure regime of the stress-strain relation of figure 3.14 causes numerical instabilities due to large changes in the material/element response. The second problem might be that the fracture strain of the ductility damage module is set at a value lower than the ultimate strain of the plasticity module. This will cause a cut-back behaviour leading to numerical instability.

2. The results of the tensile coupon test shown in figure 3.6 could be well estimated using parametric isotropic hardening as is illustrated in figure 4.10. The obtained values to put into the analysis on CT specimen level will be $\sigma_{y,0} = 39.53$ [MPa], $Q_\infty = 250$ [MPa] and $b = 300$.

3. The tensile coupon test was performed, but figure 3.6 reveals that the specimens were not loaded until failure. The parametric values allow easy extrapolation of the values until the ductile damage model defines failure.

4. Using a parametric approximation allows smoother interpolation of the input parameters as is shown in figure 4.10. If tabular values are used, leap backs in the plastic strain lead to numerical instability.

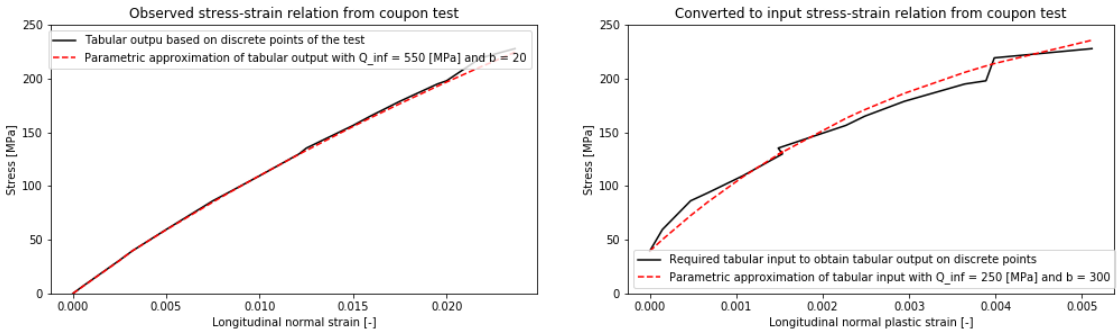


**Figure 4.10:** In the left plot is the observed stress-strain relation shown as is directly obtained from the tensile coupon test of figure 3.6. In black discrete values of the average curve are entered in a tabular form. The red dotted line gives a parametric approximation as an alternative with $\sigma_{y,0} = 39.53$ [MPa] $Q_\infty = 550$ [MPa] and $b = 20$. This should not be used as input due to the conversion from input to output, but proves it is possible to approximate the same behaviour. To obtain the input the conversion of the tabular values have to be done according to equation 4.4. The results of this conversion is shown in the right plot in black. Now an approximation of the tabular input is obtained with $\sigma_{y,0} = 39.53$ [MPa], $Q_\infty = 250$ [MPa] and $b = 300$ as is shown in red.

**Table 4.1:** Input table containing the parametric values for the bi-linear stress-strain relation used in the plasticity module for the one element model.

| | One element stable | One element unstable |
|---|---|---|
| $E$ [MPa] | 5000 | 5000 |
| $\nu$ [-] | 0 | 0 |
| $\sigma_{y,0}$ [MPa] | 50 | 50 |
| $\varepsilon_{ult}$ [-] | 0.08 | 0.08 |
| $\sigma_{ult}$[MPa] | 100 | 100 |
| $f_U$ [Hz] | 1 | 1 |
| $U_{max}$ [mm] | 0.04 | 0.041 |
| $U_{min}$ [mm] | 0 | 0 |

**Table 4.2:** Input table containing the temporary parametric values used in the ductile damage module used for the one element model.

| | One element stable | One element unstable |
|---|---|---|
| $\varepsilon_f$ [-] | 0.2 | 0.2 |
| $\eta$ [MPa] | 0.33333 | 0.33333 |
| $\dot{\varepsilon}$ [-] | 1 | 1 |
| $G_f$ [N/mm] | 6 | 6 |

### 4.5.3. Effects of plasticity model

The output of the one element model will be provided in a so called hysteresis plot. A hysteresis plot shows the stress-strain output for an element or force-displacement for a structure that is fatigue loaded. Due to the nature of fatigue loading the curve will move back and forth for each cycle. Whether there will be a difference in response between loading, unloading and reloading depends on the material model. The plasticity model has an influence on the hysteresis plot as the plastic response leads to a different unloading response resulting in energy dissipating. The energy dissipated in a cycle is the area that is enclosed during that cycle until the stress-strain curve intersects the stress-strain curve of the previous cycle. Adding up the enclosed areas should lead to the same value as was entered as a total of the fracture energy of the material or structure for the ductile damage and the enclosed area by the plasticity curve. In short it will be the area between the material curve and the horizontal axis of figure 3.14. The hysteresis plot also allows to deduct if hardening or softening occurs as during hardening either the stresses will increase or the strains decrease over the sequential cycles for a displacement controlled analysis and a force controlled analysis respectively. Analogously, it will be a decrease in stresses or an increase in strains over the sequential cycles for a displacement controlled analysis and a force controlled analysis respectively. As composites show a degradation of residual stiffness, isotropic softening has to be investigated if one element should represent the entire CT specimen. For that to happen, one major assumption is made: the isotropic softening must describe the effects of inter fibre failure and delamination. This is certainly a mere rough approximation of the reality. However, it is a good exercise to understand what happens during softening of the material. First the output for material hardening will be explained with the input given for figure 4.9. The second column of table 4.1 provides an overview of these input parameters for an element that remains stable for at least ten [cycles]. The third column of table 4.1 provides these for an element that fails within ten [cycles]. The used temporary values for the ductile damage models are provided in table 4.2 for an overview. Notice that for both models these values were kept equal. Figure 4.11 shows the output given for the one element model with the discussed parameters.

At first sight the output does not resemble the input, but there is a pattern in it that is correct. For verification the hypothesis based on the lectures of plasticity by Hoogenboom[38] is calculated using a code written in Python[58]. This code will act as a prediction of the fatigue analysis on one element under the given boundary conditions of figure 4.1. It is able to predict the longitudinal normal stress in the element and the applied forces due to the prescribed displacement on the top four nodes of the cubic element. It has proven not only to be useful to check the analysis, but also to predict the number of cycles that have to be analysed by Abaqus[3] to reach the end point. This Python[58] script is provided in appendix A. The hypothesis is not able to predict the entire analysis with accuracy as there were assumptions made, these assumptions lead to the limitations of the Python[58] script. These assumptions are:

1. No ductile damage is included, therefore no stiffness degradation parameter is taken into account. There will be only effect of the plasticity model present. Thus an over-prediction on the fatigue life is made. Moreover, if in Abaqus[3] the element does not have a ductile damage model included, then it will never fail even if a small residual strength is used to compensate the effects of the absence of a the ductile damage model.

2. The Poisson's ratio is either $0$ or the lateral contraction shall not be hindered by the boundary conditions. Only a longitudinal normal stress is taken into account by the hypothesis, thus the longitudinal normal stress must equal the Von Mises stress as the material is defined on the Von Mises stress. The proposed boundary conditions in figure 4.1 satisfy this restriction. This is required to avoid the effect of moving (relatively) along the yield contour.

3. The Python[58] script is currently written for a displacement controlled analysis in the variants of isotropic hardening and isotropic softening with a linear plastic response. More options could be modelled but are considered as unnecessary to prove the hypothesis for the one element model.

The hypothesis is based on the definition of isotropic hardening where yielding leads to an increase of the yield contour as is explained in figure 3.8a. Although the numerical prove is done for a load with $U_{max} = 0.04$ [mm], the hypothesis will be explained for $U_{max} = 0.05$ [mm] which will be $5\%$ strain for the element. The visualisation of the hypothesis is provided in figure 4.12. Upon loading the element for the first time it will start-off just as a static linear elastic analysis until the yield stress is reached at $50$ [MPa]. The second part of the analysis does no longer follow the elastic response of the material, but will follow the plastic response just as the plastic static analysis will do and increase the size of the yield contour continuously according to the isotropic hardening formulation. However, it will no longer be called a linear elastic analysis. Upon reaching the maximum displacement, the increase in stress stops at $71$ [MPa] as it is no longer needed. This stress of $71$ [MPa] is the new yield stress for both tension and compression. In the third part the stress will reduce in a linear elastic fashion as reducing the applied displacement means moving away from the contour. Since every displacement within the (new) boundaries of the yield contour corresponds with elastic response, the element will respond elastic passing the zero stress point (as the displacement will still be larger than zero). It continues elastically passing the original yield stress for compression until it reaches the new yield stress of $71$ [MPa] in compression. Now it will continue in the plastic response mirrored from the tensile plastic response. In other words the plastic stiffness of the tensile input will be used during compression to reach $0$ [mm] of longitudinal displacement. Note that this fourth part results in additional compressive stresses that pushes the yield contour even further instead of reducing it. The proportion in which it occurs depends on the hardening formulation, here it is proportional to the tensile hardening as a perfect isotropic hardening is formulated. Upon finally reaching the $0$ [mm] displacement the new cycle starts, but with a residual stress of $-84$ [MPa] which means the new yield stress will be $84$ [MPa]. In the new cycle the response will be first elastic as the fifth part moves away again from the yield contour on the compression side. It

passes again the horizontal axis at about $0.16$ [mm] until the new yield stress of $84$ [MPa] of tensile stress is reached. In the sixth part it will continue with a plastic response to $96$ [MPa]. Parts 3 to 6 will repeat itself in a longer fatigue analysis and part 7 is nothing more than part 3 of cycle 1 applied on cycle 2. However, if the yield stress reaches the final stress that has been entered in the input, then it is considered to be failed. Failure due to plasticity is best modelled by applying a small residual strength afterwards until the ductile damage module completely degrades it. This is the last part (part 8) drawn in figure 4.12 where the stress reaches $-100$ [MPa] which is the ultimate compressive/tensile yield limit.

Sometimes a little change in the applied load may lead to a large change in the number of cycles it could handle before failure due to plasticity occurs, even on a logarithmic scale. This could be seen as the difference between figure 4.11 and figure 4.13 where the former is considered to be stable for at least ten cycles and the latter fails at the fourth cycle. In this case the difference is accelerated by the ductile damage model kicking in or not, but the main cause is reaching the ultimate limit of the plasticity module. The Python[58] code is not so good in predicting this as some of it is caused by numerical side effects leading to slight inaccuracies in stresses in the Abaqus[3] model while for the Python [58] code the boundary conditions and zero Poisson's ratio are assured perfectly. Nevertheless, a small change in load may lead to a large change in fatigue life. The critical load level that would induce infinite fatigue life is to be calculated. For these bi-linear material parameters it could be done by hand as is done in equation 4.5. The thought behind the critical load level is that the stress obtained as maximum stress in cycle $N$ must equal the maximum stress in cycle $N-1$. This constrained is formulated by setting the maximum stress and minimum stress to be equal, therefore it must be reached by linear elasticity. Only in that case no energy dissipation happens as there is no enclosed area, thus no degradation of the material is observed. The maximum stress formulated in equation 4.5 refers to the bi-linear plasticity module.

$$\begin{cases} \sigma_{max} = f_y + \frac{(f_u - f_y)\left(u - \frac{f_y}{E}\right)}{\varepsilon_{u,desired} - \frac{f_y}{E}} \\ \sigma_{min} = \sigma_{max} - Eu \\ \sigma_{min} = -\sigma_{max} \end{cases} \tag{4.5}$$
$$\implies u = \frac{f_y\left(1 - \frac{f_u - f_y}{E\varepsilon_{u,desired}}\right)}{\frac{E}{2} - \frac{f_u - f_y}{\varepsilon_{u,desired} - \frac{f_y}{E}}}$$

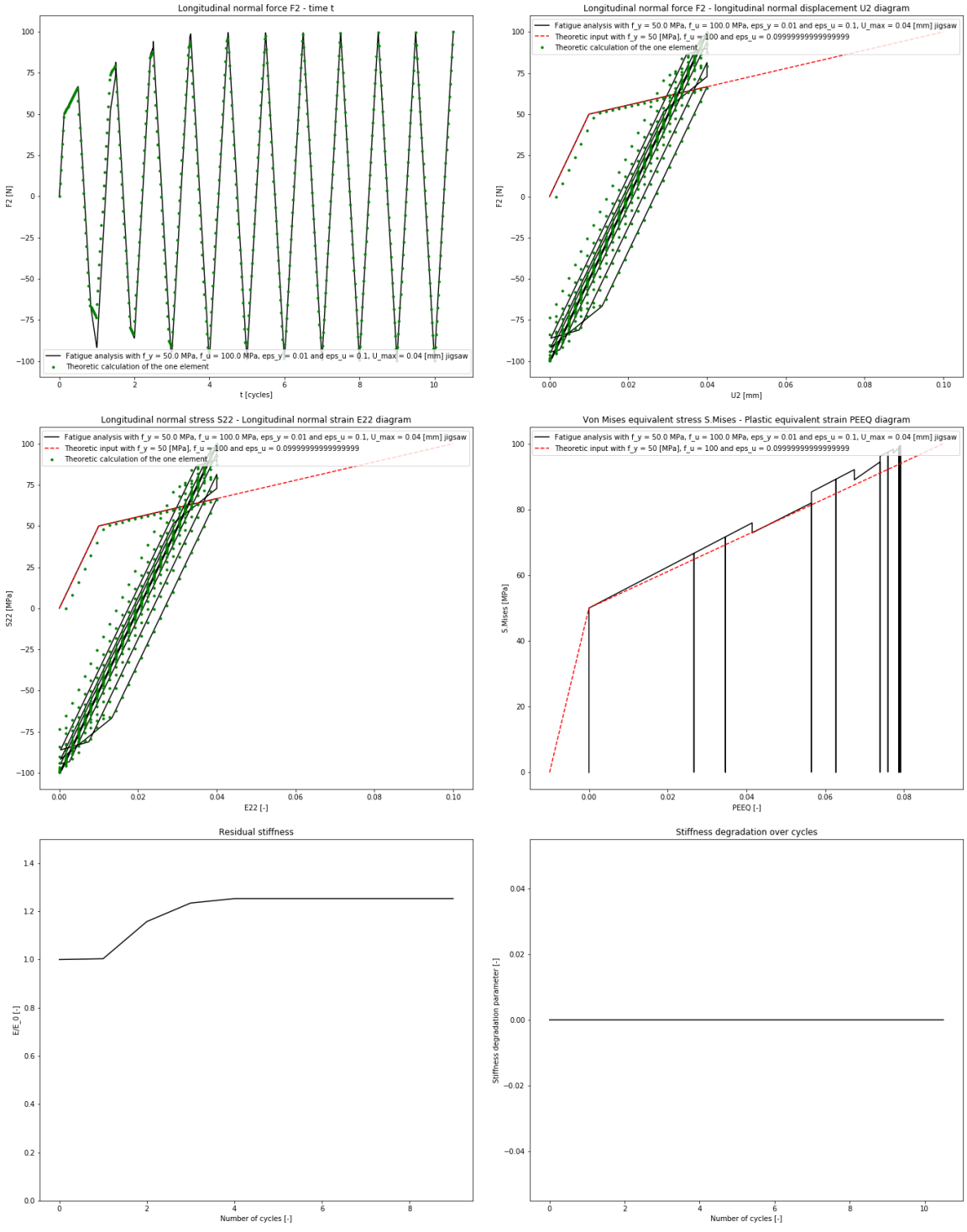


**Figure 4.11:** In the six plots the entire (relevant) output of the fatigue analysis for the one element model with an applied displacement of 0.040 [mm] failing after more than ten cycles is represented. The input of the model is given in the second columns of tables 4.1 and 4.2. The black lines are the results of the analysis and the green line is the predictions based on the Python[58] script. Counting from left to right and from top to bottom the load history plot is given first. This plot shows the applied force as resultant of a constant applied displacement amplitude function. The second plot is the force-displacement diagram which acts as the hysteresis plot of the element as structural response. The third plot shows that hysteresis plot in terms of stresses and strains of the element's internal response which is equal to figure 2 due to the unit size of the element. The fourth plot shows the plastic equivalent strain versus the Von Mises stress to see if it relates to the input parameters which are given in a red dotted line. The fifth plot shows the stiffness of the structure relative to the response of the first cycle and the sixth plot shows the value of the damage parameter that leads to stiffness degradation (0 equals no damage and 1 equals fully damaged).

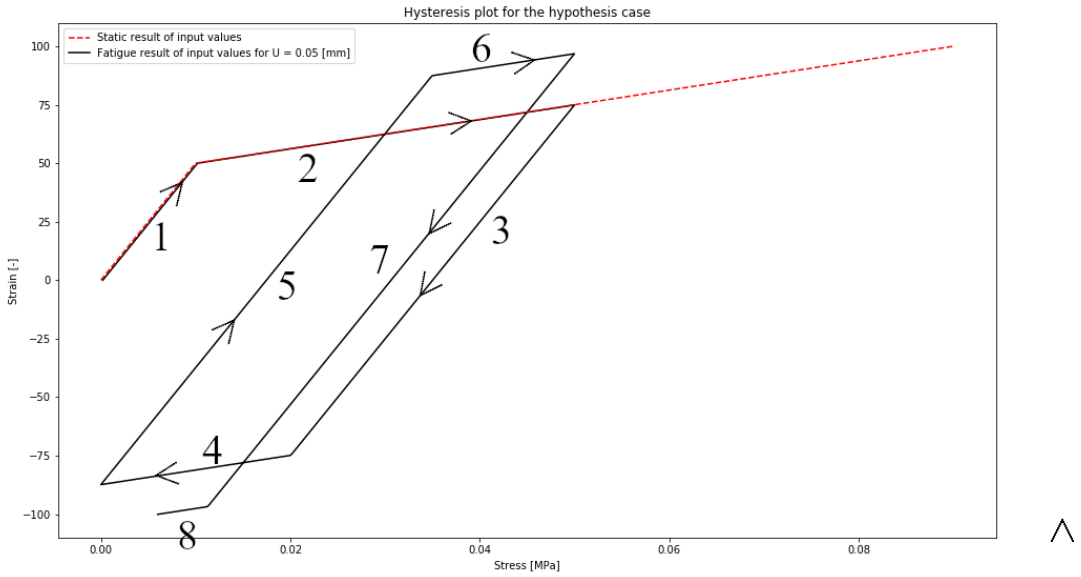


**Figure 4.12:** The visualisation of the explanation of the hypothesis showing the hysteresis loops for the material of tables 4.1 and 4.2, but with an imposed displacement of $U = 0.05$ [mm]. This leads to failure in the second cycle. The red line is the output for the model loaded with a static loading and the black line the output of the fatigue analysis.

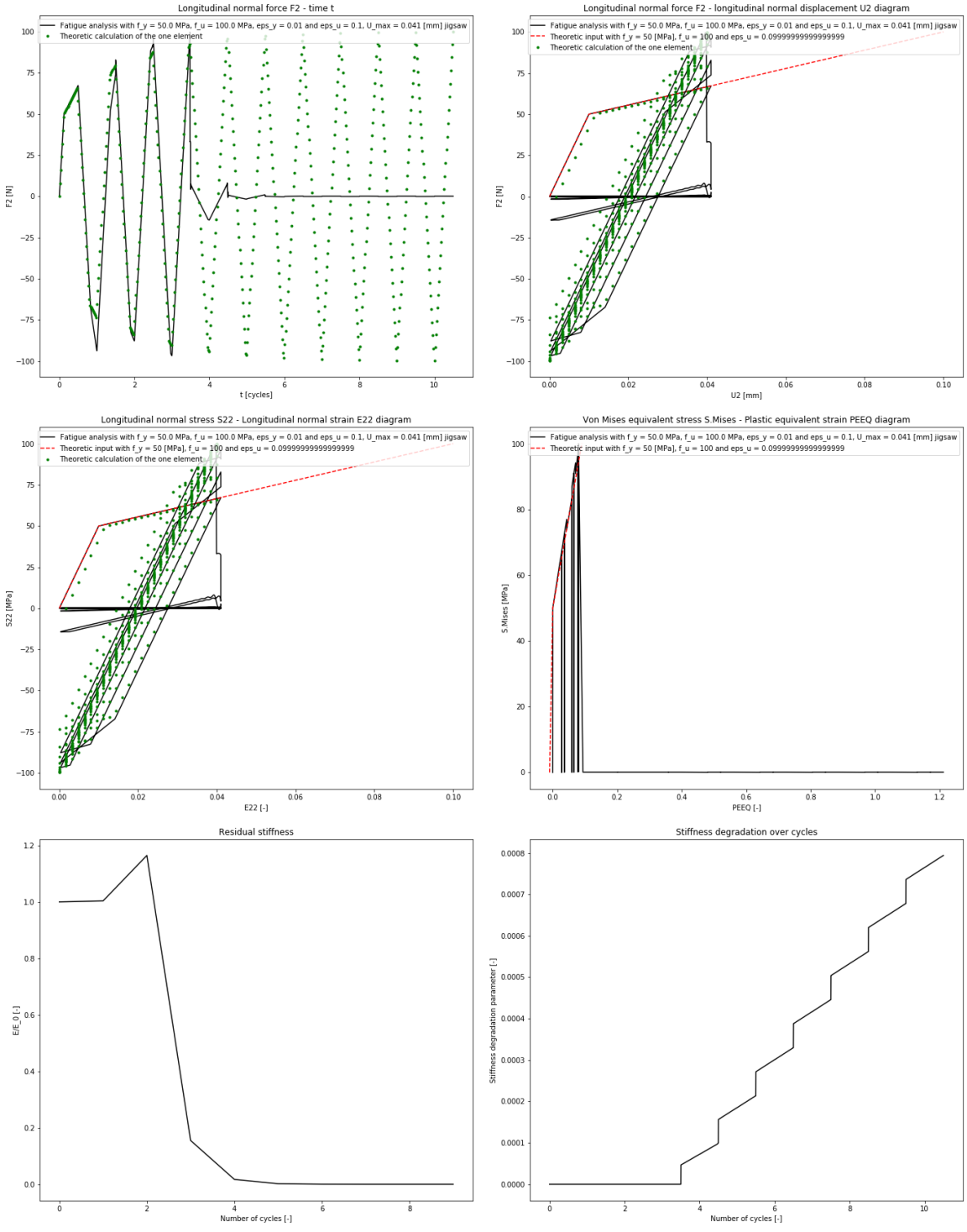


**Figure 4.13:** In the six plots the entire (relevant) output of the fatigue analysis for the one element model an applied displacement of 0.041 [mm] failing after four cycles is represented. The input of the model is given in the third columns of tables 4.1 and 4.2. The black lines are the results of the analysis and the green line is the prediction based on the Python[58] script. Counting from left to right and from top to bottom the load history plot is given first. This plot shows the applied force as resultant of a constant applied displacement amplitude function. The second plot is the force-displacement diagram which acts as a hysteresis plot of the element as structural response. The third plot shows that in terms of stresses and strains of the element's internal response which is equal to figure 2 due to the unit size of the element. The fourth plot shows the plastic equivalent strain versus the Von Mises stress to see if it relates to the input parameters given in a red dotted line. The fifth plot shows the stiffness of the structure relative to the response of the first cycle and the sixth plot shows the value of the damage parameter that leads to stiffness degradation (0 equals no damage and 1 equals fully damaged).

## 4.6. Application of ductile damage model

### 4.6.1. Implementation of material parameters for ductile damage model

The ductile damage module is implemented in the analysis as a damage model to represent the fibre fracture in the material. This is a meso-scale mechanism as its effect is too large to be considered on the individual fibre level. These fibres break at individual stress levels as there is a slight deviation in strength of each fibre. Hence the maximum allowable stress will be at the stress level of the first fibre breaking. Upon breaking the fibre, the stresses have to be redistributed over the nearby fibres causing a stress increase on the neighbouring fibres until the next one fails and the process is repeated. The absence of a fibre reduces the overall strength of a control volume, despite the nearby fibres might be slightly stronger. The ductile damage model will be used as a material module in the elements that represent the composite material under fatigue loading. The damage module introduces a damage parameter called the stiffness degradation (SDEG) that describes the amount of damage that is done to the element on a meso-scale level. This is not the amount of relative reduced stiffness. Since it is applied in combination with the elastic and plastic module, there is no longer a direct relation. The stiffness degradation parameter will describe a percentage of the broken fibres in the element. The ductile damage module is an augmentation of the plasticity module, therefore it kicks in when all or a large part of the plasticity module has taken effect. Some limitations of the ductile damage module are challenged as the composite material behaves in a brittle manner. Therefore one of the questions is: how good is the ductile damage module in handling brittle material parameters?

### 4.6.2. Input for ductile damage model

The ductile damage parameters are introducing a traction-separation law for the smeared cracking model. The easiest manner to visualise the traction-separation law and its effect on the fatigue analysis is to (re)view figure 3.13. Despite the simplicity of the description in figure 3.13, the real response is described in figure 3.14. There are four parameters that have to be described which together determine the maximum stress allowed in the element before failure. Therefore if a tabular input is used, then it is required to have the input parameters in such a way that the maximum stress matches the maximum stress in the plasticity module. Otherwise there is an over-constraining that leads to discontinuous formulation of the material model. For that reason the parametric approximation of the plasticity of the material is preferred as it will always be continuous. The damage parameters are irreversible and determine the newly (reduced) maximum stress allowed.

The first to discuss parameter is the fracture strain $\varepsilon_f$. This parameter determines at how much input of plastic strain the material has completely failed. If this value is too low, it provides a cut-back in the material response that results in numerical instability. Currently the value is set at $0.2$ [-] for the one element model which is higher than the ultimate strain put into the plasticity model. Hence continuity is preserved. Later this value will be set at $0.0062$ [-] for composites as a calibration of the earlier models from joint tests performed by He[52]. The model of He[52] also provided values for the stress triaxiality and strain rate. These are set at $\eta = 0.33333$ and $\dot{\varepsilon} = 1$. These parameters are used to define the onset of damage as described in the MIT manual[59]. However a parametric investigation already concluded that the influence of these parameters is negligible for all the models discussed in this report. Therefore standard values for the stress triaxiality and strain rate are chosen.

The last value is a fracture energy $G_f$ in the damage evolution suboption. On the contrary to the stress triaxiality and the strain rate, the fracture energy has a lot of influence on the fatigue life of an element. During the one element model this value is set at 6 [N/mm$^2$] with a linear degradation as this value is compatible with the plasticity model. In order to obtain energy values that are compatible with the bi-linear plasticity module, the energy value must fulfil equation 4.6. This equation is set on the principle that the fracture energy is the surface area underneath the stress-strain relation as is shown in figure 3.14. For a linear degradation this is relatively simple. Calibration is required based on tests specialised in determining the value for the in-plane tensile fracture energy ($G_{Ic}$). Do keep in mind the difference in unit which has to be converted with the height of the element.

$$G_f = \frac{(\varepsilon_f - \varepsilon_{ultimate,input})\sigma_{ultimate}}{2} = \frac{(0.2 - 0.08)100}{2} = 6[\text{N/mm}^2] \tag{4.6}$$

### 4.6.3. Effects of ductile damage model

The output will show an exponential increase of the stiffness degradation factor. This will lead to a progressive decrease of residual strength. The start of the increase is shown in figure 4.13 where it is still rather slow. Therefore most of the failure is by the plasticity definition with a sudden drop in stress. In the upgraded models of chapter 5 it is more clear what the effect of the ductile damage model will be.

Once the damage parameter of an element has reached the value 1, then the element has no more residual strength and is considered to be failed. It is possible for Abaqus[3] to remove such elements from the visualisation if element deletion is turned on in the element mesh properties and the visualisation effect is enabled in the results section of the visualisation. By default the element will become invisible with a damage of $0.99$ in one of its integration points, but this value could be changed in the visualisation as long as this value is between $0$ and $1$ for numerical and physical reasons. If the broken elements are deleted, then the empty space left behind could be interpreted as a crack somewhere in that element. No exact location of the crack is obtainable as it is a smeared crack model.

## 4.7. Application of the Virtual Crack Closure Technique

### 4.7.1. Implementation of VCCT interfaces

The Virtual Crack Closure Technique (VCCT) introduces a failure criterion that is capable of predicting the interply failure mechanisms such as delamination. It uses a phenomenological description to make its prediction. The fatigue and the static analysis have therefore different input templates. The VCCT is applied on two adjacent surfaces of different parts in a so called master-slave relation. The nodes of the master surface determine which nodes of the slave surface are related to it. One master node can have multiple slave nodes, but a slave node can not have multiple master nodes. This leads to problems when applying VCCT in multiple direction as is the case for the slicing model which is explained in appendix B. One of the methods to circumvent this problem is by creating narrow partitions around all edges. By doing so, not all of the contacting surface area will be in the VCCT contact bond. However, the partitioning is done in such a way that only one node at the edge will not be bonded in a particular contact slicing. This edge is made at most with a tenth of the thickness, as only then the influence will be negligible. This contact bond is a discrete manner of describing a crack. The main advantage of using the VCCT is that the crack will be very precisely displayed in terms of debonded

nodes. The second advantage is that this model obtains precise results for the crack along that interface. However, the location of the crack must be known in advance, otherwise it will have a different crack pattern since the VCCT module could only crack through a predefined enriched interface. If a different crack pattern is observed in reality, then it is unlikely that the model makes a good prediction of the reality.

### 4.7.2. Input for VCCT

For a static analysis the VCCT bond is introduced in the interaction module of Abaqus. First the contact property has to be defined. Upon creating a new property as a fracture criterion several choices have to be made. First of all the direction of the crack growth has to be defined. By default this will be the maximum tangential stress which is also correct for the CT specimen, otherwise crack growth should be in perpendicular direction to the stresses. That option would be useful to model intraply failure modelled as local delamination as is done in the VCCT slicing model of appendix B. The tolerance and viscosity are by default $f_{tol} = 0.2$ and $\zeta = 0$ respectively. The tolerance defines how much extra margin is taken on the crack initiation criterion before a crack has to propagate. In theory the crack initiation criterion is set as defined in equation 4.7 for mode I, but a tolerance increases the limit of $1$. Thus the VCCT module will look at an equivalent/combined energy release rate to determine crack initiation as is given in equation 4.8. That will eliminate the dependency on the crack direction. For the static VCCT criterion a tolerance $f_{tol}$ is defined to determine if a crack propagation has to be initiated or a cutback in the increment size has to be performed. The advised value is $\zeta = 0.1$. If a crack propagation is supposed to release multiple nodes in one increment, then the crack is considered not to be stable anymore. In that case it is advised to allow a tolerance $f^u_{tol}$ for unstable crack propagation. The default value is fine, but a specific value could be defined for it. Now the cut back in increment size only happens if $f > 1 + f_{tol} + f^u_{tol}$ with $f$ defined in equation 4.8. The larger the tolerance, the larger the increments will be if automatic incrementation is chosen according to the MIT manual[56] until Abaqus[3] finds out more than one node has to be released. The viscosity also helps to improve the stability of the system. It is advised by Dassault système[60] to have a small viscosity when using composite materials.

$$f = \frac{G_I}{G_{I,c}} = \frac{v_{1,6} F_{v,2,5}}{2bdG_{Ic}} > 1 \tag{4.7}$$

$$f = \frac{G_{eq}}{G_{eq,c}} = \frac{v_{1,6} F_{v,2,5}}{2bdG_{eq,c}} > 1 \tag{4.8}$$

Here the energy releases values $G_I$ and $G_{eq}$ are the values for mode I and the equivalent respectively. The augmented subscript $c$ indicates the critical value of these which are provided as input of the interaction property. $v_{1,6}$ is the crack opening displacement between nodes 1 and 6 caused by the release of nodes 2 and 5. $F_{v,2,5}$ is the force on the nodes 2 and 5 that is required to close the crack again at nodes 2 and 5 to its original state as described in figure 3.16. The area of the surface that will be debonded is described by the (sub)elemental thickness $d$ and length $b$. Basically this criterion determines if the surface of the enclosed triangle on the right of figure 3.16 as result of the energy required to break the bond between these elements is larger than the performed work. If not, then the unity check is larger than one and the nodes 2 and 5 will get released.

The last choice to make is choosing a mixed mode behaviour to determine the critical equivalent energy release rate. Do not mix the critical equivalent energy release rate with the equivalent

energy release rate. The equivalent energy release rate is defined in equation 4.9. The first option is the Benzeggagh-Kenane law (BK-law)[28] which has equation 4.9 to define the equivalent energy release rate and equation 4.10 for critical equivalent energy release rate. What has to be noticed is that the critical equivalent energy release rate is dependent on the equivalent energy release rate. In other words, the limit point of crack initiation has to be found iteratively. Fortunately, it is not required to find this limit. It is only required to calculate the fraction $f$ as defined in equation 4.8.

$$G_{eq} = G_I + G_{II} + G_{III} \tag{4.9}$$

$$G_{eq,c} = G_{I,c} + (G_{II,c} - G_{I,c}) \left( \frac{G_{II} + G_{III}}{G_I + G_{II} + G_{III}} \right)^{\eta} = G_{I,c} + (G_{II,c} - G_{I,c}) \left( \frac{G_{II} + G_{III}}{G_{eq}} \right)^{\eta} \tag{4.10}$$

The second formulation to choose from is the power law[29]. The formulation is rather intuitive compared to the other two laws as it is merely a weighted summation of the individual unity checks for each failure mode. The weights of the individual unity checks are given by the powers $a_m$, $a_n$ and $a_o$ which have to be provided by the user as input. The formulation directly gives the final formulation of $f$ instead of its counter and denominator. The formulation is provided in equation 4.11.

$$f = \frac{G_{eq}}{G_{eq,c}} = \left( \frac{G_I}{G_{I,c}} \right)^{a_m} + \left( \frac{G_{II}}{G_{II,c}} \right)^{a_n} + \left( \frac{G_{III}}{G_{III,c}} \right)^{a_o} \tag{4.11}$$

The third formulation to choose from is the Reeder law[30]. The Reeder law looks very similar to the BK-law[28] as it only has an extra extension. Its extension contains the critical energy release rate for the shear energies with a similar formulation as the difference between shear and normal energies. This formulation is provided in equation 4.12. The equivalent energy release rate is still according to equation 4.9.

Which three of the equivalent energy laws is most suited has to be determined by experiments. From literature values for the energy release rates are advised as $G_{I,c} = 0.6$ [J/mm$^2$], $G_{II,c} = G_{III,c} = 7$ [J/mm$^2$] in combination with an exponent of the BK-law[28] $\zeta = 1$ as provided by Ramsaier[24].These values will be used until test results have shown differently. The crack will continue to propagate until the initiation criterion in equation 4.8 is no longer met, which means a new equilibrium is obtained. Hence the initiation criterion also acts as the evolution criterion.

$$\begin{aligned} G_{eq,c} &= G_{I,c} + (G_{II,c} - G_{I,c}) \left( \frac{G_{II} + G_{III}}{G_I + G_{II} + G_{III}} \right)^{\eta} + (G_{III,c} - G_{II,c}) \frac{G_{III}}{G_{II} + G_{III}} \left( \frac{G_{II} + G_{III}}{G_I + G_{II} + G_{III}} \right)^{\eta} \\ &= G_{I,c} + (G_{II,c} - G_{I,c}) \left( \frac{G_{II} + G_{III}}{G_{eq,c}} \right)^{\eta} + (G_{III,c} - G_{II,c}) \frac{G_{III}}{G_{II} + G_{III}} \left( \frac{G_{II} + G_{III}}{G_{eq}} \right)^{\eta} \end{aligned} \tag{4.12}$$

Furthermore, advise is given on the using surface to node discretisation, which allows more deviation between the master and slave nodes. The small sliding option in the interface allocation allows to speed up analysis because more assumptions could be made and the initial uniform clearance of $10^{-8}$ [mm] between the two surfaces could be defined. What is clear is that the VCCT slicing model to

predict crack behaviour with the VCCT requires a certain ratio between the $G_{I,c}$ from the intraply and the $G_{II,c}$ and the $G_{III,c}$ from the interply to allow numerical stability. This relation is dependent on the surface area of the neighbour elements. The relevant areas to be taken into account are illustrated in figure B.4. This hypothesis states that the total amount of energy through external work to release the next node in interply direction must be roughly equal to the required energy to release the next node in intraply behaviour. For the CT specimen provided in appendix B this was required as the most critical failure mechanisms needed to release nodes of the interply and intraply interfaces simultaneously. Some deviations from this ratio are allowed and those differences determine which failure happens slightly earlier, hence is the leading failure mode. Equation 4.13 describes the relation between the critical energy release rates that is dependent on the proportion between the contact areas.

$$\begin{aligned} &G_{I,c,intraply,n} b_{intraply,n} d_{intraply,n} \\ &= G_{II,c,interply,m} b_{interply,m} d_{interply,m} \\ &= G_{III,c,interply,m} b_{interply,m} d_{interply,m} \end{aligned} \tag{4.13}$$

Here the subscripts intraply and interply specify along which element surface it is defined. The roman numerals define which failure mode it is on an element level and the subscripts $n$ and $m$ define the order number of the node to be released along that interface surface.

For the fatigue analysis the same (critical) equivalent energy release rate could be used. These definitions are used to define the final failure point of the Paris law[9] in figure 2.7. The initiation is not defined by a ratio of equivalent energy release rates, but rather by a criterion that is an inverse Paris law equation[9] with different material parameters as is shown in equation 4.14 documented in the MIT manual[56].

$$f = \frac{N}{c_1 \Delta G^{c_2}} > 1 \tag{4.14}$$

$f$ is still the parameter that defines if the crack propagates, however neither the tolerance of the static analysis is applicable, nor that of the unstable crack growth. $c_1$ and $c_2$ are material constants that have to be defined empirically and have different values than $c_3$ and $c_4$ respectively. $\Delta G$ in [N/mm] is the effective energy release rate as the difference between the maximum and minimum energy release rates observed in the cycle caused by the loading. As $N$ is the number of cycles, the initiation criterion actually defines how many cycles are needed to reach initiation of the crack propagation. It is possible to omit the initiation criterion by leaving the parameters $c_1$ and $c_2$ blank. The crack propagation itself is defined according to a derivative of the Paris Law[9]. The version used is given in equation 4.17[56]. Although the initiation and the propagation criterion have a lot of resemblance, their purpose and values are different. The $c_3$ and $c_4$ values of equation 4.17 are the same as respectively $C$ and $b$ of equation 2.9. Advised values for $c_3$ and $c_4$ for the CT specimen are based on the findings of Liu et al.[61]. The values of their mode II failure are the most representative for the delamination of the CT specimen, because the delamination in the CT specimen is a shear failure. A conversion of units has to be made as Liu et al.[61] uses [J/m$^2$]. Since $1000$[J/m$^2$] $= 1$[N/mm], directly using Liu's parameters will result in a factor of $1000$ too low for the energy release rate if no conversion is performed. For that reason either the energy release rates have to be multiplied by $1000$ or the Paris law[9] has to be converted. For the latter the steps of equation 4.15 are performed. This leads to the expression in equation 4.16 for $c_3$ with $\Delta G$ in [N/mm]. $c_4$ is unaffected by the unit conversion, thus merely due to the change in definition $c_4 = m = 5.98$. Those result in $c_3 = 3.545 * 10^{-4}$ and $c_4 = 5.98$ with $\Delta G$ in [N/mm] and $\frac{da}{dN}$ in [mm/cycle].

$$\frac{da}{dN} = C(\Delta G_{J/m^2})^m = C(1000\Delta G)^m = C1000^m(\Delta G)^m \tag{4.15}$$

$$c_3 = 1000^m C = 1000^{5.98} * 4.07 * 10^{-22} = 3.545 * 10^{-4} \tag{4.16}$$

Also the boundaries between the first and the second stage could be changed by entering a different value for the ratio of the threshold energy release rate $G_{th}$ and the critical equivalent energy release rate $G_{eq,c}$. By default this values is $\frac{G_{th}}{G_{eq,c}} = 0.01$. The threshold value is defines a truncation value which determines if a cycle has significant influence on the propagation of the crack. Energy release rates below the threshold value are therefore omitted. An analogous definition is for the limit between the second stage and the third stage. This limit is given by the ratio of the plastic energy release rate $G_p$ and the critical equivalent energy release rate $G_{eq,c}$. The default value is $\frac{G_p}{G_{eq,c}} = 0.85$. The plasticity energy release rate indicates when stage III starts, hence defines when the Paris law[9] experiences progressive exponential growth till failure. The final (non-field) parameter that could be given is the temperature in which the specimen operates. It is not required to give a temperature as the analysis is not temperature dependent. A value of 20 [°C] is chosen as input to resemble room temperature.

$$\frac{da}{dN} = c_3 \Delta G^{c_4} \tag{4.17}$$

There is one major difference between providing input for the VCCT of the static and for the fatigue analysis. For the static analysis the interaction module of Abaqus[3] provides an input template provided by an interaction dialog box. For the fatigue analysis the input parameters have to be given directly in the keywords of the input file. The keywords have to be entered completely at the end of the fatigue step. For each interface the user has to add two lines of code. The first line is independent from the choice of mixed law, the second line is dependent on the choice of the mixed law. The template for the input lines is given in table 3.1. It is required to change the values between "<" and ">" with the intended value for the analysis or make it blank if it should not be taken into account. If not performed already, then additional lines have to be written in the keywords file. In the interaction properties section of the keywords the interaction properties have to be assigned to each interface according to lines 3 and 4 of table 3.1. Line 3 is required once per property and line 4 once per interaction. Similarly, for each interface a contact pair needs to be assigned in the interaction section according to line 5 of table 3.1.

Upon introducing the VCCT module in the next chapter to include the delamination, it is advised to keep the values for the static and the fatigue analysis equal for as many parameters as possible. In other words, the BK-law[28] will be chosen with critical energy release rates $G_{I,c} = 0.6$ [J/mm$^2$] and $G_{II,c} = G_{III,c} = 7$ [J/mm$^2$] and as exponent $\eta = 1$ for both the static and fatigue analysis. All other parameters have already been advised. An overview is given in table 4.3

There is still one step missing to let the VCCT criteria work correctly. Upon creating the interaction, it is highly recommended to define an initial bond set that has at least one node on each surface that is not bonded/selected. It is important that the nodes on which a boundary condition is applied do not take part in the bonded node set as an advise of Ramsaier[24]. Theoretically it is possible for Abaqus[3] to handle cases without a bonded node set defined and determine on its own where the crack starts accoridng to the MIT manual[56]. However, without such a set or a set with all the nodes of the interface included in the set, it will result in a overly strong response as it represents a perfect material with no existing crack tip. The set is defined as an ordinary set of nodes and in the creation of the VCCT for static hardening a separate tab allows the user to select the set. As a static analysis has to

be prior to the fatigue analysis to obtain the best results, the bonded node set will then also be applied in the fatigue analysis.

**Table 4.3:** Input table containing the suggested parametric values to be used for the static and fatigue simulations of the CT specimen model for the VCCT module.

| | VCCT static CT model | VCCT fatigue CT model |
|---|---|---|
| $f^{tol}$ [-] | 0.2 | |
| $c$ [-] (viscosity) | 0.1 | |
| $f_u^{tol}$[-] | Default | |
| Mixed mode | BK | BK |
| $G_{I,c}$ [J/mm$^2$] | 0.6 | 0.6 |
| $G_{II,c}$ [J/mm$^2$] | 7 | 7 |
| $G_{III,c}$ [J/mm$^2$] | 7 | 7 |
| $\eta$ | 1 | 1 |
| $c_1$ [-] | | Blank |
| $c_2$ [-] | | Blank |
| $c_3$ [-] | | 0.005 |
| $c_4$ [-] | | 3 |
| $\frac{G_{th}}{G_{eq,c}}$ [-] | | 0.001 |
| $\frac{G_p}{G_{eq,c}}$ [-] | | 0.9 |
| $T[^\circ$ C] | | 20 |

### 4.7.3. Effects of VCCT

The output will be the visualisation of the deformation and the bond status (BDSTAT). The deformation will show which nodes along the interaction surface will be separated allowing the crack to propagate. The bond status shows the similar result, but then in a colour plot. The blue colour indicates that the nodes are released and the red colour indicates which nodes are still connected. The colour green and yellow indicate the crack tip. In other words the release of nodes is the main output of the VCCT module. Other parametric output could be useful to better understand what is going on at the crack tip. Interesting parameters of the field output are first of all the energy release rate (ENNRRT) and effective energy release rate (EFENRRTR) that provides the value of the energy release rate at the crack tip. These values remain relatively constant once the crack starts to propagate. The bond time (DBT) and opening behind crack (OPENBC) are secondary parameters for some additional information.

The propagation rate of the VCCT could be anything according the user's definition of the Paris law[9] as there is no physical basis. Only the energy release rates are parameters that have physical meaning and origin. All other parameters are just to describe the phenomenological model. Hence the VCCT module must be based on experiments with input parameters isolated in the test. Then the VCCT could be used as an extensive calculator to inter- or extrapolate the test data.

Since the VCCT cannot be implemented in a model with only a single element, a elaborated investigation about the effects of the VCCT model will be performed in section 5.5.3 of chapter 5 on the CT specimen.

## 4.8. Hypotheses review chapter 4

### 4.8.1. Proofs to thirteen hypotheses listed section 4.2 of chapter 4

**Proof of hypothesis 4: If 10 iterations are used per load cycle for a force controlled analysis on a one element model, then equilibrium is reached for each load cycle.** Section 4.4.2 of chapter 4 showed that a forced controlled analysis on a one element has a converged solution at 10 iterations. This was confirmed by performing a force controlled analysis on a one element model that has 1 [mm] in all directions with a total force of 75 [N] on the element with a yield stress of 50 [MPa] and ultimate stress of 100 [MPa]. After ten iterations no more distinction could be plotted between the first and the last cycle which was expected to happen according to the plasticity theory of loading-unloading-reloading. After the loading in the first cycle all the unloading and reloading was performed elastically as is shown in figure 4.4. Since the shape of the yield contour is monotonically increasing for all the plasticity modules in all models, it will mean that 10 iterations are also enough for the other force controlled analyses of the one element model.

**Circumstantial proof of hypothesis 5: Using 2 iterations per load cycle for a displacement controlled analysis on a one element model that includes the plasticity and ductile damage model will result in an element response that is closest related to the input parameters of the plasticity model.** The displacement controlled analysis with an imposed displacement larger than 0.01 [mm] on a one element model with 1 [mm] in all directions that has a yield strain $\varepsilon_{y,0}$ of 0.01 [-] and an ultimate strain of 0.20 [-] will show repetitive degradation over the iterations if ductile damage is included as well as plasticity is shown in figure 4.5. As is described in section 4.4.2 of chapter 4 it is likely that Abaqus[3] makes its predictions based on the outcome of the previous iteration. That will cause an accumulate the plastic strain of each iteration since the displacement controlled analysis with $U_{max} > \varepsilon_{y,0}$ and $R = 0$ will result in having elastic and plastic response. For the force controlled analysis with $F > \sigma_{y,0}$ and $R = 0$ this is not a problem because the response will be only elastic after the first cycle.

**Proof of hypothesis 6: The direct cyclic analysis without cycle jumping with a displacement controlled fatigue loading will result in a sequence of half cycles with static loading for each half cycle.** If no cycle jump is present, then each cycle will be simulated explicitly as is shown in figure 4.3. The black line is a continuous line, therefore also defined for every time step. Since Abaqus[3] does not take into account the load history during the direct cyclic analysis, it will determine the new displacement field based on the previous displacement field and the changes on that displacement field as is explained in section 4.4.2 of chapter 4 . For that reason there is no difference in using the direct cyclic analysis without cycle jumping and modelling the fatigue with a series of half cycles.

**Proof of hypothesis 7: If the direct cyclic analysis is applied on a one element model with isotropic hardening for plasticity, which has a displacement controlled load with $R = 0$, 2 iterations per load cycle and no cycle jumping ($dN = 1$), then the stress-strain response will follow the loading-unloading-reloading principles of the plasticity theorem.** This has been illustrated in figure 4.11 with only minor discrepancies between the black line for the simulated model and the green dots for the hypothetical model. In section 4.5.3 of chapter 4 the hypothesis is explained for a similar problem as the one element model with only a difference in the maximum displacement. This situation is visualised in figure 4.12.

**Proof of hypothesis 8: If the direct cyclic analysis is applied on a one element model with the ductile damage included, which is loaded with a force causing a stress larger than the ultimate stress, then no equilibrium will be found in the degraded state leading immediately to full failure.**

This hypothesis could be reasoned as followed: the ductile damage model only allows the stress to decrease after ultimate stress, it can not find a resistance stress in any deformed state that is large enough to counter the applied stress. This is not shown on a single element model, but it could be proven by contradiction. If there was a stress large enough after the ultimate stress that could resist the force, then the new stress must be higher than every other stress before. In that case the ductile damage model must allow to describe a stress increase, but it is not able to that. Thus it is not possible.

**Proof of hypothesis 9: If the direct cyclic analysis is applied on a one element model with the ductile damage included, which is loaded with a displacement causing a strain larger than the crack initiation strain $\varepsilon_{ini}$ but smaller than the fracture strain $\varepsilon_f$, then a single equilibrium point will be found with a degraded stiffness.** By the definition of the ductile damage model this is clear. The ductile damage model has a decreasing strength branch after reaching ultimate stress. Ultimate stress is reached at the corresponding $\varepsilon_{ini}$ and zero stress will be reached at $\varepsilon_f$ which inquires full separation.

**Proof of hypothesis 14: If $\frac{C_n}{\gamma_n} = Q_\infty$ and $\gamma_n = b$, then isotropic hardening and kinematic hardening will results in the same response for the static loading on a one element model.** Since the one sided hardening is defined by equation 4.2 in section 4.5.2 of chapter 4, it is observable that the second and third term could be made equal for $n = 1$ by having $\frac{C_1}{\gamma_1} = Q_\infty$ and $b = \gamma_1$. This is also illustrated in figure 4.8. Hence it is possible to create equivalent kinematic and isotropic hardening for static loading.

**Proof of hypothesis 15: Increasing $\sigma_{y,0}$ will result in a longer fatigue life in a one element model with force or displacement controlled fatigue with $R = 0$.** It has not been investigated with Abaqus[3], but the plasticity theorem provides a quick answer. Based on hypothesis 7 it will also be true for the simulation of Abaqus[3] as well. For the displacement controlled analysis it is trivial as higher yield stress means longer elastic response, therefore less force is applied in the plastic zone, thus less plastic strain. The less plastic strain is accumulated each cycle, the longer it takes to reach ultimate stress. In a force controlled analysis it is not that much the amount of plastic stress, but rather the probability that plasticity is initiated. A higher $\sigma_{y,0}$ reduces the probability, which generally means a longer fatigue life as the material is able to take higher stress in structures with multiple elements.

**Proof of hypothesis 16: Increasing $E$ will result in shorter fatigue life in a one element model with displacement controlled fatigue with $R = 0$.** If only $E$ changes and $\varepsilon_{ult}$ is kept equal, then the amount of elastic strain reduces. That leads to more plastic strain for each cycle, thus faster plasticity accumulation. An analogous explanation is by stating that the branch of elastic response becomes steeper, thus a larger stress range is required to obtain the same strain.

**Circumstantial proof of hypothesis 17: Increasing $\nu$ will result in an equal long fatigue life in the one element model, with displacement controlled fatigue and $R = 0$, that has no redundant boundary conditions.** The boundary conditions of the one element model allow free movement in transverse direction as is shown in figure 4.1. That implies that no forces will be caused by the boundary conditions. If the one element model with no redundant boundary conditions is compared to a one element model that has redundant boundary conditions transverse to the load, then transverse forces will be present. The lack of these transverse reaction forces mean less stress. Therefore a slower plastic strain accumulation is present, thus higher fatigue life is achieved.

**Proof of hypothesis 18: Increasing $Q_\infty$ will result in longer fatigue life in a one element model with a force or displacement controlled fatigue with $R = 0$.** Analogously as for hypothesis 15. For the force controlled analysis there is a higher probability to have a force lower than the ultimate stress. A higher probability means generally a longer fatigue life as it is able to take more stress in

structures with multiple elements. This is especially true upon noticing that the unloading and reloading happens elasticly as is shown in figure 4.4. This has been investigated in early models where a range of different values for $Q_\infty$ in the range $[-50, 50]$ were investigated with different $b$ in the range $[0, 100]$. The applied yield stress was $\sigma_{y,0} = 50$ [MPa] and the load was in the range from 0 [MPa] to 75 [MPa]. The number of iterations was still kept on 1 even when it was a force controlled analysis. It showed that increasing $Q_\infty$ increased the fatigue life. There were no strange domain restrictions found. Failure is defined when Abaqus[3] was no longer able to find a converged answer which is in the case that $\sigma_{y,0} + Q_\infty(1 - e^{-b\varepsilon^p_{eq}}) \approx 0$, which happens faster if $Q_\infty$ decreases under a threshold value of $Q_\infty < -\sigma_{y,0}$. Negative values would not be obtainable. Do keep in mind that due to the number of iterations being equal to 1, the implicit solver has partly become an explicit solver. The results had to be taken with caution as the negative loads in the model indicated that equilibrium had not been achieved.

**Proof of hypothesis 19: Increasing $b$ will result in shorter fatigue life in a one element model with displacement controlled fatigue with $R = 0$.** Higher values for $b$ would mean that less plastic strain is required to reach the ultimate stress. Thus even with a constant strain accumulation rate, the number of cycles would decrease as the total strain required to reach ultimate stress decreases. In early models it has been investigated what would happen if the value $b$ was changed in a range $[0, 100]$ for different $Q_\infty$ in the range $[-50, 50]$. The applied yield stress was $\sigma_{y,0} = 50$ [MPa] and the load was in a range from 0 [MPa] to 75 [MPa]. The number of iterations was still kept on 1 even when it was a force controlled analysis. It confirmed that increasing $b$ decreased the fatigue life. There were no strange domain restrictions found. Failure is defined when Abaqus[3] was no longer able to find a converged answer which is in the case that $\sigma_{y,0} + Q_\infty(1 - e^{-b\varepsilon^p_{eq}}) \approx 0$ and which happens faster if $b$ increases. Negative values would not be obtainable. Do keep in mind that due to the number of iterations being equal to 1, the implicit solver has partly become an explicit solver. The results had to be taken with caution as the negative loads in the model indicated that equilibrium had not been achieved.

**Circumstantial proof of hypothesis 20: Increasing $\eta$ or $\dot{\varepsilon}$ will not alter the results in the one element model or the compact tension specimen model with a force or displacement controlled fatigue analysis.** In early models it has been investigated what would happen if the value $\eta$ or $\dot{\varepsilon}$ was changed in the range $[-1, 1]$ and the range $[-5, 5]$ respectively. The applied yield stress was $\sigma_{y,0} = 50$ [MPa], the stress increase $Q_\infty = 50$ [MPa], the stress convergence speed $b = 100$ and the load was in a range from 0 [MPa] to 75 [MPa]. The number of iterations was still kept on 1 even if it was a force controlled analysis. No change was observed which proves the idea that the analysis is pressure and rate independent as it should be for composite fatigue.

### 4.8.2. Eight newly posed hypotheses as a result of chapter 4

Based on the hypotheses of the one element model a lot of new hypotheses are formulated for the compact tension specimen.

**Hypothesis 21: If cycle jumping is enabled for the compact tension specimen with a ductile damage model and VCCT model included and the load leads to a local stress higher than the ultimate stress, then the damage obtained during cycle $n - x$ will be extrapolated $x$ times to obtain cycle $n$.** It is expected that Abaqus[3] is able to extrapolate damage as it states "forward damage extrapolation". It will be investigated in chapter 5 if that is the case.

**Hypothesis 22: If the element size is refined from 2 [mm] to 1 [mm] in a composite compact tension specimen model that has either VCCT or tie interactions, the fatigue life will not change more than a few percent due to the mesh refinement.** A nominal element size of 2 [mm]

evenly spread already creates two elements along the height of the crack, five in the width of the crack and fifteen elements along the length of the crack. This is already a lot of elements. Also the input parameters are not element size dependent as these are normalised to the element size. However, there is no definitive answer to this question until the simulation has been performed. There is a mesh refinement study performed in chapter 5.

**Hypothesis 23: If the element size is refined from 2 [mm] to 1 [mm] in a composite compact tension specimen model that has either VCCT or tie interactions, the transition from stage I to stage III will not change more than a few cycles due to the mesh refinement.** A nominal element size of 2 [mm] evenly spread already creates two elements along the height of the crack, five in the width of the crack and fifteen elements along the length of the crack, which is already a lot of elements. The question now is, will the first element break faster if the size is smaller. On the one hand yes, because smaller elements will also have smaller fracture energy. On the other hand, the plastic response will not be changed that much. The plasticity would allow to spread the forces already to the other neighbouring elements as it would already do with 2 [mm] elements. Since the plasticity model is dominating in the first stage of the compact tension specimen, this would result in little change in the number of cycles till failure. Only a slight increase in the fatigue life is observed, since the element is less able to release energy during the ductile damage model after reaching the ultimate stress. However, there is no definitive answer to this question until the simulation has been performed. An circumstantial proof will be provided in chapter 5.

**Hypothesis 24: Loading the compact tension specimen with a fatigue load in the direct cyclic analysis will result in a crack propagating in the weakest direction of the ply.** The VCCT module will not make a distinction in direction whether the in-plane shear is left-right or up-down. On the contrary, the plies will do as these have orthotropic stiffness. As the strength is still isotropic, it will be in the stiffest direction of the ply as a higher stiffness attracts more stress, thus the ultimate stress is reached sooner. This hypothesis will be investigated in chapter 5.

**Hypothesis 25: Changing the material properties has the same effect on the fatigue life of a compact tension specimen as on the one element model with a displacement controlled analysis.** Increasing the fatigue life for each element will also increase the fatigue life of the total structure. This hypothesis will be tested in chapter 5.

**Hypothesis 26: Increasing a critical energy release rate ($G_{I,c}$, $G_{II,c}$ or $G_{III,c}$) will increase the fatigue life**. If the critical energy release rate is increased, then the interface is able to dissipate more energy. That will result in less energy required to be dissipated by the elements, thus a slower crack propagation. A slower crack propagation means a longer fatigue life. Also increasing the critical energy release rate means that the crack through the interface will be longer in the second stage of the Paris law. The longer it is in the second stage, the longer it will be stable which in its turn results in longer fatigue life.

**Hypothesis 27: Increasing $c_3$ will decrease the fatigue life.** Increasing $c_3$ of the Paris law curve will increase the propagation speed, thus it takes less time for the crack to run through the compact tension specimen. Therefore it will result in less fatigue life.

**Hypothesis 28: Increasing $c_4$ will increase the fatigue life if $G_{eq} < 1$ for each node.** If the effective energy release rates are lower than 1, then a larger $c_4$ will result in a slower crack propagation, thus longer fatigue life. If the effective energy release rates are larger than 1, then a larger $c_4$ will result in a larger crack propagation rate, thus a shorter fatigue life.

## 4.9. Conclusion chapter 4

The values of the parameters used in the one element model are found in table 4.1 for the plasticity module and in table 4.2 for the ductile damage module. The VCCT is not implemented in the one element model as the one element model only contains one element. For the CT specimen models that will be discussed in chapter 5, table 4.3 provides literature values of the VCCT module with the second column for the static load step and the third column for the direct cyclic load step.

For the one element model with load amplitudes leading to plastic response it is possible to adjust the fatigue life. When in need of improving the fatigue life of the one element model, it could be increased by increasing one of the following parameters ordered in decreasing influence: $G_f$, $\varepsilon_f$, $\varepsilon_{ult}$, $\sigma_{ult}$. Changing $\sigma_{y,0}$ and $E_2$ only has influence on small prescribed displacements that are around the yield strain, for those it could mean the difference between a fully elastic response and a little plastic response that will accumulate each cycle. Another option to increase the fatigue life, if allowed, is by decreasing the applied load.

As the one element model is only capable of taking into account the plasticity model and the ductile damage model, the delamination can not be included. With only one element present, there is only one clear distinction between stage I and III. As soon as damage starts, it has entered stage III and its residual strength starts to reduce as is clear in figure 3.14. Thus the first stage finishes and the third stage starts as soon as the SDEG parameter becomes larger than zero. The output of the plasticity model has been verified by the prediction made with the hypothesis of plasticity, which was calculating with a Python[58] script added in appendix A. This indicates that the fatigue analysis is merely a sequence of static cycles.

Since the residual stiffness is related to the stiffness degradation parameter, which is a damage parameter, this is inherently related to the residual strength. The derivative of this damage parameter is relatable to a Paris law that describes the entire model with all its fatigue failure mechanisms as one formulation. The damage parameter will keep increasing exponentially till it reaches the value one.

For the one element model it is assumed that a single element represents the entire compact tension specimen. Also it is assumed that the fatigue load is applicable on every node at the top with only the vertical forces and stresses present as the horizontal movements are free to allow contraction. This is an oversimplification of the reality.

# Chapter 5: Upgrading the one element model

## 5.1. Introduction

In chapter 4 a model for a single element was developed with a plasticity module and a ductile damage module to mimic the fatigue behaviour in composites. Now it is time to upgrade the model step-by-step in order to fulfil the requirements that were set in chapter 1. It is easier to explain what the influence of the upgrade is when it is comparable to another directly related output. The order of improvements is defined to keep it as simple as possible to understand the effects of each individual upgrade. The step-by-step approach has also been taken to identify which upgrade causes problems. The steps taken for upgrading the model are:

1. Changing to the orthotropic material properties: composite laminates are distinctive for their orthotropic material properties. As it is also possible to test the applicability of the orthotropic stiffness in a one element model, it is investigated first.
2. Changing to the brittle material properties: in contrast to metals, composites behave in a brittle manner. As the ductile damage module is developed for ductile materials, some problems may arise upon changing the parameters to represent the brittle material. However, as it is still possible to test it on a one element model, it is checked as second.
3. Changing to the compact tension specimen (CT specimen) geometry: as the upcoming investigations require multiple elements, it is time to investigate what happens if the one element model is changed to a single layer compact tension specimen with multiple elements.
4. Including the cycle jumping: since more elements slows down the calculations, the cycle jumping helps to speed up the analysis. What would happen if cycle jumping was enabled? As cycle jumping is dictated by the user, that would definitely accelerate the analysis. Therefore cycle jumping is performed first.
5. Change to automatic incrementation: in order to speed up the analysis even further, would Abaqus[3] assign itself larger increments on less critical moments and smaller increments on more critical moments?
6. Change to multiple plies with tie constraints: as the analysis has now been sped up, it is possible to introduce more plies without waiting endlessly on the result. Tie constraints were chosen initially as these are simple to introduce and require less computational effort as there are less possibilities to crack.
7. Multiple plies with VCCT constraints: now it is time to investigate whether the full intended model is able to perform a fatigue analysis in a composite compact tension specimen that includes all three main mechanisms that were observed in tests.

During the upgrades only the upgrade changes the model. All other input is kept equal to the previous discussed model unless explicitly told differently.

Despite that no calibration of the model is performed on experimental results, some validation is still done by performing sanity checks to see if the model has the potential of modelling fatigue behaviour in composites. These checks question the plausibility of the crack pattern, the level of maximum stresses, the stress intensity factor and the fatigue life compared to other simulations done before. After the checks are completed other similar questions as for the one element model could be asked. For example, since the model has multiple elements it is interesting to know how entering a new stage is defined. Also how does the model relate to the Paris law? These two questions in itself are a part of the sanity check to see if the model still performs as it is supposed to do. Finally, which parameters have the most influence on the behaviour of the fatigue life?

## 5.2. Eleven hypotheses that will be answered in chapter 5

Chapter 5 will give answer to eleven hypotheses. These hypotheses will be answered in section 5.8.1 of chapter 5.

**Hypothesis 10: If the direct cyclic analysis is applied on a one element model with the plasticity model, then no plasticity will be extrapolated during the cycle jumping.**

**Hypothesis 11: If the direct cyclic analysis is applied on a compact tension specimen with the ductile damage included, which is loaded with a displacement or force causing the stress in an element to be larger than the ultimate stress, then it transfers its burden of load to its surrounding elements in order to find equilibrium.**

**Hypothesis 13: Using the plasticity model for the inter fibre fracture will result in an overclosure of the crack due to the plastic deformation which is not present in reality.**

**Hypothesis 21: If cycle jumping is enabled for the compact tension specimen with a ductile damage model and VCCT model included and the load leads to a local stress higher than the ultimate stress, then the damage obtained during cycle $n - x$ will be extrapolated $x$ times to obtain cycle $n$.**

**Hypothesis 22: If the element size is refined from 2 [mm] to 1 [mm] in a composite compact tension specimen model that has either VCCT or tie interactions, the fatigue life will not change more than a few percent due to the mesh refinement.**

**Hypothesis 23: If the element size is refined from 2 [mm] to 1 [mm] in a composite compact tension specimen model that has either VCCT or tie interactions, the transition from stage I to stage III will not change more than a few cycles due to the mesh refinement.**

**Hypothesis 24: Loading the compact tension specimen with a fatigue load in the direct cyclic analysis will result in a crack propagating in the weakest direction of the ply.**

**Hypothesis 25: Changing the material properties has the same effect on the fatigue life of a compact tension specimen as on the one element model with a displacement controlled analysis.**

**Hypothesis 26: Increasing a critical energy release rate ($G_{I,c}$, $G_{II,c}$ or $G_{III,c}$) will increase the fatigue life**.

**Hypothesis 27: Increasing $c_3$ will decrease the fatigue life.**

**Hypothesis 28: Increasing $c_4$ will increase the fatigue life if $G_{eq} < 1$ for each node.**

## 5.3. Improvements in material properties

### 5.3.1. Orthotropic material stiffness properties

The composite material is laid in different layers of fibre direction. Fibres cause the material to be stronger and stiffer in one direction. In order to model the composite material correctly, it is required to introduce the difference in material direction. As such the isotropic properties that are defined in the elastic module of the material properties have to be altered. Although there is an option lamina present for laminates, the orthotropic property formulation is chosen for its freedom to model a quasi-isotropic layer.

The values for the first direction are evident as tests have already been performed for the tensile coupon testing. These test results were already shown in figure 3.6. From these test results a stiffness of $E_1 = 12285$ [MPa] is obtained in accordance with ISO-norm 527[45]. The corresponding Poisson's ratio is found to be at $\nu_{12} = 0.35$. For now it is assumed that the material could be modelled as an unidirectional layer. All other material properties are at a reduced value of these two properties for unidirectional layers. The longitudinal stiffness in second and third direction are matrix dominated as it is loaded perpendicular to the fibres. Therefore a value of $E_2 = E_3 = 3000$ [MPa] is estimated as being roughly a quarter of $E_1$. $E_2$ and $E_3$ will approximately be equal as long a fibres are laid in one direction (unidirectional) for the fibre layer. If woven fabrics are used, then the value of $E_2$ ought to be approximately the value of $E_1$ as the fibres perpendicularly will have the same effect one ply-level as the longitudinal fibres. The direction difference in the properties makes that the analysis will be direction dependent. Therefore it is also required to assign a material orientation to define the first direction of the fibres.

The Poisson's ratio's in the other directions will roughly be the same, only in-plane transverse loading will have a slightly higher ratio as the longitudinal fibres pulled in transverse direction will cause the matrix to deform larger in longitudinal direction of the fibres. As the latter is known from testing to be $\nu_{12} = 0.35$, the other two Poisson's ratios are estimated at $\nu_{13} = \nu_{23} = 0.3$. The Poisson's ratios also have an effect on the shear stiffness just as in isotropic materials. Whereas the Young's modulus is fibre dominated, the shear is matrix dominated. Hence the values are considered to be low and even lower in the shear stiffness out of plane for transverse in-plane loading as the fibres have least influence in that direction. Therefore the values are set at $G_{12} = G_{13} = 2000$ [MPa] and $G_{13} = 1000$ [MPa] for the CT modelling. The overview for all these parameters is given in table 5.1.

A displacement controlled fatigue analysis has been performed on the one element with the boundary conditions provided in figure 4.1. The range of the displacement was set at $0.0065$ [mm] as maximum and $0$ [mm] as minimum. The results of including the orthotropic material properties in the one element model are provided in figure 5.1.

Some change was expected, but not exactly all of these changes. The prediction model did good in describing the first $25$ cycles. Upon the $25^{th}$ cycle in theory the ultimate stress of $24.57$ [MPa] is surpassed or better stated: its corresponding ultimate plastic strain of $0.21$ [-]. In the plasticity module prediction this concludes in failure, thus it responds with a zero response after the $25^{th}$ cycle. For the FEM analysis it is the moment that the fibre failure starts with the ductile damage module. This is already observed in the last graph in which the stiffness degradation parameter starts to rise after eighteen cycles.

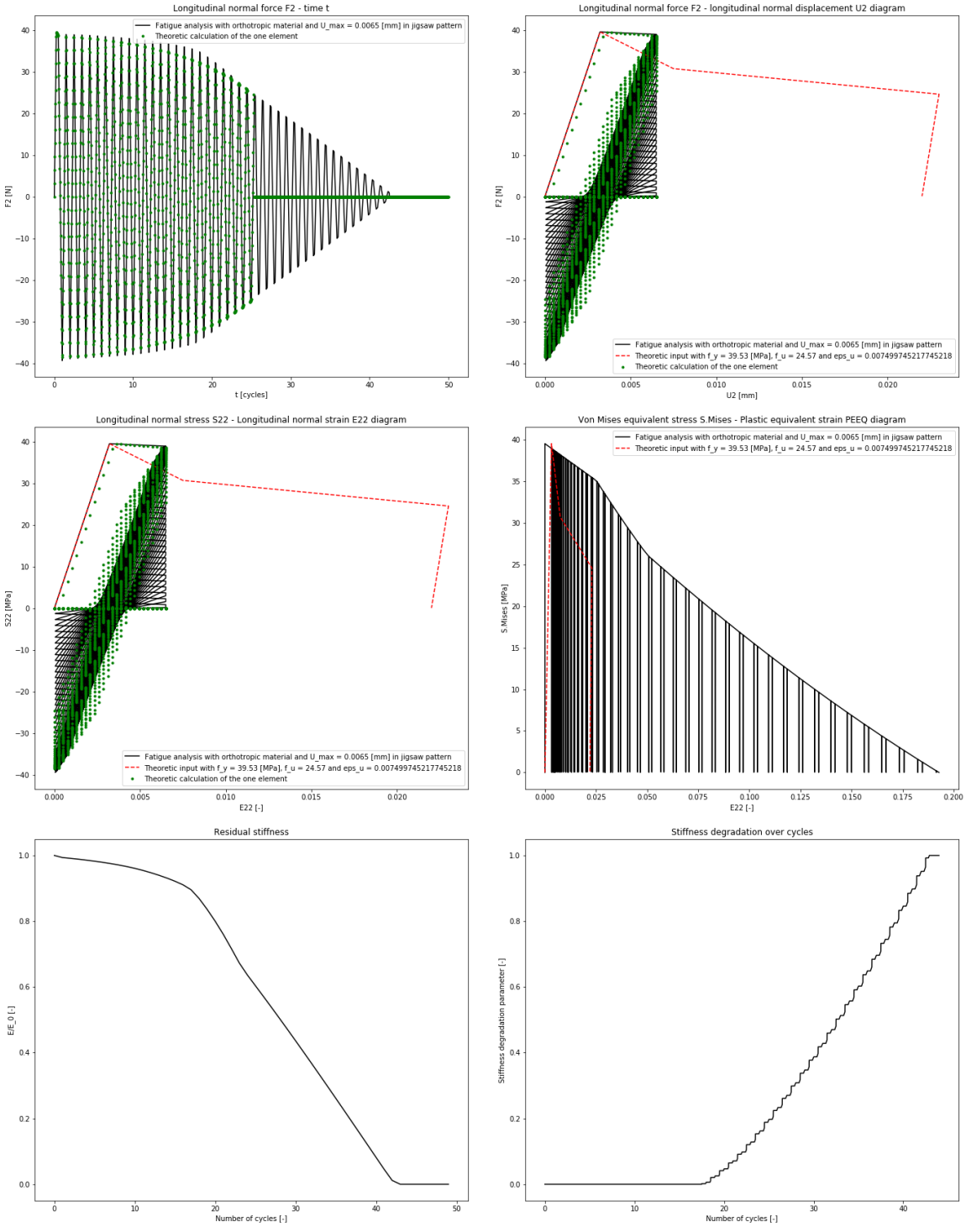


**Figure 5.1:** In six plots the output is represented of the one element model for a fatigue analysis with an applied displacement of 0.0065 [mm] failing after 42 cycles. The input of the model is given in table 5.1. The black lines is the result of the analysis and the green line is the prediction of that result using a Python[58] script for isotropic softening. Counting from left to right and from top to bottom, the load history plot is given first. This plot shows the applied force as resultant of a constant applied displacement amplitude function. The second plot is the force-displacement diagram which acts as hysteresis plot of the element as structural response. The third shows that in terms of stresses and strains showing the element's internal response which is equal to plot 2 due to the unit size of the element. The fourth plot shows the plastic equivalent strain versus the Von Mises stress to see if it relates to the input parameters given in a red dotted line. The fifth plot shows the stiffness of the structure relative to the response of the first cycle and the sixth figure shows the value of the damage parameter that leads to stiffness degradation (0 equals no damage and 1 equals fully damaged).

**Table 5.1:** The input table containing the parametric values used in the elasticity module to include the orthotropic behaviour of composite for the one element model and for the CT model. Also some changes were made in the ductility of the model such that more stability is present.

| | |
|---|---|
| $E_1$ [MPa] | 12285 |
| $E_2$ [MPa] | 3000 |
| $E_3$ [MPa] | 3000 |
| $\nu_{12}$ [-] | 0.35 |
| $\nu_{13}$ [-] | 0.30 |
| $\nu_{23}$ [-] | 0.30 |
| $G_{12}$ [MPa] | 2000 |
| $G_{13}$ [MPa] | 2000 |
| $G_{23}$ [MPa] | 1000 |
| $\sigma_{y,0}$[MPa] | 39.53 |
| $\sigma_{y,1}$[MPa] | 30.7125 |
| $\varepsilon^p_{y,1}$[-] | 0.05 |
| $\sigma_{ult}$[MPa] | 24.57 |
| $\varepsilon^p_{ult}$ [-] | 0.21 |

What is positive to observe is that the stiffness degradation starts gradually at the beginning, but at the point the ductile damage model kicks in, it reduces drastically just as is observed in preliminary fatigue tests of the joint. All in all, these results look very promising to model the inter fibre failure with a plasticity module and the fibre failure with a ductile damage module.

### 5.3.2. Brittle material properties

The brittle material property parameters of the plasticity module and ductile damage module were in the end directly implemented into the compact tension model with one ply. The material properties for the ductile damage module made by He[52] were already discussed in section 4.6 of chapter 4. In short, these parameters are based on the calibration of the static model for preliminary static tests of the joint. These are currently the most representative values available for the parameters and are certainly brittle material properties. The plasticity material properties were derived from the static coupon test shown in figure 3.6 that were investigated by He[43]. However, entering the values from figure 3.6 with converted values for the strains according to equation 4.4 in a tabular form, resulted in compatibility problems with the ductile damage model. This happened because the tabular form was too limited and could not handle the cutbacks present in the plastic strain. Therefore an extrapolation of the results was needed. For that reason and other reasons given in section 4.5 of chapter 4 the parametric formulation of hardening is used. The plasticity parameters are calibrated to represent the tabular form as accurate as possible as shown in figure 4.10. Table 5.2 provides a copy of the used parameters for the ductile damage module and the plasticity module.

**Table 5.2:** The input table containing the parametric values used in the CT model for the brittle material properties of the ductile damage module and the plasticity module.

| | |
|---|---|
| $Q_\infty$[MPa] | 250 |
| $b$[-] | 300 |
| $\varepsilon_f$ [-] | 0.0052 |
| $\eta$ [-] | 0.33333 |
| $\dot{\varepsilon}$ [-] | 1 |
| $G_f$ [N/mm] | 25 |

## 5.4. Upgrading the one element model to compact tension specimen

### 5.4.1. Compact tension geometry with one ply

As the material properties are set, it is time to increase the size of the model from one element to the full compact tension specimen geometry with multiple elements. The geometry is illustrated in figure 5.2. The CT specimen is $70$ [mm] in height, $90$ [mm] in length and $1.125$ [mm] in thickness for a single ply. The four corners are cut off with $15$ [mm] in vertical direction and $20$ [mm] in horizontal direction. A cut-out with a round tip in the centre of the left edge has a height of $4$ [mm] and a length of $27$ [mm]. Including the radius of $2$ [mm] of the round tip at the end of the crack creates a precrack of $29$ [mm] in total. The CT specimen is loaded by two pins for which the holes are symmetrically placed along the horizontal symmetry line. The offset from the centre of the hole is $14$ [mm] to the left edge from the centre and $13$ [mm] from the centre of the hole to the horizontal symmetry axis. The holes themselves have a radius of $4$ [mm]. The meshing is done in Abaqus[3] using the standard mesh algorithm. No partitions were made to ensure a symmetric meshing. A mesh with the medial axis option and hexagonal elements only provided a more or less symmetric mesh with smooth transitions. The intended mesh size was $2$ [mm], which aided the possibilities of smooth transition of the contours of the specimen. In total there are $1206$ [elements] 3D stress elements used. The default choices are taken with exception of the element deletion. The element deletion is explicitly turned on, so not left as default. In a later performance these elements could be enhanced by using continuum shell elements for a better modelling of the out-of-plane behaviour (buckling). The mesh is illustrated in figure 5.3 with the applied boundary condition. The material orientation will have its local first axis parallel to the horizontal symmetry axis and its second axis in vertical direction in parallel to the height of the CT specimen.

The boundary conditions are applied in the pins. Luckily the areas around the pins are not the most critical, hence the modelling of the embedment strength is not necessary. Thus it is allowed that the forces applied in the pins are transferred to the CT specimen by coupling the pin to the surfaces in the radial direction to the surrounding elements. This is done by setting up a reference point in the centre of the pin and use that as master node for the coupling. The slave surface is set to be the surrounding surface of every ply which makes the nodes on that surface to move in the same direction as the reference point. Thus the nodes move with the pin. Only the translations need to be transmitted as the rotations must be allowed if continuum shell elements are used. For the 3D stress elements is does not matter if the rotations are transferred since there are no bending degrees of freedoms in the 3D stress element. In the reference points there are three sets of boundary conditions applied. One set is put in place as the initial conditions and will continue throughout the entire analysis. The additional boundary conditions are step specific. The overview of the boundary conditions that is required are given in table 5.3. The lower pin will be restricted in all degrees of freedom except for the rotation in the third axis (out-of-plane). Since the pin will be clamped in the testing machine, it will eliminate the possibility for the pin to move in any

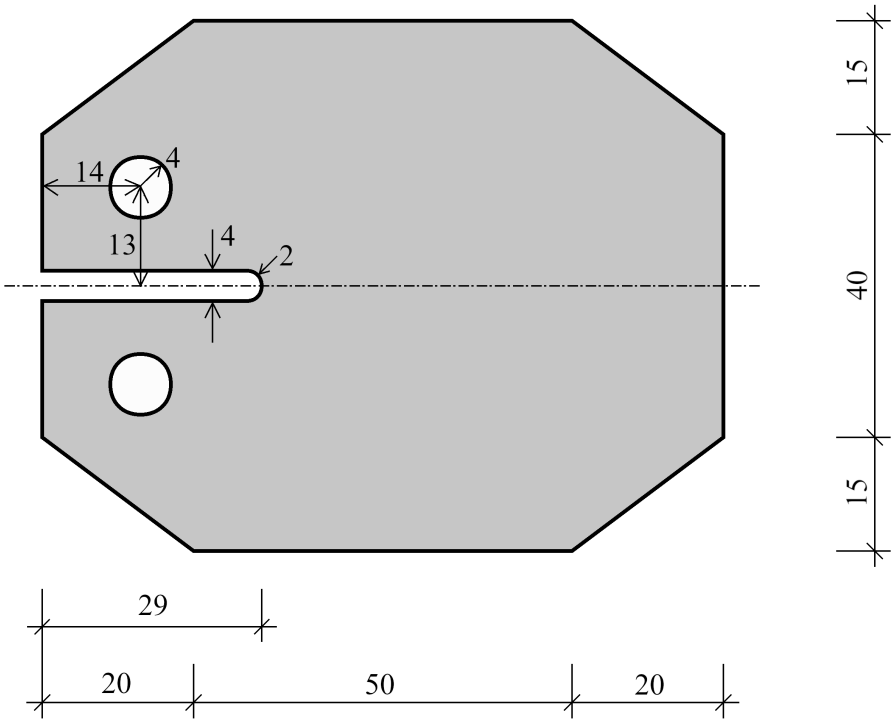


**Figure 5.2:** The geometry of the CT specimen with tapered corners. Scale is 1:1 on A4 with measurements in [mm]. The design is from the wFRP group to be used as the test specimen for fatigue. The thickness of a single ply in the model is $1.125$ [mm], the test would then have five layers to make a total thickness of $5.625$ [mm].

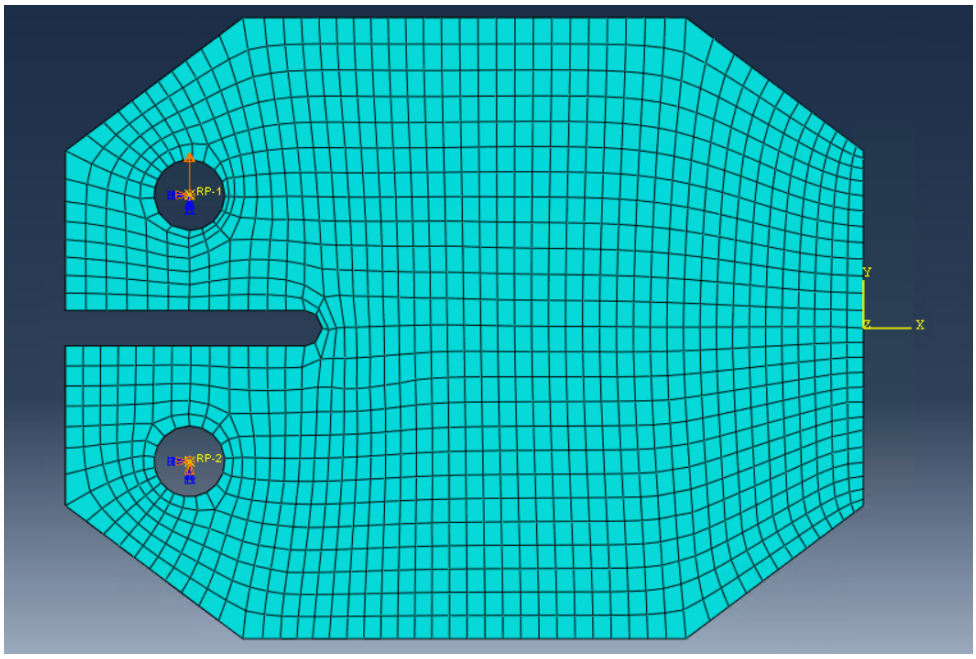


**Figure 5.3:** The mesh of a single layer of the CT specimen obtained by a global mesh size of 2 [mm], medial axis and hexagonal elements only. If multiple layers are used in further upgrades, then in the other layers have the same mesh. The boundary conditions from table 5.3 are applied in the holes showing the constrained degrees of freedom in both of the holes and the applied prescribed displacement in the top hole. The boundary condition in the centre of the hole are coupled with the degrees of freedom of the nodes of the surrounding elements. The coordinate axis indicates the material orientation with x-axis for the first direction of the material and the y-axis the second direction of the material. The third direction is perpendicular, therefore it is out of plane.

direction. However, the CT specimen could rotate around the pin, therefore $R_3 \neq 0$ [mm]. A similar situation is existing in the top, however this pin will be moved in vertical direction by the machine during the fatigue analysis. Hence in the initial conditions also the vertical translation must not be hindered as boundary conditions are passed on to the next step unless explicitly programmed otherwise. Therefore $U_2 \neq 0$ [mm] and all remaining boundary conditions are: $U_1 = U_3 = R_1 = R_2 = 0$ [mm]. In the static step (second step) only an additional boundary condition is applied on the top pin. The displacement is described for the first half cycle by defining the displacement of the top pin at $U_2 = 5$. However this is not done instantaneously as it is still part of the fatigue analysis in general, hence intermediate results have to be produced. This is done by providing the amplitude definition according to figure 4.2. The required step time is $0.5$ [s] which is exactly enough to complete the first half cycle. The amplitude that corresponds to it is provided in a tabular form. This tabular form is given in the second column of table 5.4. For the intermediate increments a linear interpolated value of the nearby values is used. This is required because Abaqus[3] is likely to cut the corner if not enough intermediate values are defined in the tabular form. This reduces the amplitude range up to $15\%$ as is shown in figure 5.4. For linear tabular form the default option of ramp could also have been chosen, but if a fatigue analysis with a dependency on time is modelled, it has to be defined in this manner. The succeeding direct cyclic analysis will have the prescribed displacement of the first half cycle disabled and a new prescribed displacement with an amplitude function enabled. Although $U_2 = 5$ [mm] still holds, the amplitude definition has to be inverted as the start time will be at $0.5$ [s] due to the static step. This inverted amplitude definition is given in the third column of table 5.4. The total amount of displacement that is applied will be the prescribed displacement times the given amplitude from the increment according to the amplitude definition. This definition is summarised in equation 5.1 for cycle $k$.

**Table 5.3:** The boundary conditions applied on the compact tension specimen for the fatigue analysis containing a static step for the first half cycle and a direct cyclic analysis to carry out the rest. Empty cells indicate the degree of freedom is free to move (unrestrained). All boundary conditions are propagated from the previous step, except for the applied displacement of 5 [mm], that one is imposed twice in total.

| | Initial boundary conditions | | Static boundary conditions | | Fatigue boundary conditions | |
|---|---|---|---|---|---|---|
| | Upper pin | Lower pin | Upper pin | Lower pin | Upper pin | Lower pin |
| $U_1$ [mm] | 0 | 0 | 0 | 0 | 0 | 0 |
| $U_2$ [mm] | | 0 | 5 | 0 | 5 | 0 |
| $U_3$ [mm] | 0 | 0 | 0 | 0 | 0 | 0 |
| $R_1$ [rad] | 0 | 0 | 0 | 0 | 0 | 0 |
| $R_2$ [rad] | 0 | 0 | 0 | 0 | 0 | 0 |
| $R_3$ [rad] | | | | | | |

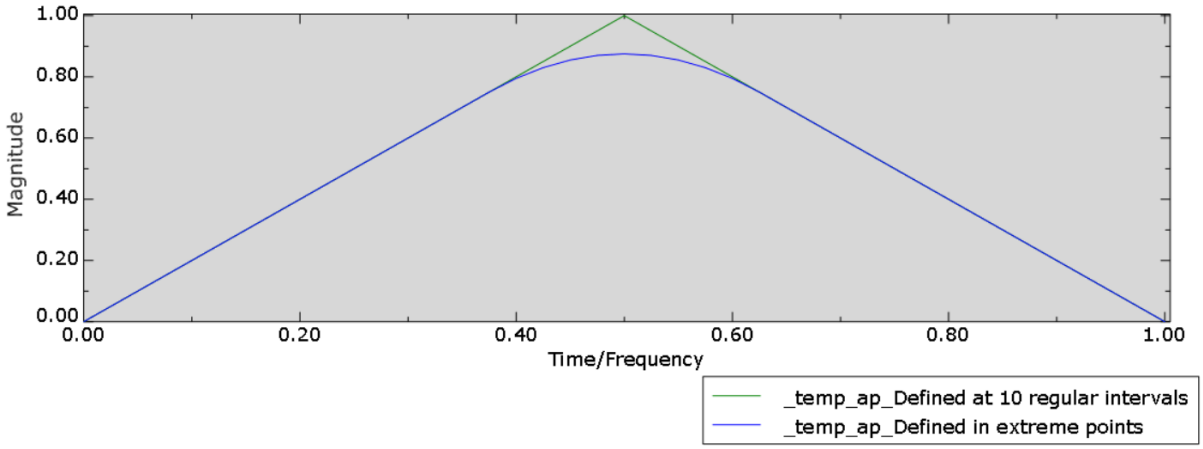


**Figure 5.4:** The applied amplitude definition according to the amplitude plotter in Abaqus[3]. The green line is the intended amplitude and is accurately obtainable by defining the amplitude every 0.1 [s] in the tabular form. If only the extreme values are defined in the tabular form (every 0.5 [s]), then the blue line is obtained as applied amplitude. Note there is a discrepancy of about 15% at 0.5 [s] which will have a large influence as the maximum tensile load is the most detrimental for the fatigue analysis.

$$U_{applied} = U_2 A_{(t)} = 5 \begin{cases} 2(t-k), & \text{if } (t-k) < 0.5 \\ 1 - 2(t-k), & \text{otherwise} \end{cases} \tag{5.1}$$

The output of the model is best described by its crack pattern shown in figure C.1 and the four graphs shown in figure C.2 of appendix C. Figure C.1 shows that the crack pattern starts under an angle of 45 [°] in both directions, but very soon becomes 90 [°] vertical. This is perpendicular to the fibre orientation. As the stiffness in first direction of the material is much higher than the other two material directions, it will also attract more stresses in that direction. As the ductile damage module neither makes a distinction between the different failure modes (I, II or III), nor between the differences in strengths of the material for the different directions, it will treat it as if the longitudinal strength equals the lateral strength. The element in the crack tip fails due to the vertical orientation of the main principal stress. However, after the first element has failed, the other elements fail due to their higher stiffness in the first direction. Now the stress has to go around the element. This increases the stress in the surrounding elements. The element above it is effected the most, because it is at the crack tip now and its first direction spans the crack opening. In other words, its first direction is perpendicular to the crack formation, which increases the stresses in the element even further. This process repeats itself until the

**Table 5.4:** Input values for the tabular form of the amplitude definition function. The first column is to define the time $t$ on the x-axis of the plot in seconds. The second column is the base amplitude function definition used in the static analysis for the first half cycle (FHC). The third column is the inverted amplitude definition of the amplitude function for the FHC as do to the step time the amplitude has shifted with $0.5$ [s].

| $t$ [s] | $A_{FHC(t)}$ | $A_{FAT(t)}$ |
|---|---|---|
| 0 | 0 | 1 |
| 0.1 | 0.2 | 0.8 |
| 0.2 | 0.4 | 0.6 |
| 0.3 | 0.6 | 0.4 |
| 0.4 | 0.8 | 0.2 |
| 0.5 | 1 | 0 |
| 0.6 | 0.8 | 0.2 |
| 0.7 | 0.6 | 0.4 |
| 0.8 | 0.4 | 0.6 |
| 0.9 | 0.2 | 0.8 |
| 1 | 0 | 1 |

last elements breaks. The top element breaks with the last element in the crack since the bending moment causes large compression stresses in the top element. Since the model is not able to distinguish between the compressive and the tensile strength, both elements will fail simultaneously. This is not true in reality where the strength in fibre direction is the stronger direction and tensile strengths in composites being much higher than the compressive strengths. This directional strength difference between the first and second direction is much higher than the relative stiffness difference. In other words, the ratio of the strength in first direction over the second direction $\frac{f_1}{f_2}$ is larger than the ratio of the stiffness of the first direction over the second direction $\frac{E_1}{E_2}$. Since $\frac{f_1}{f_2} > \frac{E_1}{E_2}$, in reality the element will not fail perpendicular to the fibre orientation. The force-time diagram shows that the material resists less force under equal displacement, hence degradation in stiffness is observed. Some of the applied force is negative which means that the structure requires compression forces to return to zero-displacement state. This is caused by a phenomenon called the crack closure effect. The hysteresis plot has to be interpreted by reading the cycles from the top to the bottom at $5$ [mm] displacement.

At certain moments more cycles are closer packed meaning that the CT specimen needs a mesh refinement as the final failure of each element is clearly visible. The residual stiffness diagram unfortunately does not show a clear stage I that stabilises itself, but stage III has a constant large degradation. The cumulative stiffness degradation parameter plot clearly dictates the pattern of the structural relative stiffness degradation. As the cumulative stiffness degradation parameter increases, the residual relative structural stiffness decreases.

### 5.4.2. Cycle jumping

Cycle jumping is one of the two methods that will be discussed to decrease computational time. It does so by extrapolating the damage that has been acquired during a cycle for a certain set of consecutive cycles instead of calculating the acquired damage in those consecutive cycles. Thus if cycle jumping is applicable, then it is a powerful tool. The same model as in section 5.4.1 of chapter 5 will be investigated, but instead of explicitly computing a $100$ cycles, only every tenth cycle will be computed. Hence a cycle jump of $dN = 10$ is created. Abaqus[3] allows to include the cycle jumping in the low-cycle fatigue tab of the direct cyclic step definition. The user could give an upper and a lower boundary of the cycle jump size. However, Abaqus[3] automatically will take half of the upper boundary as the size of all the cycle jumping. Hence the input values provided to obtain $dN = 10$ is $1$ for minimum and $20$ for the maximum number of cycles to be jumped. The allowed damage extrapolation is kept at the default value of $1$ and the maximum number of cycles to be investigated is kept at a $100$ cycles. Abaqus[3] automatically makes sure that the $100$ is the total number of cycles applied including the cycles through damage extrapolation. So it is not that a thousand cycles are simulated with $dN = 10$, neither cycle $101$ is simulated because it would not fit otherwise. In the latter case it makes a cycle jump of $9$ instead.

The cycle jumping results are provided in figures C.3 and C.4. Figure C.3 provides a visualisation of the damage done to the specimen and indicates the Von Mises stresses in the specimen. Clearly the cycle jumping results in less elements reaching the critical damage such that element deletion is applied to them. Hence the crack is less long, about a tenth of without cycle jumping. This is worrying for the fact that the fatigue life of the prediction made is therefore dependent on the cycle jumping. Figure C.4 gives more insight in what is happening. As only every tenth cycle is simulated as shown by the spikes in the top left figure of figure C.4, it still represents the $100$ cycles. Strangely enough, the hysteresis plot on the top right shows that the analysis with cycle jumping follows exactly the same pattern of the first ten cycles of the analysis without cycle jumping. This factor of $10$ is also shown in the residual stiffness of the structure. There the formatted output of the analysis with cycle jumping exactly follows the first ten cycles of the analysis without cycle jumping. Based on this outcome it would be stated that cycle jumping is not implemented in a correct manner in at least the plasticity module and perhaps the ductile damage module as well. It only stretches the time span according to the users liking. In contrast to the first three graphs, the bottom right graph of figure C.4 shows that the cycle jumping does lead to an extrapolation of damage. It is roughly in the order of ten as would be expected. Roughly a factor ten seems evident as the jumping in the graph is every ten cycles. A slight underestimation was made which is visible as the damage jumps every ten cycles. The scaled down results with factor ten is shown by the red stripped line. This is the scaled down result of the original results represented by the red continuous line. In other words, that would be calculated by simulating ten cycles without extrapolation of damage. So Abaqus[3] does take into account cycle jumping in terms of damage extrapolation, thus the most likely is that the cycle jumping is applied to the ductile damage model correctly. However, it is not seen correctly in the response of the hysteresis loops. In other words, till now the only correct cycle jump size would be no cycle jumping for this model.

### 5.4.3. Automatic incrementation

An increment is the relative amount of force increase in the analysis to obtain intermediate results that take into account the non-linear effects. Automatic incrementation helps to speed up the analysis without jeopardising the accuracy of the output significantly. Abaqus[3] determines by itself how large the next increment should be to avoid cutting the corners on the most critical moments. These critical moments are where large deviations per increment happen. In order to set the automatic incrementation, Abaqus[3] allows users to define a maximum amount of increments allowed per cycle, a minimum increment size, an initial increment size and a maximum increment size. These are provided in the incrementation tab of the direct cyclic step definition. It is advised to have a small enough initial increment size of $0.001$ such that Abaqus[3] does not directly overshoots the important steps. The maximum incrementation is best set at $0.1$ as larger would likely miss the peak in the applied force, similar to the difference in tabular input as is shown in figure 5.4. The minimum incrementation needs to be set at such a point that it is small enough to allow Abaqus[3] to decrease increment size to maintain accuracy, but not too small such that analysis takes forever. If the incrementation desired is below the allowed incrementation, then Abaqus[3] will report back an error message and stop the analysis. Currently the minimum incrementation is set at $0.0001$. The total number of increments allowed may be any number ranging between $\frac{1}{maximumincrementsize}$ to $\frac{1}{minimumincrementsize}$. Values smaller than this range will lead to an incomplete analysis and Abaqus[3] will report this back with an error message. Values larger than this range will make no difference, but it will allow Abaqus [3] to use continuously the smallest size of increments during the entire analysis. For this analysis the maximum allowed increments is set at $10000$, thus giving Abaqus[3] the opportunity to use the smallest increment size allowed during the entire analysis. The rest of the model is kept the same as in section 5.4.2 of chapter 5.

The automatic incrementation does have influence on the speed as the analysis was $10\%$ faster to finish. This manner of incrementation obtains the result provided in figures C.5 and C.6. In figure C.5 it is clear that the incrementation has no effect on the visualisation of the model. In other words, it had no influence on the crack propagation. In figure C.6 it is clear that automatic incrementation also has no influence on the load history cycles, the hysteresis curve and the structural stiffness degradation. However, the cumulative stiffness degradation parameter of all the elements does tell that the automatic incrementation leads to different results. Whether the automatic incrementation is better than a fixed incrementation, is not yet clear.

### 5.4.4. Multiple plies with tie constraint

As the automatic incrementation and the cycle jumping proved not to be successful, these techniques are left aside until further investigation is done. The next step forward is to implement multiple plies. At first these plies are connected to the adjacent plies using tie constraints, later these plies will be connected using VCCT interaction. The tie constraints are much easier to implement, thus less errors. Additionally there will be less degrees of freedom which makes computations somewhat faster. To aid computational speed, the incrementation is set to a $100$ fixed increments with each $0.01$ of the load.

Instead of one ply with thickness $1.125$ [mm], five layers of $1.125$ [mm] each are introduced creating a total thickness of the ply at $5.625$ [mm]. The layup is made from unidirectional plies which have the order from back to front as follows: $[0|-45|90|45|0]$. This layup is almost a quasi-isotropic layup. Each ply of the layup has the same geometry as in figure 5.2, the same boundary conditions as in figure 5.3 and the same mesh as in figure 5.3. In order to fulfil the new load introduction to make sure that every ply has the same imposed displacement, the coupling will now be from one reference point to the surrounding surfaces of the five plies instead of a reference point for each ply. This leads to small out-of-plane bending for the layers that are off-centre.

The major difference is that each ply will now be tied to at least one other ply. There will be four tie constraints in total: one between the first $0[^\circ]$ layer and the $-45[^\circ]$ layer, the second one between the $-45$ [°] and the $90$ [°] layer, the third one between the $90$ and the $45$ [°] layer and the final one between the $45$ and the second $0$ [°] layer. A tie constraint is imposed in the interaction section of Abaqus[3]. All the degrees of freedom between two layers will be permanently fully coupled. It will act thus as a superglue. This contact definition between the two surfaces of each layer needs to have a slave and a master surface. Since all the ties are parallel, it makes is no difference whether the one or the other layer is set a master or slave when using 3D elements. For convenience, the layer with the back surface taking part in the tie constraint will be the master surface and the layer with the front surface taking part will be the slave surface. Node to surface discretisation will be used to allow some deviation in the mesh discrepancies.

The results of the maximum load in the final cycle that is investigated (cycle $100$) are given in figure C.7 per ply. Clearly at first sight all five plies are less damaged than an individual ply under the same displacement. In a moment the reason will be given why this smaller crack pattern per ply has been developed. Also both plies (1 and 5) with the same material orientation show the similar response in stress and crack pattern, slight differences are caused by the material orientation of the adjacent ply. Figure C.8 shows the results of the five plies as one structure working together in four plots. The five plies together are stronger than five individual plies, because not all plies take the same load. So the load is less at certain points in one ply, but also the loads redistribute the neighbouring plies once the element fails. The weakness for one ply is the strength of the other. As the plies are now mainly loaded in the direction they act best, the resultant strength is larger than the summation of the individual plies as is shown in the top right plot of figure C.8. This effect is what would be expected of composites and what makes composites more advantageous than other materials.

What needs to be noted is that the crack formation is perpendicular to the material orientation. That means the crack rather propagates through the fibres instead of through the weaker matrix material. It is also observable in the single ply simulations shown in figure C.1. This is based on how the material model is defined. The stiffness of the material has been defined using orthotropic behaviour with higher $E_1$, which means that the stiffness is higher parallel to the material orientation. As the material has a higher stiffness in the longitudinal direction, the stresses will be higher in that direction as well. This results in reaching the ultimate Von Mises stress mainly by the longitudinal normal stress. Since the

**Table 5.5:** Input table containing the parametric values used in the compact tension model for unidirectional and quasi-isotropic material parameters.

| | Unidirectional | Quasi-isotropic |
|---|---|---|
| $E_1$ [MPa] | 12285 | 12285 |
| $E_2$ [MPa] | 3000 | 12285 |
| $E_3$ [MPa] | 3000 | 3071 |
| $\nu_{12}$ [-] | 0.35 | 0.35 |
| $\nu_{13}$ [-] | 0.30 | 0.30 |
| $\nu_{23}$ [-] | 0.30 | 0.30 |
| $G_{12}$ [MPa] | 2000 | 4550 |
| $G_{13}$ [MPa] | 2000 | 4725 |
| $G_{23}$ [MPa] | 1000 | 4725 |

material model does not make a distinction again between the different strengths in different directions, it will be the longitudinal normal direction that will fail first, despite being the strongest direction. This is a similar explanation to what happens in a single ply. At first this effect is not so clear as the first two elements just around the crack tip have to fail independently from the material orientation before a crack pattern occurs. This is due to the induced stress concentration by the cut-out in the CT specimen forcing the main principal stress to be vertical. As soon as the first element has failed, the next elements around the failed element have increased stresses as the crack tip is now closer to these elements. Now these multiple elements are present at the crack tip, thus the crack is free to move in any direction. As the elements located at the crack tip in the direction perpendicular to the material orientation attract the highest stresses due to the orientation of highest stiffness crossing the crack tip perpendicular, those elements will fail next. In other words the crack tip is diverted to those elements as they are supporting the crack tip most and remember there is no distinction yet in the orientation of the strengths. Thus the crack propagates in that direction.

Although the unidirectional material shows an incorrect crack path, the final material uses quasi-isotropic material. In other words, the first and second normal direction share the same stiffness and strength. As there is no more distinction between strength and stiffness in-plane, this problem is no longer a problem in predicting the crack path and fatigue life. The same analysis has been repeated as for the earlier described multiple ply with its results in figures C.7 and C.8, but with new elastic stiffness properties that are described in table 5.5. All other parameters are kept equal. For the quasi-isotropic parameters $E_1$ and $\nu_{12}$ are kept equal to that of the material testing. Since it is quasi-isotropic $E_2 = E_1$ and $\nu_{13} = \nu_{23}$. $\nu_{12}$ is set to a value of $0.3$ just as before. This means that for laminates the other material properties are defined using equations 5.2 up to and including 5.4. The output of this analysis is given in figures C.9 and C.10. The observant reader will notice that the mesh has been updated to be completely symmetrical now. Mesh size is still kept to 2 [mm] in each direction.

$$G_{23} = \frac{E_2}{2(1+\nu_{23})} = \frac{12285}{2(1+0.3)} = 4725\text{[MPa]} \tag{5.2}$$

$$G_{13} = \frac{E_1}{2(1+\nu_{13})} = \frac{12285}{2(1+0.3)} = 4725\text{[MPa]} \tag{5.3}$$

$$G_{12} = \frac{E_1}{2(1+\nu_{12})} = \frac{12285}{2(1+0.35)} = 4550\text{[MPa]} \tag{5.4}$$

The first and most obvious result to see was that all the plies show the same stress and cracking now they are quasi-isotropic. For that reason only one ply is shown for multiple cycles instead of multiple plies of the last cycle. This is to obtain an insight in the crack propagation speed. The crack pattern looks similar to what is expected in reality and from the input in the model. In other words, with quasi-isotropic stiffness the problem of different strengths in different material orientations is insignificant. For proper modelling, it is still better to implement it when out-of-plane effects come to play. The crack propagation speed slows down as the amount of cycles progress, this is because the structure becomes more flexible due to less material present. Therefore under displacement controlled analysis the crack slows down instead of speeding up. This is also observed in the stiffness degradation parameter reaching an upper limit. This limit is much higher for quasi-isotropic plies as more elements are involved in the damage as at the start there is no clear crack path, but rather a hole.

The hole is partly caused by the quasi-isotropic stiffness resulting in no precise weakest direction immediately. That would be improved by implementing different strengths in different material directions. The quasi-isotropic material is also much more flexible after the first 20 cycles than five unidirectional plies as is observed in the first three plots of figure C.10, despite the higher overall stiffness input. This is because much more damage happens faster at the start due that in-distinctive crack pattern. The initial stiffness during the first load cycle is much higher than that of the unidirectional model as is shown in the top right plot of figure C.10. This is expected, but the rapid decrease leading to more flexible response than unidirectional plies is not, especially considering the fact that the layup of the unidirectional plies is almost quasi-isotropic itself.

The second reason why the hole is present becomes clear when the analysis for figures C.9 and C.10 are compared with that of figures C.11 and C.12. These last two figures will be discussed in depth during the mesh refinement study. In the analysis for figure C.9 the first half cycle has not been simulated separately by a static step. In the analysis for figures C.11 and C.12 this has been performed. There are no more differences between these analyses. Hence the inclusion of the static analysis must be causing this. A possible explanation for this is that the fatigue analysis performs two iterations per increment while the static analysis performs at least three equilibrium iterations per increment according to both status files. The number of iterations during the fatigue analysis was limited to two. Therefore Abaqus[3] has been forced to take larger steps to obtain enough equilibrium. These larger steps result in a stiffer response. Therefore a larger area has been activated which in its turn results in the hole as more elements were already close to their limit. This indicates that the solution of C.9 is not yet converged enough during the first half cycle.

## 5.5. Improvements for the interply modelling

### 5.5.1. Replacing tie constraints with VCCT interactions

The final step would be to upgrade the model with the VCCT interactions instead of tie constraints. The geometry, layup, boundary conditions and mesh of the second model in section 5.4.4 of chapter 5 are used. The tie constraints from the TIE MS2 model are deleted and the VCCT interactions replace them to create the VCCT MS2 0053 model. The properties of the VCCT interaction are defined according to the values advised in table 4.3. That implements that a slightly different formulation is required for the VCCT interactions for the static load step for the first half cycle and the VCCT interactions for the direct cyclic load step as continuation of the fatigue analysis. For the static load step the interaction module of Abaqus[3] will help to correctly define the interactions. For the direct cyclic step the input is given in terms of data lines. For each interaction line 1 and line 2 BK of table 3.1 must be used in an added block as last part of the direct cyclic step definition in the keywords input. With the parameters defined in table 4.3 these will become the lines given in table 5.6. The VCCT interaction also requires a set of bonded nodes to be defined which act as an initial boundary condition. The unbonded nodes act as a precrack, the bonded nodes are showing virgin connection. These bonded nodes are highlighted in figure 5.5. Each VCCT interaction will have the same bonded node set. The output of the analysis is given in figures C.14 and C.15.

**Table 5.6:** Template for the input data line to provide a VCCT interface for the fatigue analysis of the five ply CT.

| | |
|---|---|
| Line 1 | *Debond, slave="Front_ply_$< n >$", master="Back_ply_$< n-1 >$", debonding force=STEP, frequency=1 |
| Line 2 BK | *FRACTURE CRITERION, TYPE=fatigue, MIXED MODE=BK, TOLERANCE=<tolerance><br>„0.005,3.0,0.001,0.9,7,<br>7,1,20 |

Again all the plies show equal cracking behaviour, but the crack is different compared to using tie constraints for interaction as is shown in figure C.14. With tie interaction the stress severity around the crack tip is slightly lower (280 [MPa]) than with VCCT interaction (290 [MPa]), but the area of increased stress levels continues more to the supports as visualised in figure C.9. Hence the VCCT interaction works more as a concentration of stress. This is caused by the fact that tie constraints do not have a bonded node set with a precrack defined. Hence the interaction always has perfect bonding. The VCCT interaction has initial cracking defined by a bonded node set. This defines already a precrack with the crack tip between the layers. The crack is for the same reason much more directed in one direction from the start as the precrack already defines the weaker direction in the quasi-isotropic material. Recognise that the crack is wider with the VCCT interaction, therefore more symmetrical than with tie constraints which will be improved upon mesh refinement. It does result in a larger and intenser stress intensity front, which is counter intuitive as larger peak stresses are expected for cracks with smaller radii as is described for the ellipse in equation 2.11. Another point of difference is the increased number of cycles needed to propagate the crack. This is partially caused by the VCCT interaction defined with the Paris law[9] which is apparently defined so optimistic that it slows down crack growth. In other words, where the crack propagation speed was limited by the breaking of the elements, it is now limited by the breaking of the interface.

Figure C.15 shows that the VCCT and tie interaction models give similar response, but after a couple of cycles the VCCT MS2 0053 model outperforms the TIE MS2 model in terms of number of cycles for a certain amount of damage and residual stiffness. The top left plot of figure C.15 shows that the VCCT MS2 0053 model degrades its force response much slower. That results in a much more elastic response in the hysteresis plot on the top right of figure C.15, thus less energy has been required

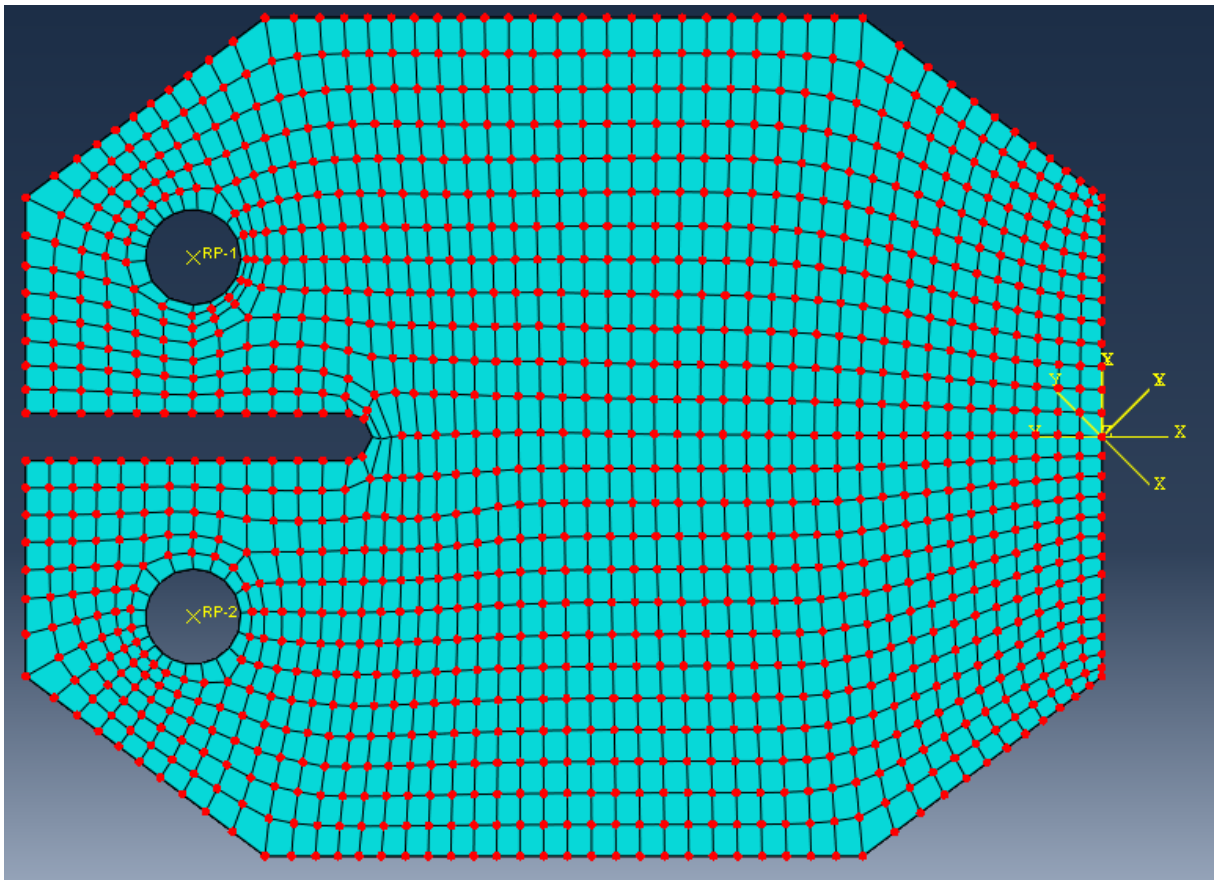


**Figure 5.5:** The bonded nodes between two plies as a definition of precracking of the VCCT interaction. The red highlighted nodes are bonded meaning that the other nodes are not bonded. These not bonded nodes are located around each hole where the boundary conditions are applied and at the centre of the round crack tip to create a micro crack present at the crack tip.

**Table 5.7:** An overview table with the differences in input for each simulation to investigate the relation with the Paris law[9]. In the last column the figure that correspond to the output of the simulation is given.

| Simulation | $c_3$ | $c_4$ | Mesh size [mm] | Figures corresponding to output |
|---|---|---|---|---|
| VCCT MS2 11 (benchmark) | 1 | 1 | 2 | C.17, C.18 and C.19 |
| VCCT MS2 101 | 10 | 1 | 2 | C.20, C.21 and C.22 |
| VCCT MS2 011 | 0.1 | 1 | 2 | C.23, C.24 and C.25 |
| VCCT MS2 103 | 10 | 3 | 2 | C.26, C.27 and C.28 |

to be dissipated in the elements. The lower energy dissipation results in less stiffness degradation, thus much more cycles till failure. That is also observed in the bottom right plot of figure C.15 where it takes many more cycles to increase the relative stiffness degradation parameter while the mesh remains the same. This is the result of two reasons: the reason described above where a crack propagation is slowed down by the interaction failure and the second reason being that the interaction also dissipates energy, degrades in stiffness and takes damage which is not taken into account in these plots.

### 5.5.2. VCCT parameteric influence

For further investigation of the VCCT with respect to the relation with the Paris law[9], some additional simulations have been performed. These additional simulations use the geometry, the boundary conditions, the mesh, the bonded nodes sets and the material properties that are used to generate the results of the VCCT MS2 0053 model. The results of these simulations are provided in figures C.17 up to and including C.28. Table 5.7 provides an overview of the simulations that are performed with their input and corresponding figures for the output.

The benchmark simulation VCCT MS2 11 has a slightly larger and a slightly more stubby stress concentration area in front of the crack tip shown in figure C.17 compared to the simulation of the tie constraint in figures C.11 and C.12. That results in more material being activated. This is caused by the VCCT interaction being less rigid than a tie constraint. A tie constraint is nothing more than defining two nodes on different parts acting as one. No energy could be dissipated if that is case. The VCCT interaction is able to release the nodes if enough energy is absorbed. If more energy is dissipated by the interface, then less energy needs to be dissipated by the material. Therefore a slightly lower maximum peak stress is observed. Thus it takes longer for the crack to propagate through the material. Hence it increases the fatigue life.

The maximum stress observed in figure C.17 is almost 290 [MPa]. This level is in coherence with the desired stress level of the static coupon testing. Since the use of a parametric formulation of the plasticity model implies that the ultimate stress is determined by the fracture energy of the ductile damage model, it shows that the used fracture energy of 25 [N/mm] is a realistic value in terms of order of magnitude. A peak stress of 290 [MPa] implies that there is a stress concentration factor of about six during the first cycle according to the definition $K_t$ provided in equation 5.5. This is an average value for compact tension specimen. In other words, the values for the stress intensity factor that are obtained from the ISO-norm 15850[4] could be used to make an initial estimation of $\sigma_{y,0} + Q_\infty$. $\sigma_{y,0}$ is determined with ISO-norm 527[45], thus that also estimates $Q_\infty$.

$$K_t = \frac{\sigma_{peak}}{\sigma_{nom}} = \frac{\sigma_{peak}}{\frac{F_{max}}{A_0}} = \frac{290}{\frac{17000}{5.625*(90-29)}} = 5.9 \tag{5.5}$$

The stress level of the maximum stress is not directly at the crack tip in the a layer, but rather an element in front of it. The element in-between is being degraded due to the ductile damage model. Therefore it is less able to resist stresses and will eventually break down which propagates the crack. Even more interesting to note is that the bondline has been observed at the border with the highest stresses. That means that the maximum stress and the VCCT failure happens at roughly the same time.

The crack propagation rate in figure C.17 looks as if it is logarithmically decreasing as the number of elements broken per frame is relatively constant while the frames are with a log base of 2. This is what would be expected for a displacement controlled fatigue analysis. It is decreasing since the structure gets more flexible if more elements are broken. It is logarithmically decreasing as the amount of elements that will break will reduce each step.

The hysteresis plot of figure C.18 shows that the boundary conditions have been correctly applied to the VCCT MS2 11 simulation. It is clear in both the load history plot as the hysteresis plot that the forces get less. From figure C.17 is known that the maximum stress will not get less. Hence the stresses will concentrate towards the crack tip as the crack propagates. The load history plot shows this happens in a logarithmic regression. The hysteresis plot shows that a significant amount of energy is dissipated each cycle.

The residual stiffness plot and the stiffness degradation parameter plot show that the ductile damage model starts to have effect on the structure at about $20$ [cycles]. That is also the moment when the first element fails. In the residual stiffness plot this is observed as the material has a drop in stiffness. A second drop in the residual stiffness indicates that the second element fails soon after. This transition from the first stage to the third stage is also observed in the stiffness degradation plot. At $20$ [cycles] the stiffness degradation parameter starts to increase significantly. That happens progressively to about $100$ [cycles]. The reason for this phenomenon will be explained by comparing the other three simulations to the benchmark simulation VCCT MS2 11.

In figure C.19 an investigation is made if there is a Paris law[9] relationship between the crack propagation rate and the equivalent fracture energy. Each row represents a different interface. Interface $1$ is the interface between the $0$ [°] layer and the $-45$ [°] layer. The second interface is between the $-45$ [°] layer and the $90$ [°] layer. Sequentially the third interface between the $90$ [°] layer and the $45$ [°] layer and finally the fourth interface is between the $45$ [°] layer and the second $0$ [°] layer. The final row is not related to one interface, but to all interfaces as it contains the sum of the energies of all interfaces. This order will be kept for further investigations. Clearly the total is mostly affected by the fourth interface. In the first column the sum of the equivalent energy release rates observed in all the nodes in a specific interface has been plotted with black dots for the different cycles. This has been done on a double logarithmic scale. A representative regression line has been estimated by hand. A straight line on this logarithmic scale means that a exponential relation is present between the data points. An exponential relation has the standard form of $aN^b$. The green line represents the overall behaviour of the data well, but with a large scatter. The last two plots clearly indicate a plateau starting at about $100$ cycles. Also the crack propagation has been plotted on a double logarithmic scale. The data is extracted by looking per layer when the next element has cracked. This has only been done for the most critical row of elements. In other words, if the crack was two elements thick initially, then only the row that propagates furthest has been accounted for. This data is plotted with blue dots in the plots of the second column of figure C.19 with double logarithmic axes. These plots are identical as the elements broke in all layers simultaneously due to the quasi-isotropic stiffness properties. It confirms the hypothesis based on the crack observed in figure C.17 that the propagation rate is logarithmic over cycles. Again a regression line is estimated for the data. This time the red regression represents the crack propagation rate over the number of cycles in an exponential relation.

Based on these regression lines a new set of data where the number of cycles that have passed for each observation is kept equal for both regression. This is done for $10^0$, $10^1$, $10^2$,$10^3$,$10^4$ and $10^5$ cycles. This allows to compare the regression line of the equivalent energy release rates with that of the crack propagation speed as not every calculated increment leads to failure of an element. The obtained values for the equivalent energy release rate (EERR) and the crack propagation rate based on the regression lines are plotted in the third column for each interface with blue dots on a double logarithmic scale. To no surprise these dots are on one line as both regression lines are exponential. The regression line through these six dots is calculated as the new values for $c_3$ and $c_4$ are related to that of the previous regression lines. The equations for finding these constants are given in equations 5.6 and 5.7. Being able to obtaining this regression line shows there is a Paris law relation[9] obtainable between the energy release rate and the crack propagation speed if a large filter is used. However, the values for these regression lines are not equal to that of the input values of the interface which were $c_3 = 1$ and $c_4 = 1$ for all interfaces.

$$c_{4,new} = \frac{c_{4,da/dN}}{c_{4,EERR}} \tag{5.6}$$

$$c_{3,dadN} = \frac{c_{3,dadN}}{(c_{3,EERR})^{c_{4,dadN1}}} \tag{5.7}$$

Changing the value $c_3$ to $10$ changes the crack pattern as is performed in the VCCT MS2 101 model. Figure C.20 shows that the crack width starts at $4$ [mm] (2 elements) and becomes $2$ [mm] (1 element) wide at around $1500$ cycles. Note that the figure at $1000$ cycles is actually the figure of $600$ cycles. The analysis automatically made the cycle jump from $600$ cycles to $1500$ cycles. Since the frame of $600$ is closer to $1000$ cycles than $1500$, the frame of $600$ cycles is shown. The smaller crack width decreases the area of peak stress thus the area is sharper around the crack tip. The decrease in area is caused by a weaker VCCT interaction. Increasing $c_3$ leads to the weaker interaction as the effect of the equivalent energy release rate ($G_{eq}$) on the crack propagation rate is proportional according to the Paris law[9]. A decrease in area means less material is activated to dissipate the energy of the fatigue load cycle. Thus the crack is focused which causes the crack propagation speed to increase for the rest of the analysis. Eventually it will stabilise itself again to a new propagation rate, but that has not been simulated.

The weaker VCCT interaction of the VCCT MS2 101 is also observed in figure C.40. At about $800$ cycles an acceleration of degradation is observed. This is due to the crack becoming narrower, but there is a difference between the number of cracks at the start of this process compared to the point at which the narrowing results in less elements being broken in width. However, more energy is dissipated during the narrowing resulting in more energy being dissipated as is observed in hysteresis plot of figure C.40. This results in an acceleration of the crack propagation rate which starts at about $700$ cycles. The acceleration is also observed in the residual stiffness and the residual stiffness degradation plot of figure C.40. Based on these two plots it is observed that now less distance is present between the crack tip and the maximum stress as the stiffness degradation parameter progresses much faster than the degradation of the residual stiffness. This is also observed at the crack tip in figure C.20. Stage III still starts at the same amount of cycles as the benchmark simulation.

The opposite effect should be observed if $c_3$ is decreases from $1$ to $0.1$. Now the crack should progress slower according to the Paris law[9] in the VCCT MS2 011 model. That is exactly what is

observed in figures C.23 and C.24. The stronger VCCT slows down the crack propagation rate in stage III. Thus the VCCT is governing over the ductile damage model causing a delayed response in residual stiffness degradation. Only a minor difference is observed for stage I. Thus the crack acceleration in the VCCT MS2 101 model is due to the VCCT no longer being governing for the crack propagation rate.

A similar response of deceleration is observed by increasing $c_4$ as is shown in figure C.26 and C.21 for the VCCT MS2 13 model. At first this is counter intuitive as increasing the value $c_4$ from 1 to 3 would increase the propagation rate as the power is increased. However, the equivalent energy release rates are lower than 1. In that case the higher powers make the outcome of the function lower, thus slower crack propagation. Again the VCCT is governing in this case. To come back at the plateau of 100 cycles during the simulation of VCCT MS2 11, this is now explained by the VCCT interface becoming governing over the ductile damage model. Now the ductile damage model moves in the same pace as the VCCT model.

It was already mentioned that both $c_3$ and $c_4$ have influence on the crack propagation rate. Since increasing $c_4$ decreases the crack propagation rate, it must be that the $G_{eq} < 1$. In figure C.21 is observed that the degradation of VCCT MS2 103 is slowed down from 300 cycles onwards compared to VCCT MS2 011. So from that point $G_{eq} < 1$ holds. In the first 300 cycles the $G_{eq}$ has to be large enough such that the influence of a ten times larger $c_3$ compensates the power three ($c_4 = 3$). That means that the $G_{eq}$ values in VCCT MS2 103 must be in the order of 0.1. This order of magnitude of the $G_{eq}$ is also observed in figure C.19, C.22, C.25 and C.28. That shows there is a relation according to the Paris law[9] defined for the VCCT between the input and the output. That means the crack propagation is VCCT dominated. However, there is no Paris relation[9] found with the input parameters.

In short, compared to the TIE MS2 model in figure C.9 the crack propagation rate in the VCCT models is lower, even with the narrowing. This is due to the rigidity of the tie constraint. The increased rigidity also increases the number of elements in front of the crack tip that are loaded with the peak stress. Add on top of that, that there is no material as interface for a tie constraint. Thus no energy could be absorbed and there is no interaction that could lag behind. Therefore the material itself has to dissipate all the energy. This leads to a faster degradation in the ply.

### 5.5.3. Isolation of the VCCT effect

Not much investigation has yet been performed into the VCCT of the model. Therefore it is difficult to grasp the idea what VCCT does to the model. So extra simulations have been performed on the CT specimen model with the plasticity module and the ductile damage module excluded. This resulted in the VCCT isolated MS2 11 U5.0 model with: an element size of 2 [mm], $c_3 = 1$, $c_4 = 1$ and $U_{max} = 5$ [mm].

The most obvious difference in results of the VCCT isolated MS2 11 U5.0 model versus the results of the VCCT MS2 11 model is the lack of in-plane cracking, because there is no damage module in the elements present that deletes the elements. For that reason it is more interesting to look at the bondstatus (BDSTAT) of the interfaces. In figure C.32 and C.33 the bondstatus between the layer in 90 [°] direction versus the 45 [°] direction has visualised. The red area indicates that nodes are bonded while the blue area indicates the nodes that have been released. The precrack that has been made is clearly visible in figure C.32. Since there is no weakest direction anymore present in the material due to the quasi-isotropic stiffness, the crack first expands vertically till it has become a circular pattern with a cut-out due to the absence of the material. Hence the delaminated area will form an arc around the cut-out in the CT specimen. Once it has become an arc, the crack propagates radially (equal crack propagation in

all directions) as the influence of the stress concentration around the crack tip no longer has a significant influence anymore to cause a preference in crack propagation. This slows down the crack propagation drastically as the crack front, the borderline between the blue and red area, has become so large that much of the material is activated to dissipate the energy from the external load.

What has to be stated is that the maximum stress in the VCCT isolated MS2 11 U5.0 model is $\sigma_{ult} > 1000$ [MPa], although it is only visualised for VCCT isolated MS2 11 U2.5 in figure C.29. This value of peak stress is absurdly high. This high value is caused by the plasticity module being defined with parameters and by the absence of a ductile damage module. Generally there would be a limit in place due to the end of the stress-strain definition for the plasticity module. If the stress-strain relation is entered using a tabular input, then that would be true. However, the stress-strain relation is provided with the exponential function given in equation 4.2. Therefore the plasticity module is defined continuously and indefinitely for positive strains. Thus it will never reach an end-value despite $\sigma_{ult}$ reaching $\sigma_{y,0} + Q_{\infty}$ closer for higher plastic strains. The absence of the ductile damage module removes the second limit given to $\sigma_{ult}$ to reach zero stress at $\varepsilon_f$ with a enclosed plastic surface area with a size of $G_f$. These two options combined allows to reach high peak stresses at the crack tip. Therefore caution has to taken if only the VCCT module is used.

The lack of degradation is also observed in figure C.37. The absence of the plasticity module and the ductile damage module resulted in only a little force degradation for the same applied displacement. That resulted in the hysteresis plot in only a small enclosed area, which means not much energy has been dissipated in the structure. In other words, the load is applied almost entirely in the elastic regime of the structure. For that reason only a little stiffness degradation is observed. Hence the load degradation has to come from the plasticity module or the ductile damage module. From the one element models it is known that the hardening of the material leads to an increase in the residual stiffness degradation. Thus lack the stiffness degradation must come from the absence of the ductile damage module.

Another observation has to be made from figure C.37. There are no negative forces present in the model. That excludes the possibility of the VCCT causing negative forces in VCCT MS2 11. Additionally, the one element model showed already negative forces present in the element. In the one element model the element would degrade quickly as soon as the ductile damage model becomes governing. This is not the case in figure 4.11. Thus plasticity module is suspected to cause the negative forces. From a physical point of view this is also understandable. The plasticity module is actually designed to describe the non-linear behaviour of a metal. A metal does deform plasticly. This plastic deformation during the tensioning of the specimen causes permanent deformation in one direction. After releasing the forces, the element will undo its elastic deformation, but not its plastic deformation. But before that point is reached the original crack has already been closed due to the plastic deformation. This premature closing of the crack causes a phenomenon called "crack overclosure". This overclosure effect will be amplified by requiring the displacements in the pins to become zero. In metals it is perfectly fine as that phenomenon is present in reality, but in composites it is a misrepresentation as composites would crack or crush instead of deform plasticly. Thus the VCCT MS2 11 model has to be taken with caution regarding the use of the plasticity module to describe a damage mechanism.

To continue on the radial expansion observed in figures C.32 and C.33, the sum of the effective equivalent energy release rates (EFENRRTR) per interface has been plotted in figure C.38. The EFENRRTR of the different interfaces of VCCT isolated MS2 11 are in the same order of magnitude as that of VCCT MS2 11. That also indicates that the Paris law[9] of the combined trendlines have the same order of magnitude. For that reason it is concluded that the model is governed by the delamination mechanism. That will come to no surprise as the two other mechanisms are excluded. In other words, the slow down of the crack propagation is also reflected in the EFENRRTR, thus there is still a Paris law[9] present in

**Table 5.8:** An overview table with the differences in input for each simulation to investigate the mesh refinement. In the last column the figure that correspond to the output of the simulation is given.

| Simulation | Interaction | Mesh size [mm] | Figures corresponding to output |
|---|---|---|---|
| VCCT MS2 11 (benchmark) | VCCT | 2 | C.17, C.16, C.18 and C.19 |
| VCCT MS1 11 | VCCT | 1 | C.39, C.40 and C.41 |
| VCCT MS05 11 | VCCT | 0.5 | C.42, C.43 and C.44 |
| TIE MS2 | Tie | 2 | C.11, C.12 and C.13 |
| TIE MS1 | Tie | 1 | C.45, C.46 and C.47 |
| TIE MS05 | Tie | 0.5 | C.48 and C.49 |

the model.

These figures also show that the EFENRRTR bends of to constant values just over 1000 [cycles]. Each interface will have ten constant values present. These constants are related to the increments that are exported in the output of the analysis. It has to be mentioned that Abaqus[3] was assigned to only show the results for every ten increments to reduce the file size of the output. This was required to prevent the workstation from crashing due to extreme file sizes. These values are constant over the cycles and proportional with the load applied in the increment. Thus EFENRRTR is load dependent even if no nodes are released. That could either mean that the mesh is not refined enough to release a node in every cycle that has been calculated or EFENRRTR includes more than only the energy that has been released due to the release of a node. No definite answer has been investigated on this issue.

## 5.6. Mesh refinement study

The goal of the mesh refinement study is to check if a correct mesh size is chosen by observing the convergence. Also if there are parameters that are size dependent, then it will be recognised in these analyses. A new set of analyses has been performed that will be compared to the benchmark analysis VCCT MS2 11. Table 5.8 provides an overview of the differences in the analyses. All other aspects such as the geometry, the mesh, the boundary conditions and the material properties are equal to that of the benchmark VCCT MS2 11 model.

The mesh refinement for the tie and the VCCT analyses resulted in a better defined area where the peak stresses are present. For the VCCT MS1 11 analysis with 1 [mm] nominal element size this resulted in a larger area during the first cycle than the VCCT MS2 11 analysis with 2 [mm] nominal element size as is visible upon comparing figure C.39 with figure C.16. On the other hand, for the TIE MS1 11 analysis with 1 [mm] nominal element size the area remains roughly equal during the first cycle compared to the TIE MS2 11 analysis with 2 [mm] element size. This is observed by comparing figures C.11 and C.12 with figures C.45 and C.46. These figures also show that with the element size of 2 [mm] it is less clear which elements are under influence of the plasticity model and which elements are under influence of the ductile damage model. Here one element is present between the crack tip and the maximum stress leading to a degradation of maximum stress to zero stress in one element. With the 1 [mm] size of the elements this is distinguished better as over the distance of 4 elements the material degrades from the maximum stress to zero stress in the ductile damage model.

Despite the increase in peak stress area in the VCCT MS1 11 analysis, the crack length does not alter that much. The opposite is true for the tie constraints. Upon decreasing the element size from 2 [mm] to 1 [mm], the crack propagates less far while the intial peak stress area has the same size. This is

caused by the decrease in area in the sequential cycles of TIE MS2 while the area for TIE MS1 remains equal for longer. For the VCCT MS2 11 and the VCCT MS1 11 analyses the areas of peak stress are equal in size from cycle 2 onwards, only the shape is somewhat different.

Refining the mesh even further to an element size of $0.5$ [mm] does not change the results compared to a mesh with element size $1$ [mm]. Both the crack length, crack shape and area of peak stress remain equal as is observed by comparing figure C.48 with figure C.45 and figure C.42 with figure C.39.

A note has to be given that for the VCCT MS05 11 analysis the analysis has been stopped at $4.3$ [mm] of the $5$ [mm] displacement during the first half cycle. The analysis has been stopped as this mesh size resulted in extremely long computation time. For the VCCT analyses the computational time (simulated cycles per hour) decreased with a factor of $50$ each time the nominal element size decreased by a factor $2$. For the tie analyses this was less severe with only a factor $5$ if the element size was decreased by a factor $2$.

Only upon comparing the forces of the VCCT MS2 11 model and the VCCT MS1 11 model in figure C.40 it is visible that the smaller mesh size results in less degradation. This is observed in the load history plot of figure C.40 by having larger forces for more cycles. It is not that the CT specimen has failed at $50$ [cycles], but the analysis has been stopped due to computational time. This lesser degradation is also observed in the residual stiffness plot of figure C.40. The shape of the degradation is followed, but with an increasing delay. That delay is also observed in the stiffness degradation parameter plot of figure C.40. Do not underestimate that delay as the plots are given on a logarithmic time axis. In other words, after $50$ [cycles] with $1$ [mm] element size the same degradation is observed as $25$ [cycles] with a $2$ [mm] element size. This is a factor of two even if the crack is not double in length. This factor of two is not directly related to the fact that the element size has been decreased by a factor of $2$. That is shown in the simulations with the tie constraints. In the load history plot of figure C.48 it is clear that some delay is present. For an element size of $0.5$ [mm] versus $1$ [mm] that delay is larger than that for an element size of $1$[mm] versus $2$ [mm]. The effect of the delay is also visualised in the stiffness degradation diagram of figure C.48. The degradation observed at $50$ cycles with $0.5$ [mm] elements is equal to the degradation observed at about $35$ [cycles] with $1$ [mm] elements and about $20$ [cycles] with $2$ [mm] elements. It is expected that this delay will become less for both refinements of the mesh. Although this is not explicitly simulated, TIE MS1 shows that it catches up with the residual stiffness degradation of TIE MS2 at $300$ [cycles] of figure C.49. This behaviour is also expected based on the crack lengths and the crack propagation rates observed in figure C.50. The crack propagation rate plot on the right shows a convergence in crack propagation rate for decreasing element sizes.

However, this catching up is not observed in the stiffness degradation parameter plot of figure C.49. Here the mesh refinements lead to exponential growth of the stiffness degradation parameter while that of the $2$ [mm] elements levels off. This is related to the number of elements that are under the influence of the ductile damage model, not necessarily the intensity of the degradation per element alone. As already explained, the smaller elements in the tie analyses lead to maintaining the initial size of the peak stress area for longer. Therefore more elements are involved. Since the crack size does not change in width or length with the change in the element size, the elements that do resolve in a crack will not have a higher degradation intensity.

In other words, mesh with element size of $2$ [mm] is fine enough to predict the fatigue life. For the VCCT analyses it will even result in an underestimation of the fatigue life which is safe to do. However, decreasing the element size from $2$ [mm] to $1$ [mm] does improve the stress distribution without compromising too much on the computational time. This does give more accurate result on the

crack pattern of the CT specimen. Decreasing the mesh size from 1 [mm] to 0.5 [mm] does not improve the accuracy of the results, but does lead to much longer computational time. Therefore 2 [mm] elements size is advised for quick simulations and 1 [mm] for accurate simulation.

The energy values from the VCCT MS1 11 analysis is similar to that of the first part of the VCCT MS2 11 analysis. This supports the idea that the mesh refinement does not lead to different results. However, there is less scatter in the energy values upon comparing figure C.41 with figure C.19. Thus the mesh refinement decreases the scatter due to having less outliers, therefore it is more accurate. For that reason the trend line for the energies of the VCCT MS1 11 analysis are better estimates than that of the VCCT MS2 11 analysis since the VCCT MS1 11 model only has the first governing mechanisms simulated. In other words, it stops before the bend in data occurs due to entering a new stage with a different governing mechanism.

Unfortunately there is only one point in the crack propagation plots of figure C.19. That means that any regression line could be drawn through that point. However, it could be checked if the point itself is on the line that it is supposed to be on. This line is based on the Paris law of the input parameters. This is performed according to equation 5.8 for interface 4 which has the most influence. The propagation rate is based on the fact that the first element fails after 36 cycles. The energy value is based on the regression line found for that interface as it resembles the data point quite accurately. Since there is a large discrepancy in equation 5.8, there is no Paris law relation found with regard to the input parameters.

$$\frac{da}{dN} = \frac{1}{36} \neq 0.098 = 1 * 0.098^1 = 1 * (1.2 * 36^{-0.7})^1 = c_3 * (1.2 * t^{-0.7})^{c_4} \tag{5.8}$$

Figures C.51 up to and including C.55 investigate if there is any Paris law relation observable between stress intensity factor and the crack propagation speed. The stress intensity factor is calculated according to equation 5.9 where it is based on the stress field of the simulations, the definition of the stress intensity factor in equation 2.15 and the stress concentration factor in equation 2.10. It is assumed that the FEM automatically takes into account all the geometric effect ($K_t$ and $\beta$) in representing the peak stresses. The peak stresses are about constant at the ultimate stress $\sigma_{ult}$ of the material. Therefore it is assumed that the peak stress of the resultant cross-section will always equal the ultimate stress $\sigma_{peak,res} = \sigma_{ult} = 290$ [MPa]. The resultant cross-section is the thickness of the cross-section ($t = 5 * 1.125$ [mm]) multiplied with residual length ($l_{res} = 90 - a$). Remember that the crack length $a$ is the length of the initial precrack plus the crack added due to the fatigue loading. Then stress intensity factors are compared to the crack propagation rate in the cycle that the crack propagates (the next element breaks).

$$K = \beta K_t \sigma_{max,nom} \sqrt{\pi a} = \sigma_{peak,res} \sqrt{\pi a} = \sigma_{ult} \sqrt{\pi a} \tag{5.9}$$

Based on these results a Paris law is observed with a negative material parameter of $c_4$ in figures C.51, C.53 and C.55. This is opposite to what should be observed.

**Table 5.9:** An overview table with the differences in input for each simulation to investigate the differences in load level. In the last column the figure that correspond to the output of the simulation is given.

| Simulation | Modules included | Load level: displacement [mm] | Figures corresponding to output |
|---|---|---|---|
| VCCT MS2 11 (benchmark) | Plasticity, VCCT, Ductile damage | 5.0 | C.17, C.16, C.18 and C.19 |
| VCCT MS2 11 U2.5 | Plasticity, VCCT, Ductile damage | 2.5 | C.56, C.57, C.58 and C.59 |
| VCCT MS2 11 U7.5 | Plasticity, VCCT, Ductile damage | 7.5 | C.60, C.61, C.62 and C.63 |
| VCCT isolated MS2 11 U2.5 | VCCT | 2.5 | C.29, C.30 and C.31 |
| VCCT isolated MS2 11 U5.0 | VCCT | 5.0 | C.32, C.33, C.34 and C.35 |
| VCCT isolated MS2 11 U7.5 | VCCT | 7.5 | C.36, C.37 and C.38 |

## 5.7. Influence of different load levels

Since the material is supposed to be applied in design, it is important to know what different load level does to the material. Therefore it is common practice to formulate S,N-curves of the material, even if it is mainly about the crack propagation as is explained in section 2.3.2 of chapter 2. In order to create these theoretical S,N-curves of the material, the model should be applied at different load levels. It has been chosen to investigate the different load levels based on the different maximum displacements applied on the benchmark model (the VCCT MS2 11 model). It has to be stated that different levels of applied displacement $U$ are applied, not different levels of stress $S$. Therefore it will be called U,N-curves from now on instead of S,N-curves to emphasise this difference. The analysis that have been performed with the differences and output figures are summarised in table 5.9.

Figures C.56 and C.57 of the VCCT MS2 11 U2.5 model show a decrease in the material being activated to respond plasticly compared to figures C.17 and C.16 of the VCCT MS2 11 model. Not only in longitudinal direction of the crack formation, but also in transverse direction. Especially the transverse direction indicate it requires less material to resist the forces. For that reason the peak stress area is merely bulb in front of the crack tip of about 6 [mm] in diameter (3 elements). In contrast to the reduces load, the increased load of the VCCT MS2 11 U7.5 model shows that an increase in load results in a larger peak stress area as is shown in figures C.60 and C.61. Thus the load level dictates how many elements are hardening due to the plasticity model.

Also the more elements that are loaded in the plastic regime due to a higher load, the more energy that is dissipated as is shown in the hysteresis plot of figure C.62. Larger enclosed areas show that more energy is dissipated each cycle. That implies a faster degradation as more elements are reaching $\sigma_{ult}$ earlier, thus reaching $\varepsilon_f$ earlier. This faster degradation is also observable as the applied forces decrease faster. The faster an element reaches $\varepsilon_f$, the faster the crack propagates. Thus the load level dictates how fast the crack propagates. The faster the crack propagates, the shorter the fatigue life. What has to be noted is that the VCCT MS2 11 U7.5 model is able to support two cracks. Although it is not fully understood why this happens, currently the best explanation is that the amount of energy that is dissipated within one cycle is enough to propagate two cracks at once. The peak stress area in front of each crack tip is much smaller. It is as if these areas are joint to one during one crack propagating. In short, a higher load level results in a faster crack propagation, therefore a shorter fatigue life. This is conform the intuition and the formulation of S,N-curves.

Furthermore, a larger applied load also results in a higher maximum force initially as is shown in figure C.62. This is observed in the first half cycle where the structural response for all three load levels the same for the first $2.5$ [mm] and for VCCT MS2 11 U5.0 and VCCT MS2 11 U7.5 also for the next $2.5$ [mm]. This is not so strange as the starting conditions for the first half cycle is identical for the three models. Thus that means it are three identical static analyses, only the $7.5$ [mm] displacement will allow to monitor the structure for longer. What is more interesting to observe is that the ultimate force applicable to the structure during a static analysis will be at about $17$ [kN] as the force decreases during the first half cycle after $U = 5.7$ [mm]. Also next load cycle this maximum force is exceeded between $7.0$ [mm] and $7.5$ [mm] displacement in the top pin. It now reached an overall maximum force of $20$ [kN]. Although this is not expected to happen for composites in reality, it is still explainable for the model. This is again due to the plasticity model. The hardening of certain elements allow the second cycle to reach higher stress levels as even more elements are now able to go beyond the initial yield stress $\sigma_{y,0}$. In other words, the plasticity model has to be taken with caution.

In figures C.59 and C.63 there is not much change in the regression of the EFENRRTR observed. The only difference that is observed is that the higher load level also induces more outliers. Thus the results are relatively less accurate. That means that higher load levels require smaller mesh sizes at the end of analysis. Contrary, smaller load levels require smaller mesh sizes at the start of the analysis to allow a more accurate result in the first cycles.

Upon comparing the intraply crack length over the cycles, figure C.64 reveals that the crack propagation rates are converging, but the crack lengths themselves are diverging. This indicates that from a certain moment onward the cracks will propagates roughly at the same pace. Thus after applying a certain amount of cycles the load size influence becomes less important and the crack length itself becomes more important to determine the crack propagation rate. This is conform the theory of the Paris law.

However, figure C.65 reveals that the crack propagation slows down to much for the increase in $K$. Moreover, it should not slow down, it should speed up. Although a slow down in crack propagation rate would be expected since it is a displacement controlled analysis instead of a force controlled analysis. The increase in crack length buffs $K$ so much that overall the crack should still accelerate. This is in contrast to the Paris law.

A load size effect has also been performed for the isolated VCCT models. For the VCCT MS2 11 U2.5 model the same effects are observed as for the VCCT MS2 11 U5.0 with only two differences. First of all, a difference is observed in how much reaction force is observed. To no surprise the reaction forces are smaller for the smaller displacement. They are about half of the VCCT MS2 11 U5.0 as is shown in figure C.34. This is not so strange since the applied displacement is half of the original. This reduction in load caused a reduction in crack propagation rate. Thus a smaller crack is observed. This is reflected upon comparing figure C.29 with figures C.32 and C.33.

The VCCT MS2 11 U7.5 does not show much results in figures C.36 and C.38. Abaqus[3] was unable to find a converged solution during the first half cycle within a reasonable amount of time (2 days of simulations). For that reason Abaqus[3] has been interrupted and the simulation is considered computationally too heavy. From figure C.37 some indication is concluded: applying a larger displacement would also result in a larger reaction force.

## 5.8. Hypotheses review chapter 5

### 5.8.1. Proofs to eleven hypotheses listed in section 5.2 of chapter 5

**Circumstantial proof of hypothesis 10: If the direct cyclic analysis is applied on a one element model with the plasticity model, then no plasticity will be extrapolated during the cycle jumping.** This hypothesis is tested in section 5.4.2 of chapter 5. Figure C.4 shows that the output of the model with cycle jumping actually follows the first part of the model without cycle jumping by Abaqus[3]. The first part of the model without cycle jumping is dominated by the plasticity model, therefore it could be concluded that the plasticity is not extrapolated during a cycle jump. Is this a problem? Perhaps it is not a problem when cycle jumping is applied after the transition point between stage I and III on a structural level.

**Proof of hypothesis 11: If the direct cyclic analysis is applied on a compact tension specimen with the ductile damage included, which is loaded with a displacement or force causing the stress in an element to be larger than the ultimate stress, then it transfers its burden of load to its surrounding elements in order to find equilibrium.** As the proof of contradiction was already stated, the fact that the compact tension specimen does not fail in one cycle after the first element has failed, proves the hypothesis.

**Circumstantial proof of hypothesis 13: Using the plasticity model for the inter fibre fracture will result in an overclosure of the crack due to the plastic deformation which is not present in reality.** The overclosure of the crack is observable by the fact that the triple mechanism compact tension models of chapter 5 show negative forces at the end of the first several cycles. These negative forces are the result of the plastic deformation caused during the tensile loading. In order to bring the pin back to zero displacement it requires a negative force to have enough compression at the crack tip to deform plasticly again. This deformation is called the overclosure. The isolated VCCT compact tension specimen models show that the overclosure is not caused by the VCCT as there are no more negative forces present.

**Circumstantial proof of hypothesis 21: If cycle jumping is enabled for the compact tension specimen with a ductile damage model and VCCT model included and the load leads to a local stress higher than the ultimate stress, then the damage obtained during cycle $n - x$ will be extrapolated $x$ times to obtain cycle $n$.** The VCCT MS2 11 model shows that Abaqus[3] still performs cycle jumping, even if it was explicitly assigned not to do so. The cycles that were jumped were the cycles without a change in nodes being released or elements that reached final degradation. That means that the plasticity is the only part that was changing. This is not extrapolated. However, figure C.18 shows that the damage done is still extrapolated. This is clearly visible between cycle $40$ and $80$. The SDEG increases with a straight line indicating that there is a damage difference between the end of cycle $40$ and the start of cycle $80$. As such the damage is still extrapolated, but do notice that this is not performed linearly.

**Circumstantial proof of hypothesis 22: If the element size is refined from 2 [mm] to 1 [mm] in a model that has either VCCT or tie interactions, the fatigue life will not change more than a few percent due to the mesh refinement.** As is observed in the mesh refinement study in section 5.6 of chapter 5, not much change in results is observed in the long run. Only temporary differences are observed that could be related to the accuracy depending on the element size that determines if the element would have failed in cycle $x$ or cycle $x + i$ with $i$ a small natural number. It is even noticed in figure C.47 that a catching up in structural stiffness degradation is present after some local deviations.

**Circumstantial proof of hypothesis 23: If the element size is refined from 2 [mm] to 1 [mm] in a model that has either VCCT or tie interactions, the transition from stage I to stage III will not change more than a few cycles due to the mesh refinement.** Figures C.40 and C.49 show only a slight delay in transition between stage I of about 3 cycles.

**Proof of hypothesis 24: Loading the compact tension specimen with a fatigue load in the direct cyclic analysis will result in a crack propagating in the weakest direction of the ply.** Section 5.4.1 of chapter 5 explained that the direction with the highest stiffness will determine the direction of the principal stresses. Since there is no distinction made between the strengths in different directions, the direction with the highest stiffness will fail first. This is shown in figure C.1 where the crack propagates perpendicularly to the first direction of the unidirectional material.

**Proof of hypothesis 25: Changing the material properties has the same effect on the fatigue life of a compact tension specimen as on the one element model with a displacement controlled analysis.** Increasing $\sigma_{y,0}$ increases the fatigue life as less plastic response will occur. Decreasing $E_i$ decreases the amount of force needed to allow the displacement, thus more fatigue life. Increasing $Q_\infty$ increases the amount of stress allowed till failure, thus higher resistance against load. Increasing $b$ would increase the plastic loads faster, thus reaches ultimate stress earlier. Increasing $\varepsilon_f$ will allow more strain till failure, thus more elements are still involved in the analysis that could take load. Increasing $G_f$ would decrease the ultimate stress with parametric values for the plasticity model, thus an element will reach ultimate stress faster. Although this is the opposite compared to the one element model with tabular input, the decrease would also be present in the one element model if the one element model is based on the parametric formulation. This is explained as followed: with the tabular input a change in $G_f$ requires a corresponding change in $\varepsilon_f$ to avoid errors, while with the parametric formulation, to a certain extend, a change in $G_f$ will automatically change $\sigma_{ult}$ as well. The model is still strain rate and pressure independent, thus $\eta$ and $\dot{\varepsilon}$ will not have any effect on the model.

**Proof of hypothesis 26: Increasing a critical energy release rate ($G_{I,c}$, $G_{II,c}$ or $G_{III,c}$) will increase the fatigue life**. It has not been simulated. However, as the slow down of the VCCT interaction improves fatigue life as will be shown for hypotheses 27 and 28, increasing the energy release rates will also increase the fatigue life.

**Proof of hypothesis 27: Increasing $c_3$ will decrease the fatigue life.** This has been investigated in section 5.5.2 of chapter 5. Figure C.24 shows that increasing $c_3$ with a factor of ten will decrease the fatigue life with about a factor ten as well. This has to be taken with caution, because in order for this to happen, the VCCT interaction must be governing. There is no restriction on the applied range, nor a dependency on the range of the equivalent energy release rate $G_{eq}$ due to the relation with the Paris law. In other words, this will hold for all $G_{eq}$ and $c_3$ as long as the VCCT of a certain ply stays governing.

**Proof of hypothesis 28: Increasing $c_4$ will increase the fatigue life if $G_{eq} < 1$ for each node.** This has been investigated in section 5.5.2 of chapter 5. Figure C.27 shows that increasing $c_4$ with a factor of three will increase the fatigue life about the same as reducing the $c_3$ value with a factor 100. That would mean that the equivalent energy release rates $G_{eq}$ must be in the order of magnitude of $0.1$ to allow this equivalent fatigue life to happen. This order of magnitude for $G_{eq}$ has been observed in the simulations of VCCT MS2 11 and VCCT MS2 103 as is shown in figures C.19 and C.28 respectively. Note that the increase in fatigue life is due to $G_{eq} < 1$. If $G_{eq} > 1$, then a decrease in fatigue life is expected for an increasing $c_4$ based on the Paris law. This has to be taken with caution, because in order for this to happen, the VCCT interaction of a certain ply must stay governing.

## 5.9. Conclusion chapter 5

Starting from the one element with ductile isotropic material properties and having no interactions, the model has been upgraded successfully on multiple fronts. Changes were made in the material properties to become brittle material properties, having orthotropic stiffness properties and the geometry from one element to that of the compact tension specimen to include multiple plies. These changes were successful. Additionally, the upgrade to include VCCT interaction shows promising results. However, two hurdles remain to overcome: the calculation speed and the crack pattern. Despite the quasi-isotropic stiffness properties of the layer do not require different strength of the material in different material directions to obtain a crack path in the weakest direction of the layer, the different strengths have to be included to obtain more accurate results. Moreover, this is certainly required to obtain the correct crack path if composites are simulated that do not have quasi-isotropic material properties in a single layer. A solution would be to implement the Hashin damage model[10] which is already available in Abaqus[3] for the general static analysis, but not for the direct cyclic analysis. Thus a user-defined material[1] would be the solution to that problem. The increase in calculation speed in particular with regard to cycle jumping is a more difficult problem. This requires extensive programming of a user-defined subroutine or the software developers of Abaqus[3] need to implement a version in Abaqus[3] that is capable of handling extrapolation of plasticity.

As already discussed in chapter 3, the second stage of residual relative stiffness will not be present in the compact tension specimen model as it is in-plane bending instead of out-of-plane bending. Even if the VCCT is included for interply failure, it is merely to enhance the prediction of the first and third stage. In other words, stage II will be overlapping with stages I and III where the delamination is only present to allow extra crack path opportunities that involve a combination of interply and intraply cracking. This provides opportunities to identify crack paths which have less resistance than individual intraply paths. That will be more interesting if two cracks start at different locations or if non-quasi-isotropic layers are modelled with the VCCT interaction included. Since more elements are involved, stage I and III will no longer be separated by the definition of the SDEG parameter of the structure being equal to zero or larger than zero. It is perfectly possible that the first element undergoes damage degradation while the next element is just in its plastic phase and further down the future crack the material is still in its virgin elastic state. Therefore a slightly new definition is needed that is more closely related to the overall definition between crack initiation and crack propagation phase on a structural level. Stage I of the stiffness degradation of the structure, caused by the inter fibre failure mechanism, shall be considered to have ended as soon as the first element has fully degraded. Once the first element has fully degraded, stage III of the stiffness degradation of the structure has started which is dominated by the fibre failure mechanism. Now stage I is related to the crack initiation phase and stage III to the crack propagation phase. One downside of this definition is the fact that it will be element size dependent.

The crack propagation rate $\frac{da}{dN}$ is in coherence with a Paris law curve based on the energy release rates of the VCCT interaction. The fatigue life of the CT specimen could be controlled by the strength of the VCCT interaction if the VCCT mechanism is governing. However, the tie constraints will always result in a faster crack propagation as the tie constraints lead to a smaller but more concentrated peak stress area. For the Paris law based on the calculated stress intensity factor a negative material parameter is observed. That should not happen, therefore it is questionable if the crack propagation is modelled correctly.

[1] A user-defined material is implemented by creating an external input file for the material parameters that contain a standard formulation in Abaqus[3] listed in section 3.4 of chapter 3. These options were not investigated as these are outside the scope of this thesis

The CT specimen models allows to extract the force and the displacement over time in the pins (holes) and the stiffness degradation parameter of the integration points. Since the elements, that are used, only have one integration point, it means that the stiffness degradation parameter of the element will be extracted. These three outputs are required to perform a fatigue assessment of the structure. The forces and displacement could be combined to obtain hysteresis plots which give insight in the amount of energy dissipated during a cycle and how the cycles progress towards failure. This progression is then plotted as a residual relative stiffness curve. This curve allows to identify the different stages happening in the composite structure and determine after how many cycles stage I is left and stage III starts. The residual strength could be obtained by stopping the fatigue analysis at a certain number of cycles and perform a static test to obtain the remaining strength. The stiffness degradation parameter shows how much overall damage has been brought to the structure which is the cumulative over all elements (even the elements which are not close to the crack). S,N-curves could be obtained by running the model for different load levels. The constant life diagrams (CLD) could be obtained if the model is not only run for different load levels, but also with different load ratios. It is always important to check the stages of the stiffness degradation, the evolution of the speed of the increasing stiffness degradation parameter and the crack pattern itself. These are simple checks to see whether a simulation resulted in a plausible result or not.

The parameters that influence the fatigue life include the ones that were already discussed in the one element model: $G_f$, $\varepsilon_f$, $\varepsilon_{ult}$, $\sigma_{ult}$ $\sigma_{y,0}$ and $E_2$. Add to that list $E_1$ as well as for plies with different material orientation, as the highest stiffness leads to faster failure. Additionally, the fatigue life of the structure is largely influenced by the interaction between two plies. Hence the critical energy values $G_{I,c}$, $G_{II,c}$ and $G_{III,c}$ with their exponents for the mixed law behaviour are important. On top of that the Paris law definition is completed with $c_3$ and $c_4$ having major influence as well. Whether the earlier parameters that define the intraply properties are more dominant in determining the fatigue life or the VCCT parameters, depends on which mechanism is the slowest. If the delamination is lagging behind, then the VCCT parameters will be dominant on the number of cycles till failure, if the intraply is lagging behind it will be the intraply parameters in order of being summed up.

A mesh refinement study has been performed to check the influence of smaller elements. Decreasing the element size from 2 [mm] to 1 [mm] does have a positive effect on the accuracy. This is observed in the crack path and the equivalent energy release rates. However, it takes the analysis 5 times as long to simulate the cycles. This is still useful if more accurate results are desired. On the other hand, reducing the mesh size from 1 [mm] to 0.5 [mm] does not increase the accuracy of the results significantly. Therefore it is a waste of time, even if the 10 times longer calculation time is not considered. Therefore the solution is considered to have converged sufficiently at a mesh size of 1 [mm].

The VCCT has been isolated for some models. The VCCT isolated MS2 11 U5.0 model revealed that the degradation in stiffness is caused by the ductile damage module. Only a minor degradation in residual stiffness was observed at the start of the VCCT isolated MS2 11 U5.0 model and it had already been eliminated in chapter 4 that a hardening formulation for the plasticity module would lead to a degradation in residual stiffness. The absence of the ductile damage model also lead to the removal of the maximum Von Mises stress allowed in the material. Now the observed maximum stress at the crack tip was at least four times as large as the previously imposed limit of $\sigma_{ult}$. It was also observed that the VCCT isolated MS2 11 models had a radial expansion of the interply crack showing there is no weak direction present in the material. This would slow down the crack propagation growth for increasing the number of cycles, but not for increasing crack length $a$. On top of that, the absence of the plasticity model meant there are no negative loads present in the material. Thus the plasticity model simulates a crack overclosure effect that is not present in composites. Therefore the plasticity model has to be taken with caution.

Although no S,N-curves, or better to state U,N-curves, were constructed, the change in load does reveal there would be a change in fatigue life. A higher load resulted in a faster crack propagation due to more material being activated plastically to dissipate the energy. Since the fatigue life is defined by the amount of cycles are required to let the first crack reach completely through the cross-section, it implies that a faster observed crack propagation rate would imminently lead to a shorter fatigue life unless a change in failure mechanism occurs. This is conform the expectations of an U,N-curve.

# Chapter 6: Discussion

Since there was no literature present that proves whether the plasticity model is compatible with the direct cyclic analysis or not, the plasticity model was tested first on a single element. The one element models of chapter 4 show that the implemented plasticity model is in line with the hypothesis of plasticity. This has been proven by comparing the one element model with a self-made program in Python[58] that calculates results for one element based on the plasticity theory. This plasticity model is used to complement the ductile damage model that is already in use to describe the onset of stage III. This improvement was required to allow one element mimic an entire compact tension specimen (CT specimen) that shows stiffness degradation in stage I due to isotropic softening component of the plasticity model. This is in line with the hypothesis that a compact tension specimen is an in-plane bending test where two stages are observed. Some important assumptions were made upon using the one element model to describe an entire full compact tension specimen.

1. The effects of the delamination (DEL) mechanism need to be included partly in the description of the inter fibre failure (IFF) and partly in the fibre failure (FF) since one element represents multiple plies.
2. The CT specimen is assumed to have free movement for side-ways contraction.
3. The CT specimen is assumed to be constrained at the top and bottom instead of two internal holes.
4. Stage III starts at increasing SDEG instead of the failure of the first element.
5. Final failure is reached if the element has failed in stage III due to the damage model instead of a crack running through the element.

Upgrading to a full compact tension specimen model with multiple plies as is performed with the two models VCCT MS2 11 and TIE MS2, did not disprove the hypothesis of a CT specimen having two stages.

However, in these two models it was no longer required to have isotropic softening to mimic stiffness degradation. Even the isotropic hardening parameters of table 6.1 based on the static coupon tests [43] still resulted in structural stiffness degradation. Thus there is a difference in concept between modelling every behaviour with one element and modelling behaviour with multiple elements. This indicates that for the general behaviour only the ultimate stress is important to model the first stage. Another option would be to model the the inter fibre failure (IFF) with a damage model. If the plasticity model is substituted by a damage model, then it is required to have a damage initiation stress $\sigma_{ini}$ to define the onset of inter fibre failure (IFF) at element level with a crack initiation strain $\varepsilon_{ini}$. If the damage model is used to define the onset of fibre failure (FF) at element level, then the ultimate stress $\sigma_{ult}$, with a corresponding strain $\varepsilon_{ult}$, has to be larger than $\sigma_{ini}$ as is shown in the static coupon test results [43]. This could be achieved either by having two damage models or in a simpler manner with one damage model that has a bi-linear degradation. For the latter the situation is illustrated in figure 3.7. For this a tabular input is required and the linear damage evolution is no longer sufficient. Notice that stage 0 is used to describe the elastic response which is small since composites crack early due to their brittleness. This option has not been investigated, thus there is no clue if Abaqus[3] allows this input. Anyway, it will not be a possibility if the evolution is based on the fracture energy since a

tabular input is not possible on the fracture energy basis. Therefore there is no readily available damage model in Abaqus[3] that explicitly describes an increase in stress after damage initiation. One could still investigate the effect of having an ultimate stress equal or slightly lower than the initiation stress on a CT specimen model with multiple elements. Perhaps the effect of $\sigma_{ult} < \sigma_{ini}$ is not as detrimental as it is thought to be. In literature only the Lemaitre model[44] is found to allow an increase of stress in an element on bases of the effective stress model. This model is not included in one of the readily available models in Abaqus[3]. All these options of a readily available damage models with fracture energies would lead to an undesired material response definition. For that reason the plasticity model is preferred to describe the IFF.

The plasticity model has a second advantage, it will not show cracking due to IFF. Thus only the ductile damage model will result in cracking. So it is always clear due to the crack visualisation when an element has failed completely. For both groups of models (the one element models and the CT specimen models) it is assumed that only three damage mechanisms are present (IFF, delamination and FF), but only the ductile damage (FF) leads to intraply cracking. IFF does lead to small cracks in reality and actually is a damage mechanism, but in all the models these cracks are considered as too small to visualise. Therefore only the stiffness degradation effect of these cracks is included. Consequently, a critical view has to be kept on using the plasticity model for the IFF with respect to overclosure as proven with the VCCT isolated MS2 11 U5.0 model. For now it is the most convenient solution with the limitation of using readily available techniques in Abaqus[3]. Preferably IFF is modelled with a damage model as well. Perhaps a solution could be to define the stiffness degradation due to damage based on displacements instead of on energy as already mentioned.

For now a choice has been made to use the ductile damage model for FF as is explained in section 3.7.2 of chapter 3, but the XFEM would have been a valid choice for a CT specimen. In CT specimen the crack initiation location is known. Moreover, the crack propagation path is to a certain extend already known as well. The general direction of the crack is based on the fibre orientation. A damage model has to be included to limit the observed $\sigma_{ult}$ to realistic values as is demonstrated by the VCCT isolated MS2 11 U5.0 model.

For the CT specimen the transition from stage I to stage III is much more nuanced. This is more nuanced since one element could be already fully degraded while the next element in the crack pattern could still have had only an elastic response. For that reason it has been chosen to define the end of stage I and the start of stage III in the CT specimen at the moment that the first element has failed. This is at the same moment when the degradation of the residual stiffness levels off. This is detected by observing the shape of the residual stiffness plots of the VCCT MS2 11 model and the TIE MS2 model. It is in resemblance with the results of the discontinuous-continuous specimen loaded at $69\%$ of ultimate tensile load [2]. The value of the decrease in stiffness on the other hand is $3$ and $5$ times larger for the VCCT MS2 11 model and the TIE MS2 model respectively.

The VCCT MS2 11 model and the TIE MS2 model discussed in sections 5.5.2 and 5.6 of chapter 5 respectively show promising results. The crack path is in horizontal direction as is expected for a material with quasi-isotropic stiffness and one failure strength. The quasi-isotropic stiffness results in that no extra stresses are attracted in any direction and the strength is equal in all directions even in tension as well as compression. Therefore it has no preferred direction to crack based on the material model as is mentioned already in section 5.4.4 of chapter 5. The compact tension specimen (CT specimen) does have a preferred direction due to its geometry. The CT specimen has a stress intensity at the crack tip with the highest stresses a bit in front of the crack tip. Therefore the element in front of the crack tip is degraded more, thus the crack moves straight ahead (horizontally). During the CT specimen testing the crack has to move horizontally within a certain deviation as is required by ISO-norm 15850[4]. Thus it

**Table 6.1:** Input table containing the parametric values used in the compact tension model for unidirectional and quasi-isotropic elastic stiffness parameters.

| | Unidirectional | Quasi-isotropic |
|---|---|---|
| $E_1$ [MPa] | 12285 | 12285 |
| $E_2$ [MPa] | 3000 | 12285 |
| $E_3$ [MPa] | 3000 | 3071 |
| $\nu_{12}$ [-] | 0.35 | 0.35 |
| $\nu_{13}$ [-] | 0.30 | 0.30 |
| $\nu_{23}$ [-] | 0.30 | 0.30 |
| $G_{12}$ [MPa] | 2000 | 4550 |
| $G_{13}$ [MPa] | 2000 | 4725 |
| $G_{23}$ [MPa] | 1000 | 4725 |

is in coherence with reality.

The orthotropic stiffness properties are included in the models VCCT MS2 11 and TIE MS2. The values that are used for these two models are summarised in table 6.1. The longitudinal normal stiffness $E_1$ and Poisson's ratio $\nu_{12}$ are based on an earlier performed static tensile coupon test [43] in accordance with ISO-norm 527-1 [45]. Based on the fact that these test specimen have a quasi-isotropic layup, the other stiffness parameters are worked out. Only the value of either one of the Poisson's ratios in the other direction had to be assumed to complete this. With these quasi-isotropic stiffness properties a good representation of the stress distribution and stress intensity is obtained.

The unidirectional (UD) stiffness properties are also summarised in table 6.1, but these were used in earlier models discussed in section 5.3 of chapter 5 and the first model of section 5.4.4 of chapter 5. From these models it is observed that the UD stiffness properties lead to false crack patterns. The crack propagates through the material perpendicular to the first direction of the material with the first direction of the material being in fibre direction as was shown in figures C.1 and C.7. This is contradictory to the expectations as the crack is expected along the fibre, therefore parallel to the first material direction. This is caused by modelling one ultimate stress for all failure directions of the composite. Hence no strength parallel or perpendicular to the fibre is distinguished. There is even no compressive strength distinguished from the tensile strength. The UD model suffers from the lack of orthotropic strength definition, but the quasi-isotropic model does not since the quasi-isotropic material has equal in-plane stiffness and strength. Additionally, the material is mainly loaded in tension thus defining a weaker compression strength is of lesser importance.

The VCCT MS2 11 model and the TIE MS2 model include brittle material properties for the ductile damage model. The material properties for the ductile damage model are summarised in table 6.2. The fracture strain $\varepsilon_f$ is based on the assumption that the material was about to fail during the static tensile coupon test [43]. This leads to a brittle failure which is a well-known property of glass fibre composites. The stress triaxiality $\eta$ and strain rate $\dot{\varepsilon}$ do not have influence on all the models as the problem is not stress nor strain dependent as was discussed in section 4.6.2 of chapter 4. Although it was successful in obtaining results with the brittle material input, the ductile damage model is originally designed for ductile materials such as metals. Metals are isotropic, therefore the ductile damage model acts as if the composite is isotropic in strength and stiffness. This has been shown earlier in models and raises concern as the strength and the stiffness are actually orthotropic in composites. Especially the compression strength and the tensile strength are different for a single direction. For the quasi-isotropic models VCCT MS2 11 and TIE MS2 this is not that big of a deal.

**Table 6.2:** The input table containing the parametric values used in the CT model for the brittle material properties of the ductile damage module.

| | |
|---|---|
| $\varepsilon_{fracture}$ [-] | 0.0052 |
| $\eta$ [-] | 0.33333 |
| $\dot{\varepsilon}$ [-] | 1 |
| $G_f$ [N/mm] | 25 |

**Table 6.3:** The input table containing the parametric values used in the CT model for the brittle material properties of the plasticity module.

| | |
|---|---|
| $\sigma_{y,0}$[MPa] | 39.53 |
| $Q_\infty$[MPa] | 250 |
| $b$[-] | 300 |

Similarly both models include brittle material properties for the plasticity model. These values are summarised in table 6.3. It is rather contradicting to have a plasticity model for brittle materials as brittle materials are defined not to have a plastic response; unlike metals. For all the models discussed in chapter 5 the definition of plastic response is adapted. Now the plastic response is defined as the response for which the initial stiffness no longer applies. In other words, the plasticity model is only used to model the stiffness degradation up to the point where damage starts. The values for the plasticity model in the VCCT MS2 11 and the TIE MS2 model are based on the stress-strain relation of the static tensile coupon test results[43]. The initial yield strength $\sigma_{y,0}$ is based graphically on the pen line of the initial stiffness $E_1$ leaving stress-strain relation as is shown in figure 3.6. The values for the stress increase $Q_\infty$ and conversion speed $b$ are based on calibration according to the conversion explained in section 4.5.1 of chapter 4. This calibration is shown in figure 4.10. It is not required for the plasticity model to have reached conversion. Lastly the fracture energy $G_f$ of the ductile damage model determines the precise point on which the maximum stress is reached.

There are two final models: the VCCT MS2 11 model and the TIE MS2 model. The VCCT MS2 11 model has the virtual crack closure technique (VCCT) defined as interface between two plies while the TIE MS2 uses tie constraint for the interfaces resulting in some differences between the two final models. The input values of the VCCT criterion are summarised in table 6.4 for the VCCT MS2 11 model. Some typical characteristics are observed for the VCCT model such as the peak stress area in front of the crack tip and the crack propagation rate, but the residual stiffness remained about equal. The peak stress area is slightly larger and more stubby, therefore more elements are involved in the plasticity model as is for the ductile damage model. Also the crack propagation rate is slower. In section 5.5.2 of chapter 5 these phenomena are explained by the fact that the VCCT interaction is able to absorb energy by releasing nodes. On the other hand, the tie constraint cannot release nodes, therefore more energy must be absorbed by the elements themselves. This results in more damage in the elements, thus a faster crack propagation. By absorbing more energy in the interaction, the elements ahead of the crack tip have a slightly lower peak stress, thus could endure more cycles. However, a slightly lower maximum peak implies a larger area of peak stress is needed. For that reason more elements are involved that undergo stiffness degradation. Hence the residual stiffness diagram shows no significant difference.

**Table 6.4:** Template for the input data line to provide a VCCT interface for the fatigue analysis of the five ply CT.

| | |
|---|---|
| Line 1 | *Debond, slave="Front_ply_$< n >$", master="Back_ply_$< n-1 >$", debonding force=STEP, frequency=1 |
| Line 2 BK | *FRACTURE CRITERION, TYPE=fatigue, MIXED MODE=BK, TOLERANCE=<tolerance><br>„1,1,0.001,0.9,7,<br>7,1,20 |

There is an exponential relation between the crack propagating and the observed critical energy release rates in the VCCT MS2 11 model. The exponential relation shows that some type of Paris law exists between the crack propagation and the equivalent energy release rate. However, the exponential relation is not equal to that based on the input values of the Paris law. A further investigation of the SDEG might show resemblance with the Paris law input values.

A mesh refinement study performed in section 5.6 of chapter 5 has demonstrated that decreasing the element size from 2 [mm] in the VCCT MS2 11 model to 1 [mm] in the VCCT MS2 11 does improve the accuracy of results. There is a better defined area of peak stress in the shape of an arc instead of a bulb in front of the crack tip. This arc allows entire elements to be in stage III between the peak stress and the crack tip instead of one element with one edge at maximum stress and the other at zero stress. Refining the mesh also reduces the scatter observed in figure C.40 compared to first 50 [cycles] in figure C.18. However, this improved accuracy is at the cost of computational speed. The VCCT MS1 11 model took five times as long as the VCCT MS2 11 model to complete the first 50 [cycles]. The converging of the solution leads to an absence of further significant improvements upon decreasing the element size from 1 [mm] to 0.5 [mm]. Therefore it does not justify to increase the computational time again by a factor of 10. For that reason the mesh is best kept at 1 [mm] for accurate calculations and 2 [mm] if time is limited.

Also a load differentiation effect has been performed in section 5.7 of chapter 5. The change in load does reveal there would be a change in fatigue life. A higher load resulted in a faster crack propagation due to more material being activated plastically to dissipate the energy. Since the fatigue life is defined by the amount of cycles are required to let the first crack reach completely through the cross-section, it implies that a faster observed crack propagation rate would imminently lead to a shorter fatigue life unless a change in failure mechanism occurs. This is conform the expectations of an U,N-curve. However, this valid as long as no extra cracks are added during the analysis. In other words, as long as the cracks do not split. For the VCCT MS2 11 U7.5 a crack split was possible at the start, therefore it did not have much influence on the total crack propagation rate. But if the crack would have split after a several thousands of cycles, then a slow down in crack propagation rate would have clearly been observable as the energy would have to be distributed over two cracks instead of one. Generally this results in one crack absorbing all the energy an propagates significantly faster. As this crack propagates, then it will absorb more energy till it has arrested the other crack. Since this split is at the start, it is able to continue both cracks equally.

Other methods to accelerate the calculation speeds have been tried with varying success. It is still a debate whether cycle jumping is possible in combination with the plasticity model. Abaqus[3] is able to calculate with it, but both the one element model of chapter 4 and the CT single ply UD[0] dN=10 model showed that the amount of final plastic strain is dependent on the ratio of the number of cycles jumped over the number of cycles to be simulated $\frac{dN}{N}$ and simply on the number of cycles to be simulated $N$ as was shown in figure C.4. The VCCT criterion is well known to be compatible with cycle jumping [24]. The ductile damage model has not specifically been tested on cycle jumping as an incorrect cycle jumping during the plasticity model makes it no longer required on the ductile damage model.

The number of iterations that have to be used depends on the type of loading. It has been verified on the one element model of section 4.4.2 of chapter 4 that 10 iterations are needed for the force controlled analysis to obtain equilibrium while only 2 iterations are needed for the displacement controlled analysis. Although the VCCT MS2 11 and TIE MS2 models have displacement controlled analysis, the element itself undergoes certain forces based on the adjacent elements. Therefore it is questionable if more iterations are required.

On top of that, it is required to model the first half cycle with a static analysis. In theory this should not be required as was proven in figure 4.4 where the static analysis is only performed to visualise the first half cycle. However, comparing figure C.9 with figure C.12 does show a major influence on the fatigue behaviour of the material due to a different approach in modelling the first half cycle. For that reason it seems safer to model the first half cycle with the static analysis.

The VCCT MS2 11 model and the TIE MS2 model still holds some assumptions based on the included and the excluded mechanisms. Although Brod et al[1] and Bartkowiak et al [2] only observed the inter fibre failure, the delamination and the fibre failure mechanisms, other mechanisms could have effect in a CT specimen. These mechanisms such as the braider yarn periphery mechanism and a crack along the fibre mechanism are neglected. That means they will be included together with the other mechanism during calibration. This results in small differences between the parameters that should be used and what is obtained from tests. These differences could have influence when up-scaling the model from a CT specimen to a full size joint. For that reason there is always a trade-off between the number of mechanisms included, the number of tests required for calibration and the computational time. Including more mechanisms in a model will require more material tests to define all the parameters, but these models are more likely to need less calibration after up-scaling. However, including more mechanisms in a model definitely takes more time to simulate. There are different models developed by other research groups that are not based on the mechanisms or only describe one mechanism as a lump mechanism. If only ductile damage models are used to describe all the mechanisms that will be considered, then only the most governing ductile damage model will have its effect. A single mechanism is certainly a lot easier to model. A single predefined crack along the symmetry line of the CT specimen with a VCCT interaction would do the trick. There is one big "but" to that, you have to know the crack path in advance. An alternative has been tried as the VCCT slicing model, but that turned out to be unattainable for the current computers. It takes too much time to perform the analysis, even if the CT specimen is loaded only with static loading. Having a single ductile damage model will not suffice either. The ductile damage model is one of the two damage models compatible with fatigue and requires a definition of plasticity in order to define the ultimate stress. Finally, one could argue to use a probabilistic model. For simple problems this is possible based on one parameter providing the probability of success[62]. However, this is unattainable for full size joints. Other methods are merely a variation of the S,N-curve by providing an estimation of the scatter. These probabilistic methods need a lot of fatigue testing to obtain their parameters with a reasonably accurate prediction of the scatter.

Even if all mechanisms are accounted for, the model is phenomenological. Even the virtual crack closure technique (VCCT) for the delamination phase is phenomenological. Hence not the real mechanism is modelled, but rather the mechanism is mimicked. That implies that the model will only predict the fatigue behaviour and the fatigue life accurately for the region it has been calibrated for. A fair degree of interpolation and nearby extrapolation will be possible. Even if a prediction would be made for the joint in the jacket structure, first calibrations with the material test results will be required. It is also questionable if the precise cracking behaviour will ever be correctly presented as the model is a smeared crack model. One of the underlying assumption is that the static coupon test initially loses its stiffness due to static IFF that would be the cause of embedment failure. It is not verified if this assumption is valid. In spite of the model just being a phenomenological model, it still has to prove itself in predicting the fatigue behaviour on physical applications since the real mechanisms are modelled by a dummy mechanisms. Even then, it still has potential to obtain accurate results. This is similar to how in the medieval times the positions of the stars were predicted based on epicycles. Although those models had the Earth as the centre of the universe, those models provided more accurate results in predicting the position of the planets and the stars than the early models with the Earth moving in a constellation. However, those phenomenological models will be outdated once more knowledge and stronger computers are available. For the moment it is the best option present with today's widely available knowledge and resources. In

other words, this is the best available model with the readily available tool in Abaqus[3] to describe the mechanisms without considering user-defined materials and subroutines.

# Chapter 7: Conclusion

The master thesis is performed to investigate the applicability of a combined model that predicts the fatigue behaviour of glass fibre composites. First research was done on a one element model with a plasticity model and a continuum damage model (CDM) included in the material properties. This model has been improved in order to predict the behaviour of a compact tension specimen (CT specimen). The CT specimen consists of interconnected multiple layers which are researched with a Virtual Crack Closure Technique (VCCT) interface model. The CT specimen model was used to investigate certain aspects such as: stiffness degradation, fatigue life, the influence of the material parameters of all three modules (plasticity, ductile damage and VCCT) included in the model, cycle jumping and mesh refinement.

There are three significant failure mechanisms considered for the in-plane bending fatigue of a compact tension specimen as explained in section 2.5 of chapter 2. The significant failure mechanisms that were included are: the inter fibre failure, delamination and fibre failure. The inter fibre failure and fibre failure are intraply mechanisms. The first to occur is the inter fibre failure mechanisms starting at the crack tip that reduce the stiffness of the material, then the fibre failure mechanism occurs in the ply that reduce the strength and stiffness progressively. Delamination occurs simultaneously with either of the intraply mechanisms. The delamination allows to find more critical crack patterns than each ply individually.

A triple mechanism model with a distinctive effect for each of the mechanisms has been developed with the readily available tools in Abaqus[3]. The model consists of a plasticity model to describe the inter fibre failure, a ductile damage model to describe the fibre failure and a virtual crack closure technique (VCCT) model to describe the delamination.

The CT model with VCCT interaction discussed in paragraph 5.5.1 of chapter 5 that includes these three mechanisms shows expected results based on the requirements set in the introduction. First of all, it is possible to show simulate different fatigue life for different load levels. Secondly, the CT model with VCCT interaction is capable of handling brittle materials with orthotropic stiffness. Thirdly, it shows an expected crack pattern for quasi-isotropic material which is in the direction of the peak stress. However, the orthotropic strength of the composite is not taken into account. This resulted in a simulated crack pattern that is not correct for unidirectional materials. Fortunately, the cycle jumping for the VCCT and ductile damage model is possible since both models are damage based and Abaqus[3] is able to extrapolate damage. On the other hand, the cycle jumping is not possible for the plasticity model since the plasticity model is based on plastic strain which could not yet be extrapolated by Abaqus[3]. This results in a cycle jumping that is questionable for the CT model with VCCT interactions. Also the plasticity model has to be taken with caution as it will lead to the crack overclosure effect which is present in metals, but not in composites. Therefore the CT model with VCCT interaction is promising, but not yet qualified to predict the fatigue behaviour of composites.

There are solutions possible that are not readily available techniques in Abaqus[3]. A user-defined material could be written adapt to the Hashin damage model for the direct cyclic analysis. That would allow to handle the orthotropic strengths. Perhaps an anisotropic hardening formulation, which is readily available, is sufficient enough. Also a user-defined subroutine could be written to perform plasticity extrapolation and to allow cycle jumping in the plasticity model.

The parameters that have the most influence on the fatigue life are: the elastic stiffness, the ultimate strength, the fracture plastic strain, the fracture energy, the energy release rates and the two material constants for the Paris law of the interface.

# Chapter 8: Recommendations

The current CT specimen models are not yet ready to handle fatigue failure in composites. First a couple of issues have to be solved. The most important issue to find a solution for, is to allow cycle jumping. For the VCCT model there is a cycle jumping algorithm readily available in Abaqus[3], but not for the plasticity model. Therefore it is not applicable for the combination of these three models. A user-defined subroutine needs to be defined or future versions of Abaqus [3] should have it implemented. The second opportunity is to handle the orthotropic strength, which is not dramatic for quasi-isotropic laminates. For the static analysis the Hashin model is readily available, but it is not yet applicable for the direct cyclic step. Therefore a user-defined material needs to be written or the anisotropic plasticity must be investigated further.

For future research it is required to first calibrate the model with parameters determined by material testing. Some of the parameters could be obtained by static tests such as the elastic stiffness in the different directions. Other values have to be obtained by simple fatigue tests that determine certain values such as the critical energy values (double cantilever beam test for $G_{Ic}$ and end notch fracture test for $G_{IIc}$). The final parameters for the plasticity model and ductile damage model could initially be estimated on static tests, but will require compact tension tests to calibrate them accurately as static and fatigue input are likely to be different. There is one trick that helps to determine $Q_\infty$. As mentioned during the sanity checks, the peak stress is determined by the sum of the yield stress and $Q_\infty$. Since the yield stress is already known, $Q_\infty$ could be obtained from the stress concentration formula in ISO-norm 15850 [4]. In the end the idea is to predict the residual strength based on the residual stiffness. In order to obtain the residual strength from the model, an additional static step is required which tears the compact tension specimen apart after a certain number of cycles has been simulated. Also the S,N-curves could be determined by switching to force controlled analysis and applying different load levels. If also different load ratios are added, then constant life diagrams could be obtained. These will help to design the joints easier.

# References


[1] M. Brod, A. Dean, S. Scheffler, C. Gerendt, and R. Rolfes. Numerical modeling and experimental validation of fatigue damage in cross-ply CFRP composites under inhomogeneous stress states. *Composites Part B: Engineering*, page 108050, 2020.

[2] M. Bartkowiak, W. Liebig, and K.A. Weidenmann. Fatigue damage behaviour of continuous-discontinuous properties of thermoplastic base hybrid laminates. *Hybrid 2020 Materials and Structures*, pages 71–77, 2020.

[3] Dassault Systèmes. Abaqus 2019. *Providence, Rhode Island, USA*, 2019.

[4] NEN-ISO 15850: Plastics - determination of tension-tension fatigue crack propagation - linear elastic fracture mechanics (LEFM) approach. Norm, Nederlands Normalisatie-instituut, Delft, Netherlands, February 2014.

[5] P. Dvorak. Developments of bottom-fixed offshore wind foundations in europe. *Windpower Engineering Development*, 2017.

[6] Officer of the Watch. Alexander L. Kielland platform capsize accident – investigation report, 2013. *https://officerofthewatch.com/2013/04/29/alexander-l-kielland-platform-capsize-accident/*, accessed 9 August 2020.

[7] R.C. Dr.Ir. Alderliesten. AE4ASM005: Fatigue in structures and materials, 2019. *https://brightspace.tudelft.nl, Delft University of Technology*, accessed 9 August 2020.

[8] W. Van Paepegem and J. Degrieck. A new coupled approach of residual stiffness and strength for fatigue of fibre-reinforced composites. *International Journal of Fatigue*, 24(7):747–762, 2002.

[9] P.C. Paris, H. Tada, and J.K. Donald. Service load fatigue damage—a historical perspective. *International Journal of fatigue*, 21:S35–S46, 1999.

[10] Z. Hashin and A. Rotem. A fatigue failure criterion for fiber reinforced materials. *Journal of composite materials*, 7(4):448–464, 1973.

[11] BS 5400-10:1980: Steel, concrete and composite bridges. Code of practice for fatigue. Norm, British Standards Institute (BSI), United Kingdom, 1980.

[12] J. Schijve. *Fatigue of structures and materials*. Springer Science & Business Media, 2001.

[13] A.P. Vassilopoulos and R.P.L. Nijssen. Fatigue life prediction of composite materials under realistic loading conditions (variable amplitude loading). In *Fatigue life prediction of composites and composite structures*, pages 293–333. Elsevier, 2010.

[14] M.M. Shokrieh and L.B. Lessard. Progressive fatigue damage modeling of composite materials, part i: Modeling. *Journal of composite materials*, 34(13):1056–1080, 2000.

[15] M. Kamiński. On probabilistic fatigue models for composite materials. *International journal of fatigue*, 24(2-4):477–495, 2002.

[16] M. Naderi and A.R. Maligno. Fatigue life prediction of carbon/epoxy laminates by stochastic numerical simulation. *Composite Structures*, 94(3):1052–1059, 2012.

[17] C. Kassapoglou. Fatigue life prediction of composite structures under constant amplitude loading. *Journal of Composite Materials*, 41(22):2737–2754, 2007.

[18] J. Degrieck and W. Van Paepegem. Fatigue damage modeling of fibre-reinforced composite materials. *Appl. Mech. Rev.*, 54(4):279–300, 2001.

[19] H. Pakdel and B. Mohammadi. Experimental observation and energy based analytical investigation of matrix cracking distribution pattern in angle-ply laminates. *Theoretical and Applied Fracture Mechanics*, 92:146–154, 2017.

[20] E.K. Gamstedt and S.I. Andersen. Fatigue degradation and failure of rotating composite structures–materials characterisation and underlying mechanisms. *Riso National Laboratory, Denmark*, 2001.

[21] A. Argüelles, C. Rocandio, S. Rubiera, I. Viña, and J. Viña. Influence of the test method on the characterization of the fatigue delamination behavior of a composite material under mixed mode i/ii fracture. *Polymers*, 11(11):1788, 2019.

[22] Z. Hashin. Cumulative damage theory for composite materials: residual life and residual strength methods. *Composites Science and Technology*, 23(1):1–19, 1985.

[23] Massachusetts Institute of Technology. Damage initiation for ductile metals, 2019. *https://abaqus-docs.mit.edu/2017/English/SIMACAEMATRefMap/simamat-c-damageinitductile.htm*, accessed 28 September 2020.

[24] Manuel Ramsaier. Fracture mechanics: Cls specimen vcct debonding in abaqus part 1: Strain energy release rate, 2014. *https://www.youtube.com/watch?v=9GXppvgGmHQlist=PLE4jpqcRJiBrNlnkqCrCLJHKoIEs71mQPindex=2*, accessed 13 August 2020.

[25] Simutech solution corp. Abaqus application of fracture mechanicsxfem low cycle fatigue, 2019. *https://www.youtube.com/watch?v=hdWlqkBDZ8I*, accessed 5 November 2019.

[26] Massachusetts Institute of Technology. *FRACTURE CRITERION, 2019. *https://abaqus-docs.mit.edu/2017/English/SIMACAEKEYRefMap/simakey-r-fracturecriterion.htm*, accessed 29 September 2020.

[27] Massachusetts Institute of Technology. *COHESIVE BEHAVIOR, 2019. *https://abaqus-docs.mit.edu/2017/English/SIMACAEKEYRefMap/simakey-r-cohesivebehavior.htm*, accessed 29 September 2020.

[28] M. L. Benzeggagh and M.J.C.S. Kenane. Measurement of mixed-mode delamination fracture toughness of unidirectional glass/epoxy composites with mixed-mode bending apparatus. *Composites science and technology*, 56(4):439–449, 1996.

[29] E. M. Wu and R.C. Reuter Jr. Crack extension in fiberglass reinforced plastics. Technical report, Illinois university at Urbana Deparmtent of theoretical and applied mechanics, 1965.

[30] J. Reeder, K. Song, P. Chunchu, and D. Ambur. Postbuckling and growth of delaminations in composite plates subjected to axial compression. In *43rd AIAA/ASME/ASCE/AHS/ASC Structures, Structural Dynamics, and Materials Conference*, page 1746, 2002.

[31] Massachusetts Institute of Technology. Johnson-cook plasticity, 2019. *https://abaqus-docs.mit.edu/2017/English/SIMACAEMATRefMap/simamat-c-johnsoncook.htm*, accessed 28 September 2020.

[32] Silesian University of Technology Jaroslaw Z. What is the difference between bilinear kinematic model (availaible in ANSYS APDL) and johnson cook model(ABAQUS)?, 2020. *https://www.researchgate.net/post/What_is_the_difference_between_Bilinear_Kinematic_Model_availaible_in_ANSYS_APDL_and_Johnson_Cook_ModelABAQUS*, accessed 28 September 2020.

[33] Massachusetts Institute of Technology. Ornl – oak ridge national laboratory constitutive model, 2019. *https://abaqus-docs.mit.edu/2017/English/SIMACAEMATRefMap/simamat-c-ornl.htm*, accessed 29 September 2020.

[34] Massachusetts Institute of Technology. Annealing or melting, 2019. *https://abaqus-docs.mit.edu/2017/English/SIMACAEMATRefMap/simamat-c-annealmelt.htm*, accessed 29 September 2020.

[35] Massachusetts Institute of Technology. Anisotropic yield/creep, 2019. *https://abaqus-docs.mit.edu/2017/English/SIMACAEMATRefMap/simamat-c-anisoyield.htm*, accessed 29 September 2020.

[36] Massachusetts Institute of Technology. Models for metals subjected to cyclic loading, 2019. *https://abaqus-docs.mit.edu/2017/English/SIMACAEMATRefMap/simamat-c-hardening.htm*, accessed 1 July 2020.

[37] Massachusetts Institute of Technology. Direct cyclic analysis, 2019. *https://abaqus-docs.mit.edu/2017/English/SIMACAEANLRefMap/simaanl-c-directcyclic.htm*, accessed 14 September 2020.

[38] P.C.J. Dr.Ir. Hoogenboom. CIE4150: Plastic analysis of structures, 2017. $http://homepage.tudelft.nl/p3r3s/b19A_schedule.html, accessed 1 October 2017.$

[39] O. Copuruglo and H.M. Jonkers. CTB1320: Construction materials and sustainability, powerpoint slides. *https://brightspace.tudelft.nl, Delft University of Technology*, 2014.

[40] P. van Mourik, J. van Dam, and S. Picken. *Materials Science in Design and Engineering*. VSSD, Delft, 2012.

[41] S. Tu, X. Ren, J. He, and Z. Zhang. Stress–strain curves of metallic materials and post-necking strain hardening characterization: A review. *Fatigue & Fracture of Engineering Materials & Structures*, 43(1):3–19, 2020.

[42] Massachusetts Institute of Technology. Defining plasticity in abaqus, 2019. *https://abaqus-docs.mit.edu/2017/English/SIMACAEGSARefMap/simagsa-c-matdefining.htm*, accessed 1 July 2020.

[43] H. Pei and M. Pavlovic. Test results of the static coupon testing of the glass fibre reinforcement, 2019.

[44] Jean Lemaitre. *A course on damage mechanics*. Springer Science & Business Media, 2012.

[45] Kunststoffen - Bepalingen van de trekeigenschappen - Deel 1: Algemene beginselen (ISO 527-1:2019,IDT). Norm, Nederlands Normalisatie-instituut, Delft, Netherlands, October 2019.

[46] Prof.dr.ir. R.D. de Borst and Prof.dr.ir. L.J. Sluys. CIE5124: Computational methods in non-linear solid mechanics, lecture notes. *https://brightspace.tudelft.nl, Delft University of Technology*, 2014.

[47] J. Montesano, M. Selezneva, M. Levesque, and Z. Fawaz. Modeling fatigue damage evolution in polymer matrix composite structures and validation using in-situ digital image correlation. *Composite Structures*, 125:354–361, 2015.

[48] J. Montesano, Z. Fawaz, C. Poon, and K. Behdinan. A microscopic investigation of failure mechanisms in a triaxially braided polyimide composite at room and elevated temperatures. *Materials & Design*, 53:1026–1036, 2014.

[49] R. Hill. A theory of the yielding and plastic flow of anisotropic metals. *Proceedings of the Royal Society of London. Series A. Mathematical and Physical Sciences*, 193(1033):281–297, 1948.

[50] N. Mavrodontis. Simuleon FEA blog Abaqus hardening laws on single element model, 2020. *https://info.simuleon.com/blog/abaqus-hardening-laws-on-single-element-model*, Simuleon, accessed 30 September 2020.

[51] Massachussets Institute of Technology. Modeling discontinuities as an enriched feature using the extended finite element method, 2019. *https://abaqus-docs.mit.edu/2017/English/SIMACAEANLRefMap/simaanl-c-enrichment.htm*, accessed 30 September 2020.

[52] P. He and M. Pavlovic. Material model calibrated on joint tests. *Wrapped Fibre Reinforced Polymers work group*, Delft University of Technology, 2019.

[53] L.-J. Jia, W. Fujie, T. Ikai, S. Yoshida, and H. Ge. Dependency of mesh size and loading history on crack propagation energy of cyclic ductile fracture model. *Engineering Fracture Mechanics*, 215:117–137, 2019.

[54] Z. Zou, S.R. Reid, and S. Li. A continuum damage model for delaminations in laminated composites. *Journal of the Mechanics and Physics of Solids*, 51(2):333–356, 2003.

[55] J. Reiner, M. Veidt, M. Dargusch, and L. Gross. A progressive analysis of matrix cracking-induced delamination in composite laminates using an advanced phantom node method. *Journal of Composite Materials*, 51(20):2933–2947, 2017.

[56] Massachusetts Institute of Technology. Crack propagation analysis, 2019. *https://abaqus-docs.mit.edu/2017/English/SIMACAEANLRefMap/simaanl-c-crackpropagation.htm*, accessed 10 March 2020.

[57] Stackexchange: Electrical Engineering. Impedance matching for short-low frequency traces, 2013. *https://electronics.stackexchange.com/questions/42667/impedance-matching-for-short- low-frequency-traces*, accessed 12 August 2020.

[58] Anaconda. Python free edition, 2020.

[59] Massachusetts Institute of Technology. Damage initiation for ductile metals 2019. *https://abaqus-docs.mit.edu/2017/English/SIMACAEMATRefMap/simamat-c-damageinitductile.htm*, accessed 13 August 2020.

[60] Dassault Système. Analysis of composite materials with abaqus. *Course overview*, 21:255, 2019.

[61] Y. Liu, S. Lemanski, X. Zhang, D. Ayre, and H. Y. Nezhad. A finite element study of fatigue crack propagation in single lap bonded joint with process-induced disbond. *International Journal of Adhesion and Adhesives*, 87:164–172, 2018.

[62] Christos Kassapoglou. Fatigue life prediction of composite structures under constant amplitude loading. *Journal of Composite Materials*, 41(22):2737–2754, 2007.

# Appendices

# Appendix A: Python source code

The additional explanation is already given in the source code as string between """..."""" which will also be shown when using the function or after # which will not be shown when using the function.

Imported packages

```
import numpy as np
import matplotlib.pyplot as plt
%matplotlib inline
```

**Figure A.1:** Part 1 of the Python code to predict the response of the plasticity of one element under fatigue loading.

One element isotropic hardening

```python
def fat_prediction_iso_hardening(f_y_0,f_u,e_u,E,U,M,I):
    """This function will only work properly for fatigue analysis on a single cubic 3D stress element with
    unit size that has only isotropic hardening defined in a bi-linear response. Additionally the lateral
    degrees of freedom unrestrained and load with a jigsaw pattern.

    f_y_0 is the initial yield stress
    f_u is the ultimate stress
    e_u is the corresponding observed plastic strain to the ultimate stress
    E is the Young's modulus
    U is the amplitude of the load for R=0 for displacement controlled fatigue
    M is the maximum of cycles estimated to simulate
    I is the number of increments of the load per cycle"""

    e_y_0 = f_y_0*1.0/E #Calculating the yield strain based on the given input parameters
    t = np.linspace(0,M,M*I) #Array that defines the time during the analysis
    e = np.zeros(M*I) #Array that will be defined to have the applied strains
    dU = 2*U/I #Calculating the increment in strain
    c = 0 #Setting the counter to know when a maximum strain has been reached
    a = 1 #Derivative of the amplitude


    for i in range(int(M*I)): #Loop that defines the jigsaw load function
        if c == I/2.0:
            c = 1
            a = -a
        else:
            c += 1
        e[i] = e[i-1] + 2.0*U/(I)*a

    #e = U*( 0.5-0.5*np.cos(2*np.pi*t)) #If a sinusoidal load is prefered, than this line has to be activated

```

**Figure A.2:** Part 2 of the Python code to predict the response of the plasticity of one element under fatigue loading.

```python
    de = np.zeros(M*I) #Array that keeps track of the applied strain increments
    sigma = np.zeros(M*I)#Array that keeps track of the stresses during the calculations
    sigma_predictor = np.zeros(M*I) #Array that make the prediction of the next stress based on elasticity
    f_y = np.zeros(M*I) #Array keeping track of the change in yield stress due to isotropic hardening
    N = 0 #actual count of cycles

    for i in range(M*I): #Main loop to predict the stresses over time
        N += 1.0/I
        if i == 0: #Setting the initial conditions of the system
            de[i] = 0
            sigma[i] = 0
            f_y[i] = f_y_0
        else: #All sequential steps
            de[i] = e[i]-e[i-1] #Calculating strain increment
            sigma_predictor[i] = sigma[i-1] + E * de[i] #Calculating stress based on elasticity
            if abs(sigma_predictor[i]) > f_y[i-1]: #Checking if new stress is within yield contour
                if abs(sigma[i-1]) < f_y[i-1]: #Stress out of yield contour, checking if there is still elasticity
                    if sigma[i-1] < 0: #Elastic and plastic response, initial point inside contour and compression
                        sigma[i] = -f_y[i-1] - (f_u-f_y_0)/(e_u-e_y_0)*(abs(de[i])-(f_y[i-1]-abs(sigma[i-1]))/E)
                    else: #Elastic and plastic response, initial point inside contour and tensile loading
                        sigma[i] = f_y[i-1] + (f_u-f_y_0)/(e_u-e_y_0)*(de[i]-(f_y[i-1]-sigma[i-1])/E)
                else: #Plastic response only, start point already on yield contour
                    sigma[i] = sigma[i-1] + (f_u-f_y_0)/(e_u-e_y_0)*de[i]
            else: #New stress is within yield contour, thus elastic response
                sigma[i] = sigma_predictor[i]
            f_y[i] = max([abs(sigma[i]) , f_y[i-1]])
        if abs(sigma[i]) > f_u: #Stop programm if yield stress has reached ultimate stress
            break

    return t,e,sigma,N
```

**Figure A.3:** Part 3 of the Python code to predict the response of the plasticity of one element under fatigue loading.

One element isotropic softening

```python
def fat_prediction_iso_softening(f_y_0,f_u,e_u,E,U,M,I):
    """This function will only work properly for fatigue analysis on a single cubic 3D stress element with
    unit size that has only isotropic hardening defined in a bi-linear response. Additionally the lateral
    degrees of freedom unrestrained and load with a jigsaw pattern.

    f_y_0 is the initial yield stress
    f_u is the ultimate stress
    e_u is the corresponding observed plastic strain to the ultimate stress
    E is the Young's modulus
    U is the amplitude of the load for R=0 for displacement controlled fatigue
    M is the maximum of cycles estimated to simulate
    I is the number of increments of the load per cycle"""

    e_y_0 = f_y_0*1.0/E #Calculating the yield strain based on the given input parameters
    t = np.linspace(0,M,M*I) #Array that defines the time during the analysis
    e = np.zeros(M*I) #Array that will be defined to have the applied strains
    dU = 2*U/I #Calculating the increment in strain
    c = 0 #Setting the counter to know when a maximum strain has been reached
    a = 1 #Derivative of the amplitude


    for i in range(int(M*I)): #Loop that defines the jigsaw load function
        if c == I/2.0:
            c = 1
            a = -a
        else:
            c += 1
        e[i] = e[i-1] + 2.0*U/(I)*a

    #e = U*( 0.5-0.5*np.cos(2*np.pi*t)) #If a sinusoidal load is prefered, than this line has to be activated
```

**Figure A.4:** Part 4 of the Python code to predict the response of the plasticity of one element under fatigue loading.

```python
    de = np.zeros(M*I) #Array that keeps track of the applied strain increments
    sigma = np.zeros(M*I)#Array that keeps track of the stresses during the calculations
    sigma_predictor = np.zeros(M*I) #Array that make the prediction of the next stress based on elasticity
    f_y = np.zeros(M*I) #Array keeping track of the change in yield stress due to isotropic hardening
    N = 0 #actual count of cycles

    for i in range(M*I): #Main loop to predict the stresses over time
        N += 1.0/I
        if i == 0: #Setting the initial conditions of the system
            de[i] = 0
            sigma[i] = 0
            f_y[i] = f_y_0
        else: #All sequential steps
            de[i] = e[i]-e[i-1] #Calculating strain increment
            sigma_predictor[i] = sigma[i-1] + E * de[i] #Calculating stress based on elasticity
            if abs(sigma_predictor[i]) > f_y[i-1]: #Checking if new stress is within yield contour
                if abs(sigma[i-1]) < f_y[i-1]: #Stress out of yield contour, checking if there is still elasticity
                    if sigma[i-1] < 0: #Elastic and plastic response, initial point inside contour and compression
                        sigma[i] = -f_y[i-1] - (f_u-f_y_0)/(e_u-e_y_0)*(abs(de[i])-(f_y[i-1]-abs(sigma[i-1]))/E)
                        f_y[i] = abs(sigma[i])
                    else: #Elastic and plastic response, initial point inside contour and tensile loading
                        sigma[i] = f_y[i-1] + (f_u-f_y_0)/(e_u-e_y_0)*(de[i]-(f_y[i-1]-sigma[i-1])/E)
                        f_y[i] = abs(sigma[i])
                else: #Plastic response only, start point already on yield contour
                    sigma[i] = sigma[i-1] + (f_u-f_y_0)/(e_u-e_y_0)*de[i]
                    f_y[i] = abs(sigma[i])
            else: #New stress is within yield contour, thus elastic response
                sigma[i] = sigma_predictor[i]
                f_y[i] = f_y[i-1]
            #f_y[i] = max([abs(sigma[i]) , f_y[i-1]])
        if f_y[i] < f_u: #Stop programm if yield stress has reached ultimate stress
            break

    return t,e,sigma,N
```

**Figure A.5:** Part 5 of the Python code to predict the response of the plasticity of one element under fatigue loading.

# Appendix B: VCCT slicing model

## B.1. Introduction

The VCCT slicing model was the first model developed for determining the crack behaviour of composites due to fatigue. One type of formulation was enough to describe the two mechanisms that had the largest influence on the residual stiffness: delamination between the plies and matrix failure within the plies along the unidirectional fibre (UD). These mechanisms will often be referred to as interply failure and intraply failure following the idea to incorporate the effects of all interply mechanisms together in one model and the effects of all intraply mechanisms in another model. The expected failure combinations were similar to that of figure 2.27.

The basic concept of the VCCT slicing model is slicing the plies in multiple parts (not partitions). Slicing allows to define not only interfaces between plies, but also in the ply parallel to the fibre. Each interface is set to be a VCCT interface except for one as will be explained later. Each VCCT interface is a weak-spot in the model allowing a crack to propagate through. This provides a predetermined crack path as it is a discrete crack formulation. The idea is to find the crack pattern that needs the least force, energy, displacement or cycles to failure. The more slices are present, the more freedom the model has to crack in a certain manner. Therefore the accuracy is improved upon refinement. Theoretically the best solution would be to have a slicing pattern that isolates all elements. Although the intraply slices are parallel to the fibre orientation, fibre failure actually does occur. However, the idea is to predict the behaviour until fibre failure happens as until that point the stiffness degrades, but the strength not so much. The initial crack would then be created by the non-selected nodes in the bonded nodes sets as is described in paragraph 4.7.2 of chapter 4 already.

## B.2. One hypothesis will be answered in appendix B

Appendix B will give answer to one hypothesis. This hypothesis will be answered in section B.7.1 of appendix B.

**Hypothesis 12: If only the VCCT model is used to describe both the interply and intraply interactions with a delamination mechanism, then the compact tension specimen model with fatigue loading will become computational too heavy to execute.**

## B.3. Advantages of the VCCT slicing model

At first sight the VCCT slicing model seems feasible since not much trouble is expected, because the VCCT is a criterion specifically developed for the direct cyclic analysis. The advantages that come along the concept are:

- Only one type of formulation is needed that only requires energies as input. These energies could be obtained by elementary tests for which ISO-norms [4] are present.

- The VCCT interface for fatigue analysis directly uses the Paris law to calculated the crack propagation. The Paris law is well known for its capabilities of predicting crack propagation under fatigue loading condition.
- As the VCCT is a discrete formulation of the crack pattern, the results are mesh independent making calibration along different models easier.
- Despite being difficult to find the path of least resistance by hand, the final result could be checked by hand to see if the number of cycles expected for a certain crack propagation match up with the hand calculations of the Paris law.
- The VCCT is compatible with the cycle jumping algorithm.

## B.4. Disadvantages of the VCCT slicing model

The VCCT slicing model seems an elegant solution to the problem with full freedom. However, there are a lot of comprimises to be made:

- The VCCT interaction is a phenomenological model in itself, hence testing is required. As the input is directly from fatigue tests only, that means that a lot of fatigue tests are needed. Other models such as the plasticity model and ductile damage model could first attempt to calibrate their parameters on static tests. For the VCCT model this is only possible for the energy parameters.
- Although the two intraply mechanisms could be joined into one formulation, it is capable of predicting only one intraply failure mechanism. That means a compromise has to be made in optimising predictions to stages I and II or stages II and III as the most governing of these will prevail. There is no waiting out as an augmentation.
- The VCCT slicing model requires a lot of interactions to be defined which is a tedious and time consuming job to do properly and consistently.
- As the VCCT requires master and slave surfaces, it is likely to tangle up multiple masters nodes to one slave node. Sometimes it is unavoidable unless gaps are made between two interactions, especially between two intraply interactions. These corner elements belong in that case only to one of them leaving a gap on the other interaction. By making the gaps smaller, the error will be minimised. Despite the small size, the increasing number of slices also increases the number of gaps, therefore undoing the extra gained accuracy obtained by more slices.
- The VCCT model needs a large precrack in the terms of unbonded nodes in order to allow the crack propagate without convergence problems.
- Even if the precrack is large enough, sometimes the smallest allowed increment by Abaqus ($10^{-60}$) is not even small enough to obtain convergence. And if convergence is obtained, it would still take large amounts of computational time to complete the analysis.
- The last but not least, as VCCT is intended to model the weak-points in the model, slicing could only be performed in unidirectional plies with the slices parallel to the fibres to model cracking along the fibre. Slicing in perpendicular direction should make it possible to crack through the fibres, but with large resistance. This would determine if a shortcut through the fibres is still less strong than a longer crack path including more inter fibre failure and delamination. In unidirectional layers this is fine, but in woven fabrics it would mean that strong intraply properties are

present in both directions. In that case, delamination could only occur in combination with fibre failure.

## B.5. Input required for the VCCT slicing model

A simplified geometry of the compact tension specimen with two plies is made. This geometry is given in figure B.1. The thickness of each ply is $1.5$ [mm]. The total height is $60$ [mm] and total length of the specimen is $60$ [mm]. Important to note is that each part has a partition with $0.2$ [mm] offset from each border, including in thickness direction. This partitions are to create gaps between the different master and slave surfaces. The allowed failure lines (VCCT interaction lines) are highlighted with orange and green in figure B.2. The ties in both plies at the second half of the horizontal centre line are forcing the analysis to go up, go down or to split. The ties act as an infinitely strong and stiff VCCT interaction. The loads and boundary conditions are introduced over the first $14$ [mm] from the left at the top and bottom area as an alternative for the pins in the holes. A large introduction surface is required to avoid large bending stresses at the end of the load introduction that could cause premature failure. Each of the boundary conditions restricts every node attached to it in horizontal in-plane and out-of-plane translation and rotations around the two in-plane axes. That results in $U_1 = U_3 = 0$ [mm] and $R_1 = R_2 = 0$ [rad]. $R_3$ is kept free and $U_2$ has a prescribed displacement of $5$ [mm] for static loading. No fatigue loading has been applied yet successfully.

The meshing is done for each part separately and by copying one part multiple times, it is made sure that the mesh of one ply matches that of the other ply. Although Abaqus[3] is capable of handling unmatched meshes by accepting a certain tolerance, this manner of meshing avoids unnecessary problems in the interaction definitions. If the element is not in one of the border partitions, then the mesh size is about $1.5$ [mm] in all directions with a slight bias towards the Y-junction. In the border partitions the elements have a length of $1$ [mm] but a width and thickness of $0.1$ [mm]. Despite that a mesh refinement would increase accuracy, a regular mesh is a lot easier for Abaqus[3] to handle, thus less convergence problems. The current mesh used is given in figure B.3.

What seems to be important upon defining the VCCT interaction properties is to keep in mind the different element sizes due to the bias. The total energy needed to move the crack one element forward either along the entire interply interaction or intraply should be roughly equal. This concerns for the $G_{I,c}$ of the intraply with the $G_{II,c}$ and $G_{III,c}$ of the interply. Equation B.1 helps to find out the equivalence. Figure B.4 shows the visualisation of the mentioned areas. The $G_{II,c}$ and $G_{III,c}$ of the intraply could be set at values that keep the same proportion to $G_{I,c}$ of the intraply. Analogously $G_{I,c}$ of the interply with that of $G_{II,c}$ and $G_{III,c}$ of the interply.

$$G_{I,C,intraply}A_{I,intraply} = G_{II,C,interply}A_{II,interply} = G_{III,C,interply}A_{III,interply} \tag{B.1}$$

These values of energies have to be set in the keywords using the fracture criterion lines of table 3.1 along with certain value describing the speed of crack propagation. Higher values for $c_4 > 1$ means that the crack growth will be more exponential. If $c_4 = 1$, then the crack growth rate will be rougly constant through the entire analysis and if $c_4 < 1$, then the crack will slow down. The parameters used during the analysis are given in the input lines given in table B.1.

In order to finish the modelling a bonded node set has to be defined in order to get the crack started. If no set is given, then the interface is perfectly bonded either requiring ridiculous amount of

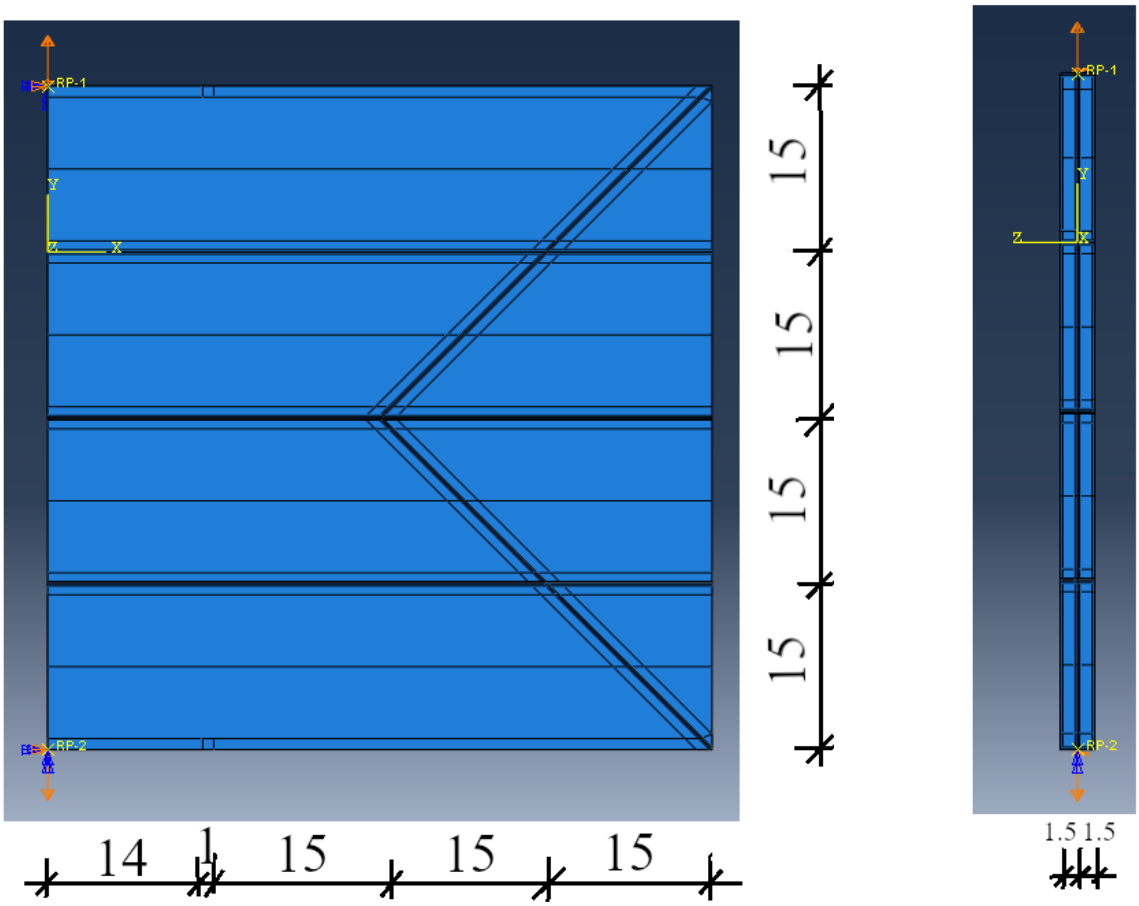


**(a)** Front view

**(b)** Side view

**(c)** Top view

**Figure B.1:** The geometry of the compact tension specimen used for the VCCT slicing model. The measurements are in [mm].

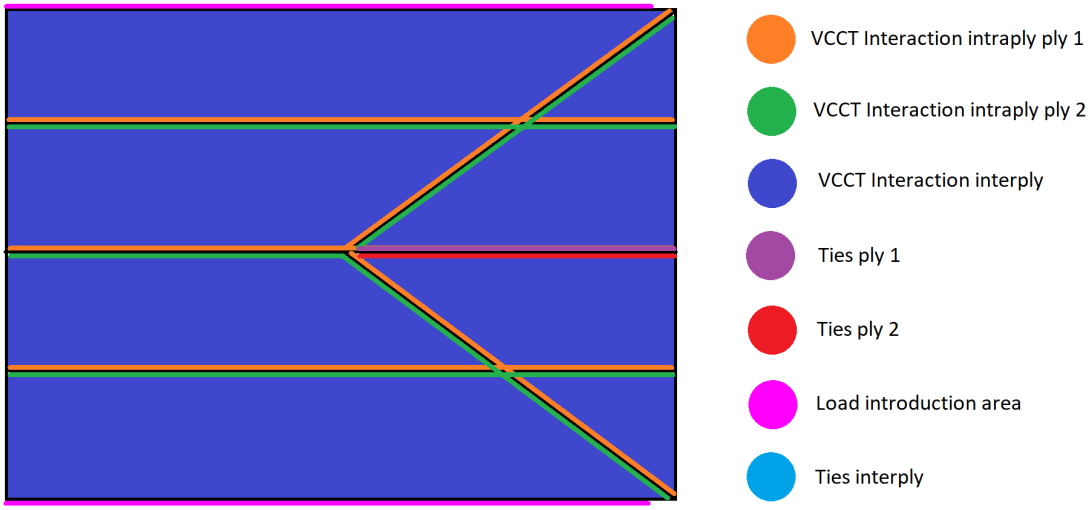


**Figure B.2:** The interaction scheme showing where ties and VCCT interactions are defined for both plies in one drawing.

**Table B.1:** Template for the input data line to provide a VCCT interface for the fatigue analysis.

| | |
|---|---|
| Line 1 | *Debond, slave="<name of slave surface>", master="<name of master surface>", debonding force=STEP, frequency=1 |
| Line 2 BK Interply | *FRACTURE CRITERION, TYPE=fatigue, MIXED MODE=BK, TOLERANCE=<tolerance><br>„$2 * 10^{-4}$,3,0.1,0.9,30,10<br>10,1,20 |
| Line 2 BK Intraply | *FRACTURE CRITERION, TYPE=fatigue, MIXED MODE=BK, TOLERANCE=<tolerance><br>„$2 * 10^{-4}$,3,0.1,0.9,30,2<br>2,1,20 |

force that will lead to broken parent material or will not fail at all. One node may result in a total different answer, but sometimes a change in a lot of nodes are needed to push it over a certain edge. The bonded node sets defined along the interply interface where the precrack is present is provided in figure B.5. For the intraply interfaces along the interply interface is nothing more than extrapolating it in thickness direction on the edge instead of ending just before it.

## B.6. Output obtained from the VCCT slicing model

The most obvious output to look at is the force-displacement diagram of the CT specimen. This diagram is provided in figure B.6. What immediately pops-out is the high peak and sudden drop at about $0.5$ [mm] of applied displacement. Moreover, the forces tend to stay flat afterwards. It looks like as if it was a stuck zipper that zips through once the obstacle has been passed. Figures B.7 up to and including B.12 show the Von Mises stress, the displacement magnitude, the bond status of the VCCT interply of the left interface on the third row and the effective energy release rate of that interface for the important increments. View these results as a comic book as an alternative to an animation. Comments on it will be provided afterwards.

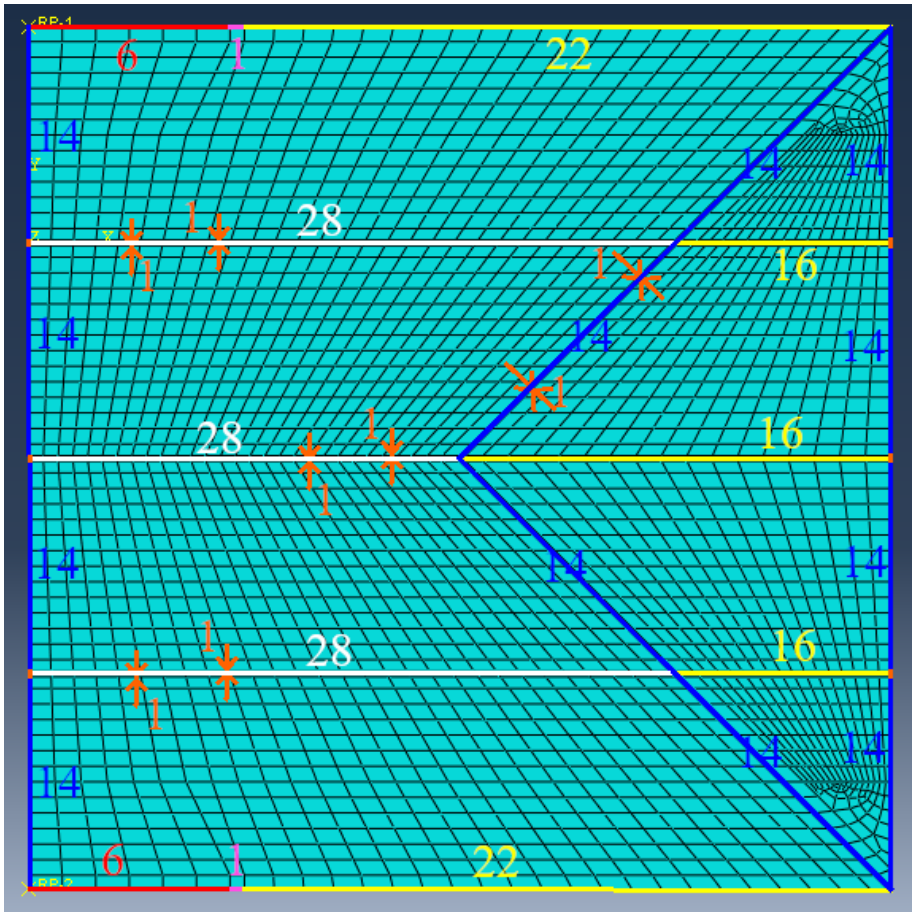


**(a)** Front view

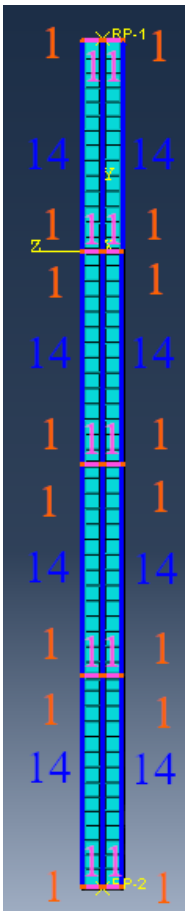


**(b)** Side view

**(c)** Top view

**Figure B.3:** The mesh of the compact tension specimen used for the VCCT slicing model. The numbers provide how many elements are used along a certain edge with the colour corresponding to the colour of the edge.

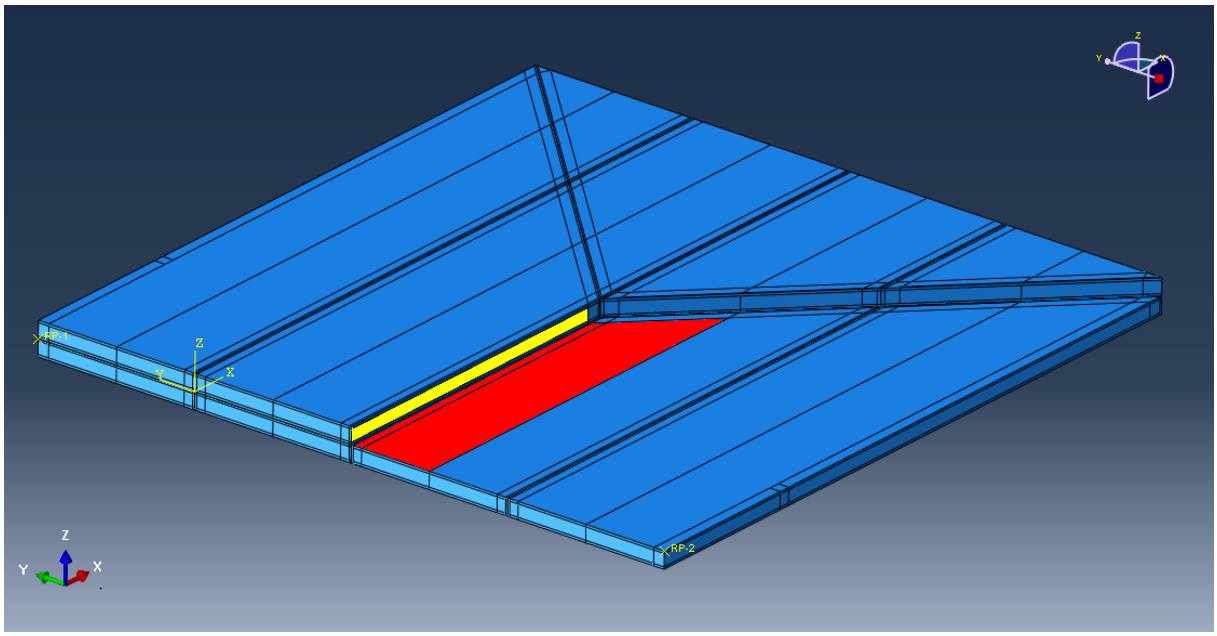


**Figure B.4:** The surfaces that need roughly equivalent energies to fracture. These interactions are: the intraply action on the second line between part one of row two and part one of row three of the zero degree ply is drawn in yellow. And the intraply action on the first part on the third row with that of the zero degree ply with that of the 45 degree ply in red.

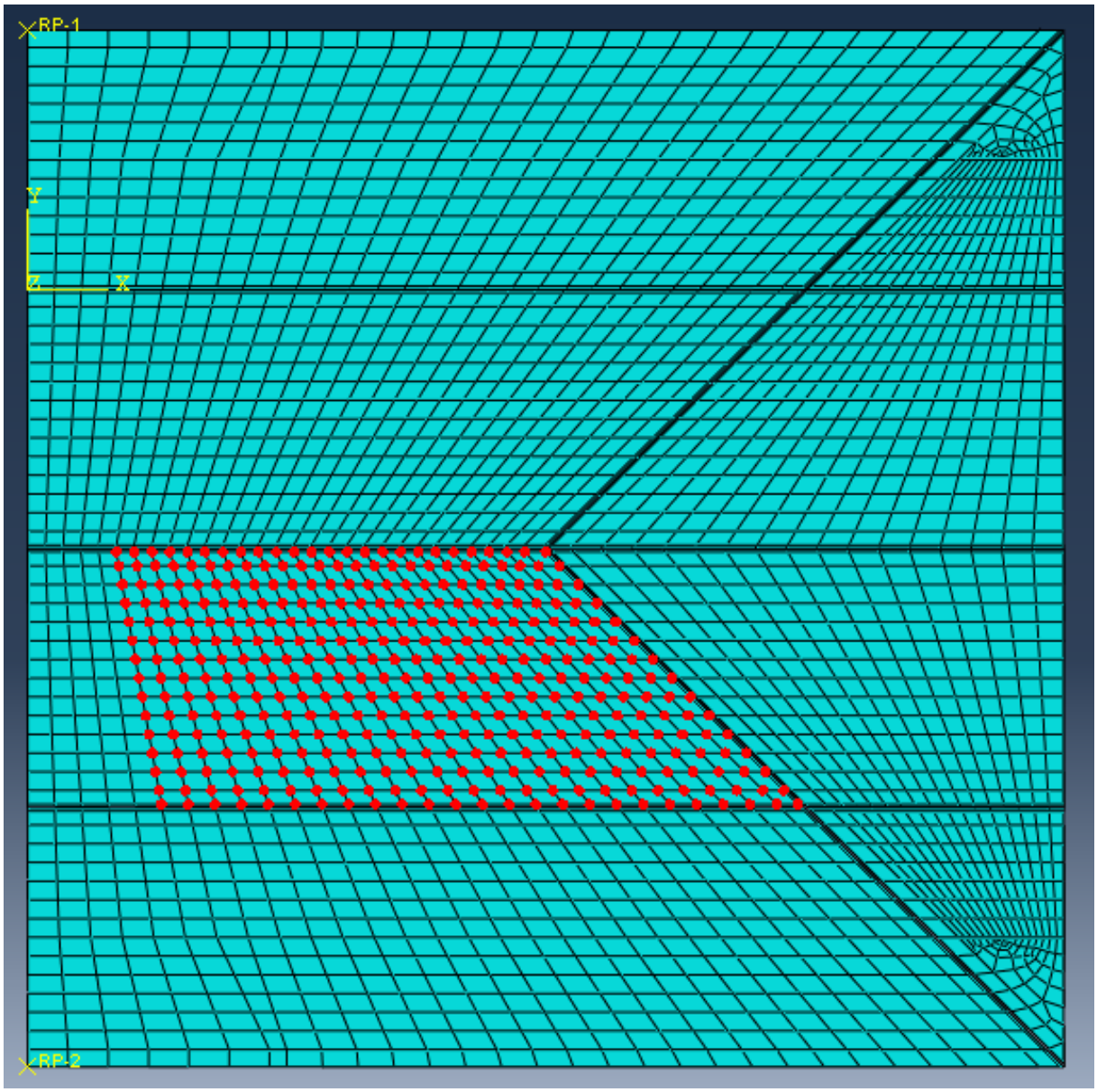


**Figure B.5:** Bonded node set with precrack in the interply interface of the left part on the third row.

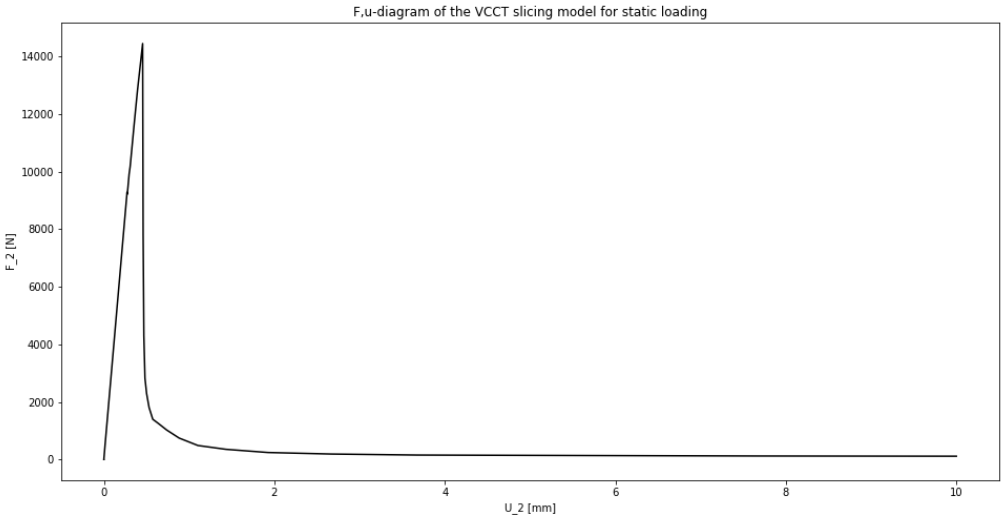


**Figure B.6:** The force displacement diagram of the VCCT slicing model for static loading.

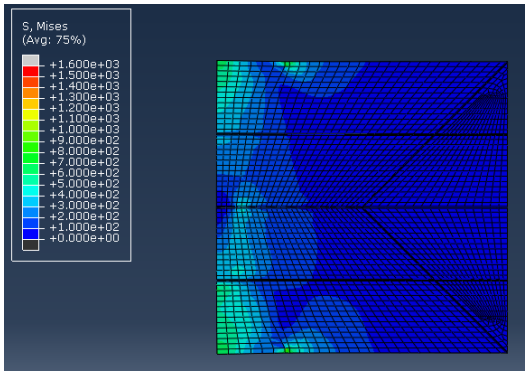


**(a)** The Von Mises stress

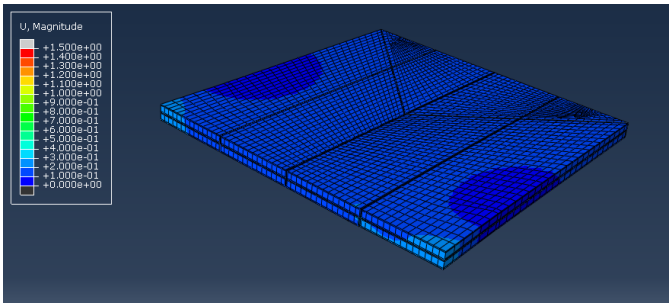


**(b)** The magnitude displacement

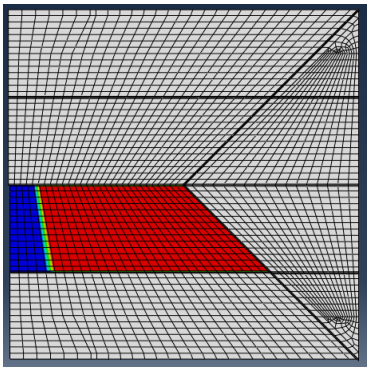

**(c)** The bond status of the interply of the left part on the third row. Red means fully bonded and blue means debonded.

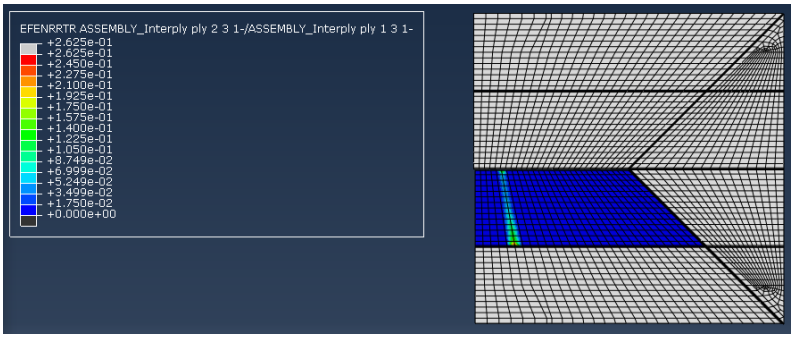


**(d)** The effective energy release rate of the interply of the left part on the third row

**Figure B.7:** The output of frame 16 at $U_{applied} = 0.272$ [mm] for the static loading of the VCCT slicing model.

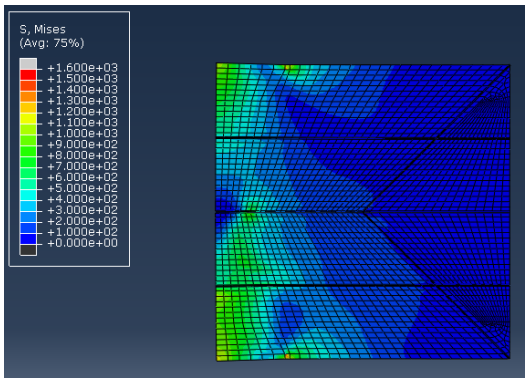


**(a)** The Von Mises stress

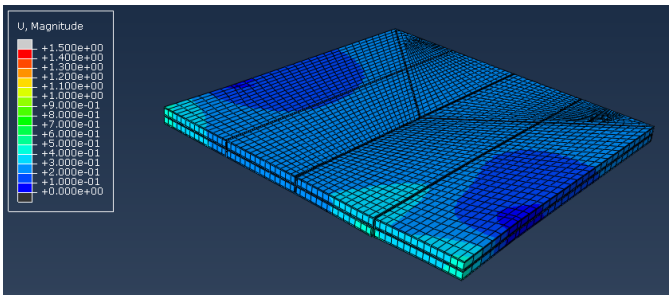


**(b)** The magnitude displacement

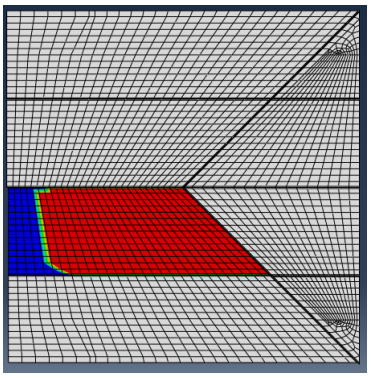

**(c)** The bond status of the interply of the left part on the third row. Red means fully bonded and blue means debonded.

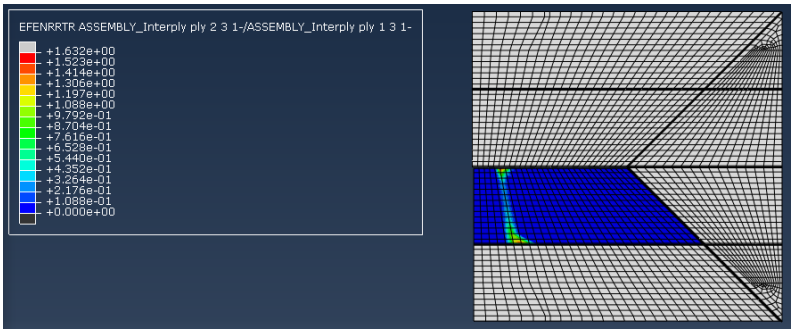


**(d)** The effective energy release rate of the interply of the left part on the third row

**Figure B.8:** The output of frame 113 at $U_{applied} = 0.455$ [mm] for the static loading of the VCCT slicing model.

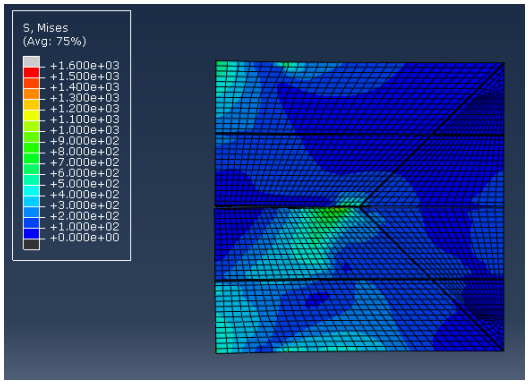


**(a)** The Von Mises stress

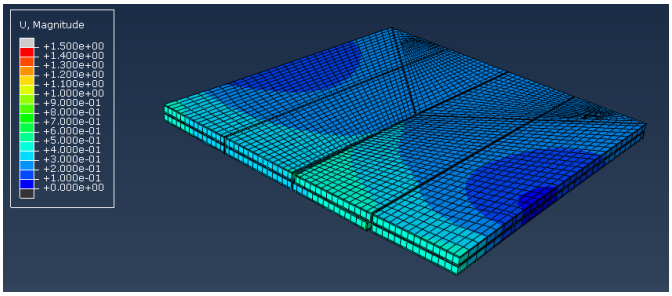


**(b)** The magnitude displacement

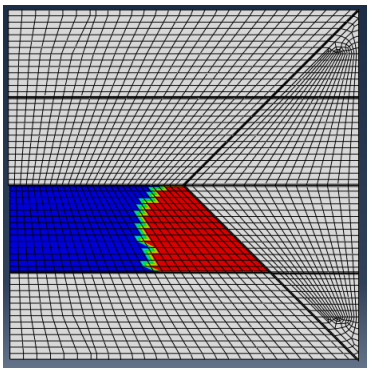

**(c)** The bond status of the interply of the left part on the third row. Red means fully bonded and blue means debonded.

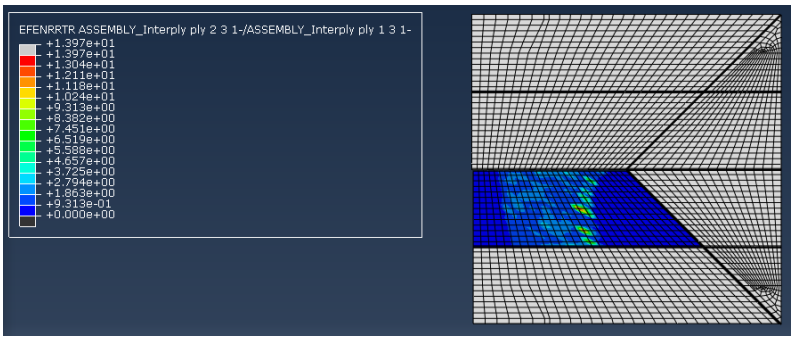


**(d)** The effective energy release rate of the interply of the left part on the third row

**Figure B.9:** The output of frame 114 at $U_{applied} = 0.461$ [mm] for the static loading of the VCCT slicing model.

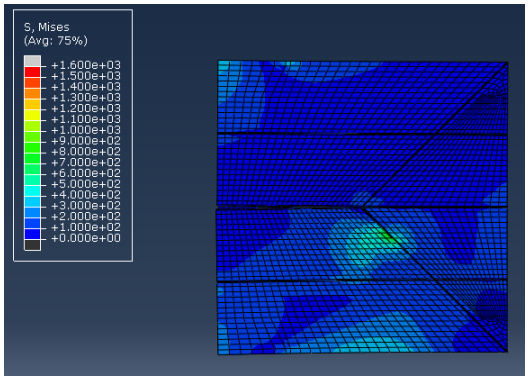


**(a)** The Von Mises stress

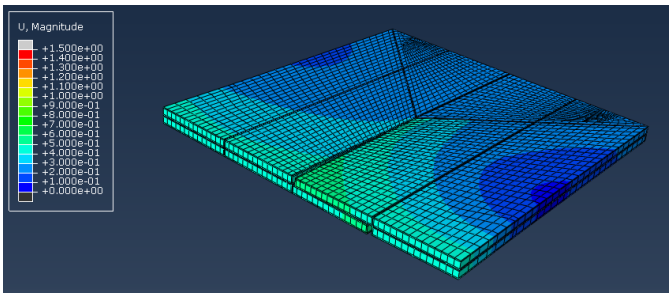


**(b)** The magnitude displacement

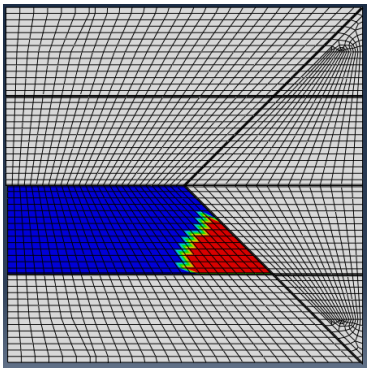

**(c)** The bond status of the interply of the left part on the third row. Red means fully bonded and blue means debonded.

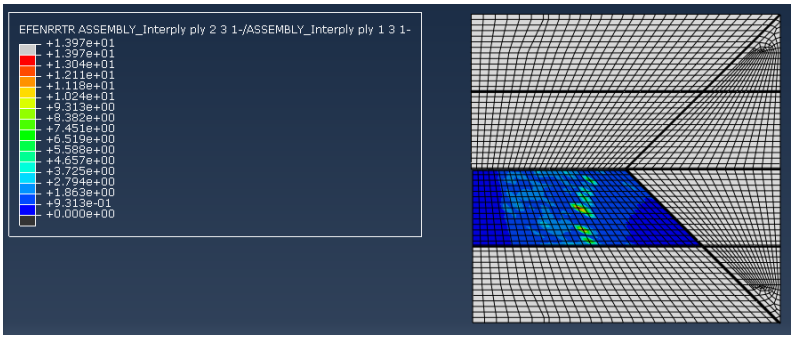


**(d)** Effective energy release rate of the interply of the left part on the third row

**Figure B.10:** The output of frame 115 at $U_{applied} = 0.469$ [mm] for the static loading of the VCCT slicing model.

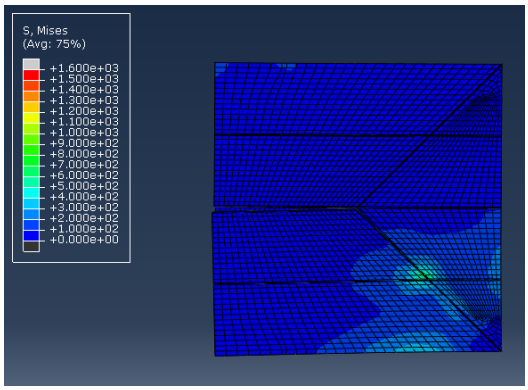


**(a)** The Von Mises stress

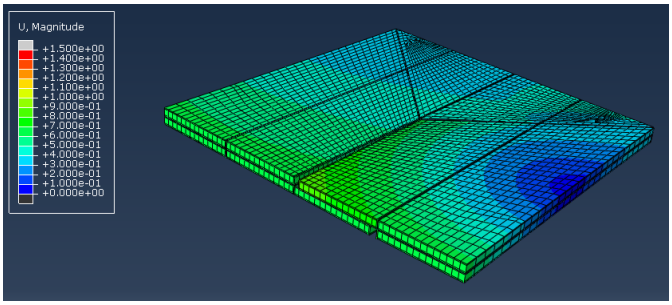


**(b)** The magnitude displacement

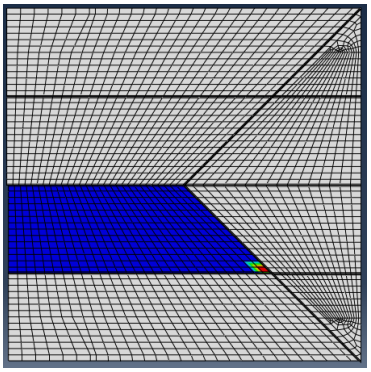

**(c)** The bond status of the interply of the left part on the third row. Red means fully bonded and blue means debonded.

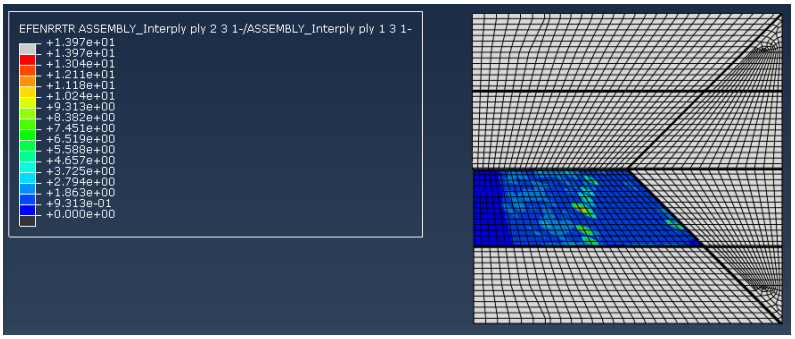


**(d)** The effective energy release rate of the interply of the left part on the third row

**Figure B.11:** The output of frame 120 at $U_{applied} = 0.639$ [mm] for the static loading of the VCCT slicing model.

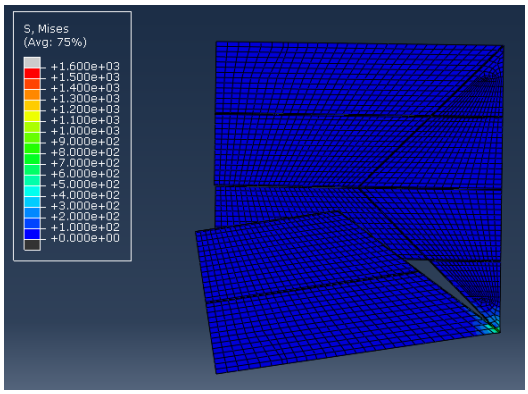


**(a)** The Von Mises stress

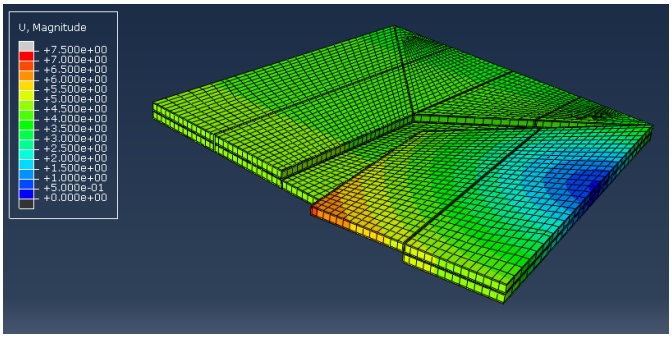


**(b)** The magnitude displacement

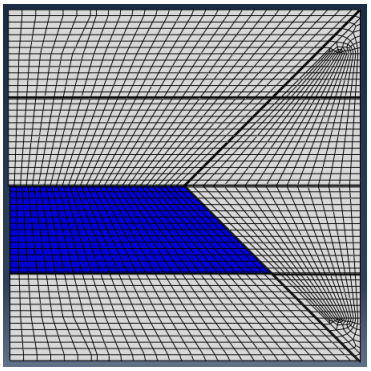

**(c)** The bond status of the interply of the left part on the third row. Red means fully bonded and blue means debonded.

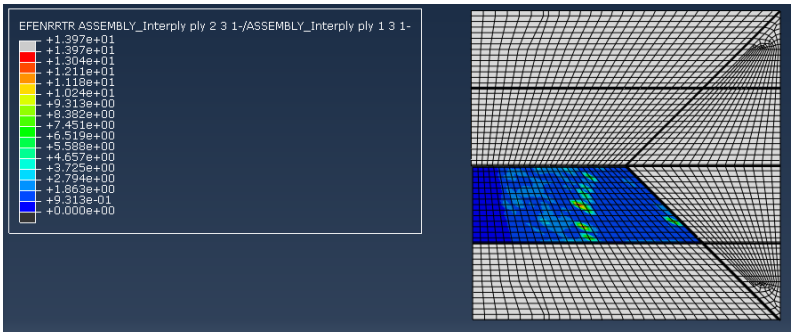


**(d)** The effective energy release rate of the interply of the left part on the third row

**Figure B.12:** The output of frame 128 at $U_{applied} = 4.66$ [mm] for the static loading of the VCCT slicing model.

The stuck zipper that suddenly unblocks and moves is actually a good description of what is happening at $U = 0.455$ [mm]. First the Von Mises stresses locally increase linearly with the applied forces. However, at a certain point the local energy release rate is high enough to start the debonding of a bonded node. The force in the structure falls drastically due to that debonding which is also observable in the effective energy release rate since forces and energies are related by displacements. Once one node had started, the next node follows quickly. Now the domino effect has started by taking the next row of nodes and the step after that multiple row of nodes as shown in the bond status. Here the unstable crack tolerance shows its purpose. Otherwise it would have had to cut back the increment size a lot of times. The debonding continues along the $-45$ [°] line until the final node where in theory an infinite rotation is possible as the 3D stress elements do not have a rotational degree of freedom. Without a rotational degree of freedom, there is also no rotational strength, thus free to rotate around that single node. The effective energy release rate shows the energy released at a certain node during a time frame of the analysis. At the crack tip (the line between the fully bonded and fully released nodes) the highest response of energy released shows up during that frame. This is not so strange as the most energy is released upon the breaking of the bonding. The area before the crack tip (the bonded area) shows no energy release as is expected since the bond is able to take up all the energy without breaking. No breaking means no energy released. Remember to look at the scales of the graphs as these may vary for the energy release rate. The energy release rates increase until that certain point of crack propagation has been reached. The energy release rate may decrease in a displacement controlled analysis as is shown in figure B.11d compared to figure B.10d. This is caused by the less force required to break the bond.

## B.7. Hypothesis review appendix B

### B.7.1. Proof to one hypothesis listed in section B.2 of appendix B

**Proof to hypothesis 12: If only the VCCT model is used in Abaqus[3] to describe both the interply and intraply interactions with a delamination mechanism, then the compact tension specimen model with fatigue loading will become computational too heavy to execute.** This option has been tried in appendix B. However, for the static analysis increments of $10^{-40}$ were sometimes needed. That leads to requiring two full days of simulation on the high performance cluster (HPC) with $64$ cores activated (that is a lot of computational power). An attempt has been made with a direct cyclic analysis with larger steps that allowed less accuracy. Even then the analysis became too heavy that the HPC gave out and resulted in an error. That means it is currently unfeasible to run such type of models, certainly when realising that these are the simple versions of the desired VCCT slicing model.

## B.8. Conclusion Appendix B

Although the VCCT slicing model is an elegant solution in terms of only using the energy equations to describe the cracking behaviour, it is impracticable to use. It is a lot of effort to set up, it needs a lot of testing and it requires strong computational resources. The advantage does not weight up against these disadvantages. Therefore this solution is perhaps possible, but certainly impracticable.

# Appendix C: Output of the compact tension specimen in chapter 5

## C.1. Compact tension geometry with one ply

### C.1.1. CT single ply UD [0]

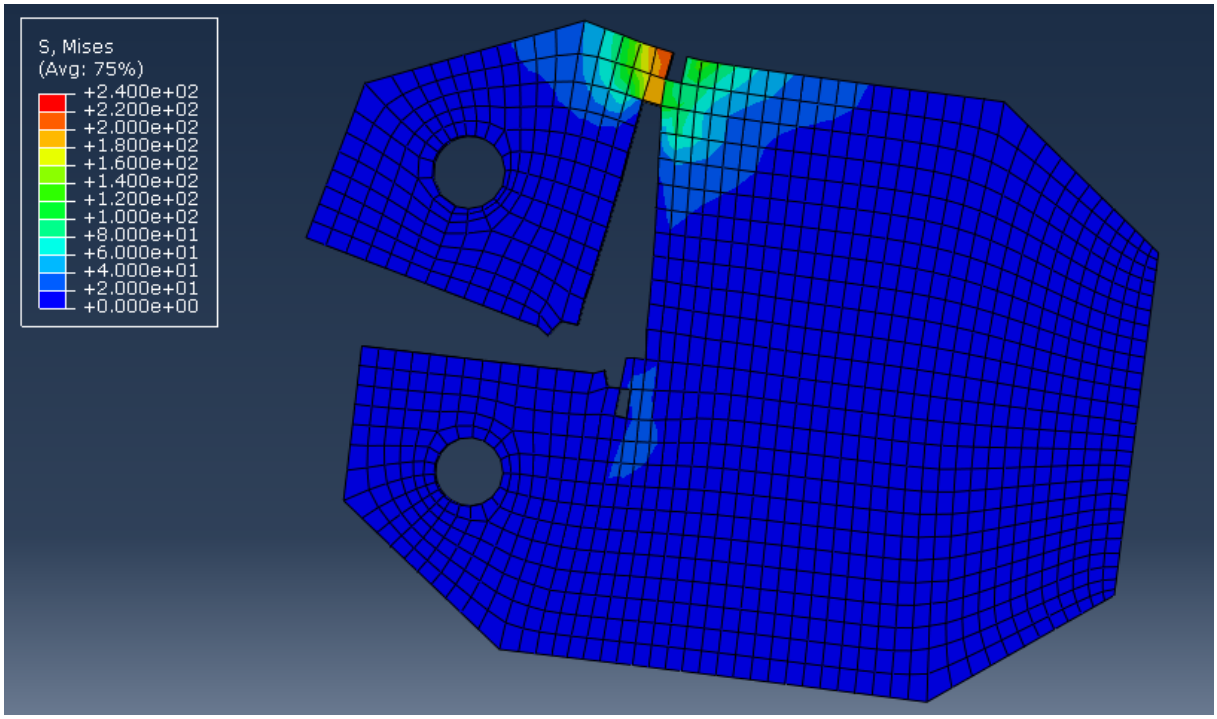


**Figure C.1:** A visualisation of the deformed compact tension specimen showing the distribution of Von Mises stresses at a maximum loading of 5 [mm] vertical displacement in the top pin in cycle 56. This is the final cycle before complete failure of the specimen.

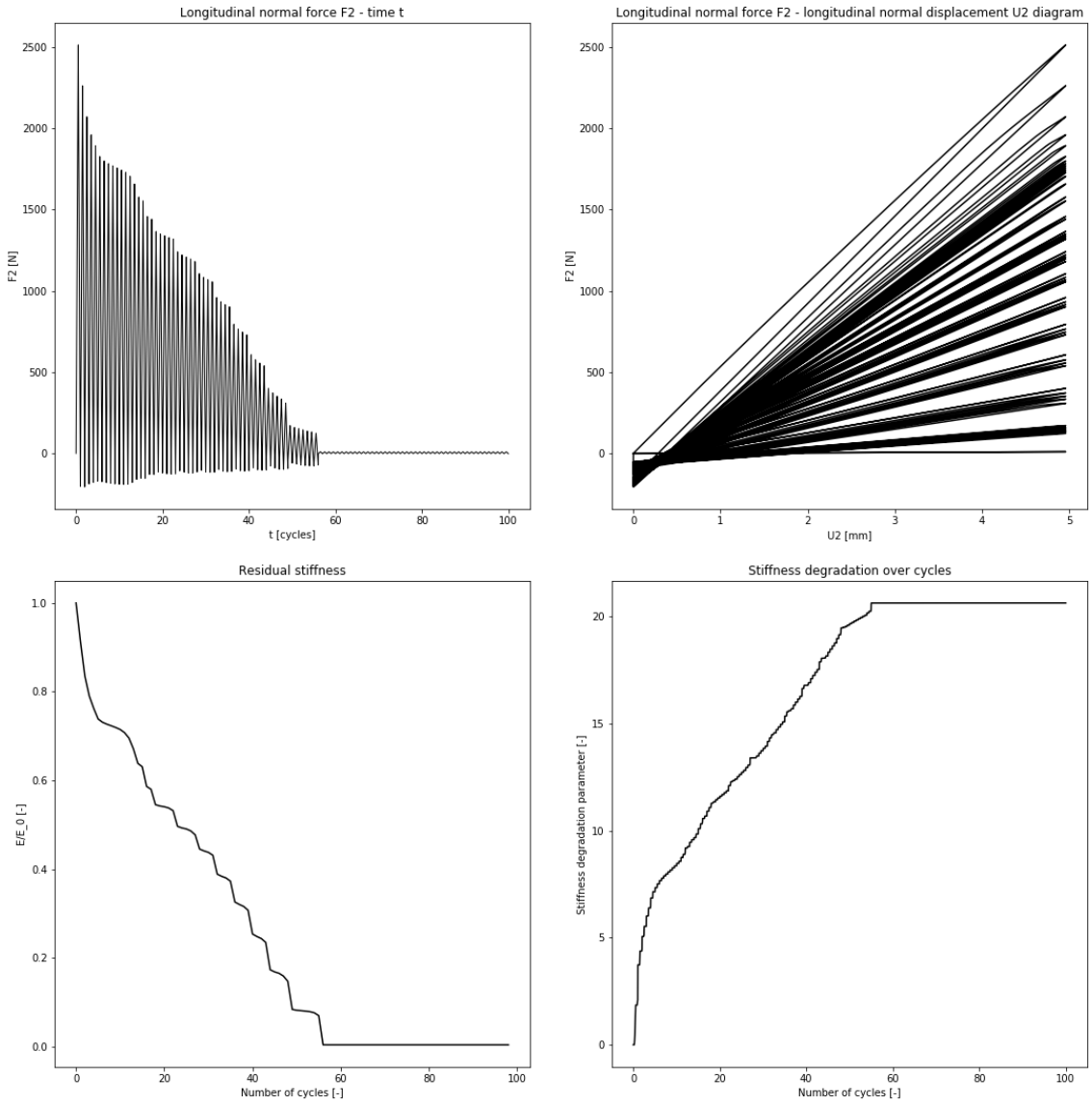


**Figure C.2:** In four plots the output is represented for the compact tension specimen that is fatigue loaded with an applied displacement of 5 [mm] failing after 56 cycles. Counting from the left to the right and from the top to the bottom, the load history plot is given first. This plot shows the applied force over time as resultant of a constant applied displacement amplitude function. The second plot is the force-displacement diagram which acts as hysteresis plot of the element as structural response. The third plot shows the stiffness of the structure relative to the response of the first cycle and the fourth plot shows the cumulative value of the damage parameters of the individual elements that leads to stiffness degradation (0 equals no damage and 1206 equals all elements fully damaged).

## C.2. Cycle jumping

### C.2.1. CT single ply UD [0] dN = 10

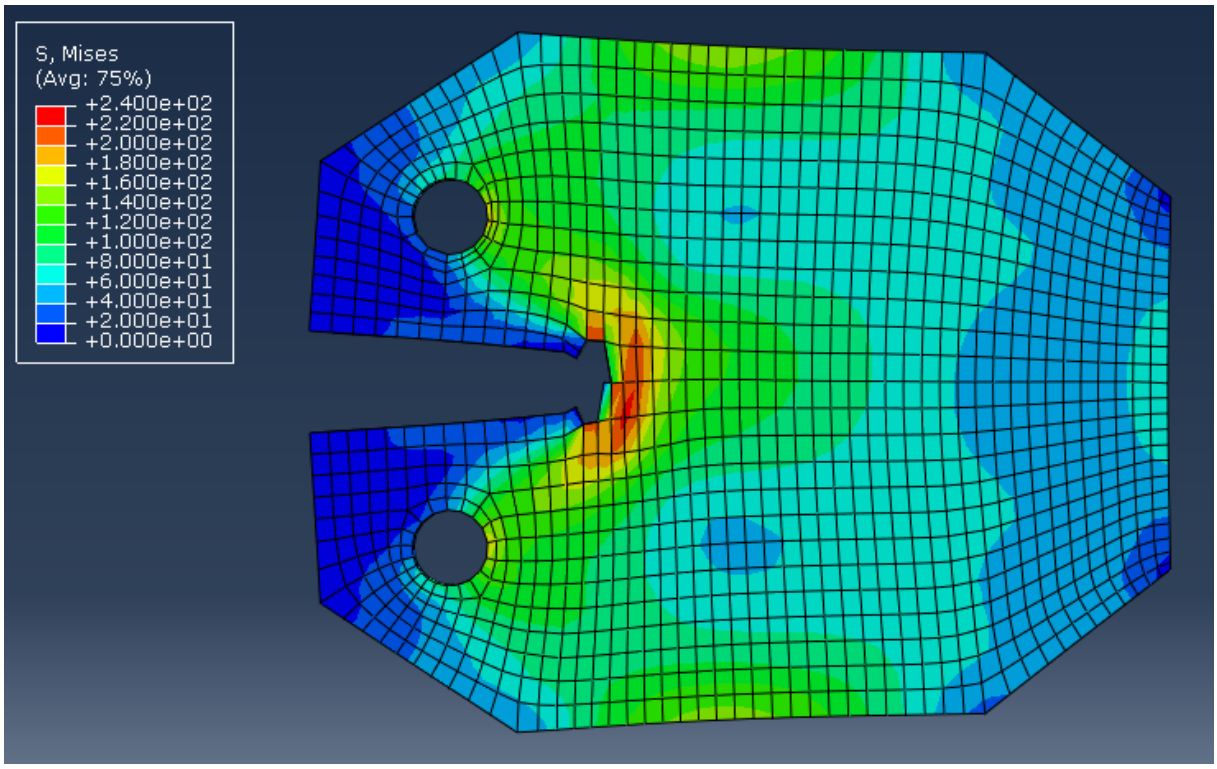


**Figure C.3:** A visualisation of the deformed compact tension specimen showing the distribution of Von Mises stresses at maximum loading of 5 [mm] vertical displacement in the top pin in cycle 100. The analysis was limited to a 100 [cycles].

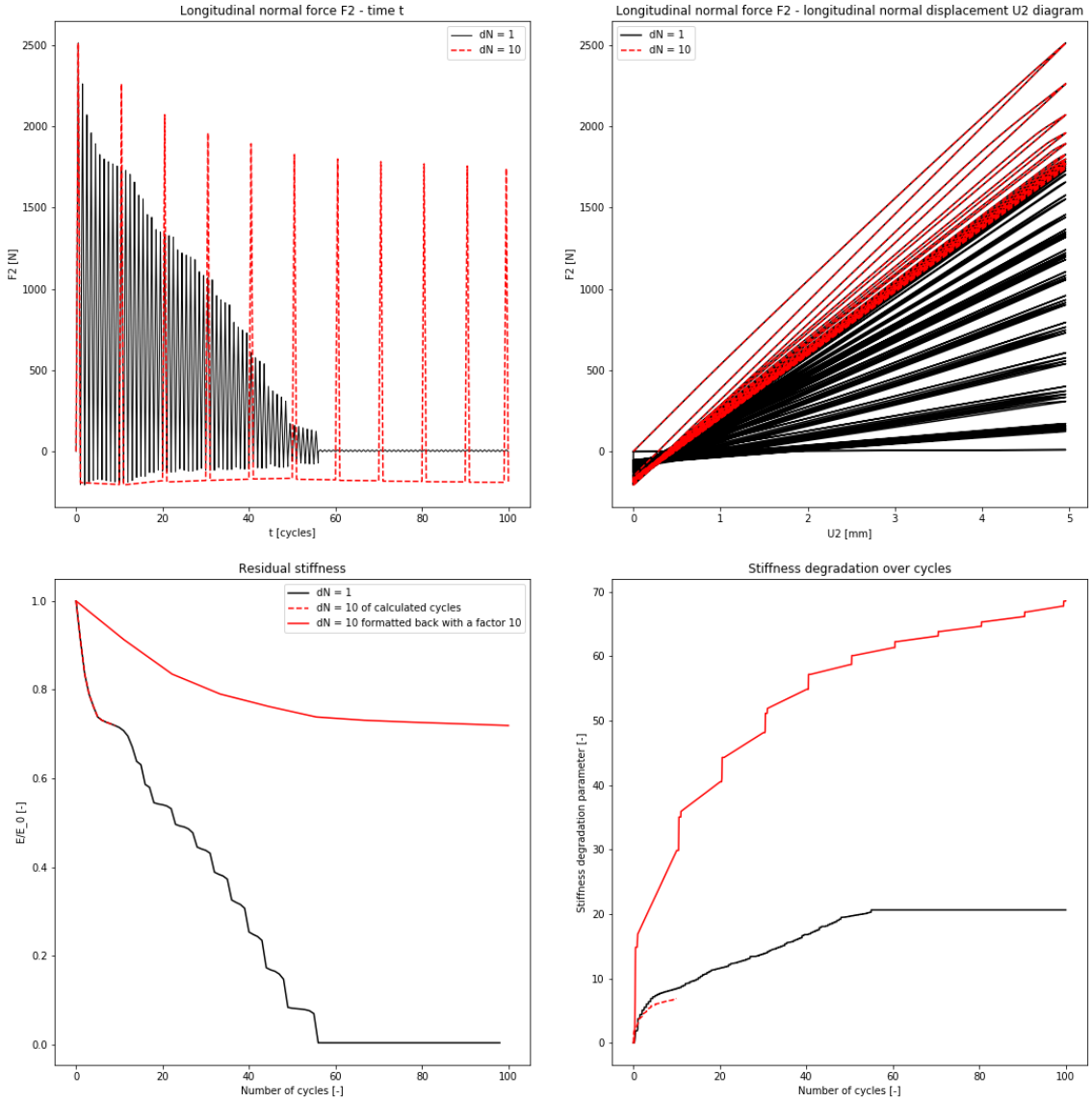


**Figure C.4:** In four plots the output is represented for the compact tension specimen for a fatigue load with an applied displacement of 5 [mm] finishing computations at a 100 [cycles]. The black line shows the output for a 100 cycles without cycle jumping which is identical to the output of figure C.2 and the red line represents a 100 cycles with cycle jumping to every tenth cycle. Counting from the left to the right and from the top to the bottom the load history plot is given first. This plot shows the applied force over time as resultant of a constant applied displacement amplitude function. The second plot is the force-displacement diagram which acts as hysteresis plot of the structural response. The third plot shows the stiffness of the structure relative to the response of the first cycle. Here is not only the stiffness degradation for with and without cycle jumping provided, but also a scaled case of the cycle jumping. This is done with a factor of 10 which results in compliance with the first part of the analysis without cycle jumping. The fourth figure plots the cumulative value of the damage parameters of the individual elements that leads to stiffness degradation (0 equals no damage and 1206 equals all elements fully damaged).

## C.3. Automatic incrementation

### C.3.1. CT single ply UD [0] dN = 10 auto increments

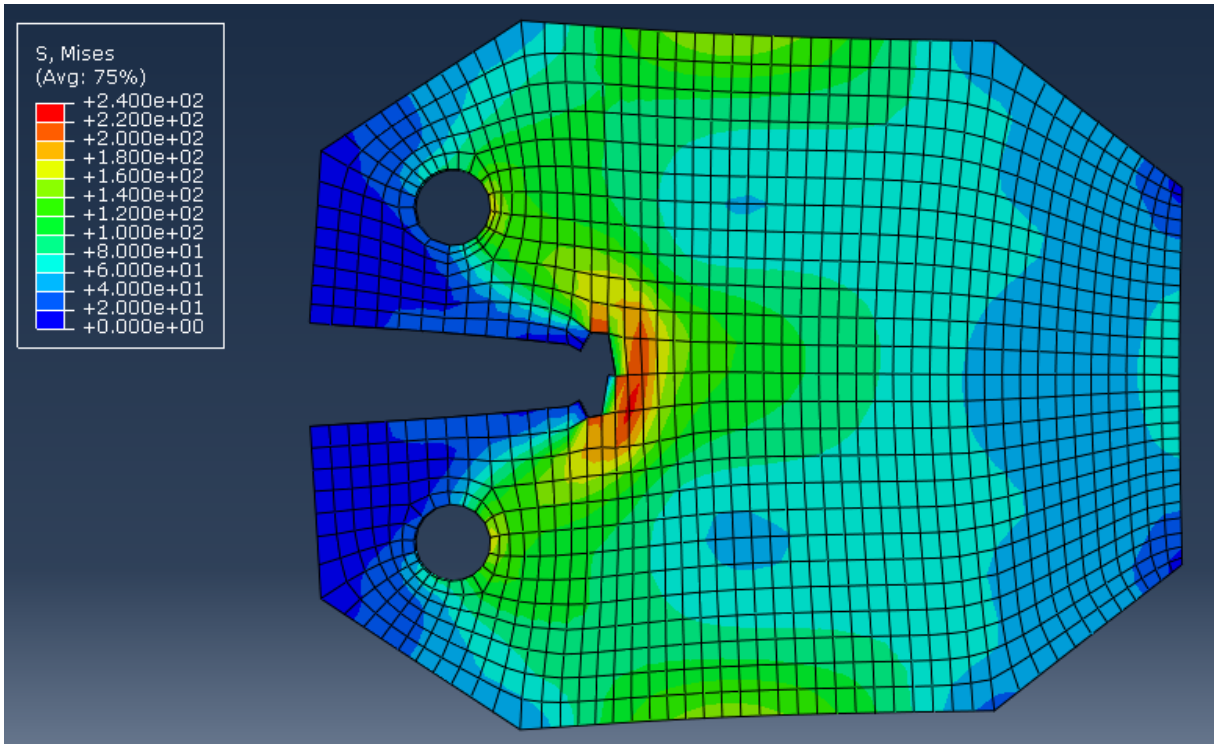


**Figure C.5:** A visualisation of the deformed compact tension specimen showing the distribution of Von Mises stresses at maximum loading of 5 [mm] vertical displacement in the top pin in cycle 100. The analysis was limited to a 100 [cycles].

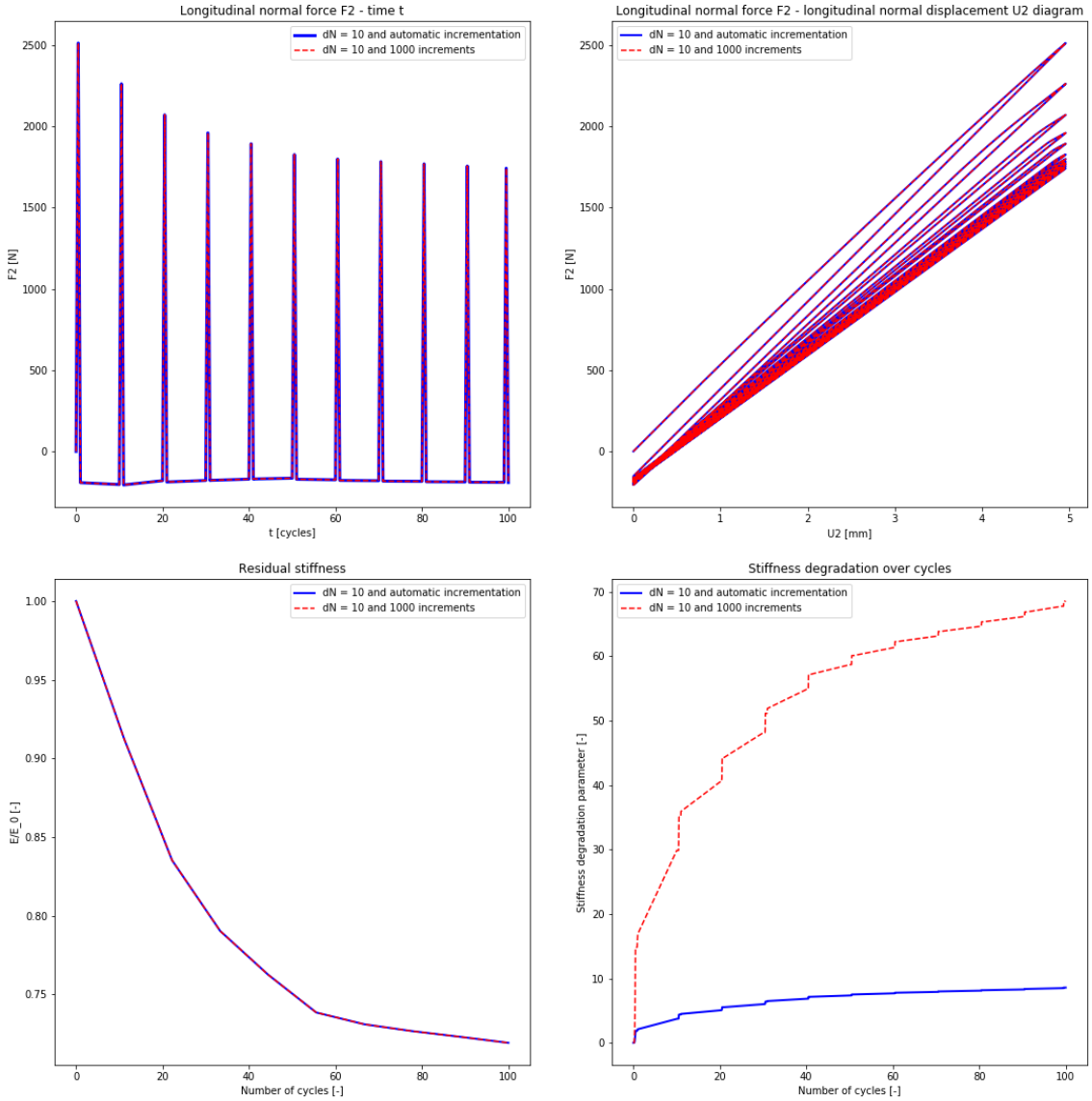


**Figure C.6:** In four plots the output is represented of the fatigue analysis for the compact tension specimen with an applied displacement of 5 [mm] finishing computations at a 100 [cycles]. The red line shows the output for a 100 cycles with cycle jumping to every tenth cycle and a fixed incrementation of size 0.001 which is identical to the red output of figure C.4. The blue line represents the analysis with a 100 cycles with cycle jumping to every tenth cycle and an automatic incrementation. Counting from the left to the right and from the top to the bottom the load history plot is given first. This plot shows the applied force over time as resultant of a constant applied displacement amplitude function. The second plot is the force-displacement diagram which acts as hysteresis plot of the element as structural response. The third plot shows the stiffness of the structure relative to the response of the first cycle. This is done with a factor of 10 which complies with the first part of the analysis without cycle jumping. The fourth plot shows the cumulative value of the damage parameters of the individual elements that leads to stiffness degradation (0 equals no damage and 1206 equals all elements fully damaged).

## C.4. Replacing tie constraints with VCCT interactions

### C.4.1. TIE MS2 UD [0|-45|90|45|0]

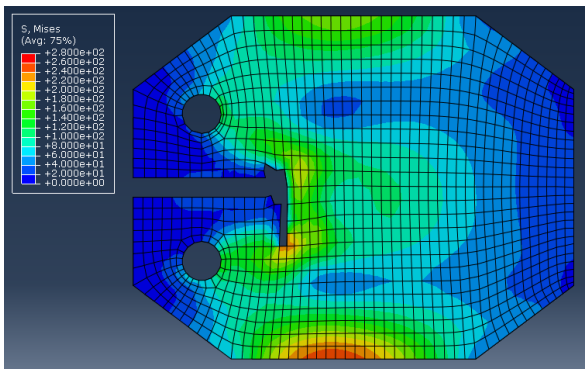


**(a)** Ply 1 at material orientation angle 0 [°]

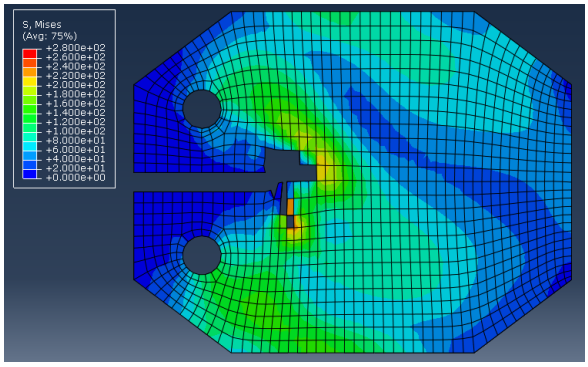


**(b)** Ply 2 at material orientation angle $-45$ [°]

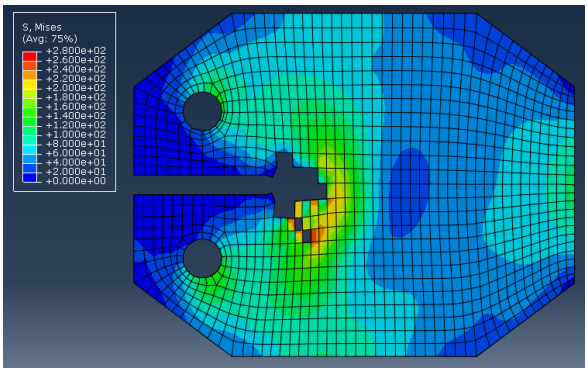


**(c)** Ply 3 at material orientation angle 90 [°]

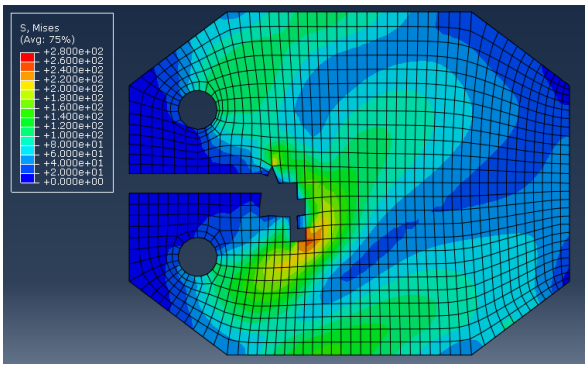


**(d)** Ply 4 at material orientation angle 45 [°]

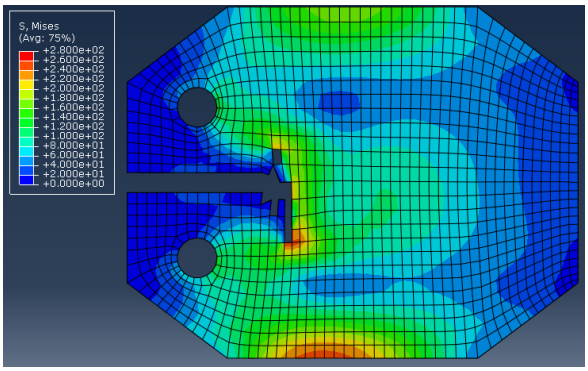


**(e)** Ply 5 at material orientation angle 0 [°]

**Figure C.7:** A visualisation of the deformed compact tension specimen of each individual ply. The distribution of Von Mises stresses at maximum loading of 5 [mm] vertical displacement in the top pin in cycle 100 are displayed in colour. The analysis was limited to a 100 [cycles].

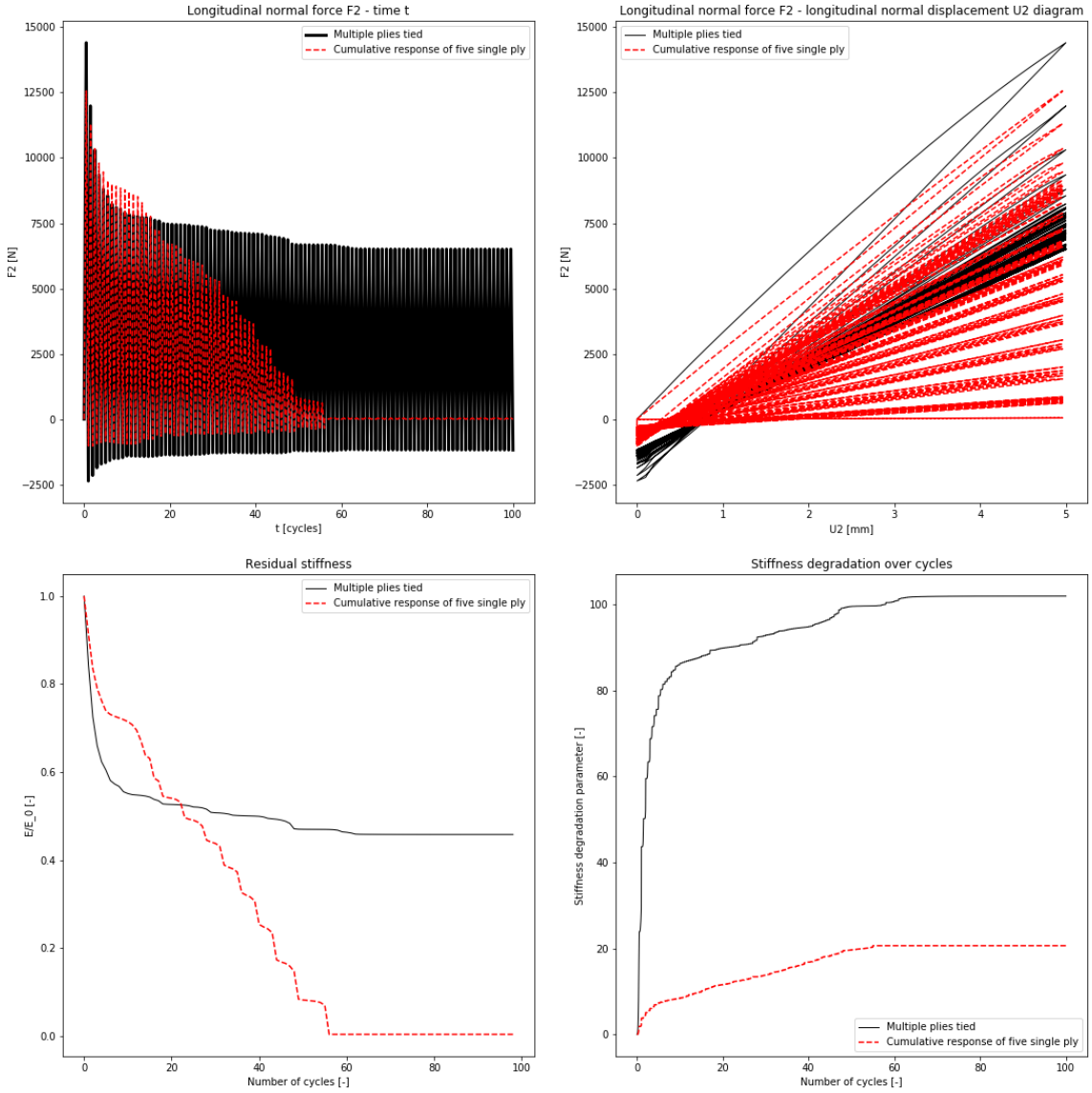


**Figure C.8:** In four plots the output of is represented of the fatigue analysis for the compact tension specimen with an applied displacement of 5 [mm] finishing computations at a 100 [cycles]. The red line shows the output for a single ply which is identical to the output provided in figure C.2. The black line represents the analysis of a compact tension specimen with five plies with a layup of $[0|-45|90|45|0]$. Counting from the left to the right and from the top to the bottom the load history plot is given first. This plot shows the applied force over time as resultant of a constant applied displacement amplitude function. The second plot is the force-displacement diagram which acts as hysteresis plot of the element as structural response. The third plot shows the stiffness of the structure relative to the response of the first cycle. The fourth plot shows the cumulative value of the damage parameters of the individual elements that leads to stiffness degradation. For the single ply 0 equals no damage and 1206 equals all elements fully damaged. For the multiply layup these values are 0 and 6030 respectively.

### C.4.2. TIE MS2 QI0

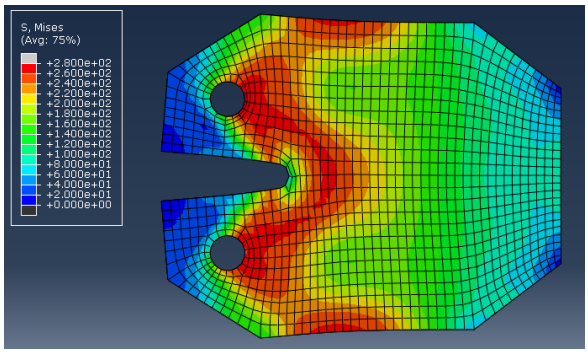


**(a)** One of the plies at cycle 1

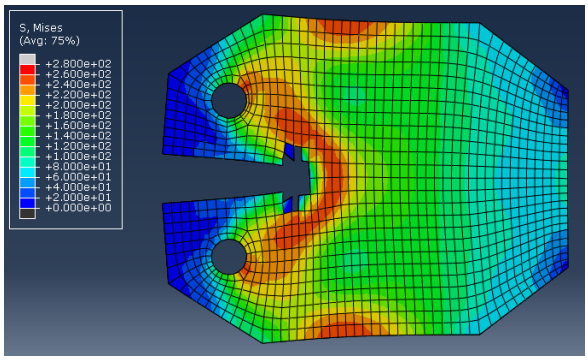


**(b)** One of the plies at cycle 2

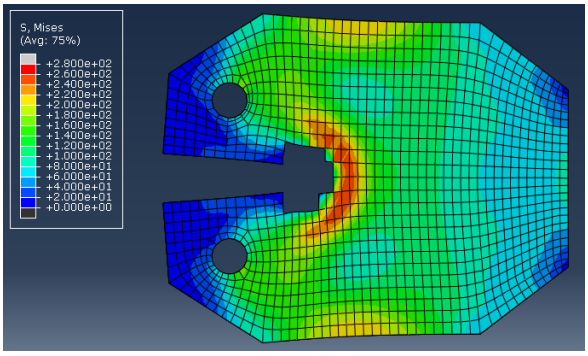


**(c)** One of the plies at cycle 5

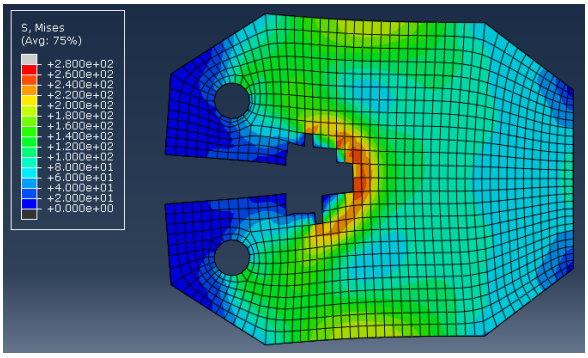


**(d)** One of the plies at cycle 10

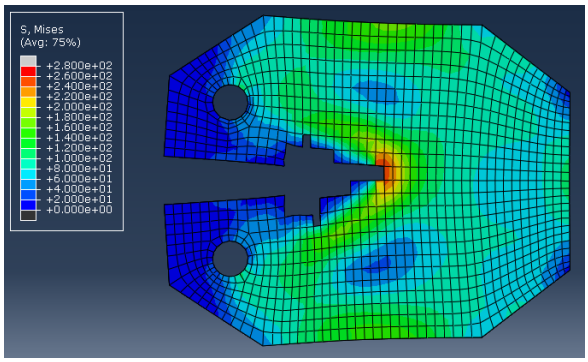


**(e)** One of the plies at cycle 20

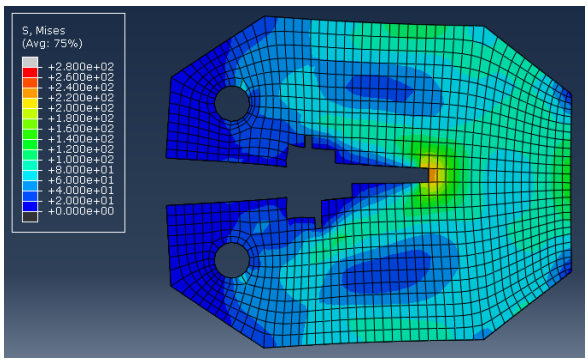


**(f)** One of the plies at cycle 100

**Figure C.9:** Visualisation of the deformed compact tension specimen of an individual ply that has quasi-isotropic stiffness and tie interactions with its adjacent plies. As all the plies had the same reaction due to quasi-isotropic stiffness, one ply is presented at different cycles to show crack propagation rate instead of each individual ply at final stage. The distribution of Von Mises stresses at maximum loading of 5 [mm] vertical displacement in the top pin are displayed in colour. The analysis was limited to a 100 [cycles].

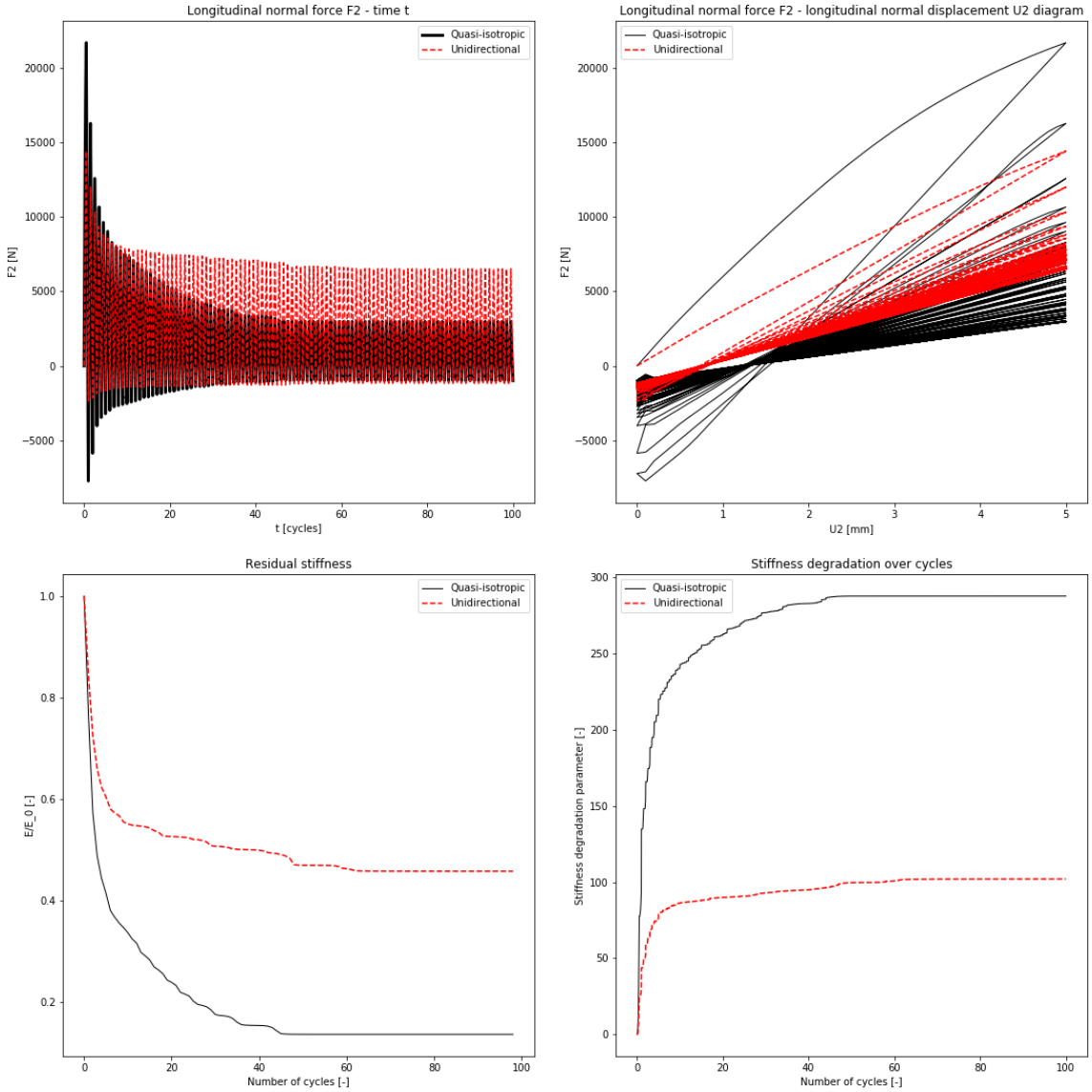


**Figure C.10:** In the entire (relevant) output of the fatigue analysis for the compact tension specimen with five quasi-isotropic plies with tie interaction is represented in these four figures. A displacement of $5$ [mm] is applied and the computations is truncated at a $100$ [cycles]. The red line shows the output for a single ply which is identical to the output provided in figure C.7. The black line represents the analysis with a compact tension specimen with five plies with a layup $[0|-45|90|45|0]$ for which only the first direction of the quasi-isotropic plies is mentioned. Counting from left to right and from top to bottom the load history plot is given first. This figure shows the applied force over time as resultant of a constant applied displacement amplitude. The second figure is the force-displacement diagram which acts as hysteresis plot of the element as structural response. The third figure shows the stiffness of the structure relative to the response of the first cycle. The fourth figure shows the cumulative value of the damage parameters of the individual elements that leads to stiffness degradation. For the multiply layup these values are $0$ and $6030$ respectively as there are $1206$ elements in each ply.

### C.4.3. TIE MS2

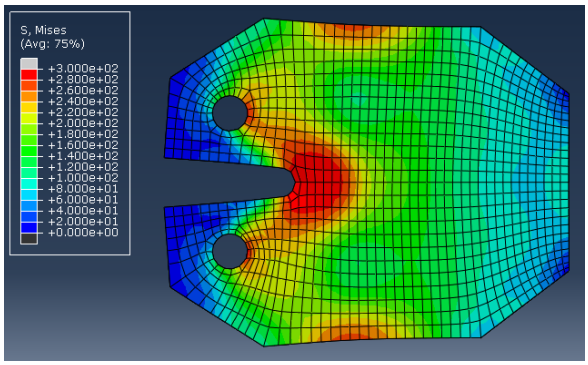


**(a)** One of the plies at cycle 1

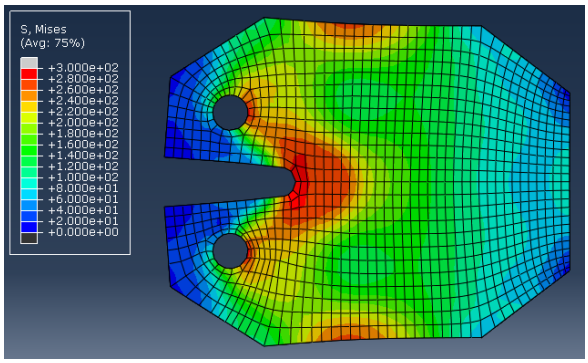


**(b)** One of the plies at cycle 2

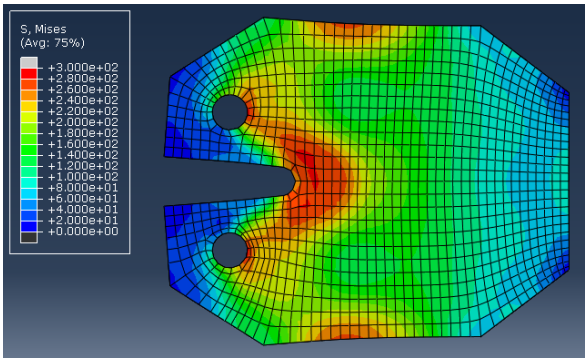


**(c)** One of the plies at cycle 5

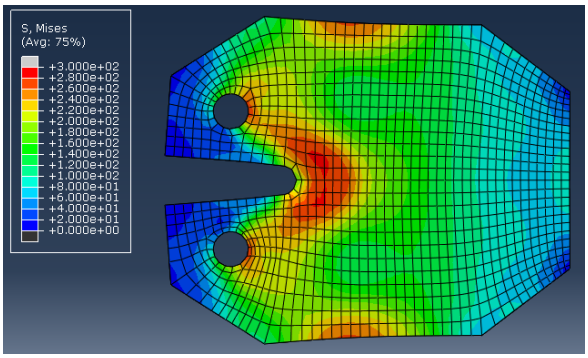


**(d)** One of the plies at cycle 10

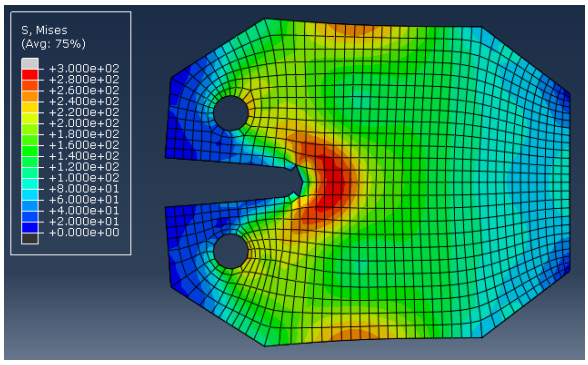


**(e)** One of the plies at cycle 20

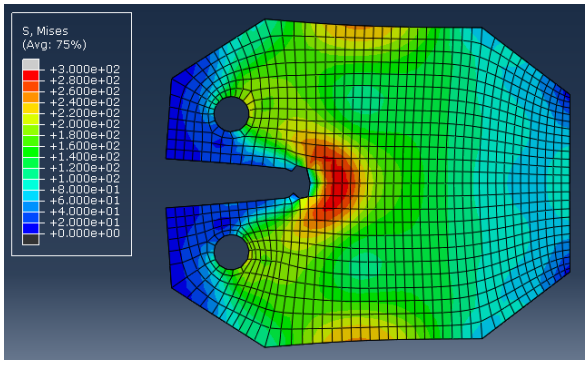


**(f)** One of the plies at cycle 30

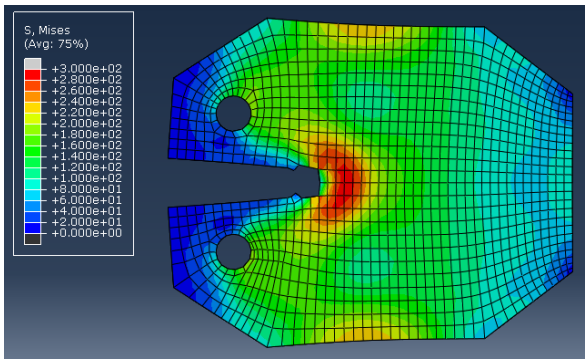


**(g)** One of the plies at cycle 40

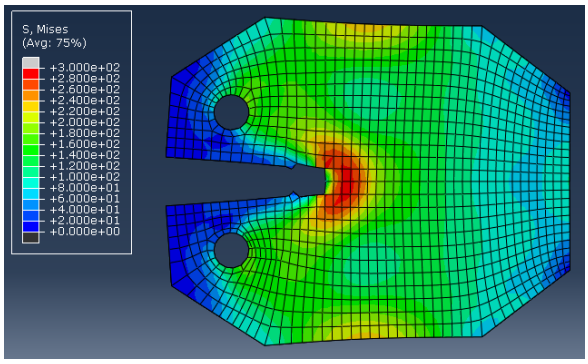


**(h)** One of the plies at cycle 50

**Figure C.11:** A visualisation of the deformed compact tension specimen of an individual ply that has quasi-isotropic stiffness and tie constraints with its adjacent plies. As all the plies had the same reaction due to quasi-isotropic stiffness, one ply is presented at different cycles to show crack propagation rate instead of each individual ply at final stage. The distribution of Von Mises stresses at maximum loading of 5 [mm] vertical displacement in the top pin are displayed in colour. The analysis was limited to a 2000 [cycles]. The used mesh size is 2 [mm].

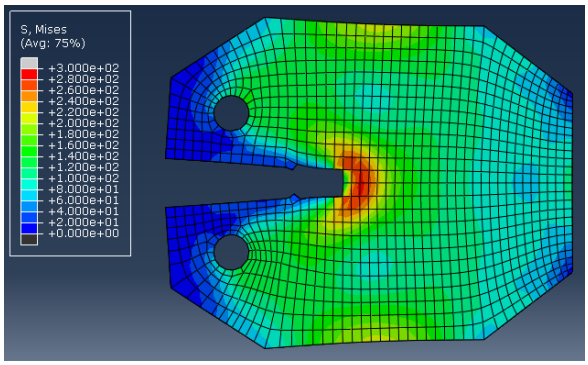


**(a)** One of the plies at cycle 100

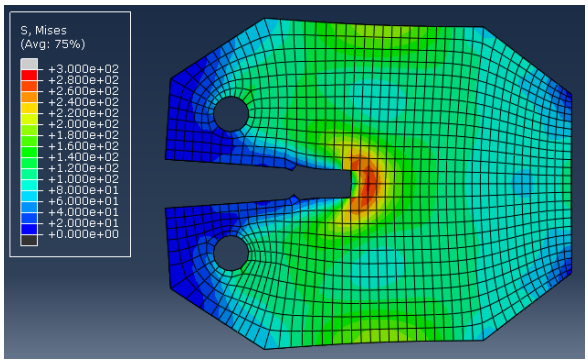


**(b)** One of the plies at cycle 150

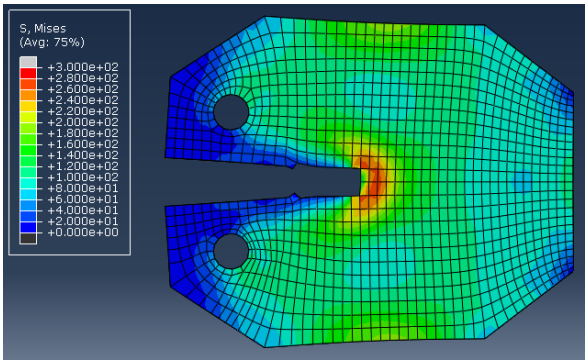


**(c)** One of the plies at cycle 200

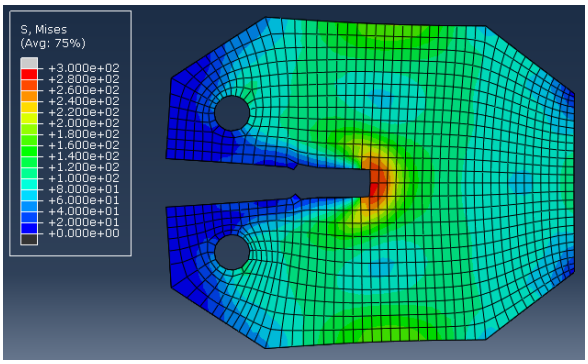


**(d)** One of the plies at cycle 250

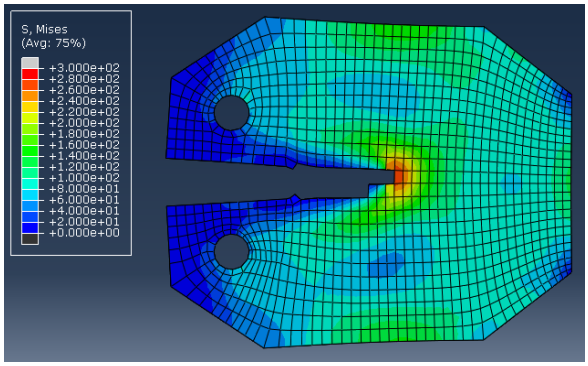


**(e)** One of the plies at cycle 500

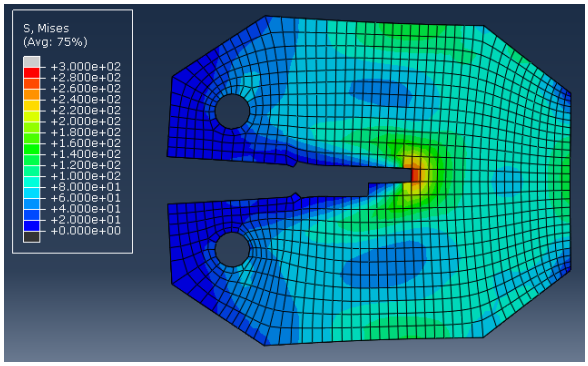


**(f)** One of the plies at cycle 1000

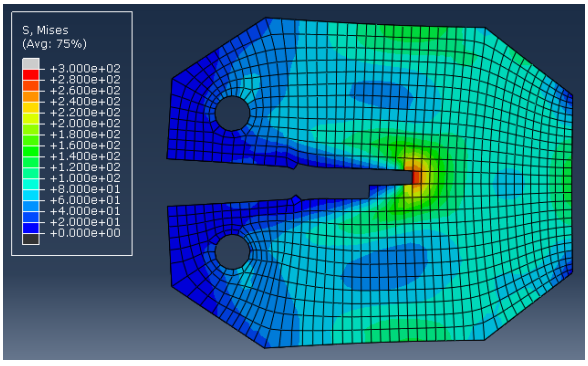


**(g)** One of the plies at cycle 2000

**Figure C.12:** A visualisation of the deformed compact tension specimen of an individual ply that has quasi-isotropic stiffness and tie constraints with its adjacent plies. As all the plies had the same reaction due to quasi-isotropic stiffness, one ply is presented at different cycles to show crack propagation rate instead of each individual ply at final stage. The distribution of Von Mises stresses at maximum loading of 5 [mm] vertical displacement in the top pin are displayed in colour. The analysis was limited to a 2000 [cycles]. The used mesh size is 2 [mm].

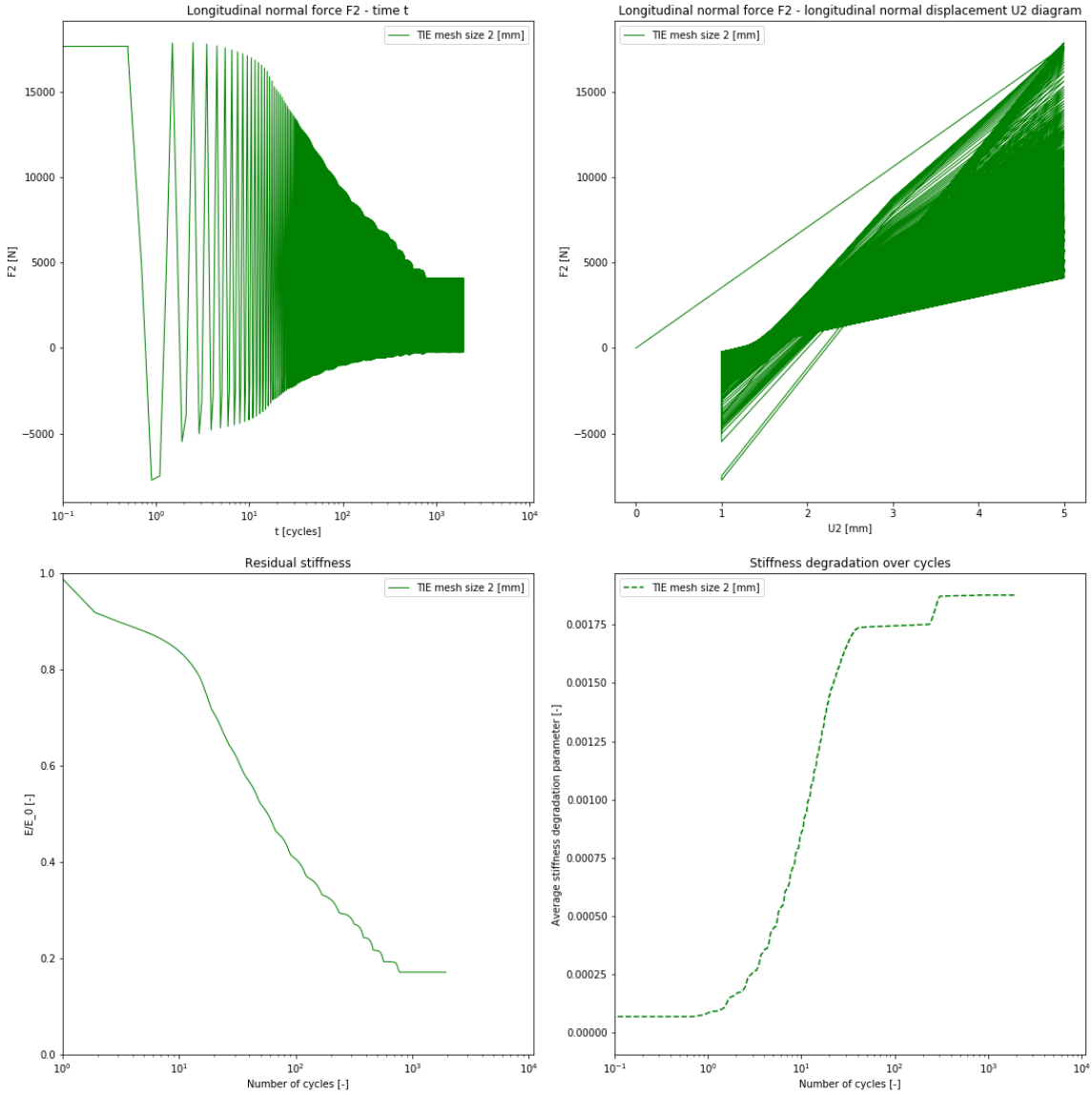


**Figure C.13:** In four plots the output is represented of the fatigue analysis for the compact tension specimen with five quasi-isotropic plies with tie interaction. A displacement of 5 [mm] is applied and the computations is truncated at a 50 [cycles]. The plots represent the analysis with a compact tension specimen with five plies with a layup $[0|-45|90|45|0]$ for which only the first direction of the quasi-isotropic plies is mentioned. The black line represents the output with a mesh size of 2 [mm]. Counting from the left to the right and from the top to the bottom, the load history plot is given first. This plot shows the applied force over time as resultant of a constant applied displacement amplitude. The second plot is the force-displacement diagram which acts as hysteresis plot of the element as structural response. The third plot shows the stiffness of the structure relative to the response of the first cycle. The fourth plot shows the average value of the damage parameters of the individual elements that leads to stiffness degradation, hence it is already normalised with the number of elements. Do recognise that the time axes are now on log scale instead of linear.

## C.5. VCCT interactions

### C.5.1. VCCT MS2 0053

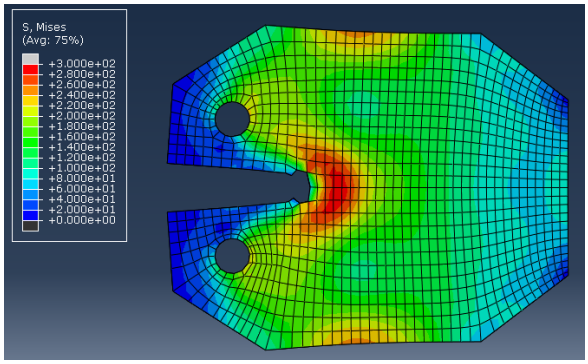


**(a)** One of the plies at cycle 500

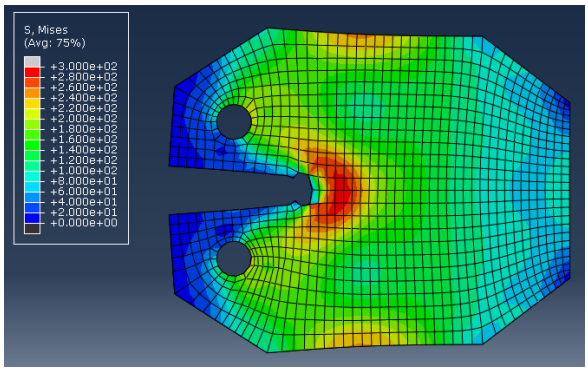


**(b)** One of the plies at cycle 1000

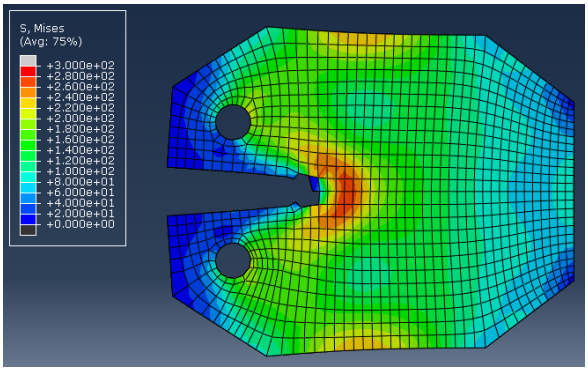


**(c)** One of the plies at cycle 2000

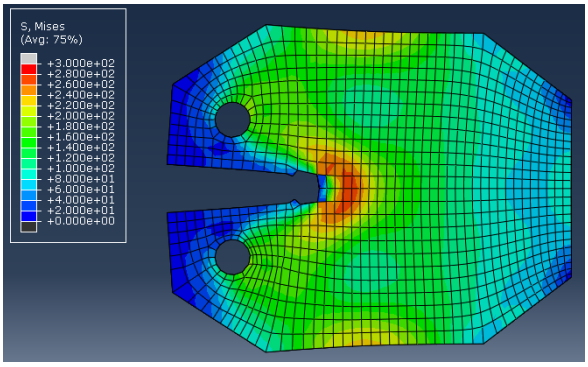


**(d)** One of the plies at cycle 5000

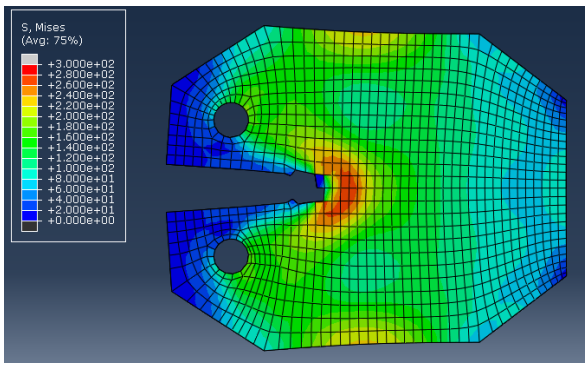


**(e)** One of the plies at cycle 10000

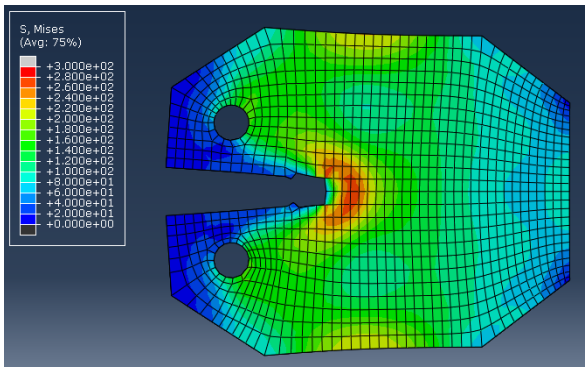


**(f)** One of the plies at cycle 20000

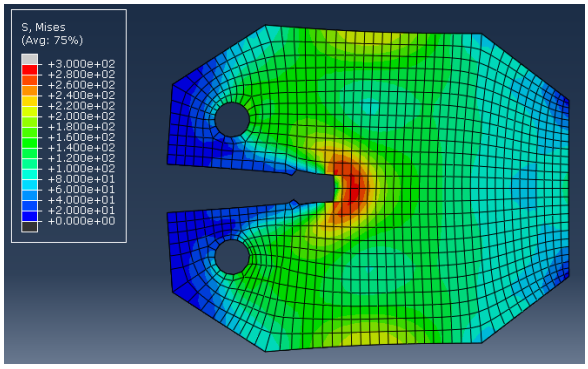


**(g)** One of the plies at cycle 50000

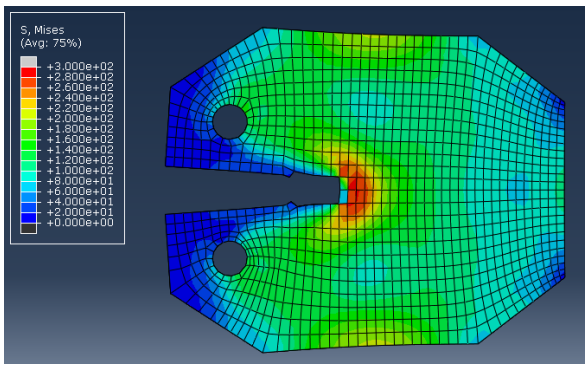


**(h)** One of the plies at cycle 100000

**Figure C.14:** Visualisation of the deformed compact tension specimen of an individual ply that has quasi-isotropic stiffness and VCCT interactions with its adjacent plies. The VCCT interaction had $c_3 = 0.005$ and $c_4 = 3$. As all the plies had the same reaction due to quasi-isotropic stiffness, one ply is presented at different cycles to show crack propagation rate instead of each individual ply at final stage. The distribution of Von Mises stresses at maximum loading of 5 [mm] vertical displacement in the top pin are displayed in colour. The analysis was limited to a 100000 [cycles].

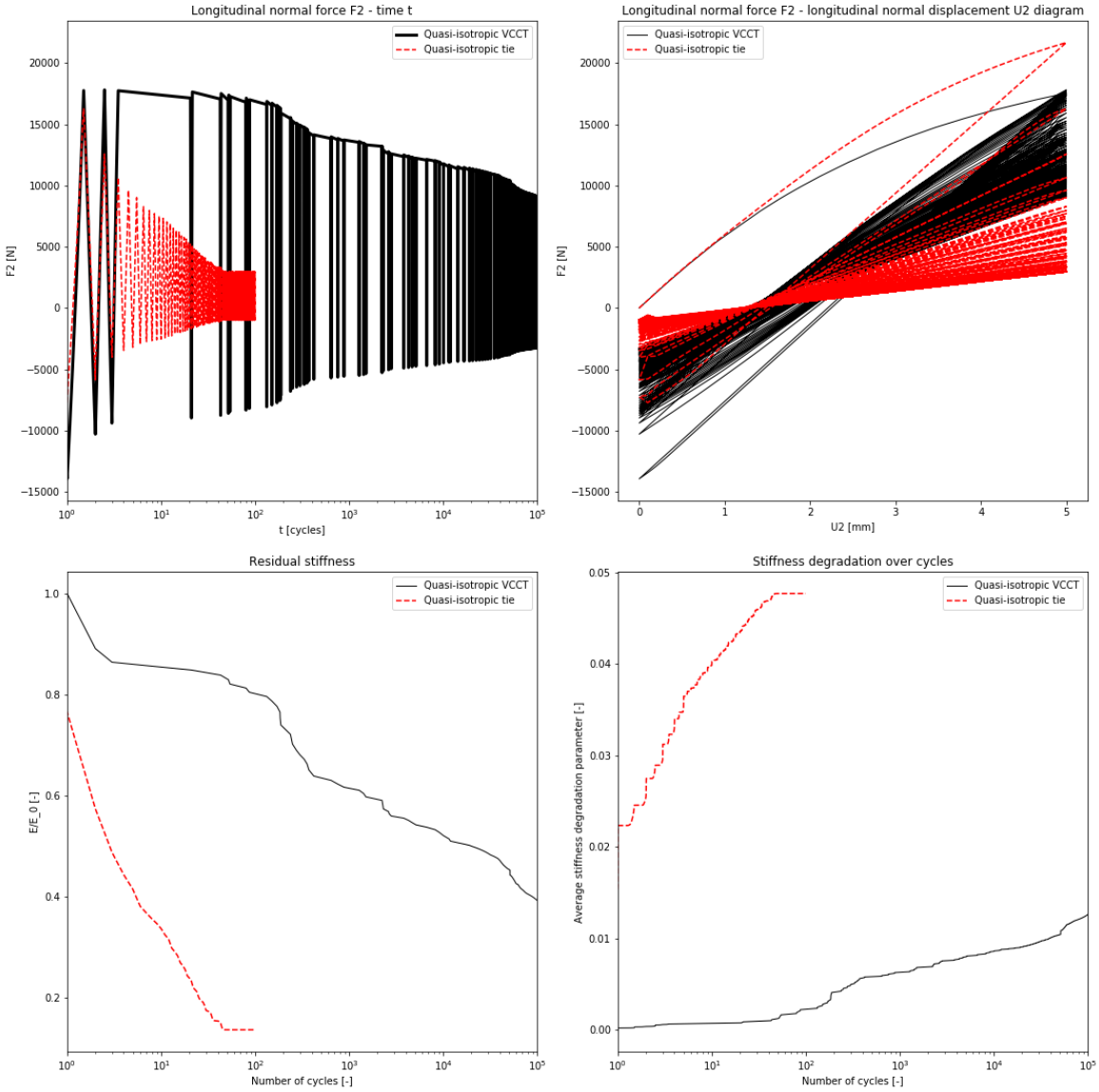


**Figure C.15:** In the entire (relevant) output of the fatigue analysis for the compact tension specimen with five quasi-isotropic plies with VCCT interaction is represented in these four figures. A displacement of 5 [mm] is applied and the computations is truncated at a 100 [cycles]. The red line shows the output for a single ply which is identical to the output provided in figure C.9. The black line represents the analysis with a compact tension specimen with five plies with a layup $[0|-45|90|45|0]$ for which only the first direction of the quasi-isotropic plies is mentioned. Counting from left to right and from top to bottom the load history plot is given first. This figure shows the applied force over time as resultant of a constant applied displacement amplitude. The second figure is the force-displacement diagram which acts as hysteresis plot of the element as structural response. The third figure shows the stiffness of the structure relative to the response of the first cycle. The fourth figure shows the average value of the damage parameters of the individual elements that leads to stiffness degradation, hence it is already normalised with the number of elements. Do recognise that the time axes are now on log scale instead of linear.

## C.6. VCCT parameteric influence

### C.6.1. VCCT MS2 11 (benchmark)

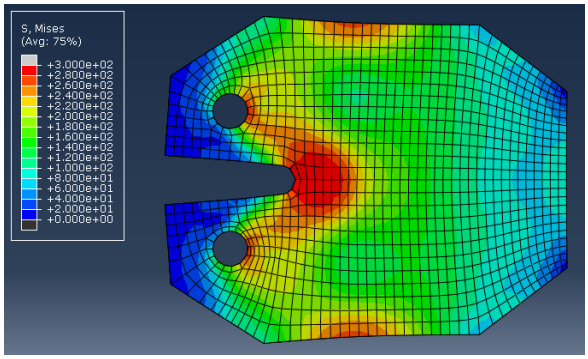


**(a)** One of the plies at cycle 1

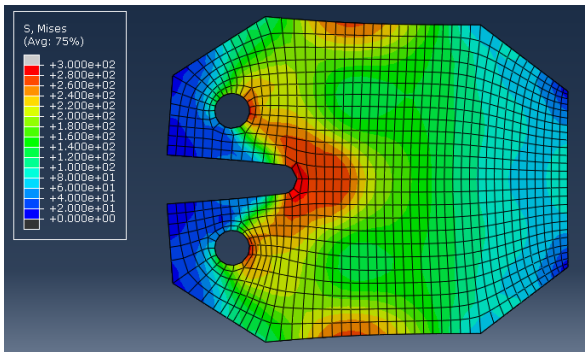


**(b)** One of the plies at cycle 2

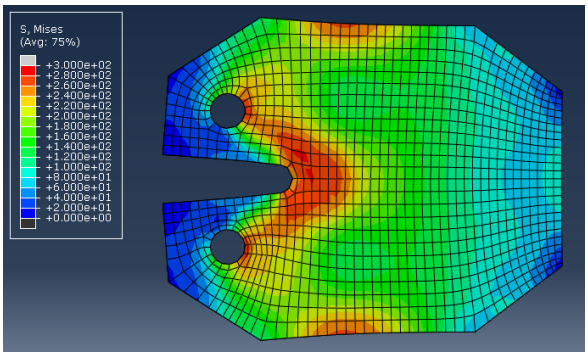


**(c)** One of the plies at cycle 5

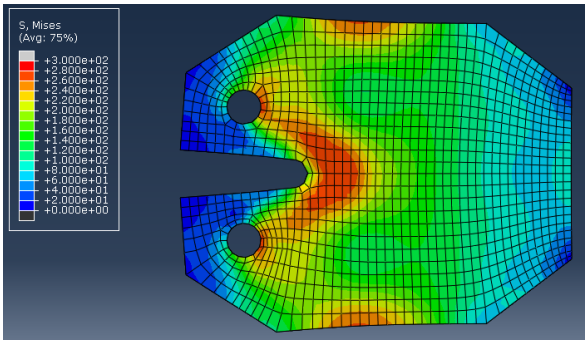


**(d)** One of the plies at cycle 10

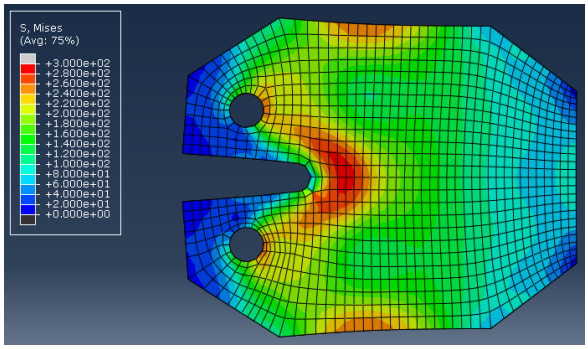


**(e)** One of the plies at cycle 20

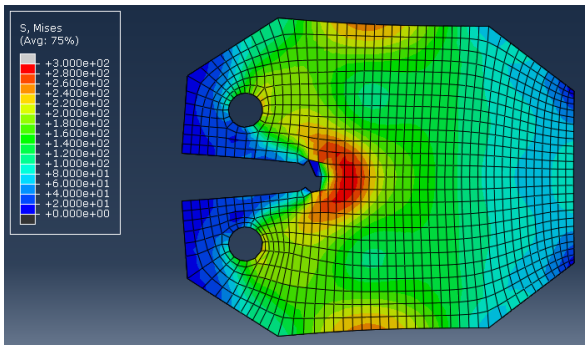


**(f)** One of the plies at cycle 50

**Figure C.16:** A visualisation of the deformed compact tension specimen of an individual ply that has quasi-isotropic stiffness and VCCT interactions with its adjacent plies. The applied Paris law material constants are $c_3 = 1$ and $c_4 = 1$. As all the plies had the same reaction due to quasi-isotropic stiffness, one ply is presented at different cycles to show crack propagation rate instead of each individual ply at final stage. The distribution of Von Mises stresses at maximum loading of 5 [mm] vertical displacement in the top pin are displayed in colour. The analysis was limited to a 5000 [cycles]. Only the first 50 cycles are shown with mesh size 2 [mm] for comparison in the mesh refinement.

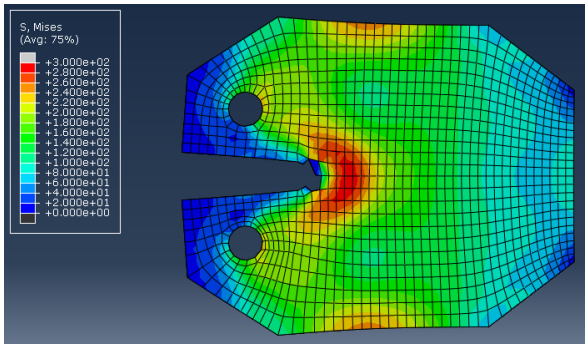


**(a)** One of the plies at cycle 50

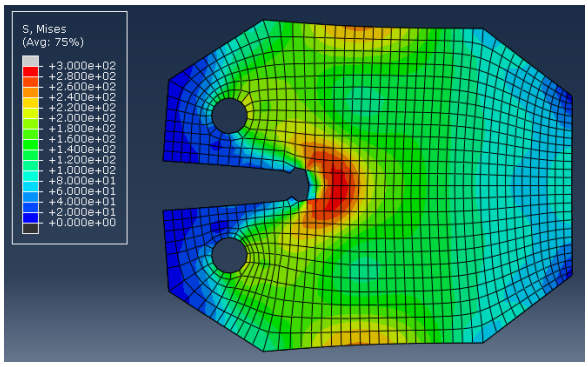


**(b)** One of the plies at cycle 100

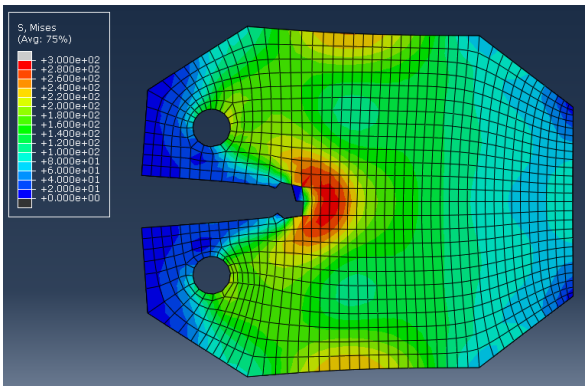


**(c)** One of the plies at cycle 200

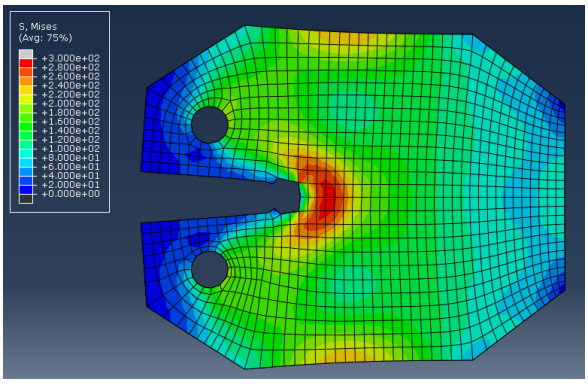


**(d)** One of the plies at cycle 500

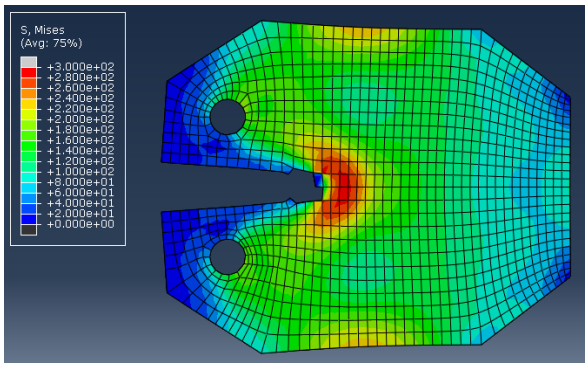


**(e)** One of the plies at cycle 1000

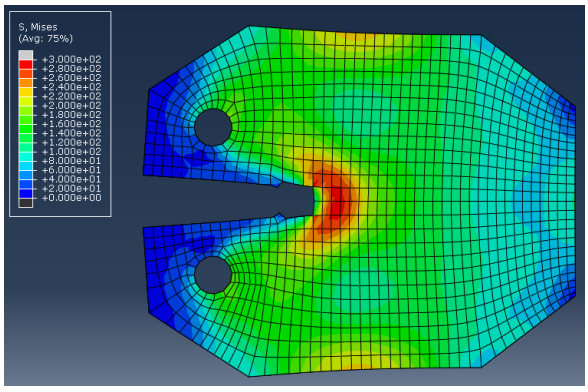


**(f)** One of the plies at cycle 2000

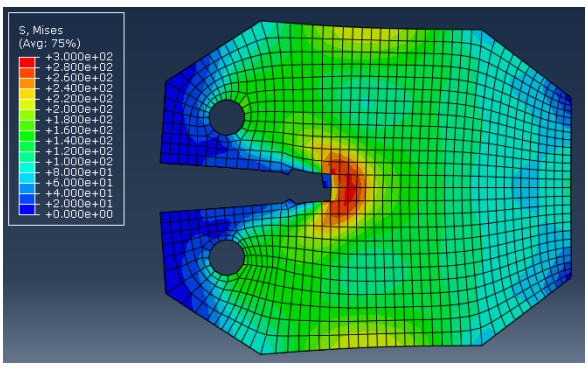


**(g)** One of the plies at cycle 5000

**Figure C.17:** A visualisation of the deformed compact tension specimen of an individual ply that has quasi-isotropic stiffness and VCCT interactions with its adjacent plies. The applied Paris law material constants are $c_3 = 1$ and $c_4 = 1$. As all the plies had the same reaction due to quasi-isotropic stiffness, one ply is presented at different cycles to show crack propagation rate instead of each individual ply at final stage. The distribution of Von Mises stresses at maximum loading of 5 [mm] vertical displacement in the top pin are displayed in colour. The analysis was limited to a 5000 [cycles].

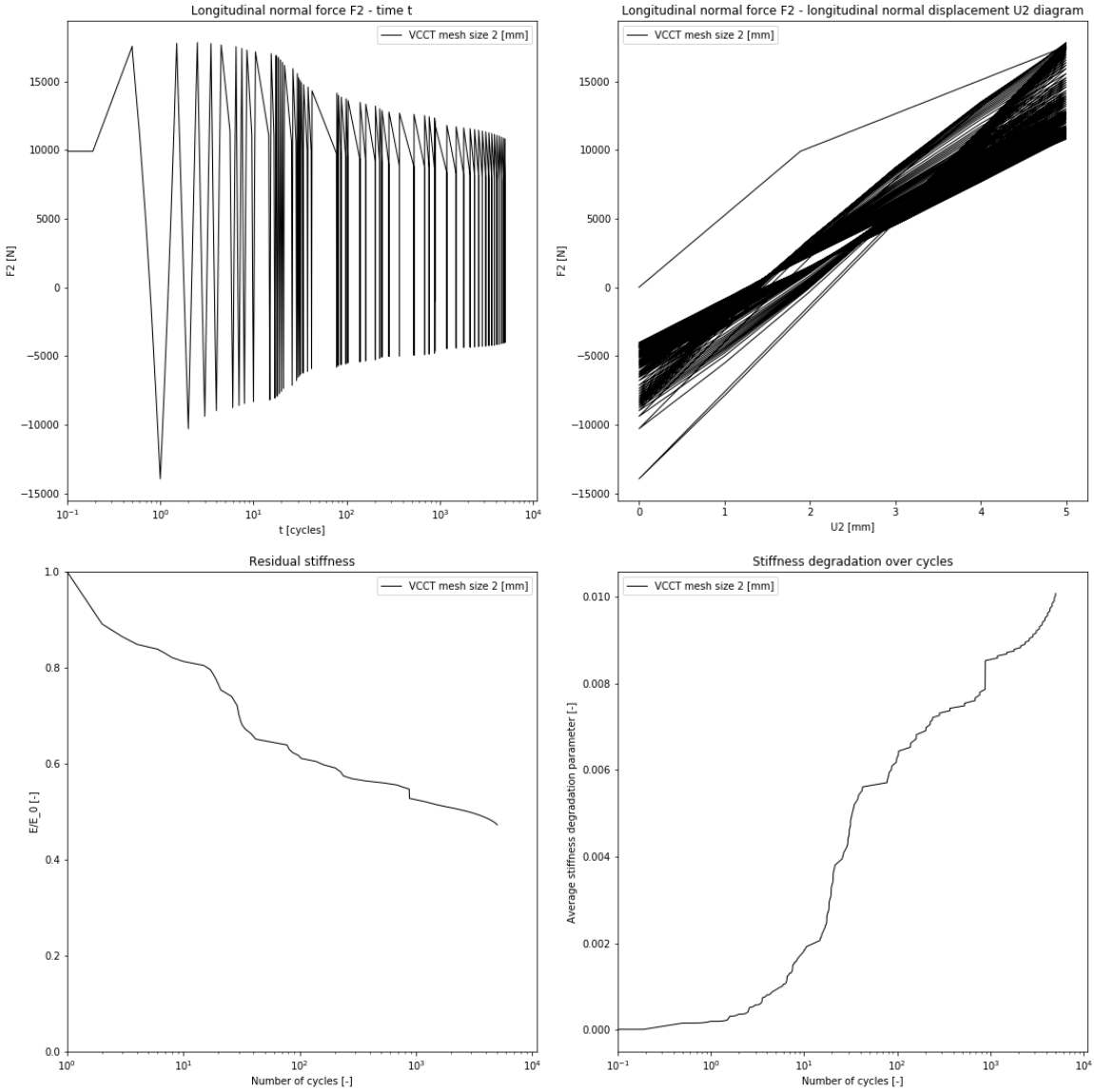


**Figure C.18:** In four plots the output is represented of the fatigue analysis for the compact tension specimen with five quasi-isotropic plies with VCCT interaction. A displacement of $5$ [mm] is applied and the computations is truncated at a $5000$ [cycles]. The plots represent the analysis with a compact tension specimen with five plies with a layup $[0|-45|90|45|0]$ for which only the first direction of the quasi-isotropic plies is mentioned. The applied Paris law material constants for the black line are $c_3 = 1$ and $c_4 = 1$. Counting from the left to the right and from the top to the bottom, the load history plot is given first. This plot shows the applied force over time as resultant of a constant applied displacement amplitude. The second plot is the force-displacement diagram which acts as hysteresis plot of the element as structural response. The third plot shows the stiffness of the structure relative to the response of the first cycle. The fourth plot shows the average value of the damage parameters of the individual elements that leads to stiffness degradation, hence it is already normalised with the number of elements. Do recognise that the time axes are now on log scale instead of linear.

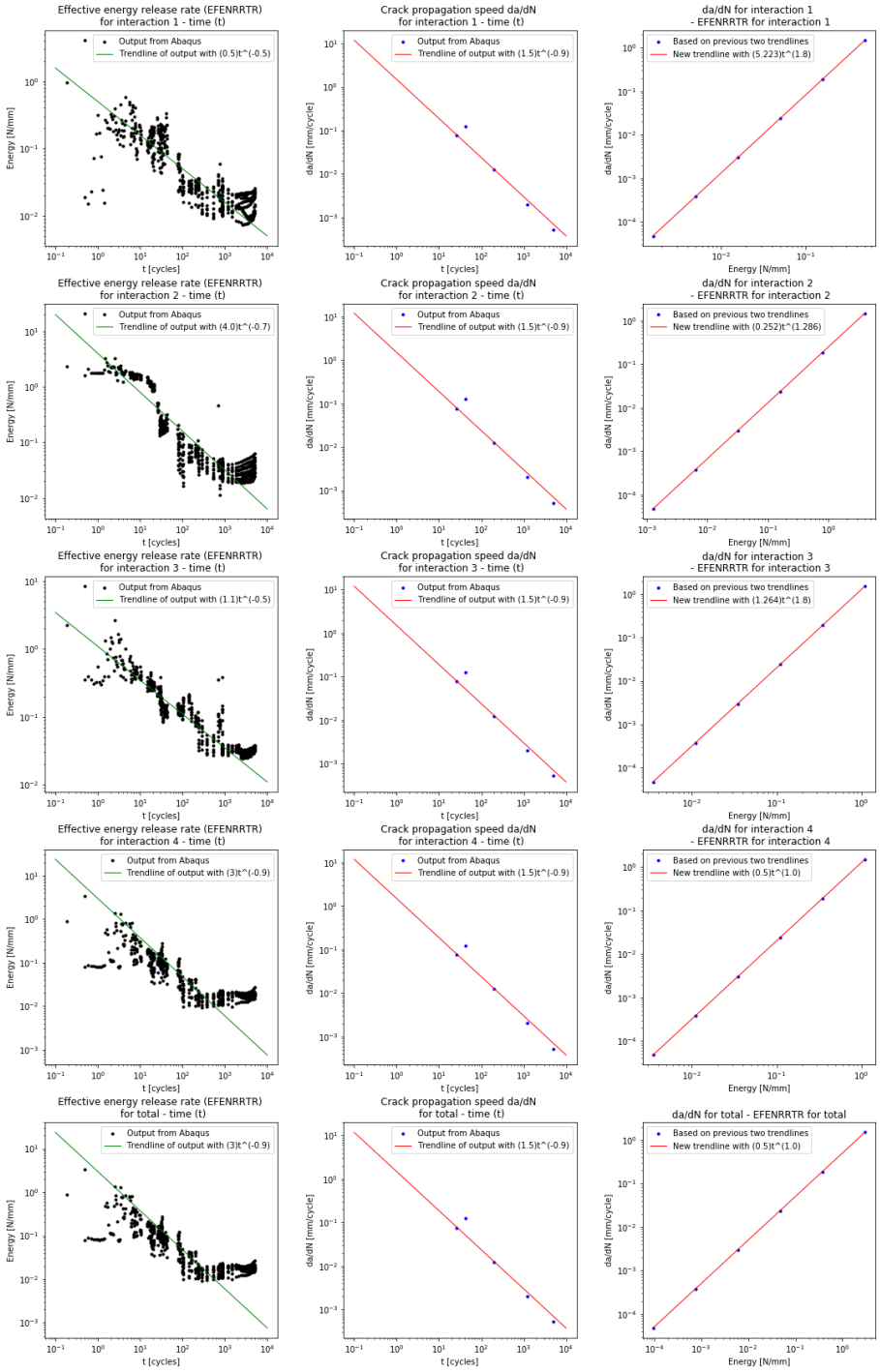


**Figure C.19:** A visualisation of the effect of the Paris law material constants on the fatigue analysis for the compact tension specimen related to figure C.18 with $c_3 = 1$ and $c_4 = 1$. Each row is for the next interface from the layup $[0|-45|90|45|0]$ and the fifth is the summation. The first column represents the equivalent energy release rate on the interface for each cycle. The second column provides the crack propagation rate for each 2 [mm] of crack propagation. The third column shows the relation between crack propagation rate and the equivalent energy release rate.

### C.6.2. VCCT MS2 101

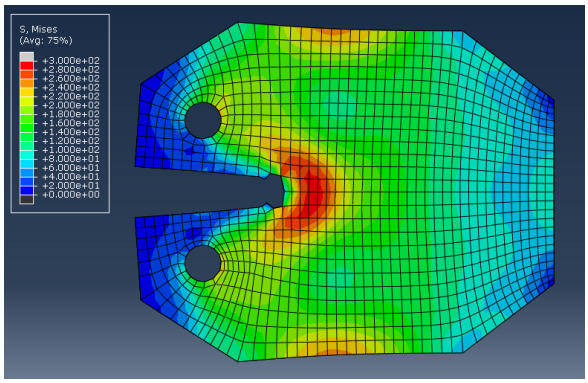


**(a)** One of the plies at cycle 100

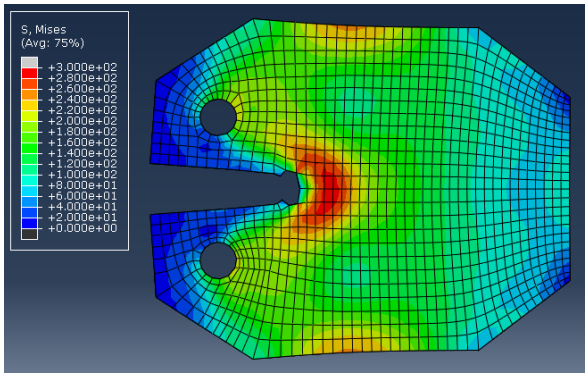


**(b)** One of the plies at cycle 200

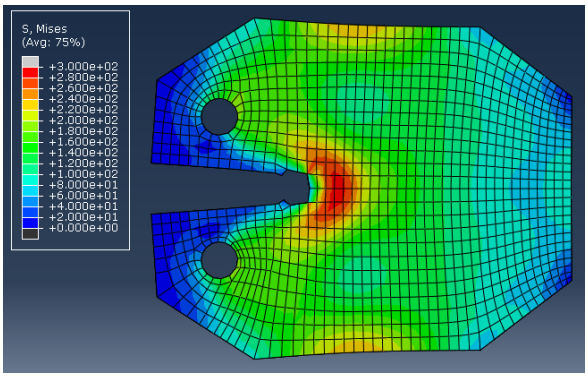


**(c)** One of the plies at cycle 500

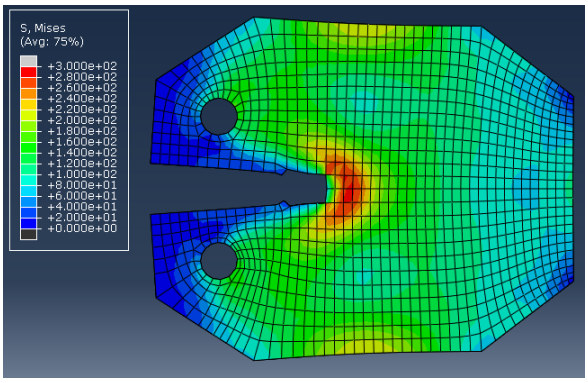


**(d)** One of the plies at cycle 1000

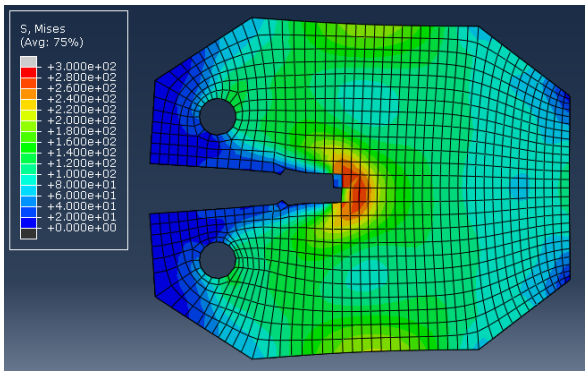


**(e)** One of the plies at cycle 2000

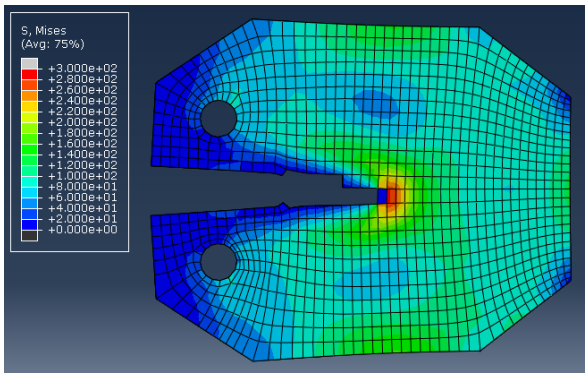


**(f)** One of the plies at cycle 5000

**Figure C.20:** A visualisation of the deformed compact tension specimen of an individual ply that has quasi-isotropic stiffness and VCCT interactions with its adjacent plies. The applied Paris law material constants are $c_3 = 10$ and $c_4 = 1$. As all the plies had the same reaction due to quasi-isotropic stiffness, one ply is presented at different cycles to show crack propagation rate instead of each individual ply at final stage. The distribution of Von Mises stresses at maximum loading of 5 [mm] vertical displacement in the top pin are displayed in colour. The analysis was limited to a 5000 [cycles].

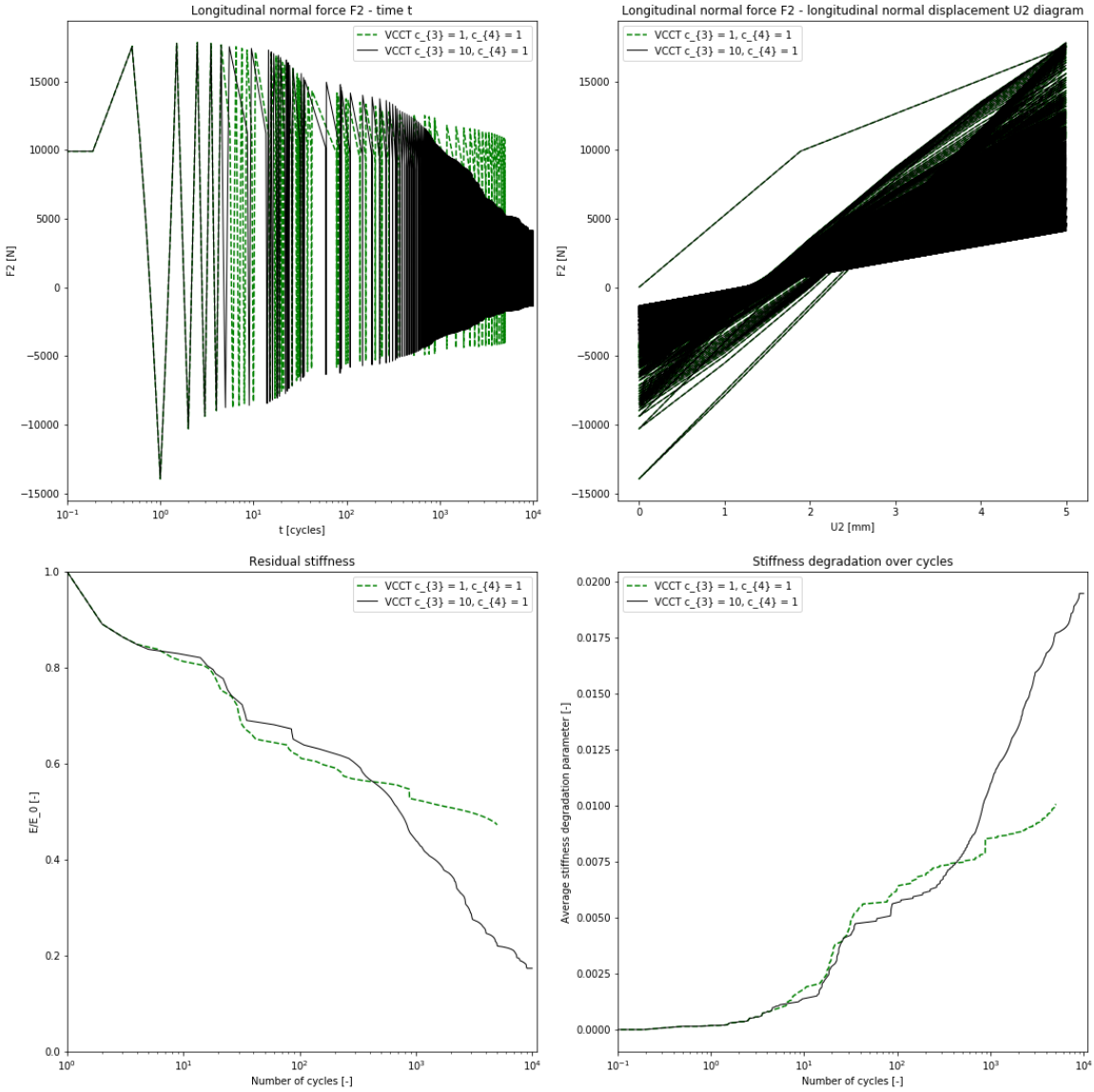


**Figure C.21:** In four plots the output is represented of the fatigue analysis for the compact tension specimen with five quasi-isotropic plies with VCCT interaction. A displacement of $5$ [mm] is applied and the computations is truncated at a $5000$ [cycles]. The plots represent the analysis with a compact tension specimen with five plies with a layup $[0|-45|90|45|0]$ for which only the first direction of the quasi-isotropic plies is mentioned. The applied Paris law material constants for the black line are $c_3 = 10$ and $c_4 = 1$. Counting from the left to the right and from the top to the bottom, the load history plot is given first. This plot shows the applied force over time as resultant of a constant applied displacement amplitude. The second plot is the force-displacement diagram which acts as hysteresis plot of the element as structural response. The third plot shows the stiffness of the structure relative to the response of the first cycle. The fourth plot shows the average value of the damage parameters of the individual elements that leads to stiffness degradation, hence it is already normalised with the number of elements. Do recognise that the time axes are now on log scale instead of linear.

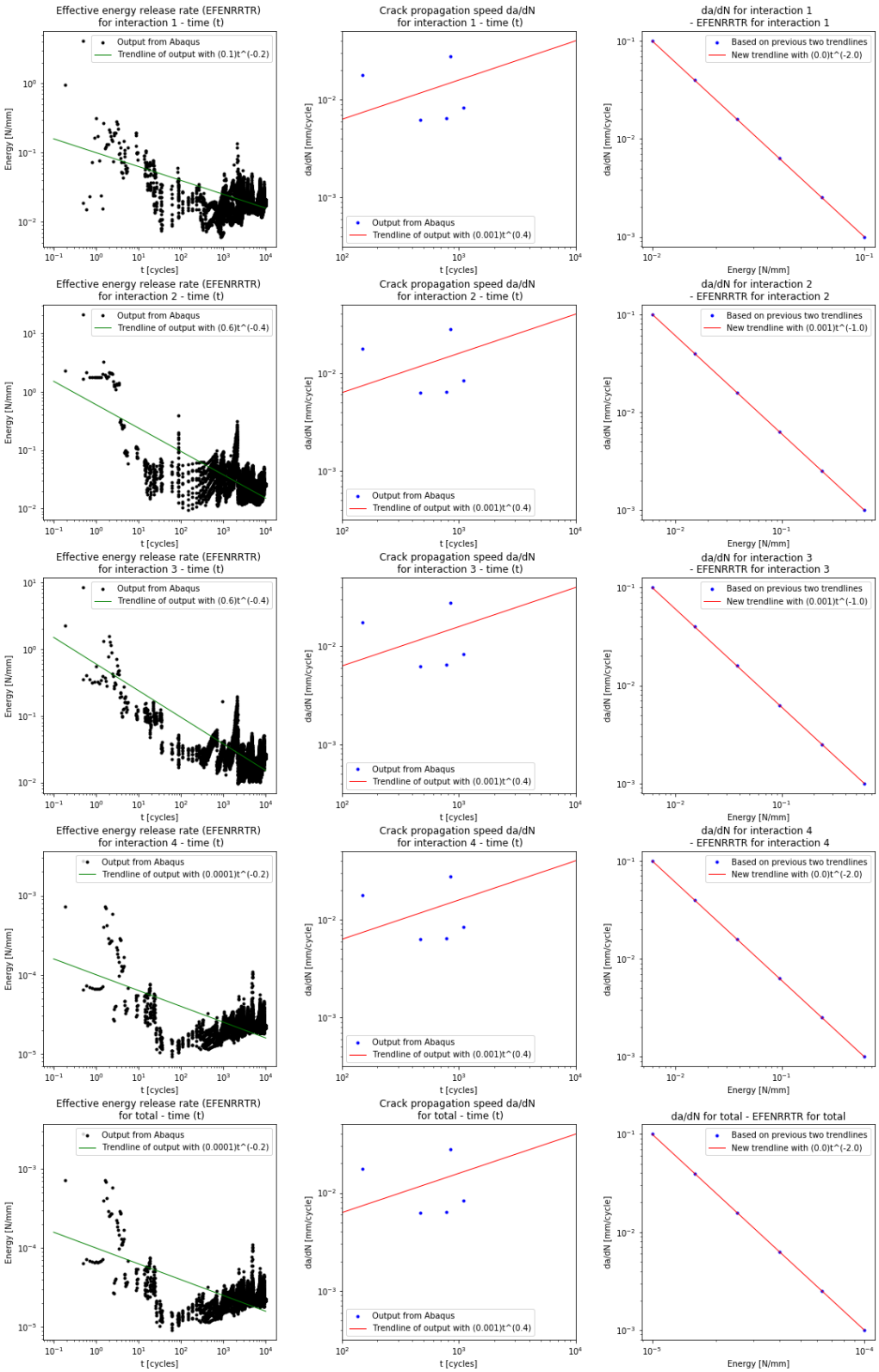


**Figure C.22:** A visualisation of the effect of the Paris law material constants on the fatigue analysis for the compact tension specimen related to figure C.21 with $c_3 = 10$ and $c_4 = 1$. Each row is for the next interface from the layup $[0|-45|90|45|0]$ and the fifth is the summation. The first column represents the equivalent energy release rate on the interface for each cycle. The second column provides the crack propagation rate for each 2 [mm] of crack propagation. The third column shows the relation between crack propagation rate and the equivalent energy release rate.

### C.6.3. VCCT MS2 011

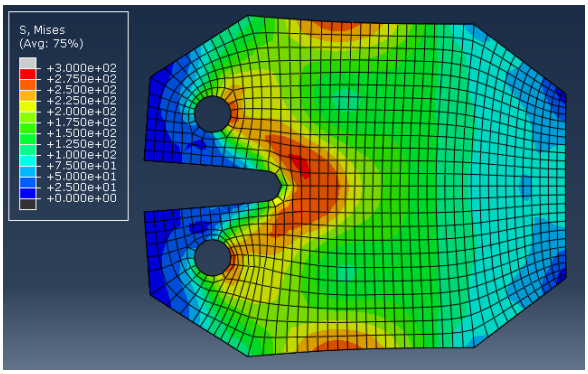


**(a)** One of the plies at cycle 100

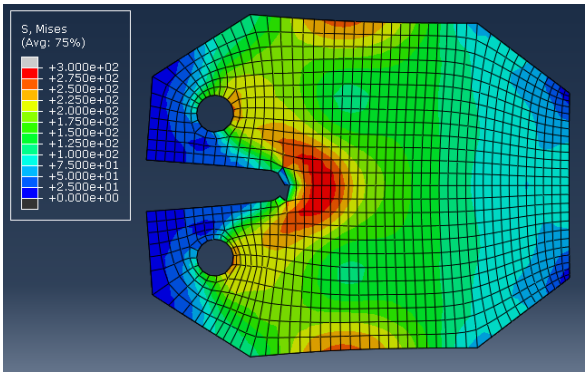


**(b)** One of the plies at cycle 200

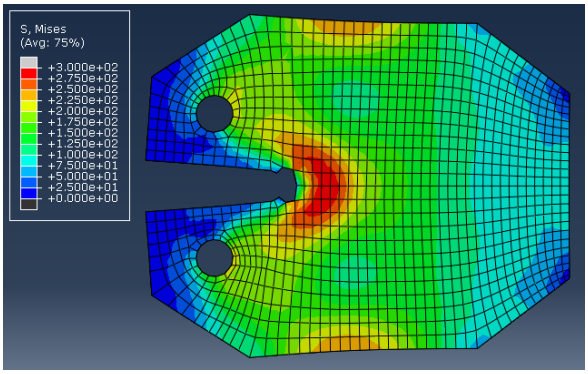


**(c)** One of the plies at cycle 500

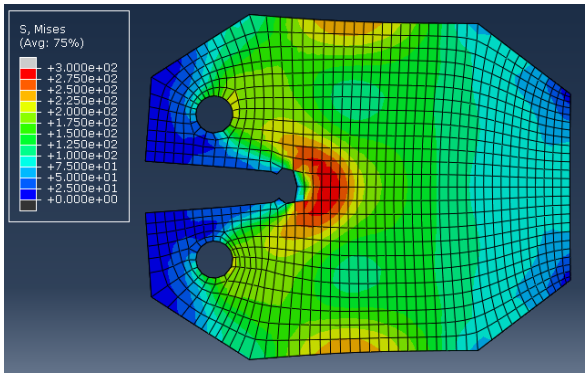


**(d)** One of the plies at cycle 1000

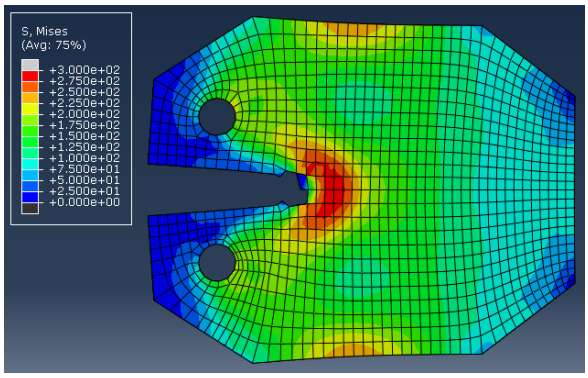


**(e)** One of the plies at cycle 2000

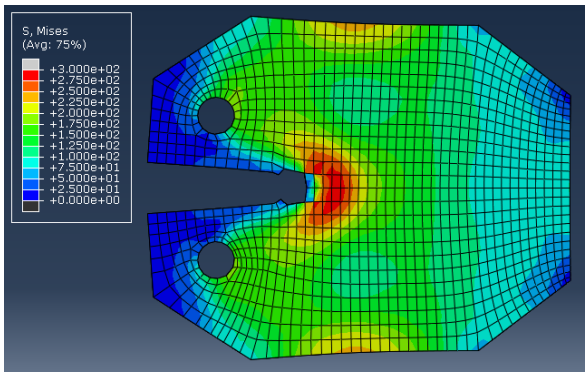


**(f)** One of the plies at cycle 5000

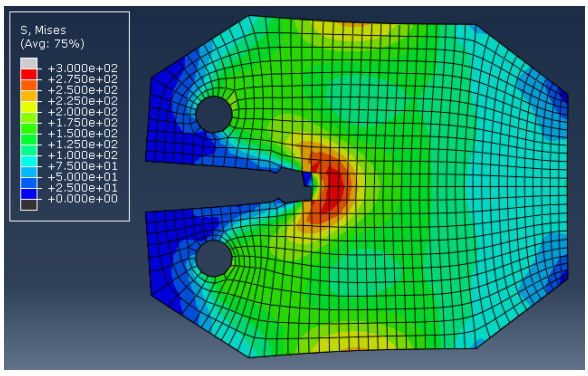


**(g)** One of the plies at cycle 10000

**Figure C.23:** A visualisation of the deformed compact tension specimen of an individual ply that has quasi-isotropic stiffness and VCCT interactions with its adjacent plies. The applied Paris law material constants are $c_3 = 0.1$ and $c_4 = 1$. As all the plies had the same reaction due to quasi-isotropic stiffness, one ply is presented at different cycles to show crack propagation rate instead of each individual ply at final stage. The distribution of Von Mises stresses at maximum loading of 5 [mm] vertical displacement in the top pin are displayed in colour. The analysis was limited to a 10000 [cycles].

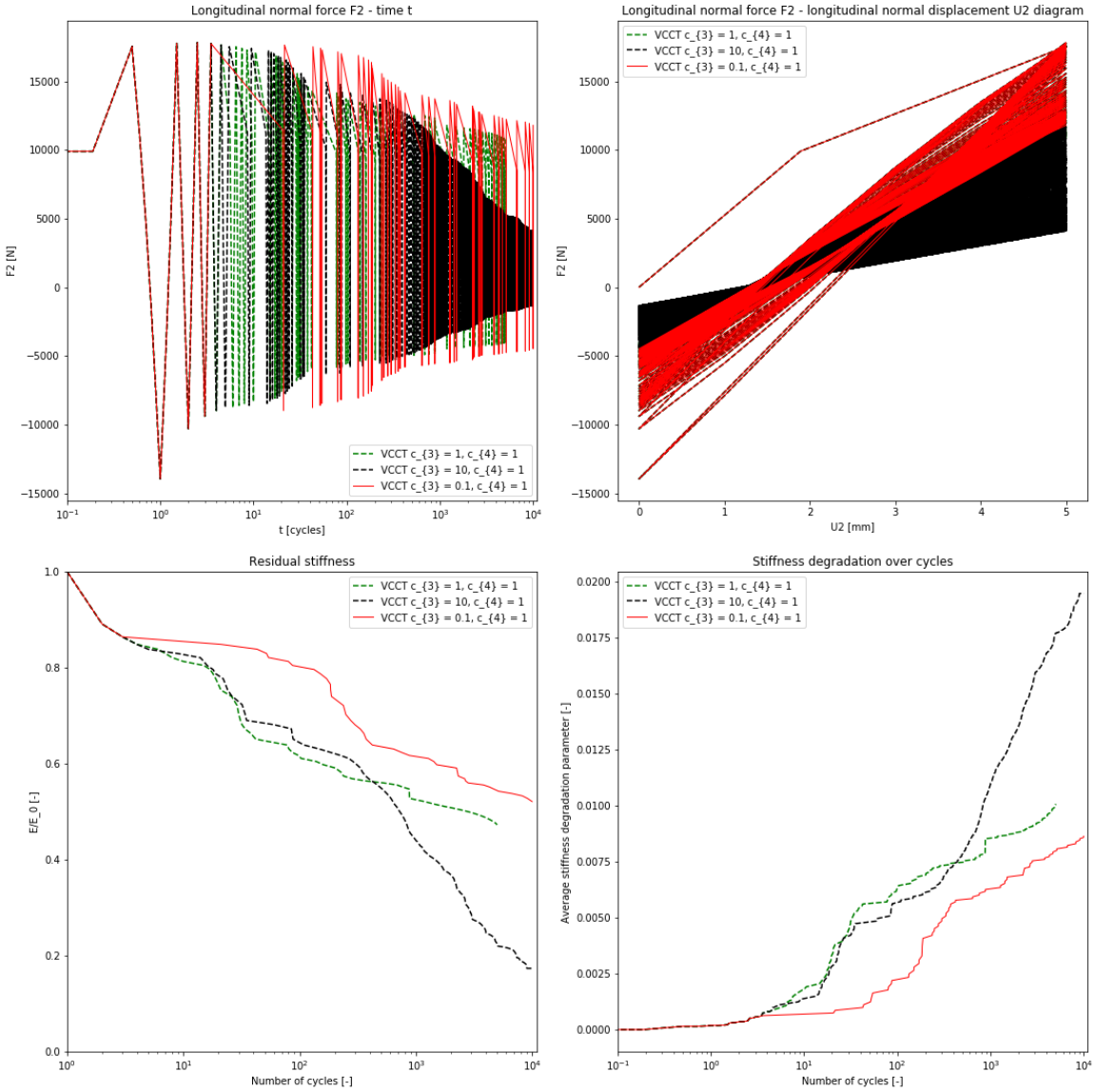


**Figure C.24:** In four plots the output is represented of the fatigue analysis for the compact tension specimen with five quasi-isotropic plies with VCCT interaction. A displacement of 5 [mm] is applied and the computations is truncated at a 10000 [cycles]. The plots represent the analysis with a compact tension specimen with five plies with a layup $[0|-45|90|45|0]$ for which only the first direction of the quasi-isotropic plies is mentioned. The applied Paris law material constants for the black line are $c_3 = 0.1$ and $c_4 = 1$. Counting from the left to the right and from the top to the bottom, the load history plot is given first. This plot shows the applied force over time as resultant of a constant applied displacement amplitude. The second plot is the force-displacement diagram which acts as hysteresis plot of the element as structural response. The third plot shows the stiffness of the structure relative to the response of the first cycle. The fourth plot shows the average value of the damage parameters of the individual elements that leads to stiffness degradation, hence it is already normalised with the number of elements. Do recognise that the time axes are now on log scale instead of linear.

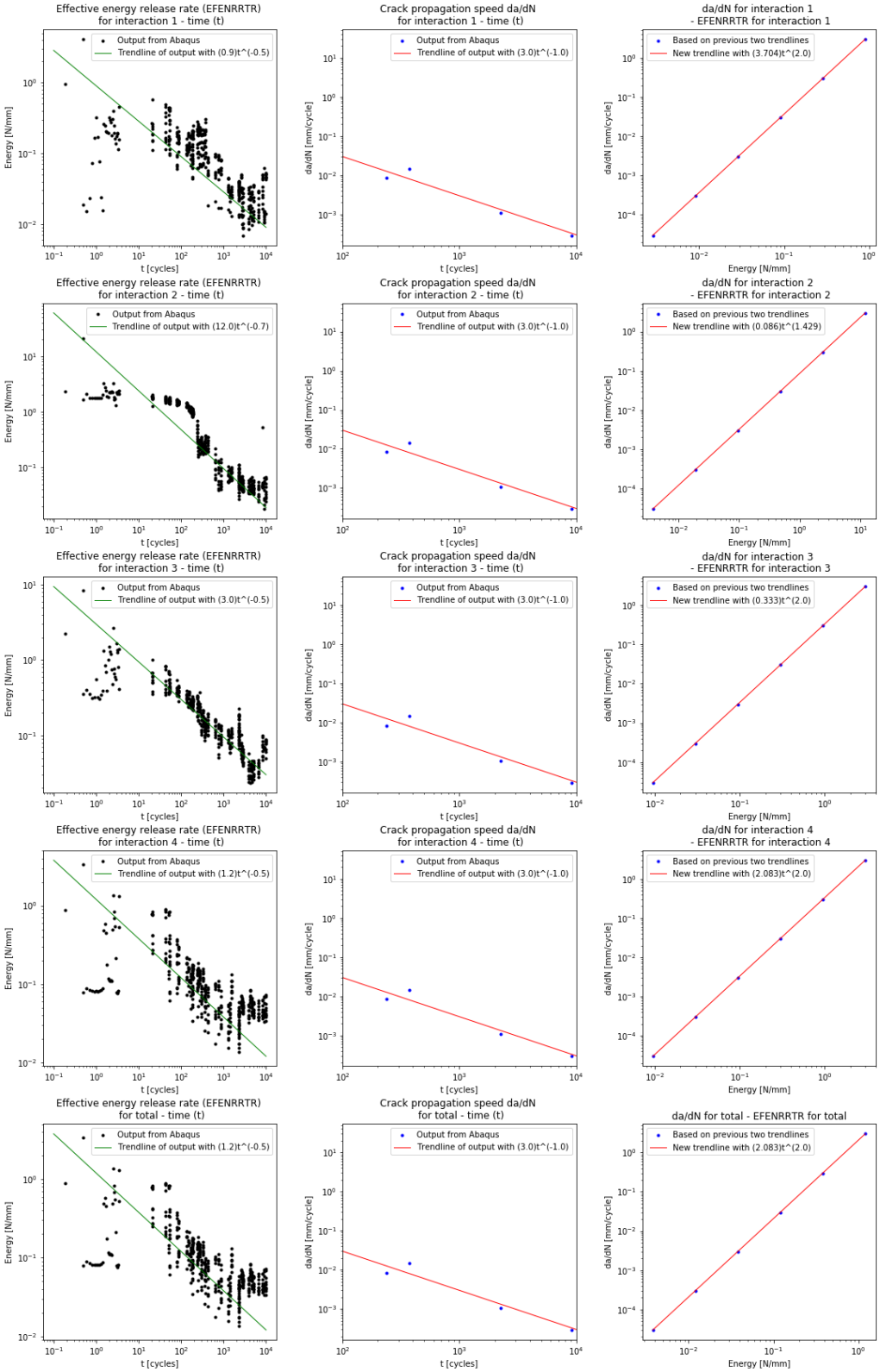


**Figure C.25:** A visualisation of the effect of the Paris law material constants on the fatigue analysis for the compact tension specimen related to figure C.24 with $c_3 = 0.1$ and $c_4 = 1$. Each row is for the next interface from the layup $[0|-45|90|45|0]$ and the fifth is the summation. The first column represents the equivalent energy release rate on the interface for each cycle. The second column provides the crack propagation rate for each 2 [mm] of crack propagation. The third column shows the relation between crack propagation rate and the equivalent energy release rate.

### C.6.4. VCCT MS2 103

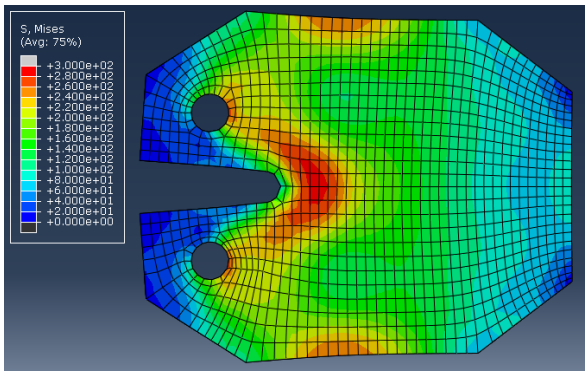


**(a)** One of the plies at cycle 50

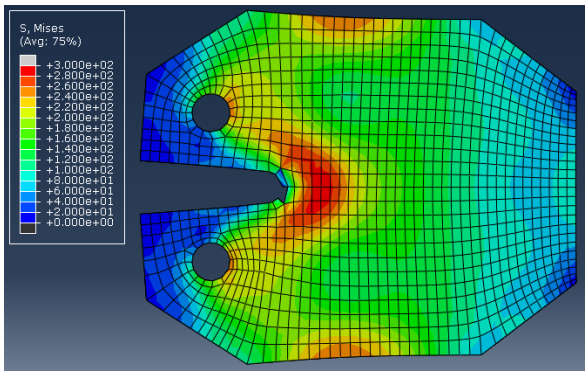


**(b)** One of the plies at cycle 100

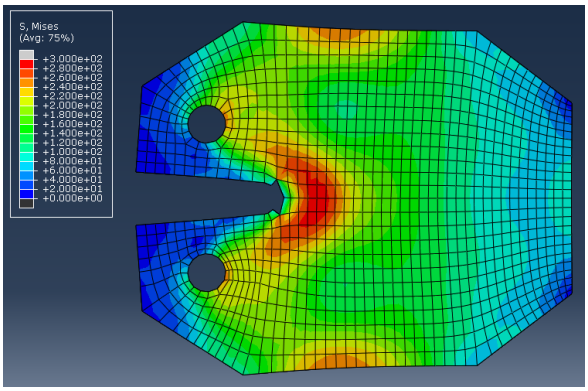


**(c)** One of the plies at cycle 200

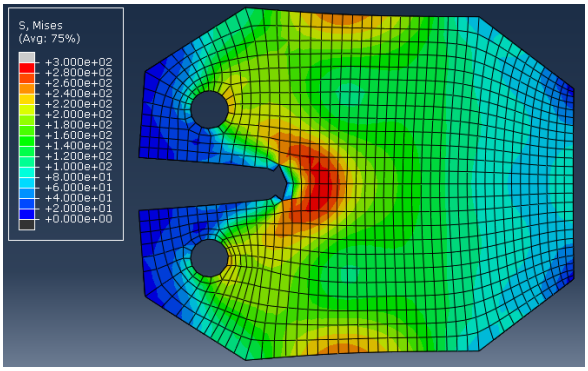


**(d)** One of the plies at cycle 500

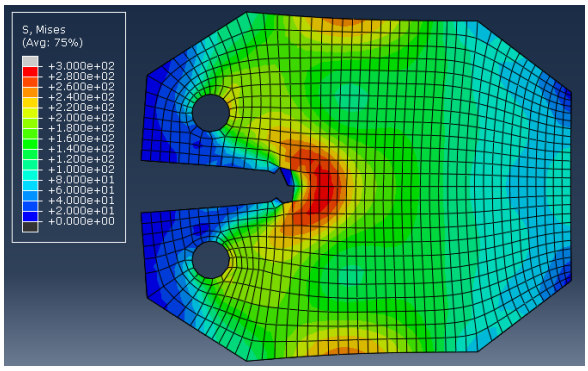


**(e)** One of the plies at cycle 1000

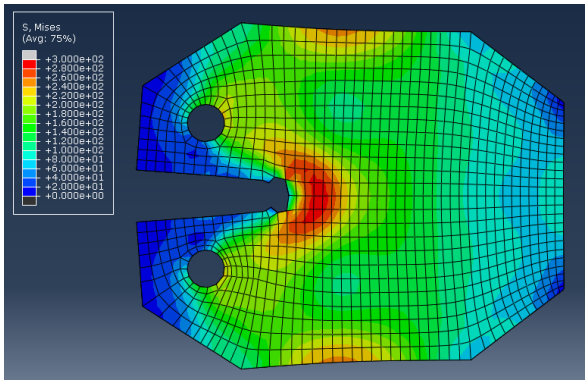


**(f)** One of the plies at cycle 2000

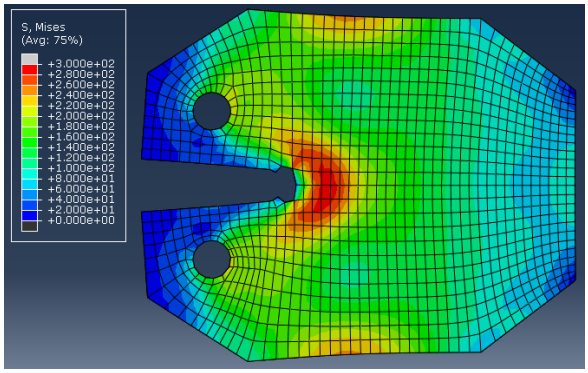


**(g)** One of the plies at cycle 5000

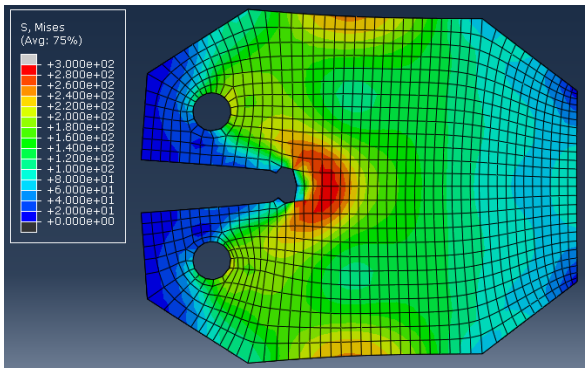


**(h)** One of the plies at cycle 10000

**Figure C.26:** A visualisation of the deformed compact tension specimen of an individual ply that has quasi-isotropic stiffness and VCCT interactions with its adjacent plies. The applied Paris law material constants are $c_3 = 10$ and $c_4 = 3$. As all the plies had the same reaction due to quasi-isotropic stiffness, one ply is presented at different cycles to show crack propagation rate instead of each individual ply at final stage. The distribution of Von Mises stresses at maximum loading of 5 [mm] vertical displacement in the top pin are displayed in colour. The analysis was limited to a 10000 [cycles].

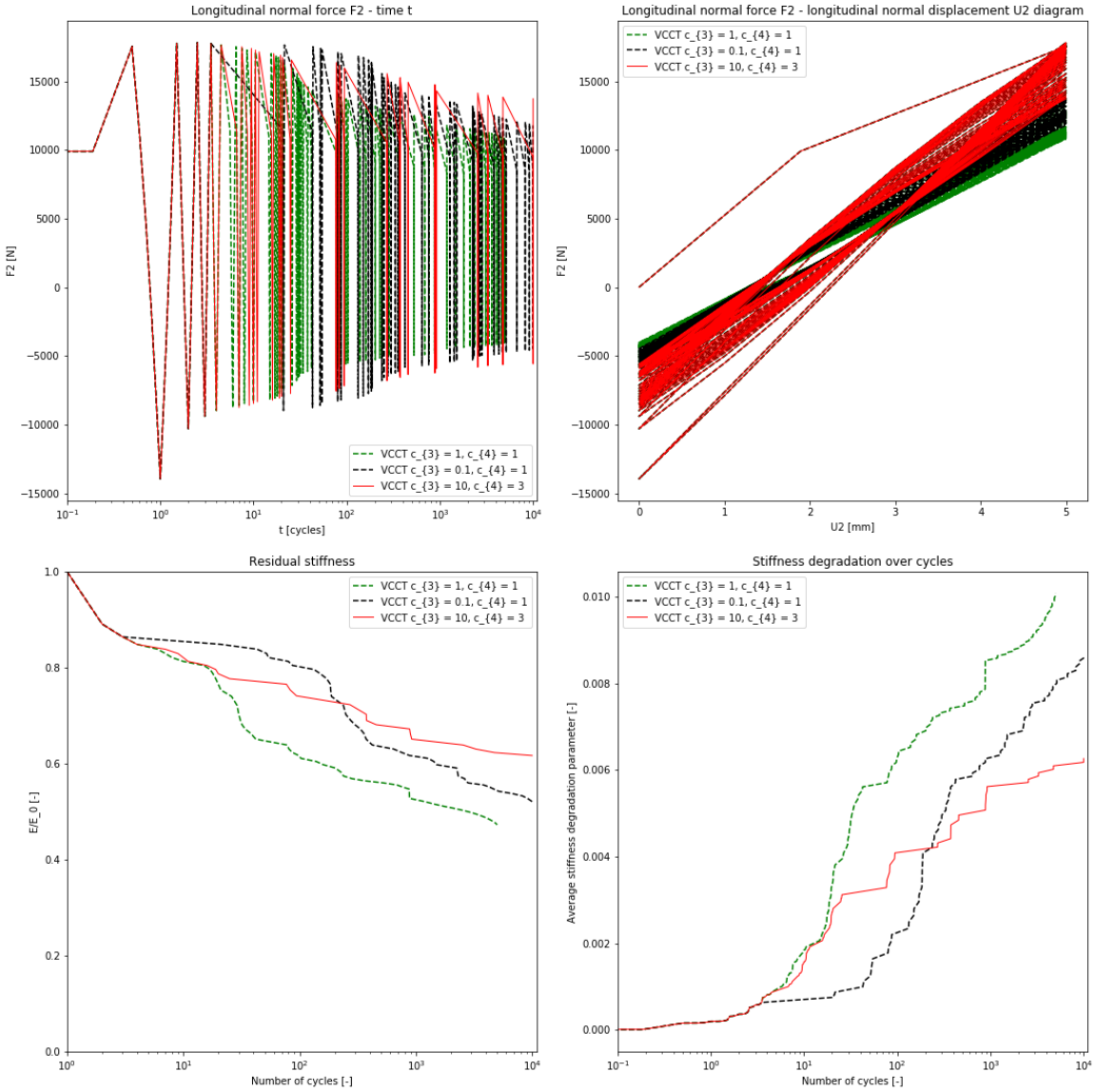


**Figure C.27:** In four plots the output is represented of the fatigue analysis for the compact tension specimen with five quasi-isotropic plies with VCCT interaction. A displacement of 5 [mm] is applied and the computations is truncated at a 10000 [cycles]. The plots represent the analysis with a compact tension specimen with five plies with a layup $[0|-45|90|45|0]$ for which only the first direction of the quasi-isotropic plies is mentioned. The applied Paris law material constants for the black line are $c_3 = 10$ and $c_4 = 3$. Counting from the left to the right and from the top to the bottom, the load history plot is given first. This plot shows the applied force over time as resultant of a constant applied displacement amplitude. The second plot is the force-displacement diagram which acts as hysteresis plot of the element as structural response. The third plot shows the stiffness of the structure relative to the response of the first cycle. The fourth plot shows the average value of the damage parameters of the individual elements that leads to stiffness degradation, hence it is already normalised with the number of elements. Do recognise that the time axes are now on log scale instead of linear.

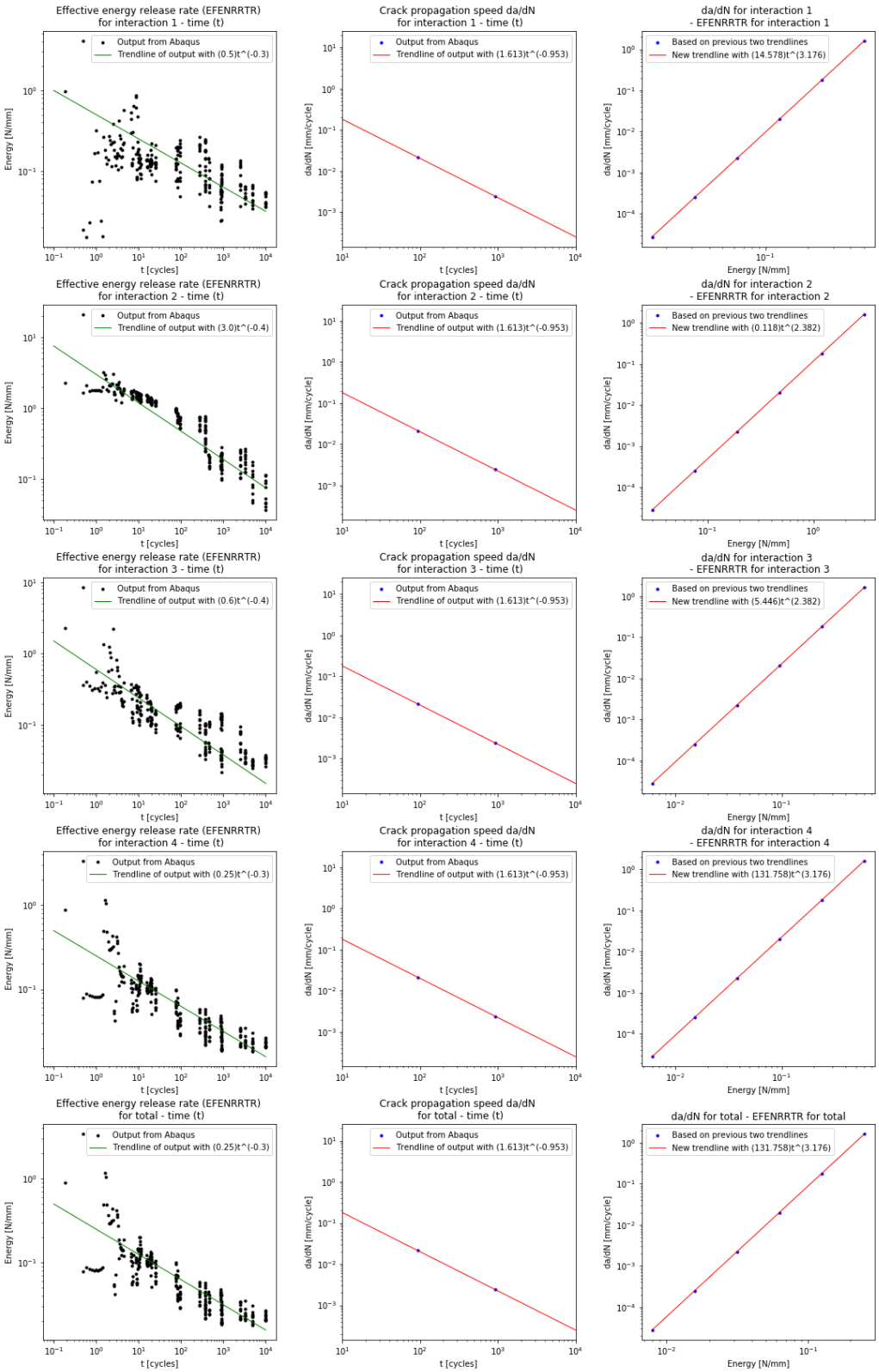


**Figure C.28:** A visualisation of the effect of the Paris law material constants on the fatigue analysis for the compact tension specimen related to figure C.27 with $c_3 = 10$ and $c_4 = 3$. Each row is for the next interface from the layup $[0|-45|90|45|0]$ and the fifth is the summation. The first column represents the equivalent energy release rate on the interface for each cycle. The second column provides the crack propagation rate for each 2 [mm] of crack propagation. The third column shows the relation between crack propagation rate and the equivalent energy release rate.

## C.7. Isolation of the VCCT effect

### C.7.1. VCCT isolated MS2 11 U2.5

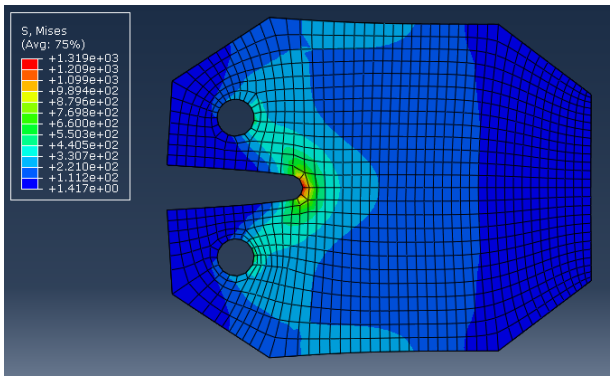


**(a)** One of the plies at cycle 1

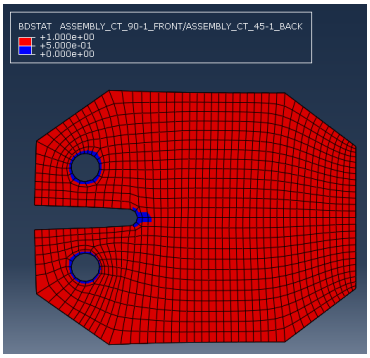


**(b)** One of the plies at cycle 10

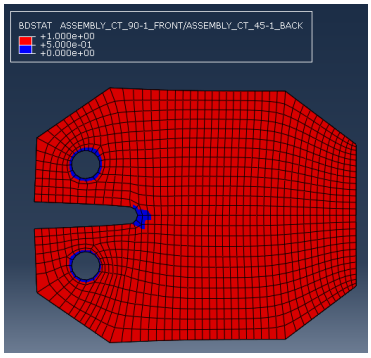


**(c)** One of the plies at cycle 20

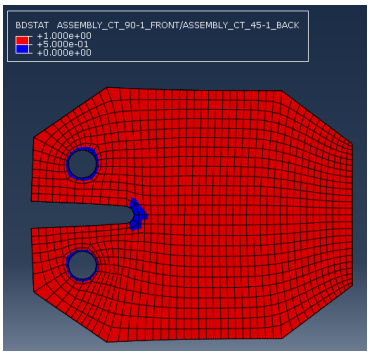


**(d)** One of the plies at cycle 25

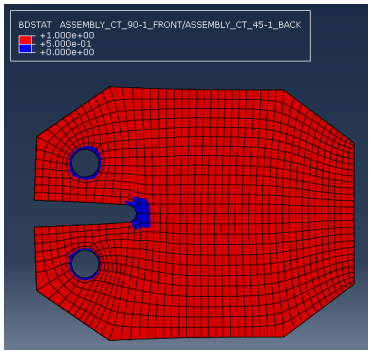


**(e)** One of the plies at cycle 116

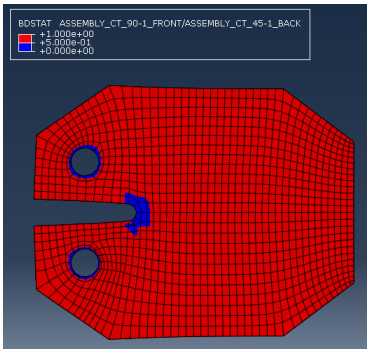


**(f)** One of the plies at cycle 195

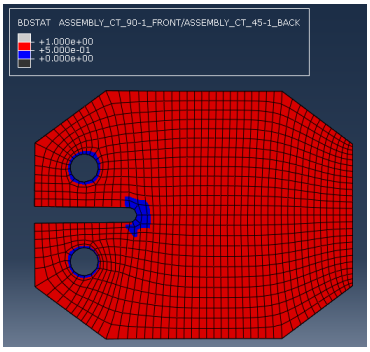


**(g)** One of the plies at cycle 20135

**Figure C.29:** VCCT isolated MS2 11 U7.5

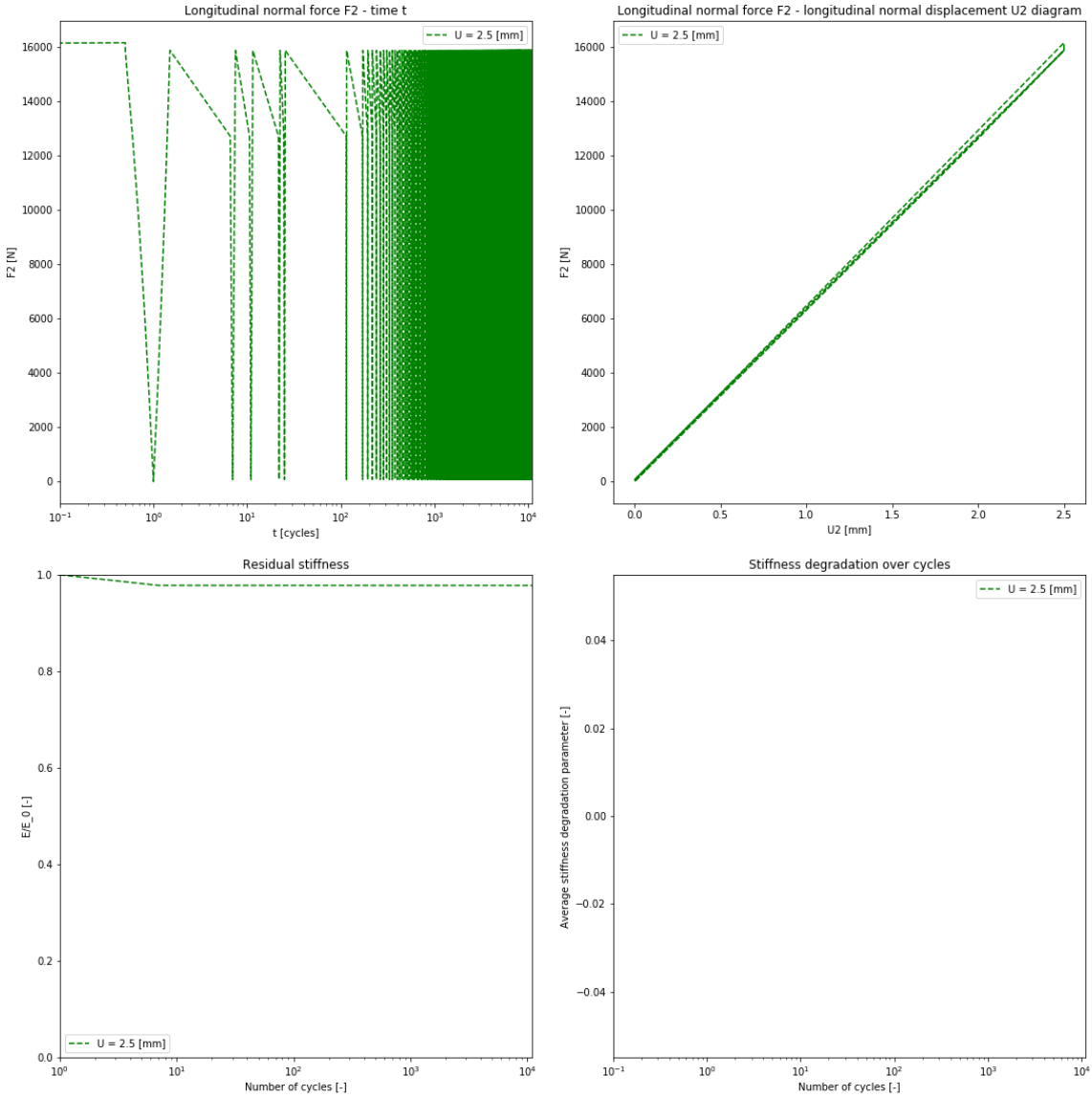


**Figure C.30:** In four plots the output is represented of the fatigue analysis for the compact tension specimen with five quasi-isotropic plies with VCCT interaction and linear elastic material. A displacement of 2.5 [mm] is applied. The plots represent the analysis with a compact tension specimen with five plies with a layup $[0|-45|90|45|0]$ for which only the first direction of the quasi-isotropic plies is mentioned. The applied Paris law material constants for the black line are $c_3 = 1$ and $c_4 = 1$ and a mesh size of 2 [mm]. Counting from the left to the right and from the top to the bottom, the load history plot is given first. This plot shows the applied force over time as resultant of a constant applied displacement amplitude. The second plot is the force-displacement diagram which acts as hysteresis plot of the element as structural response. The third plot shows the stiffness of the structure relative to the response of the first cycle. The fourth plot shows the average value of the damage parameters of the individual elements that leads to stiffness degradation, hence it is already normalised with the number of elements. Do recognise that the time axes are now on log scale instead of linear.

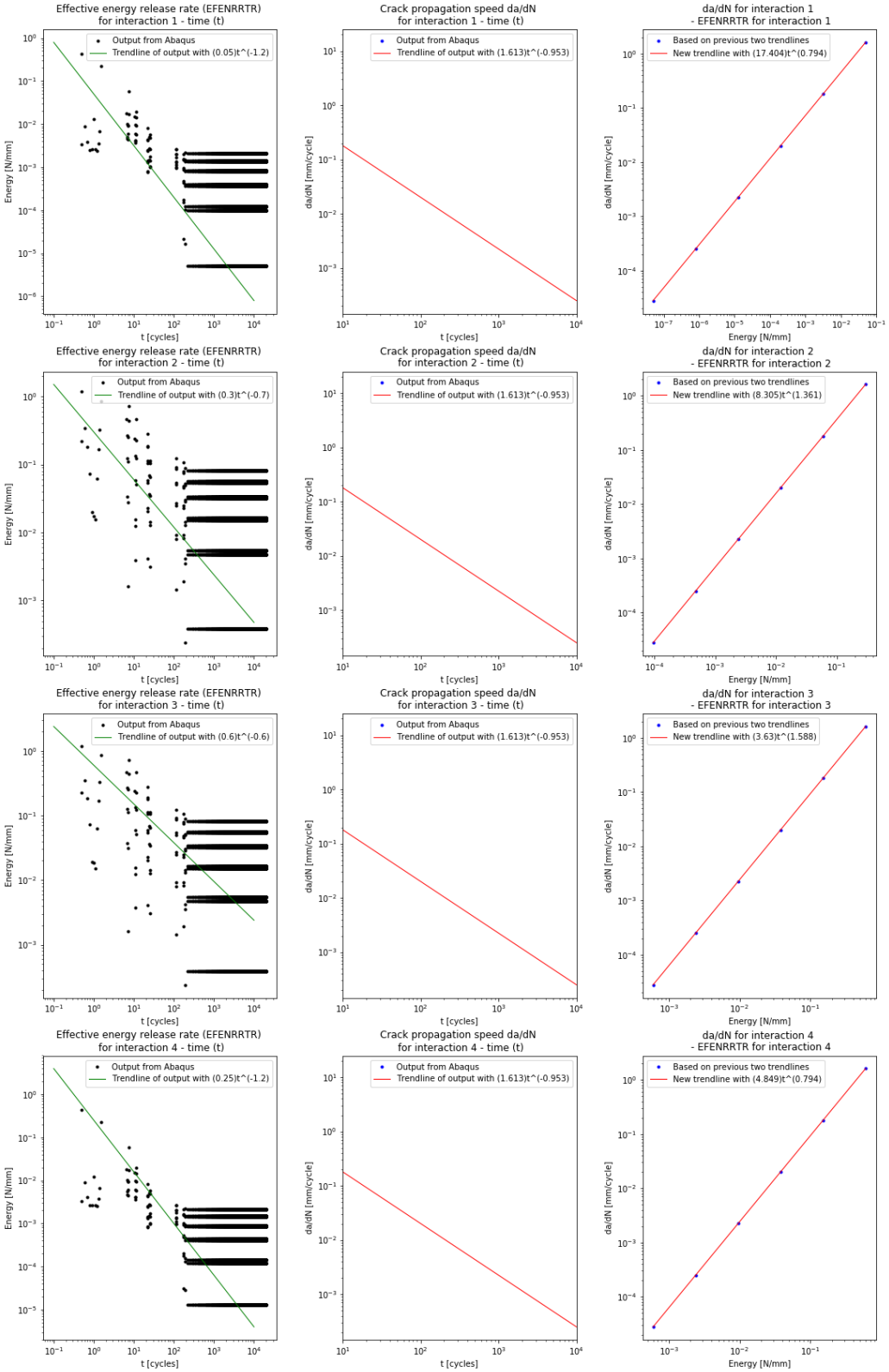


**Figure C.31:** A visualisation of the effect of the Paris law material constants on the fatigue analysis for the compact tension specimen related to figure C.30 with $c_3 = 1$ and $c_4 = 1$ and a load of 2.5 [mm]. Each row is for the next interface from the layup $[0|-45|90|45|0]$ and the fifth is the summation. The first column represents the equivalent energy release rate on the interface for each cycle. The second column provides the crack propagation rate for each 2 [mm] of crack propagation. The third column shows the relation between crack propagation rate and the equivalent energy release rate.

### C.7.2. VCCT isolated MS2 11 U5.0

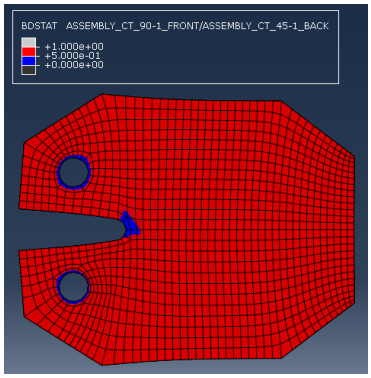


**(a)** One of the plies at cycle 1

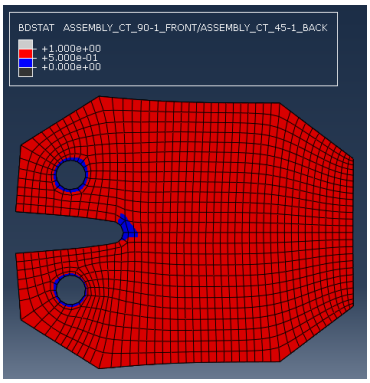


**(b)** One of the plies at cycle 2

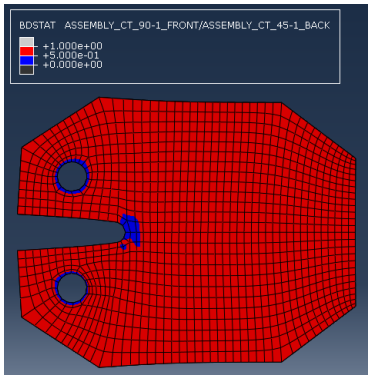


**(c)** One of the plies at cycle 5

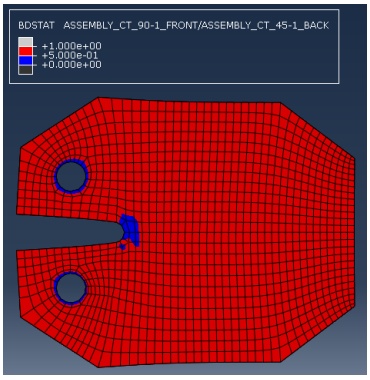


**(d)** One of the plies at cycle 6

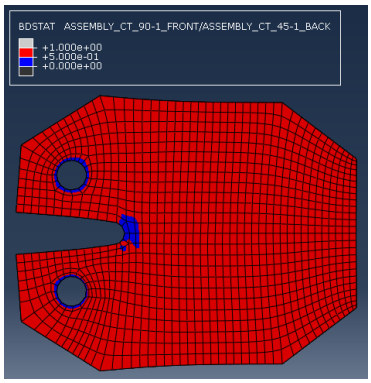


**(e)** One of the plies at cycle 7

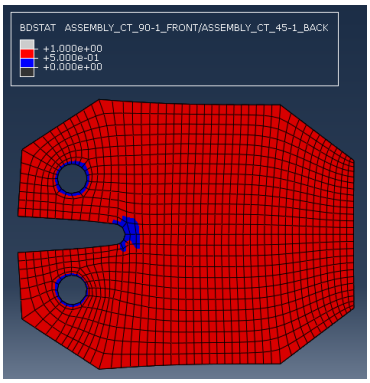


**(f)** One of the plies at cycle 31

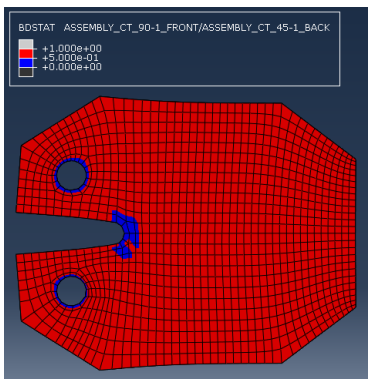


**(g)** One of the plies at cycle 47

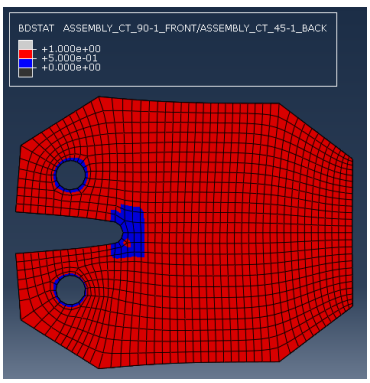


**(h)** One of the plies at cycle 98

**Figure C.32:** VCCT isolated MS2 11 U5.0

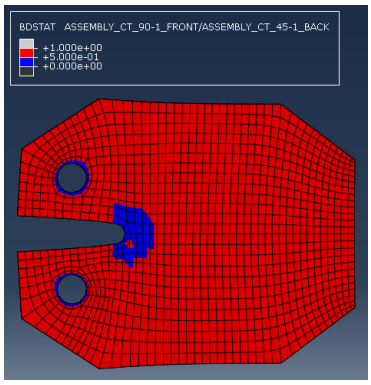


**(a)** One of the plies at cycle 211

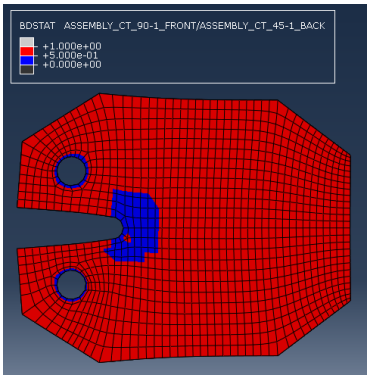


**(b)** One of the plies at cycle 465

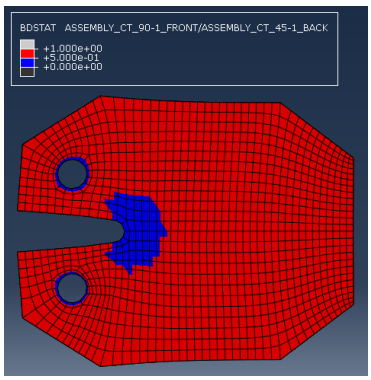


**(c)** One of the plies at cycle 910

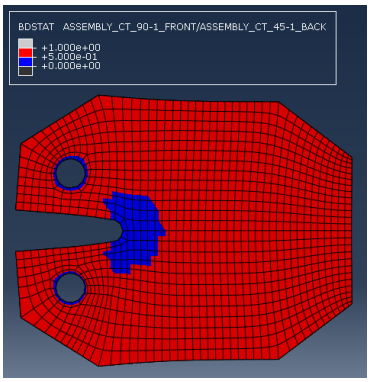


**(d)** One of the plies at cycle 1975

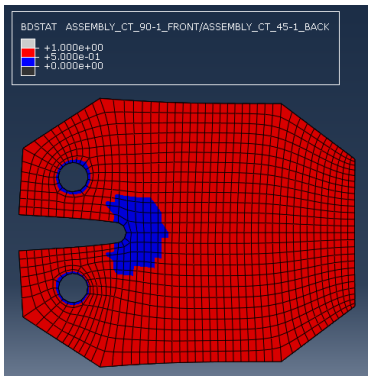


**(e)** One of the plies at cycle 5169

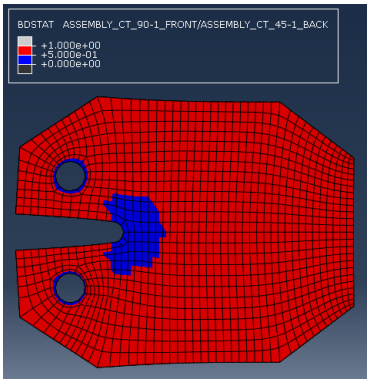


**(f)** One of the plies at cycle 10139

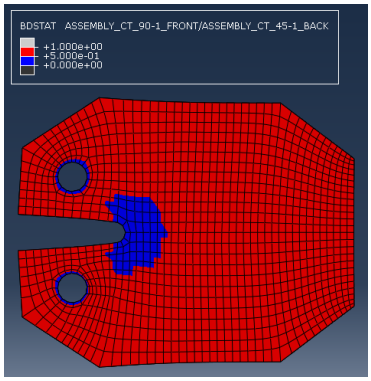


**(g)** One of the plies at cycle 20079

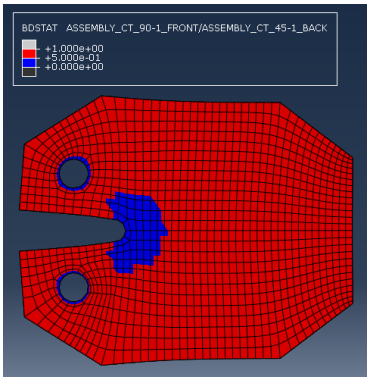


**(h)** One of the plies at cycle 50000

**Figure C.33:** VCCT isolated MS2 11 U5.0

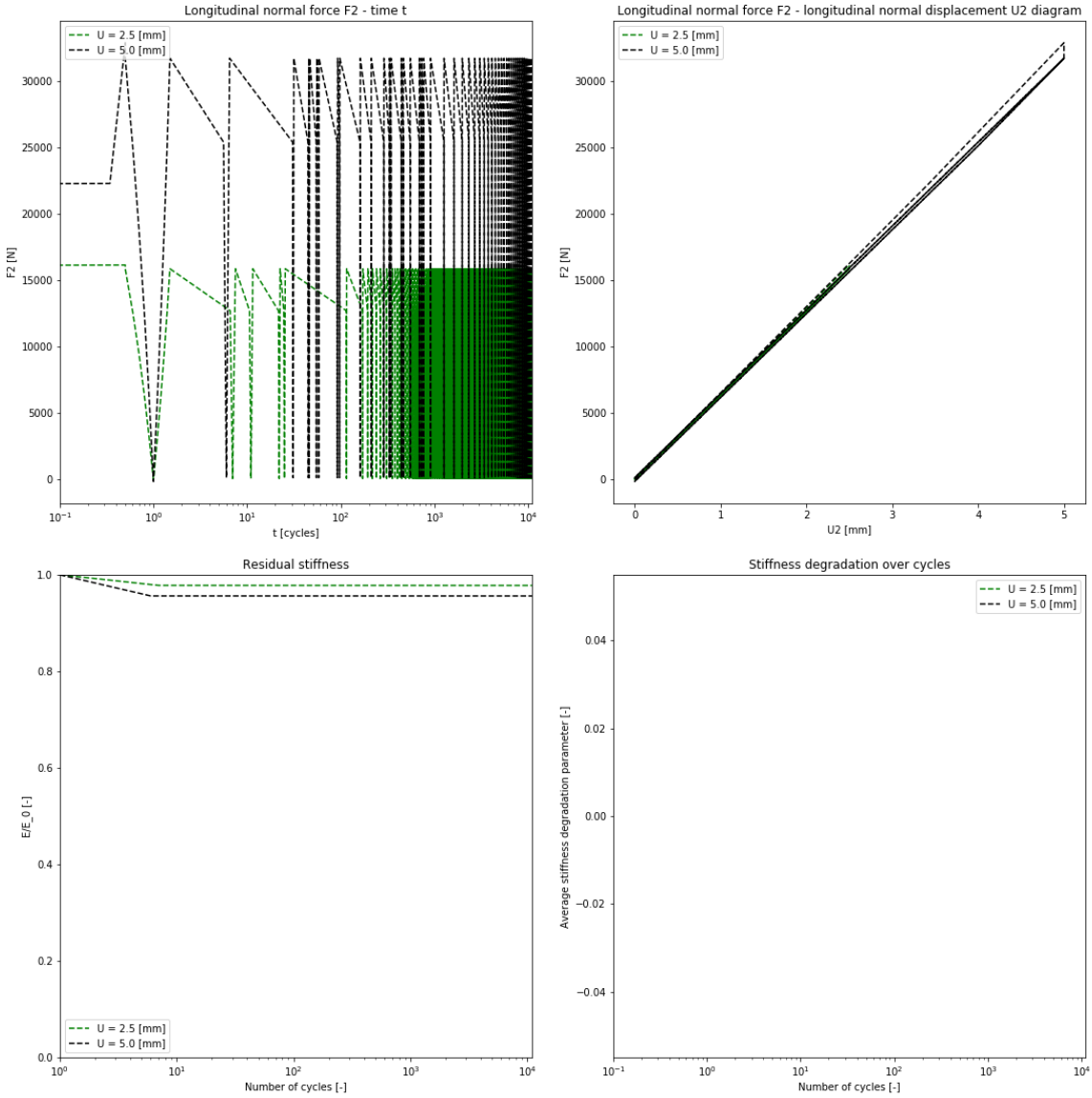


**Figure C.34:** In four plots the output is represented of the fatigue analysis for the compact tension specimen with five quasi-isotropic plies with VCCT interaction and linear elastic material. A displacement of 5 [mm] is applied. The plots represent the analysis with a compact tension specimen with five plies with a layup $[0|-45|90|45|0]$ for which only the first direction of the quasi-isotropic plies is mentioned. The applied Paris law material constants for the black line are $c_3 = 1$ and $c_4 = 1$ and a mesh size of 2 [mm]. Counting from the left to the right and from the top to the bottom, the load history plot is given first. This plot shows the applied force over time as resultant of a constant applied displacement amplitude. The second plot is the force-displacement diagram which acts as hysteresis plot of the element as structural response. The third plot shows the stiffness of the structure relative to the response of the first cycle. The fourth plot shows the average value of the damage parameters of the individual elements that leads to stiffness degradation, hence it is already normalised with the number of elements. Do recognise that the time axes are now on log scale instead of linear.

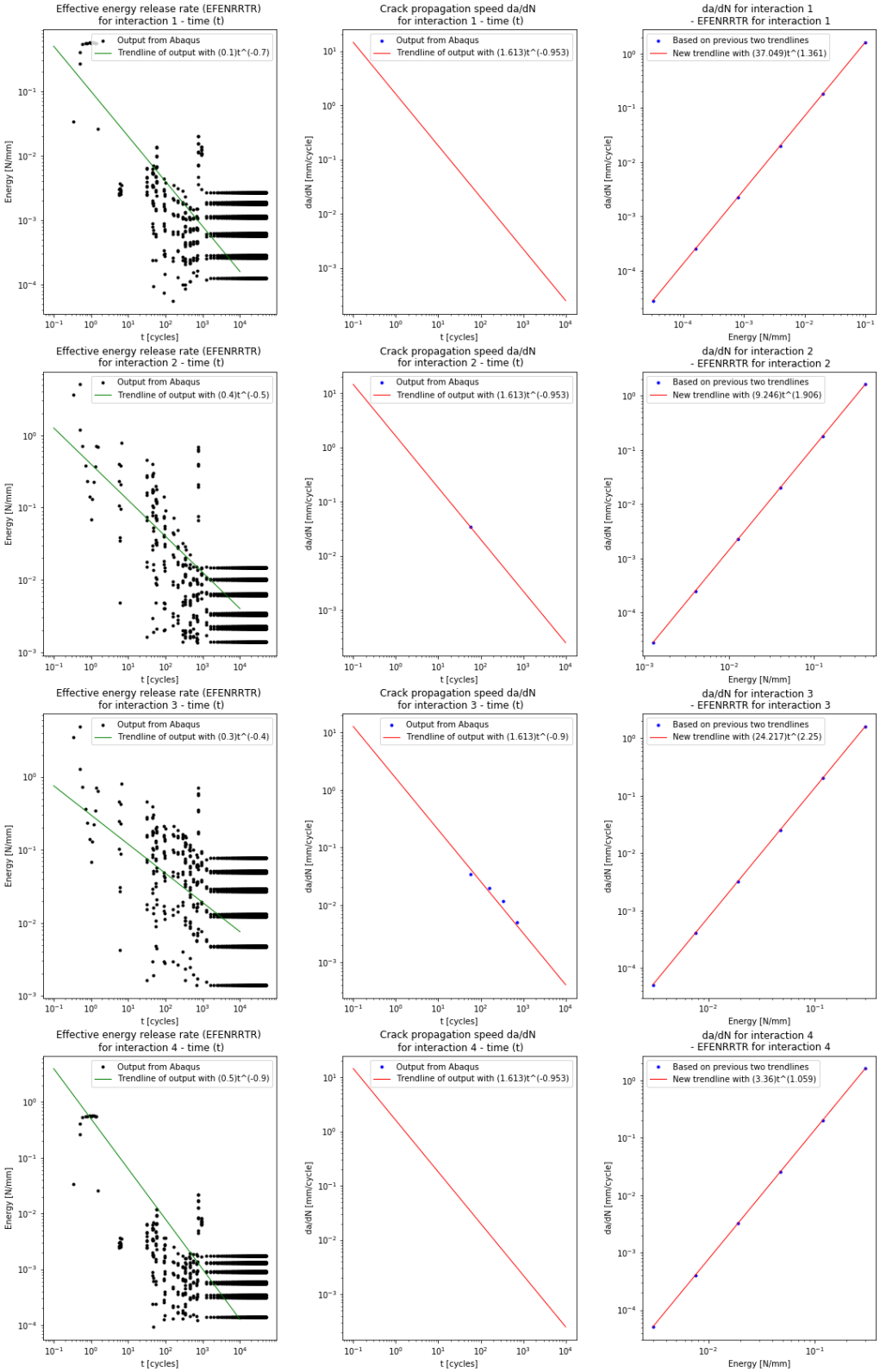


**Figure C.35:** A visualisation of the effect of the Paris law material constants on the fatigue analysis for the compact tension specimen related to figure C.30 with $c_3 = 1$ and $c_4 = 1$ and a load of 5 [mm]. Each row is for the next interface from the layup $[0|-45|90|45|0]$ and the fifth is the summation. The first column represents the equivalent energy release rate on the interface for each cycle. The second column provides the crack propagation rate for each 2 [mm] of crack propagation. The third column shows the relation between crack propagation rate and the equivalent energy release rate.

### C.7.3. VCCT isolated MS2 11 U7.5

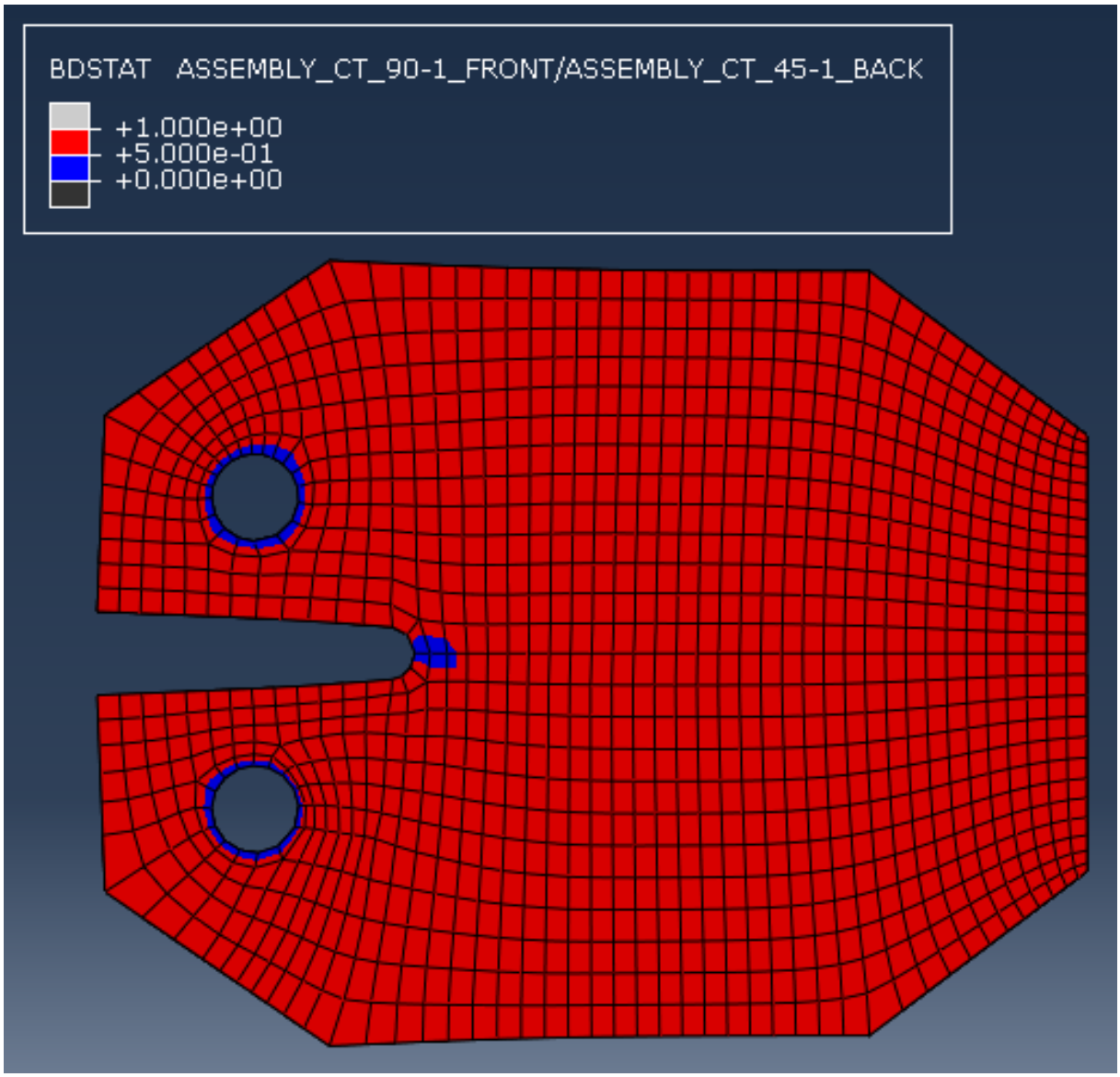


**Figure C.36:** VCCT isolated MS2 11 U7.5 at cycle 1

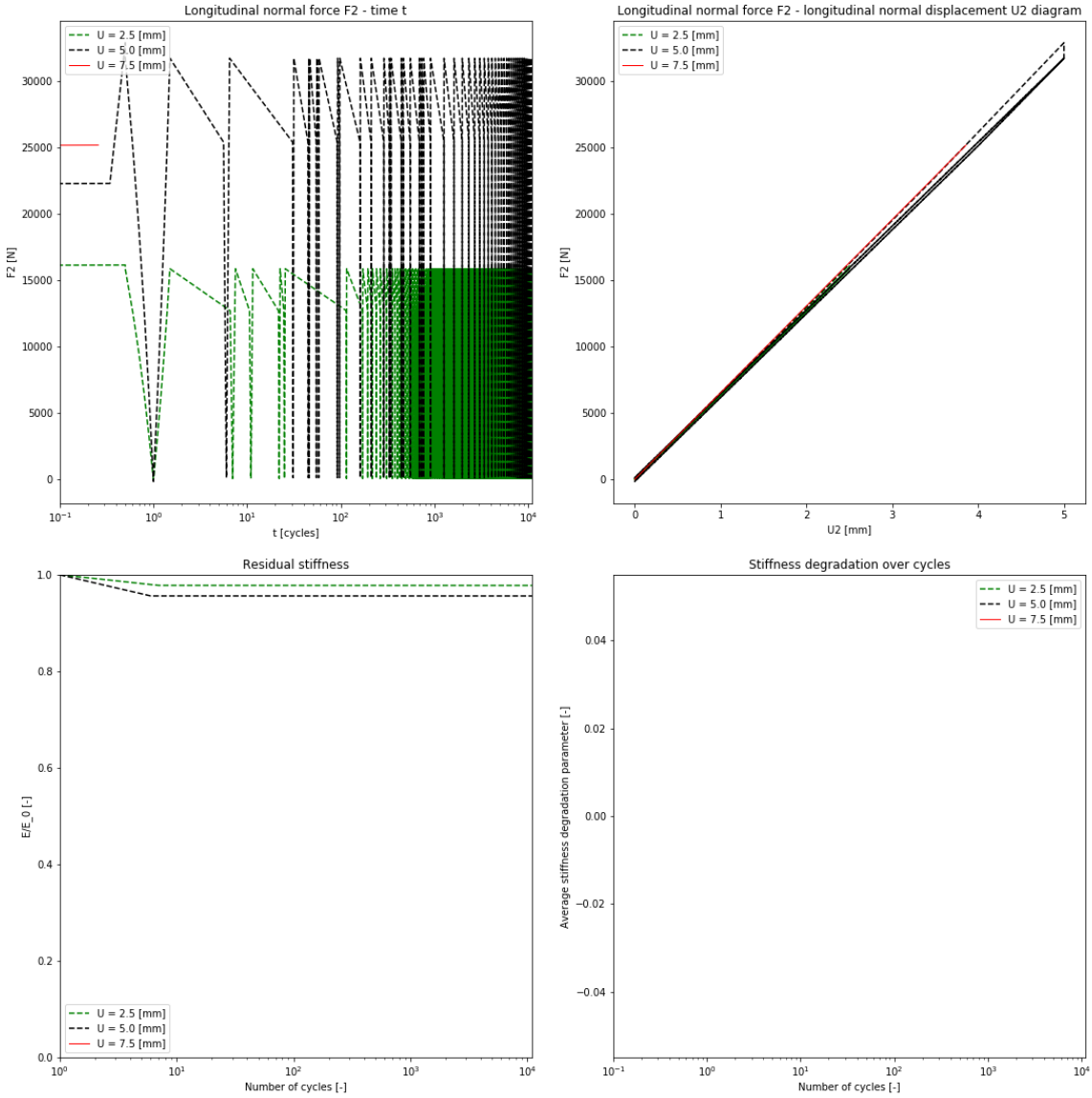


**Figure C.37:** In four plots the output is represented of the fatigue analysis for the compact tension specimen with five quasi-isotropic plies with VCCT interaction and linear elastic material. A displacement of 7.5 [mm] is applied. The plots represent the analysis with a compact tension specimen with five plies with a layup $[0|-45|90|45|0]$ for which only the first direction of the quasi-isotropic plies is mentioned. The applied Paris law material constants for the black line are $c_3 = 1$ and $c_4 = 1$ and a mesh size of 2 [mm]. Counting from the left to the right and from the top to the bottom, the load history plot is given first. This plot shows the applied force over time as resultant of a constant applied displacement amplitude. The second plot is the force-displacement diagram which acts as hysteresis plot of the element as structural response. The third plot shows the stiffness of the structure relative to the response of the first cycle. The fourth plot shows the average value of the damage parameters of the individual elements that leads to stiffness degradation, hence it is already normalised with the number of elements. Do recognise that the time axes are now on log scale instead of linear.

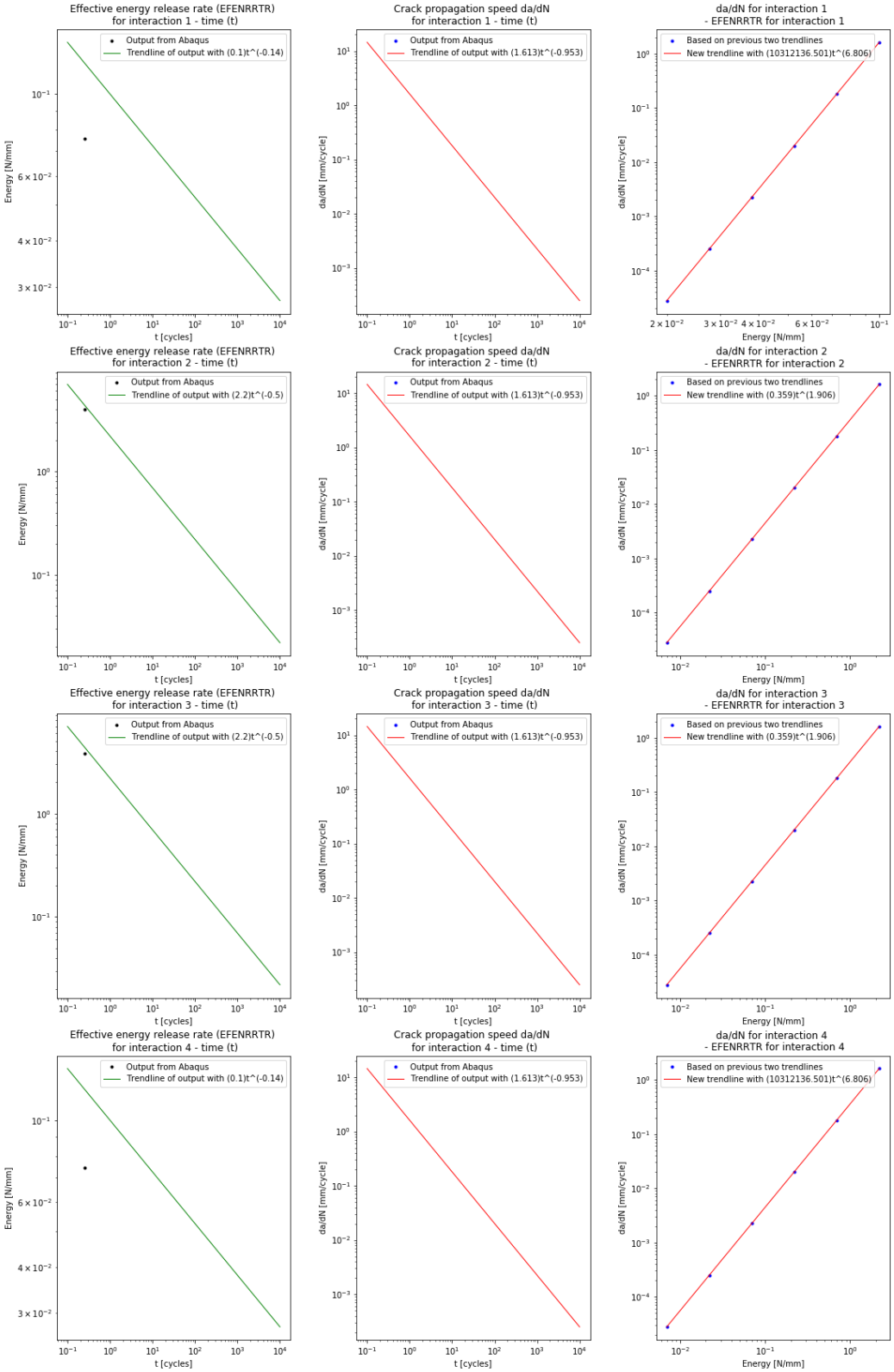


**Figure C.38:** A visualisation of the effect of the Paris law material constants on the fatigue analysis for the compact tension specimen related to figure C.37 with $c_3 = 1$ and $c_4 = 1$ and a load of 7.5 [mm]. Each row is for the next interface from the layup $[0|-45|90|45|0]$ and the fifth is the summation. The first column represents the equivalent energy release rate on the interface for each cycle. The second column provides the crack propagation rate for each 2 [mm] of crack propagation. The third column shows the relation between crack propagation rate and the equivalent energy release rate.

## C.8. Mesh refinement study

### C.8.1. VCCT MS1 11

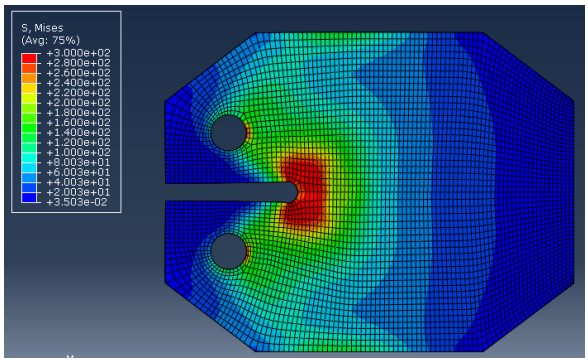


**(a)** One of the plies at cycle 1

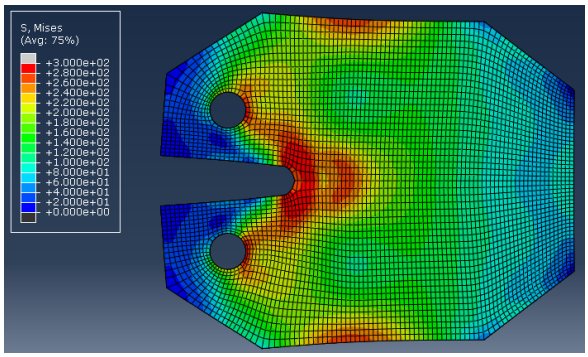


**(b)** One of the plies at cycle 2

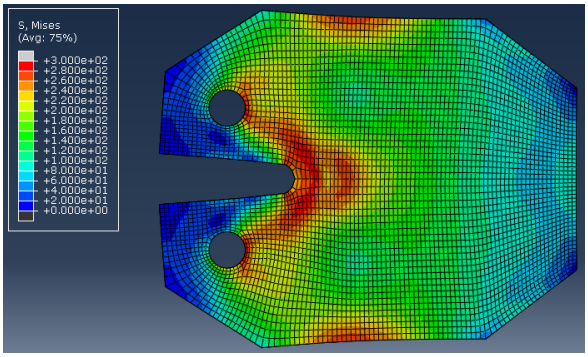


**(c)** One of the plies at cycle 5

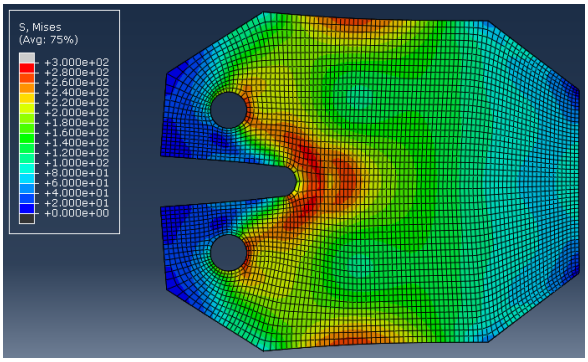


**(d)** One of the plies at cycle 10

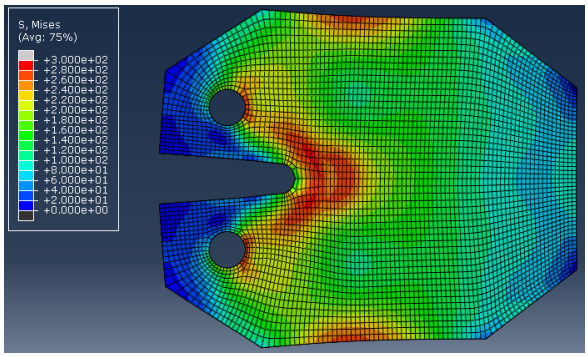


**(e)** One of the plies at cycle 20

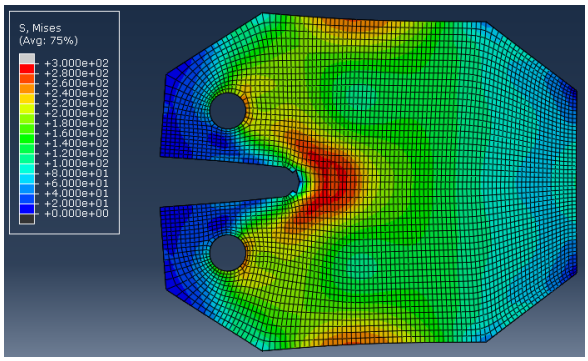


**(f)** One of the plies at cycle 50

**Figure C.39:** A visualisation of the deformed compact tension specimen of an individual ply that has quasi-isotropic stiffness and VCCT interactions with its adjacent plies. The applied Paris law material constants are $c_3 = 1$ and $c_4 = 1$. As all the plies had the same reaction due to quasi-isotropic stiffness, one ply is presented at different cycles to show crack propagation rate instead of each individual ply at final stage. The distribution of Von Mises stresses at maximum loading of $5$ [mm] vertical displacement in the top pin are displayed in colour. The analysis was limited to a $50$ [cycles]. Only the first $50$ cycles are shown with mesh size $1$ [mm] for comparison in the mesh refinement.

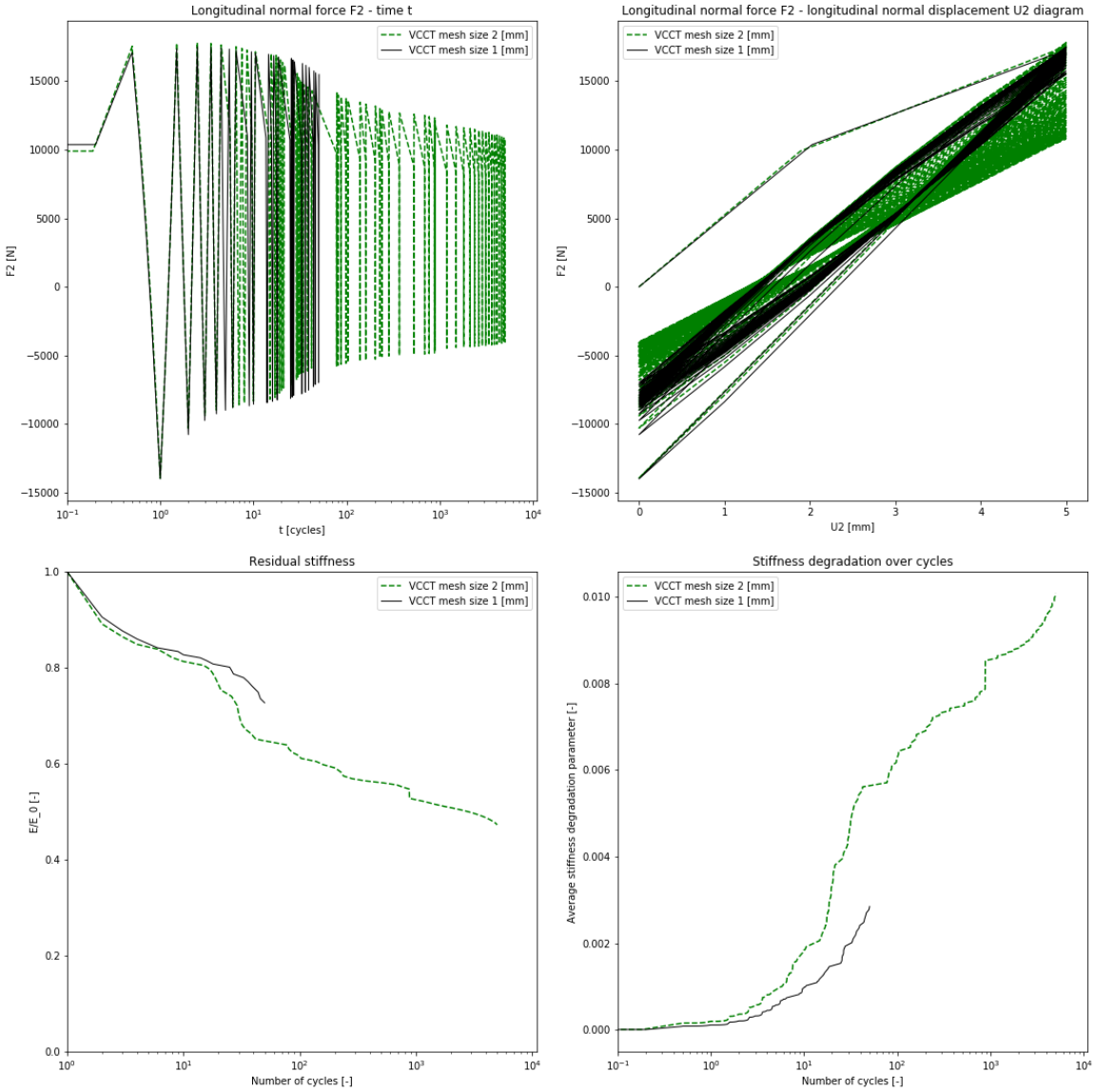


**Figure C.40:** In four plots the output is represented of the fatigue analysis for the compact tension specimen with five quasi-isotropic plies with VCCT interaction. A displacement of $5$ [mm] is applied and the computations is truncated at a $50$ [cycles]. The plots represent the analysis with a compact tension specimen with five plies with a layup $[0|-45|90|45|0]$ for which only the first direction of the quasi-isotropic plies is mentioned. The applied Paris law material constants for the black line are $c_3 = 1$ and $c_4 = 1$ and a mesh size of $1$ [mm]. Counting from the left to the right and from the top to the bottom, the load history plot is given first. This plot shows the applied force over time as resultant of a constant applied displacement amplitude. The second plot is the force-displacement diagram which acts as hysteresis plot of the element as structural response. The third plot shows the stiffness of the structure relative to the response of the first cycle. The fourth plot shows the average value of the damage parameters of the individual elements that leads to stiffness degradation, hence it is already normalised with the number of elements. Do recognise that the time axes are now on log scale instead of linear.

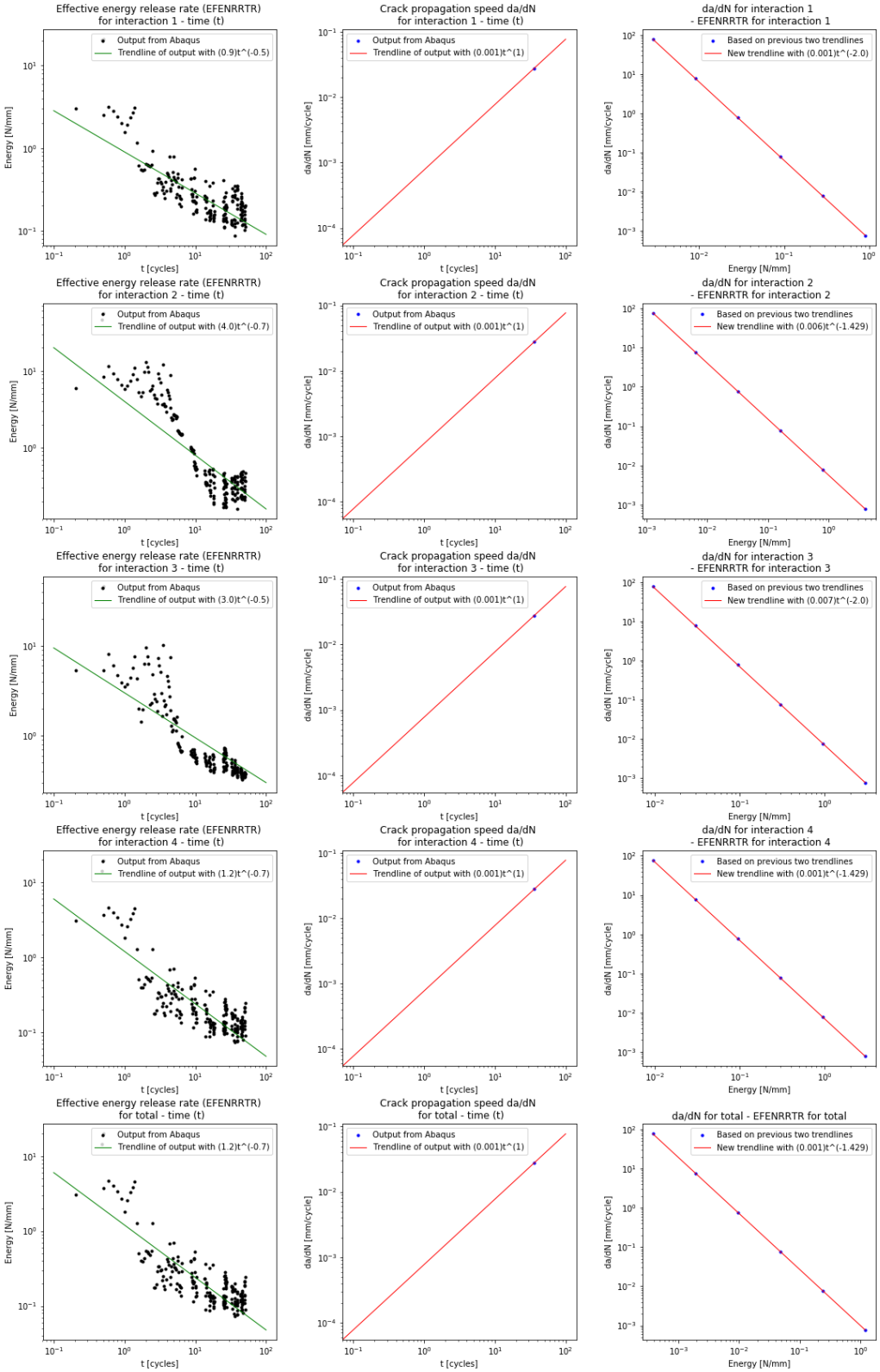


**Figure C.41:** A visualisation of the effect of the Paris law material constants on the fatigue analysis for the compact tension specimen related to figure C.40 with $c_3 = 1$ and $c_4 = 1$ and a mesh size of 1 [mm]. Each row is for the next interface from the layup $[0|-45|90|45|0]$ and the fifth is the summation. The first column represents the equivalent energy release rate on the interface for each cycle. The second column provides the crack propagation rate for each 2 [mm] of crack propagation. The third column shows the relation between crack propagation rate and the equivalent energy release rate.

### C.8.2. VCCT MS05 11

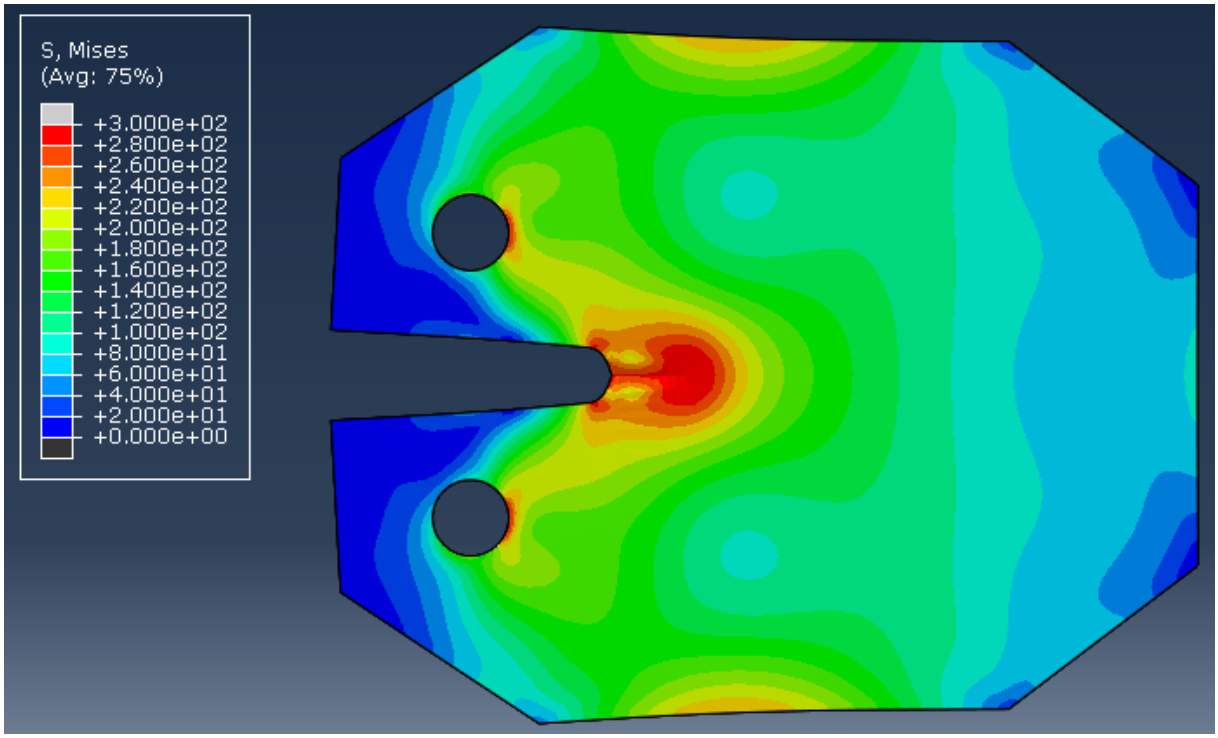


**Figure C.42:** A visualisation of the deformed compact tension specimen of an individual ply that has quasi-isotropic stiffness and VCCT interactions with its adjacent plies. The applied Paris law material constants are $c_3 = 1$ and $c_4 = 1$. As all the plies had the same reaction due to quasi-isotropic stiffness, one ply is presented at different cycles to show crack propagation rate instead of each individual ply at final stage. The distribution of Von Mises stresses at maximum loading of $5$ [mm] vertical displacement in the top pin are displayed in colour. The analysis was limited to a $50$ [cycles]. Only the first $50$ cycles are shown with mesh size $0.5$ [mm] for comparison in the mesh refinement.

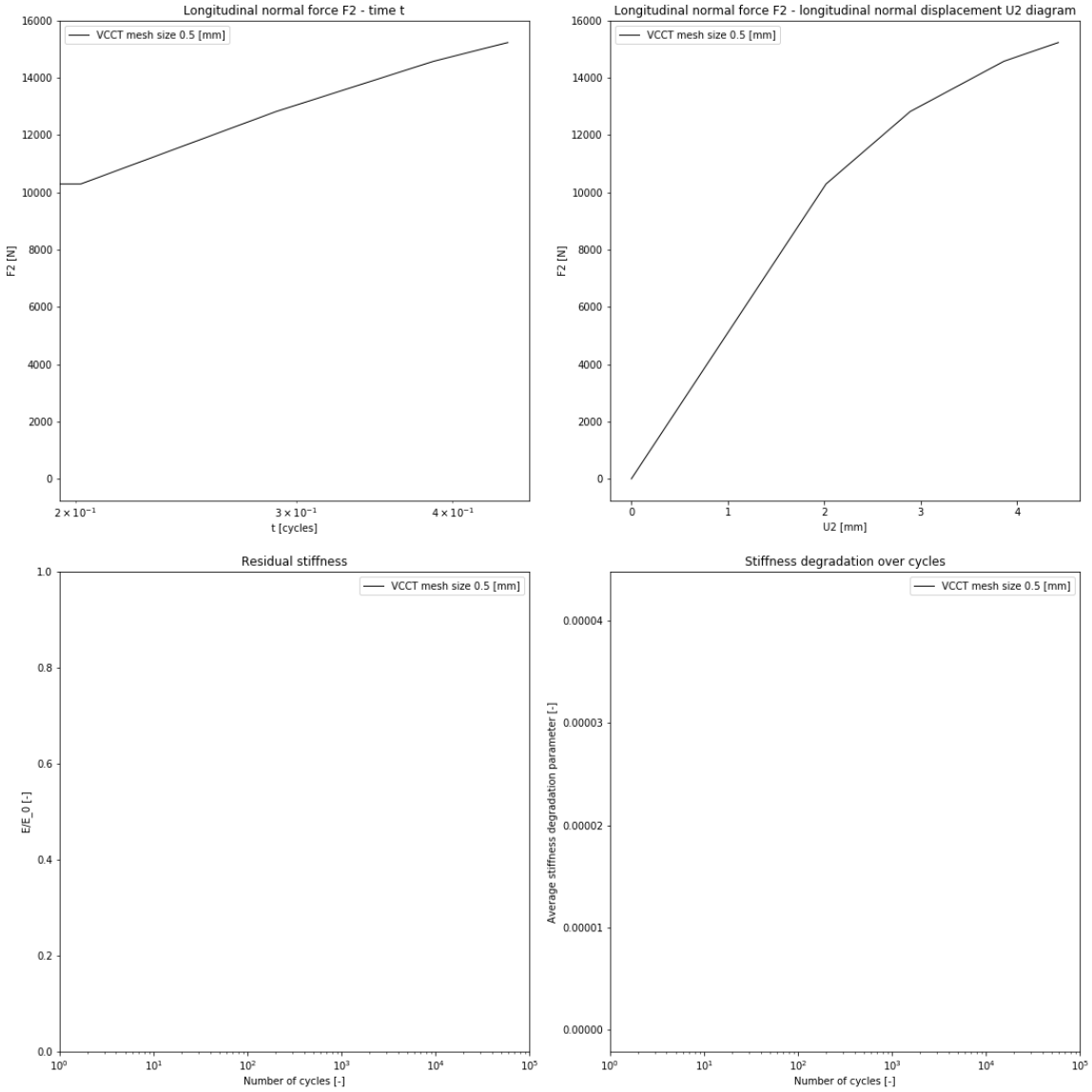


**Figure C.43:** In four plots the output is represented of the fatigue analysis for the compact tension specimen with five quasi-isotropic plies with VCCT interaction. A displacement of $5$ [mm] is applied and the computations is truncated at a $50$ [cycles]. The plots represent the analysis with a compact tension specimen with five plies with a layup $[0|-45|90|45|0]$ for which only the first direction of the quasi-isotropic plies is mentioned. The applied Paris law material constants for the black line are $c_3 = 1$ and $c_4 = 1$ and a mesh size of $0.5$ [mm]. Counting from the left to the right and from the top to the bottom, the load history plot is given first. This plot shows the applied force over time as resultant of a constant applied displacement amplitude. The second plot is the force-displacement diagram which acts as hysteresis plot of the element as structural response. The third plot shows the stiffness of the structure relative to the response of the first cycle. The fourth plot shows the average value of the damage parameters of the individual elements that leads to stiffness degradation, hence it is already normalised with the number of elements. Do recognise that the time axes are now on log scale instead of linear.

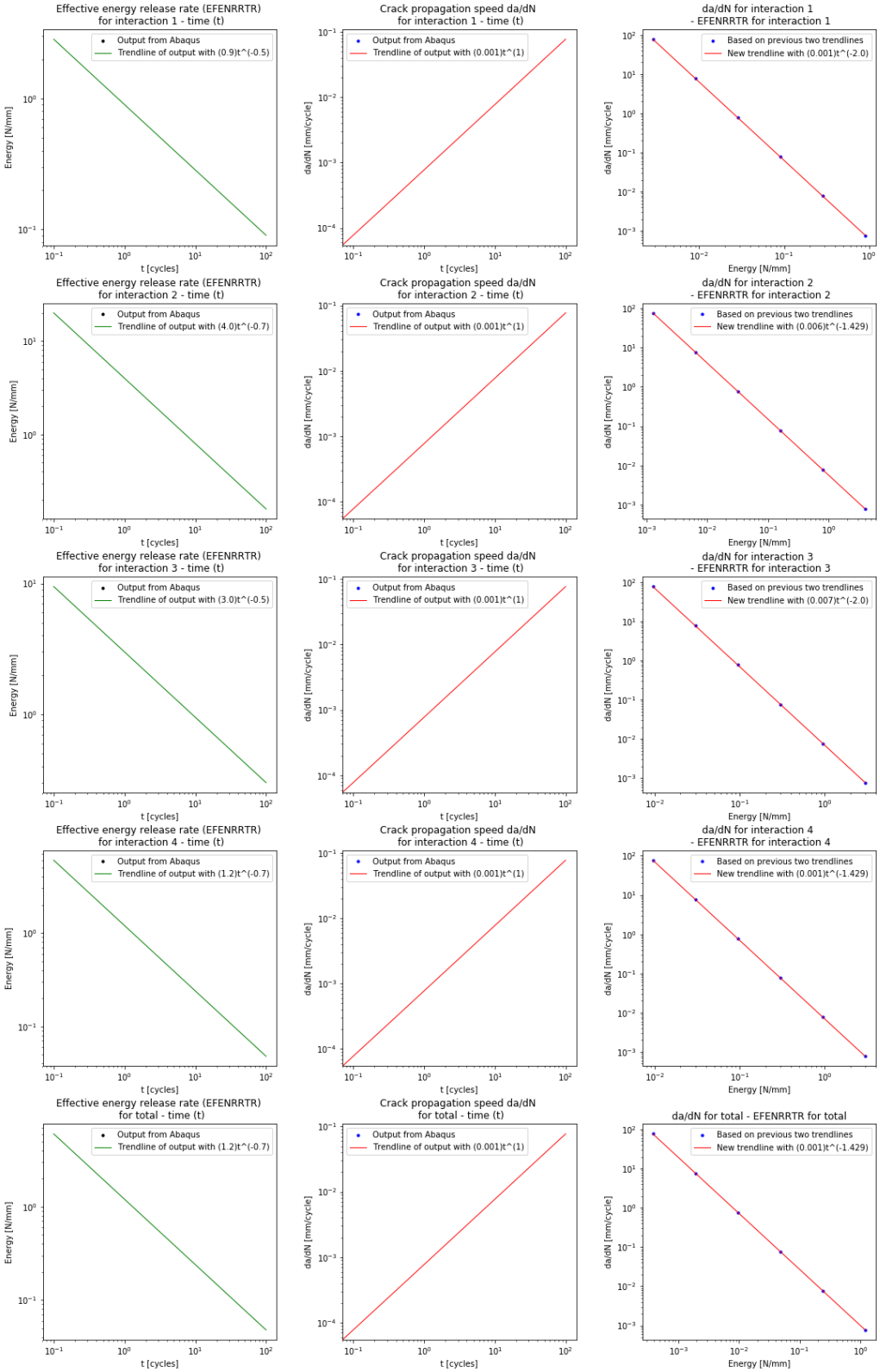


**Figure C.44:** A visualisation of the effect of the Paris law material constants on the fatigue analysis for the compact tension specimen related to figure C.43 with $c_3 = 1$ and $c_4 = 1$ and a mesh size of $0.5$ [mm]. Each row is for the next interface from the layup $[0|-45|90|45|0]$ and the fifth is the summation. The first column represents the equivalent energy release rate on the interface for each cycle. The second column provides the crack propagation rate for each 2 [mm] of crack propagation. The third column shows the relation between crack propagation rate and the equivalent energy release rate.

### C.8.3. TIE MS1

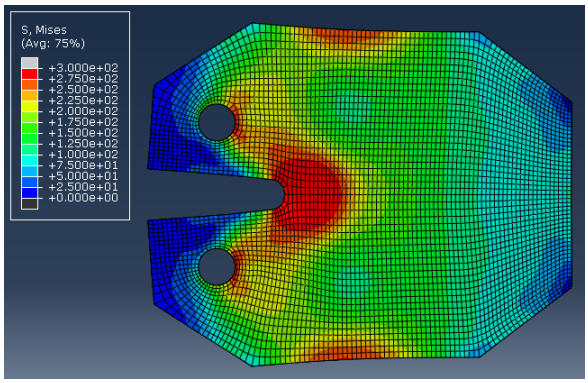


**(a)** One of the plies at cycle 1

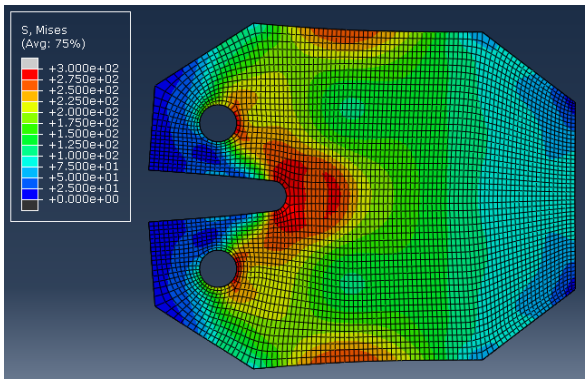


**(b)** One of the plies at cycle 2

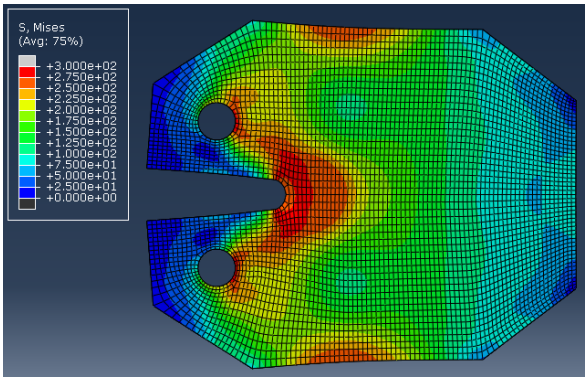


**(c)** One of the plies at cycle 5

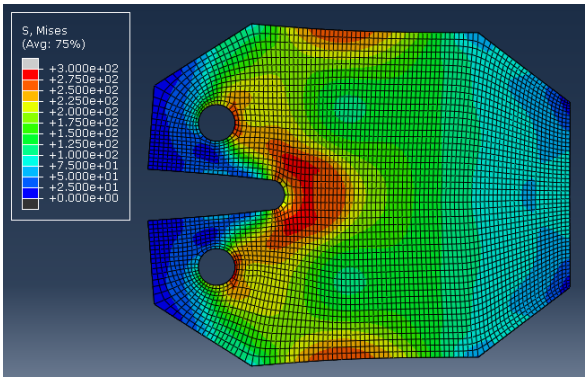


**(d)** One of the plies at cycle 10

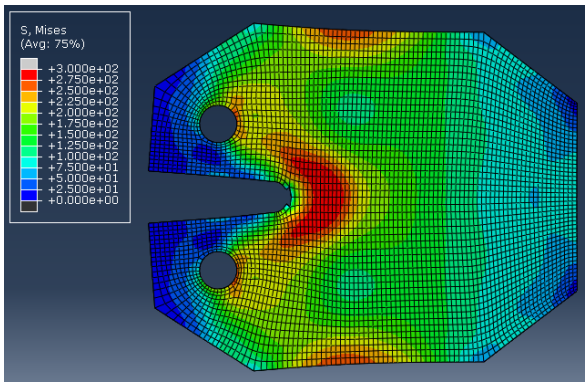


**(e)** One of the plies at cycle 20

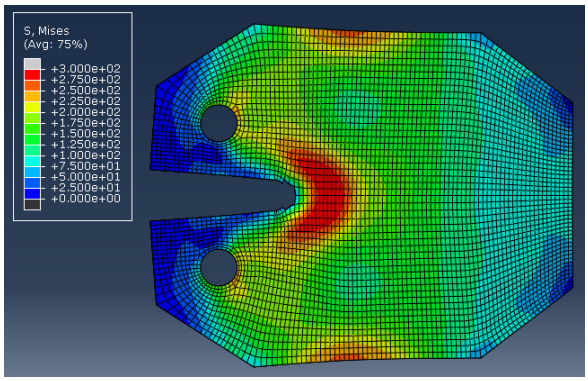


**(f)** One of the plies at cycle 30

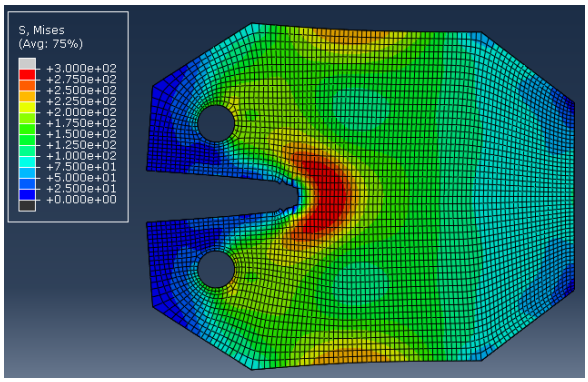


**(g)** One of the plies at cycle 40

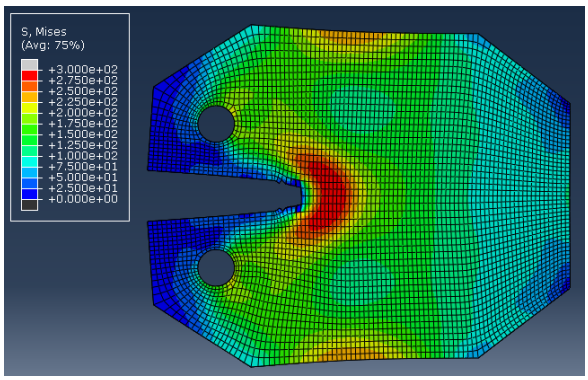


**(h)** One of the plies at cycle 50

**Figure C.45:** A visualisation of the deformed compact tension specimen of an individual ply that has quasi-isotropic stiffness and tie constraints with its adjacent plies. As all the plies had the same reaction due to quasi-isotropic stiffness, one ply is presented at different cycles to show crack propagation rate instead of each individual ply at final stage. The distribution of Von Mises stresses at maximum loading of 5 [mm] vertical displacement in the top pin are displayed in colour. The analysis was limited to a 250 [cycles]. The used mesh size is 1 [mm].

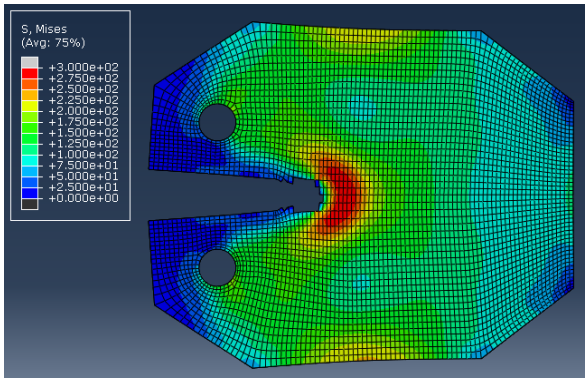


**(a)** One of the plies at cycle 100

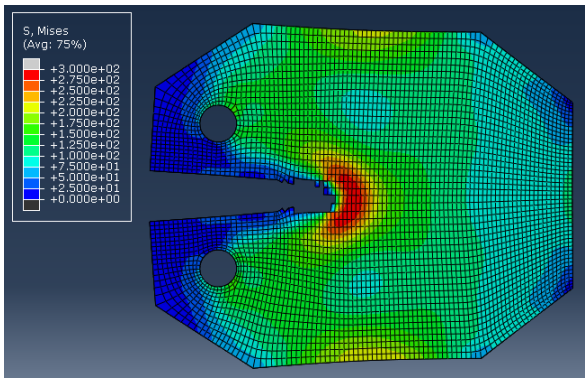


**(b)** One of the plies at cycle 150

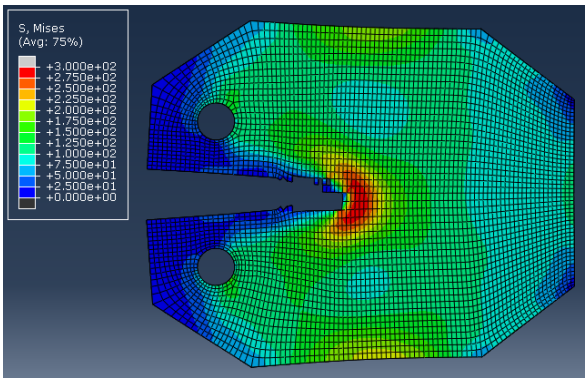


**(c)** One of the plies at cycle 200

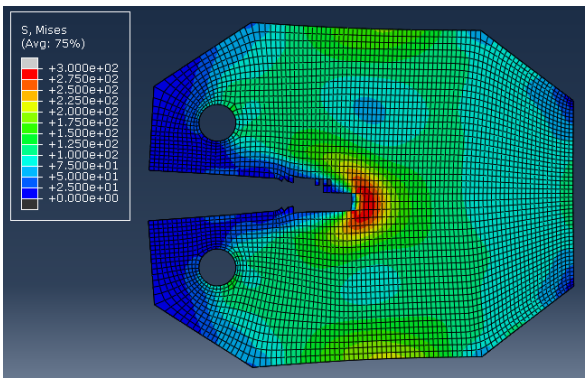


**(d)** One of the plies at cycle 250

**Figure C.46:** A visualisation of the deformed compact tension specimen of an individual ply that has quasi-isotropic stiffness and tie constraints with its adjacent plies. As all the plies had the same reaction due to quasi-isotropic stiffness, one ply is presented at different cycles to show crack propagation rate instead of each individual ply at final stage. The distribution of Von Mises stresses at maximum loading of 5 [mm] vertical displacement in the top pin are displayed in colour. The analysis was limited to a 250 [cycles]. The used mesh size is 1 [mm].

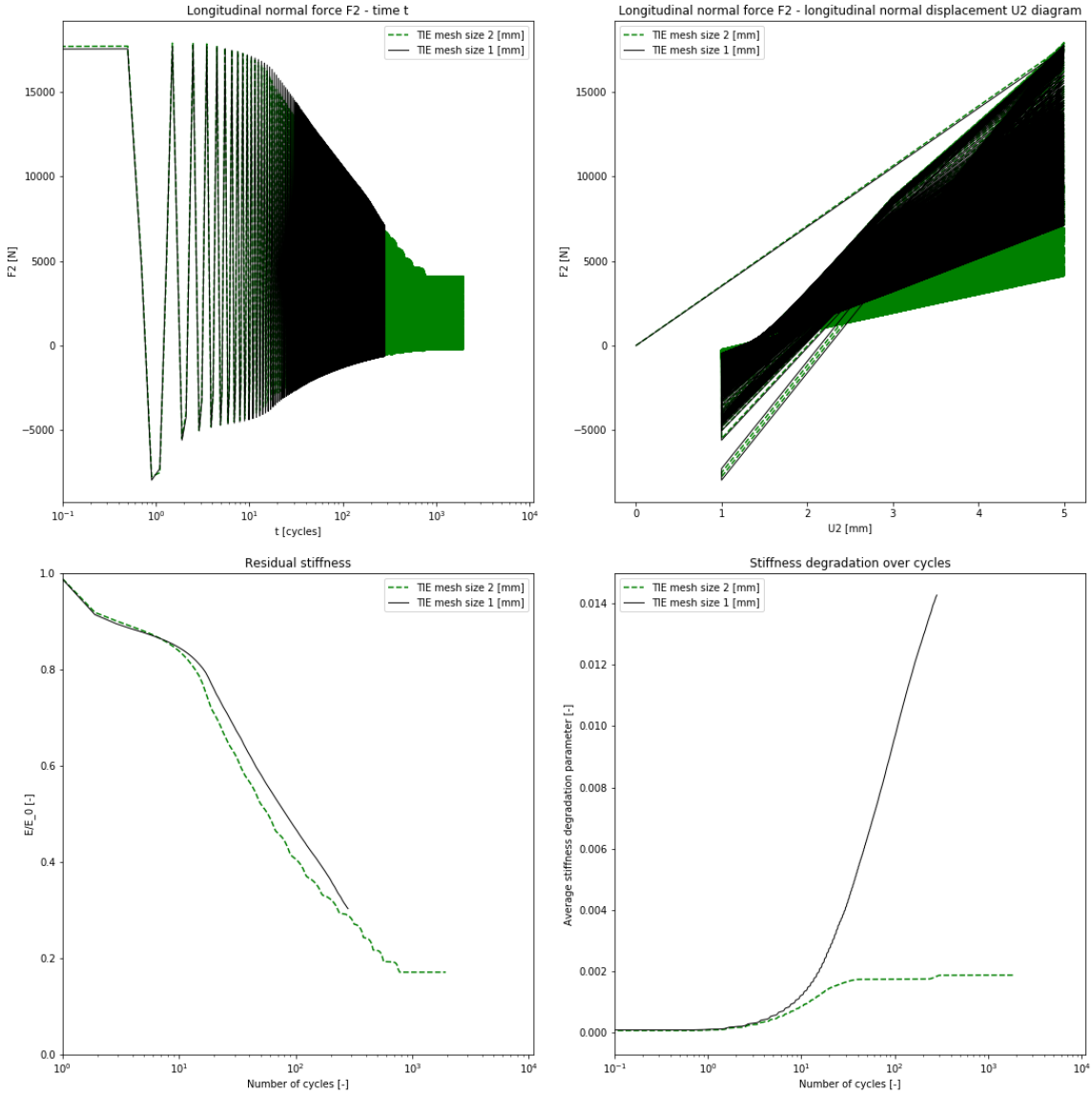


**Figure C.47:** In four plots the output is represented of the fatigue analysis for the compact tension specimen with five quasi-isotropic plies with tie interaction. A displacement of 5 [mm] is applied and the computations is truncated at a 50 [cycles]. The plots represent the analysis with a compact tension specimen with five plies with a layup $[0|-45|90|45|0]$ for which only the first direction of the quasi-isotropic plies is mentioned. The black line represents the output with a mesh size of 1 [mm]. Counting from the left to the right and from the top to the bottom, the load history plot is given first. This plot shows the applied force over time as resultant of a constant applied displacement amplitude. The second plot is the force-displacement diagram which acts as hysteresis plot of the element as structural response. The third plot shows the stiffness of the structure relative to the response of the first cycle. The fourth plot shows the average value of the damage parameters of the individual elements that leads to stiffness degradation, hence it is already normalised with the number of elements. Do recognise that the time axes are now on log scale instead of linear.

### C.8.4. TIE MS05

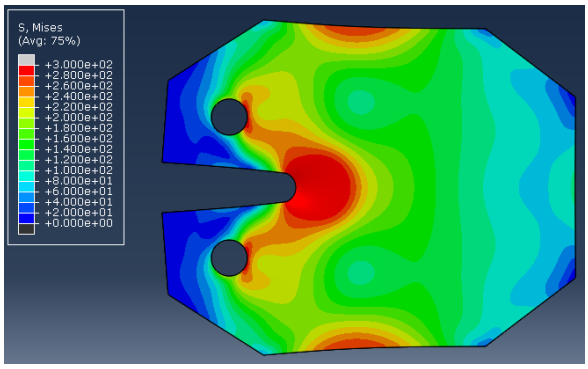


**(a)** One of the plies at cycle 1

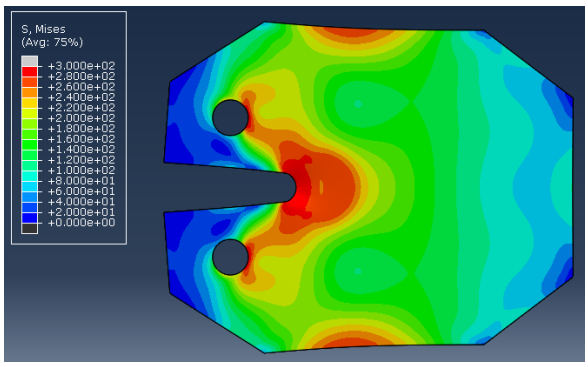


**(b)** One of the plies at cycle 2

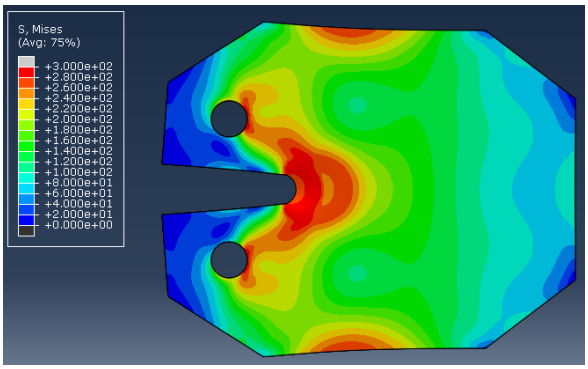


**(c)** One of the plies at cycle 5

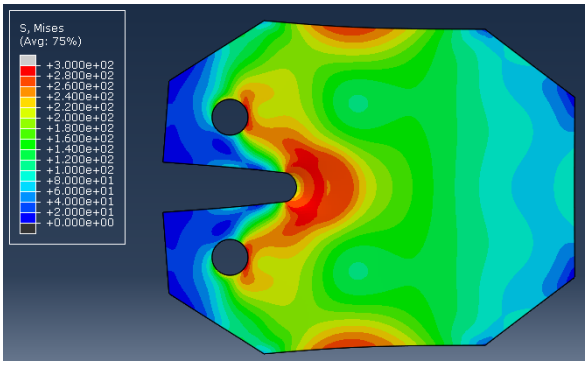


**(d)** One of the plies at cycle 10

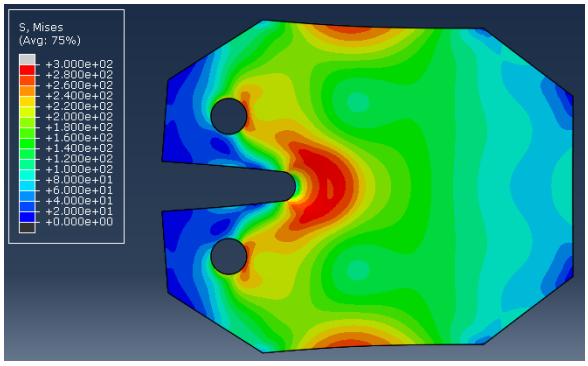


**(e)** One of the plies at cycle 20

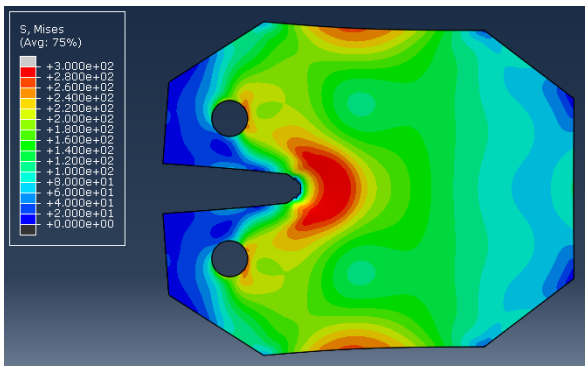


**(f)** One of the plies at cycle 30

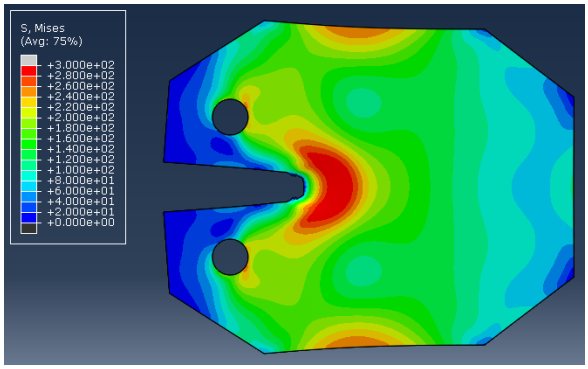


**(g)** One of the plies at cycle 40

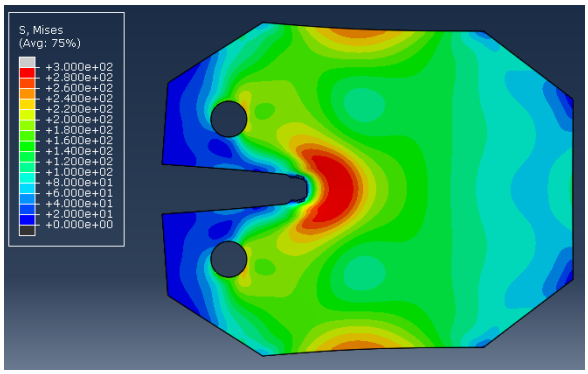


**(h)** One of the plies at cycle 50

**Figure C.48:** A visualisation of the deformed compact tension specimen of an individual ply that has quasi-isotropic stiffness and tie constraints with its adjacent plies. As all the plies had the same reaction due to quasi-isotropic stiffness, one ply is presented at different cycles to show crack propagation rate instead of each individual ply at final stage. The distribution of Von Mises stresses at maximum loading of 5 [mm] vertical displacement in the top pin are displayed in colour. The analysis was limited to a 250 [cycles]. The used mesh size is 1 [mm].

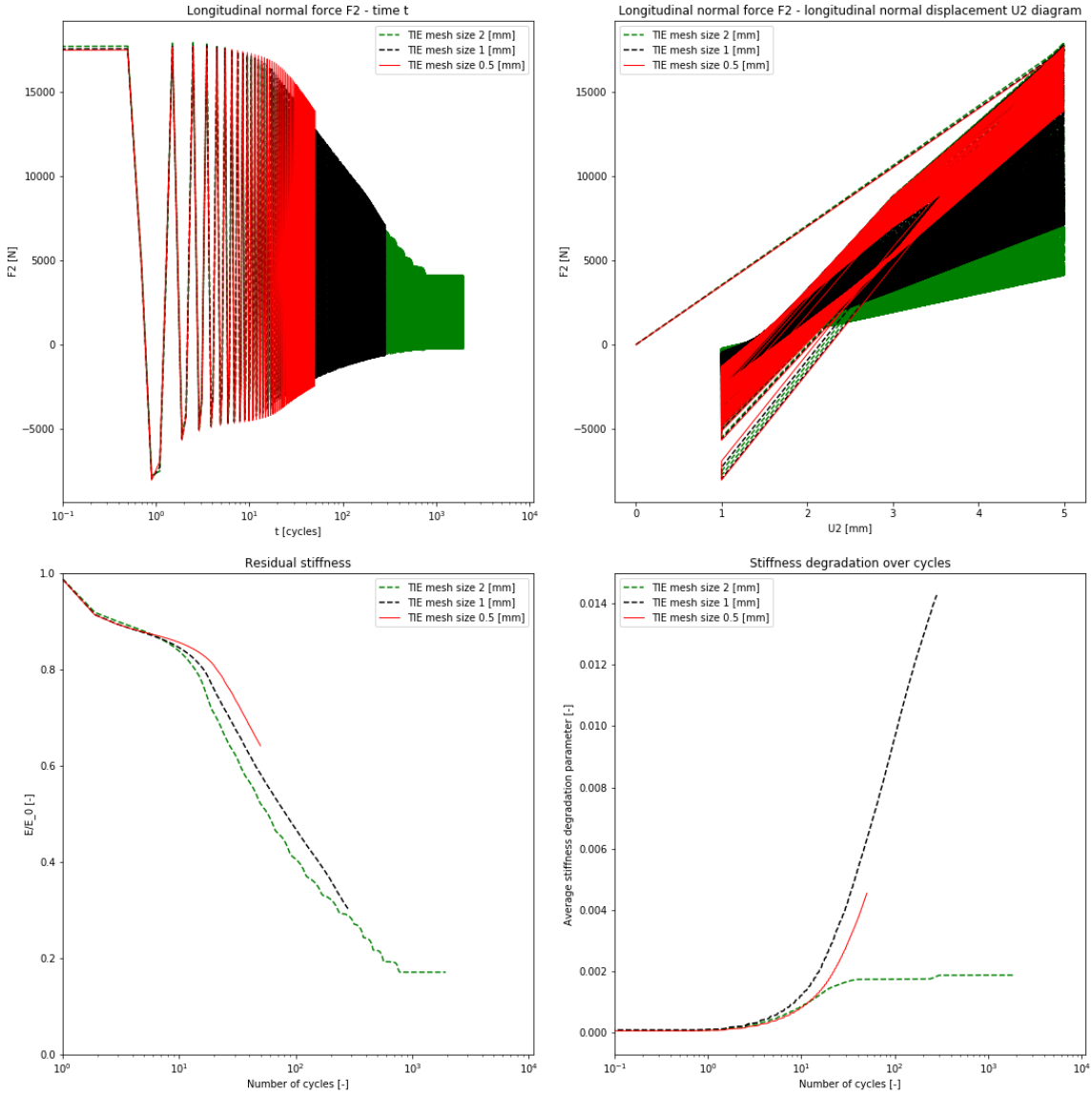


**Figure C.49:** In four plots the output is represented of the fatigue analysis for the compact tension specimen with five quasi-isotropic plies with tie interaction. A displacement of $5$ [mm] is applied and the computations is truncated at a $50$ [cycles]. The plots represent the analysis with a compact tension specimen with five plies with a layup $[0|-45|90|45|0]$ for which only the first direction of the quasi-isotropic plies is mentioned. The black line represents the output with a mesh size of $0.5$ [mm]. Counting from the left to the right and from the top to the bottom, the load history plot is given first. This plot shows the applied force over time as resultant of a constant applied displacement amplitude. The second plot is the force-displacement diagram which acts as hysteresis plot of the element as structural response. The third plot shows the stiffness of the structure relative to the response of the first cycle. The fourth plot shows the average value of the damage parameters of the individual elements that leads to stiffness degradation, hence it is already normalised with the number of elements. Do recognise that the time axes are now on log scale instead of linear.

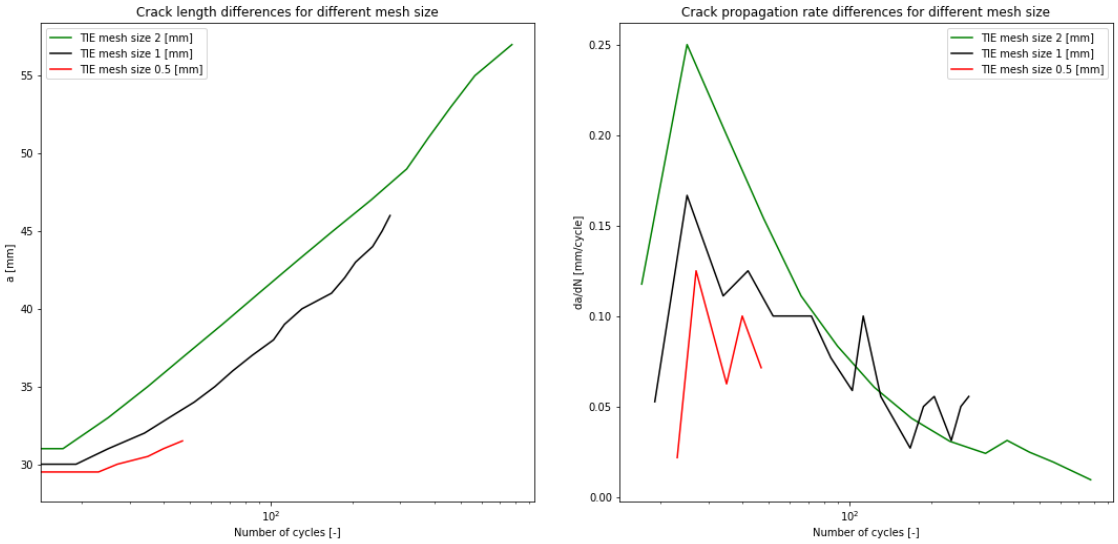


**Figure C.50:** Comparison of the crack propagation for the tie constraint mesh refinement discussed in figures C.13, C.47 and C.49. On the left the crack length over the cycles and on the right the crack propagation speed over the cycles. The green line relates to the output in figure C.13 with a mesh size of 2 [mm]. The black line relates to the output in figure C.47 with a mesh size of 1 [mm]. The red line relates to figure C.49 with a mesh size of 0.5[mm].

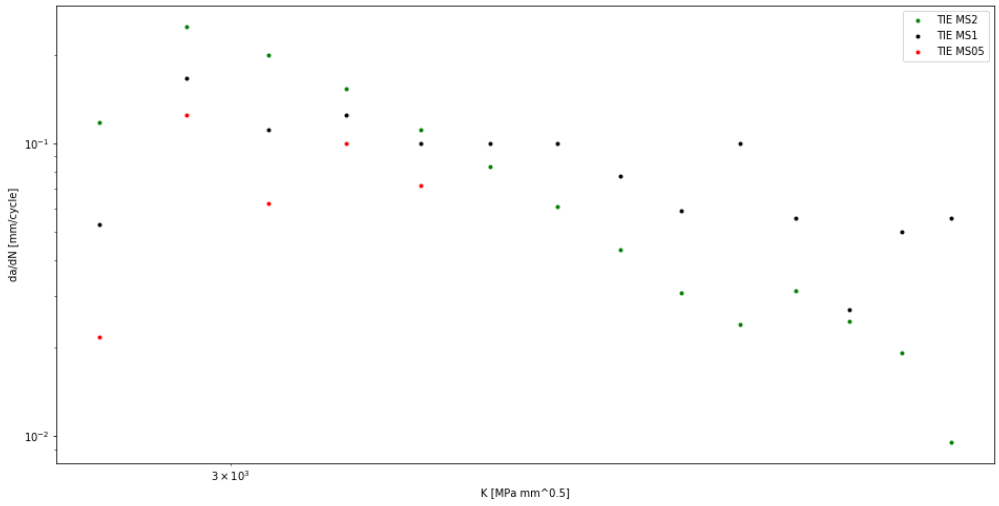


**Figure C.51:** A crack propagation plot showing the crack propagation rate versus the stress intensity factor for a CT specimen with tie constraints. In green it is performed for an element size of 2 [mm], in black for an element size of 1 [mm] and in red for 0.5 [mm].

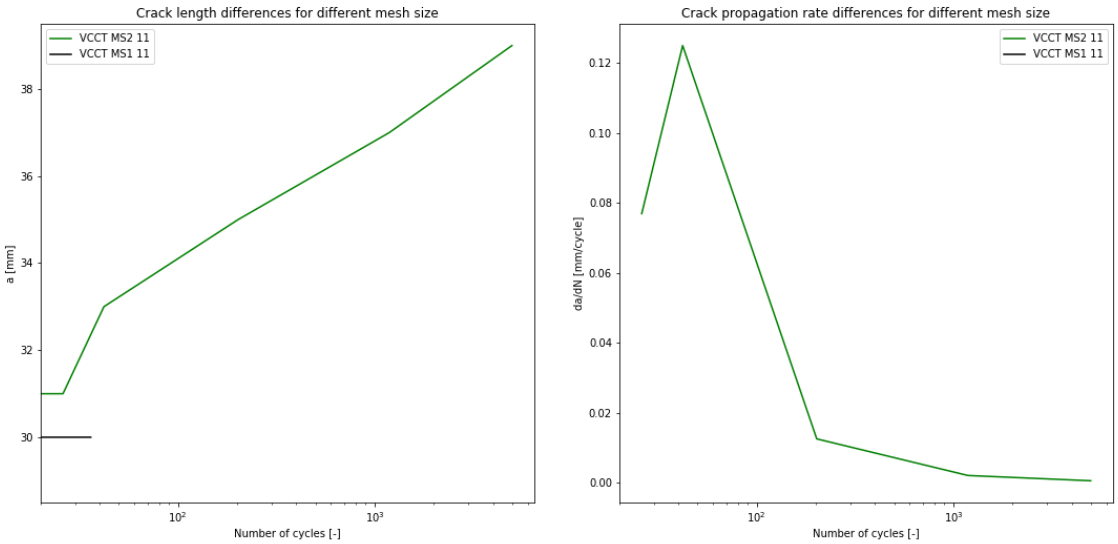


**Figure C.52:** Comparison of the crack propagation for the VCCT interface with mesh refinement. On the left the crack length over the cycles and on the right the crack propagation speed over the cycles. In green it is performed for an element size of 2 [mm] and in black for an element size of 1 [mm]. The mesh size of 0.5 [mm] had no relevant data.

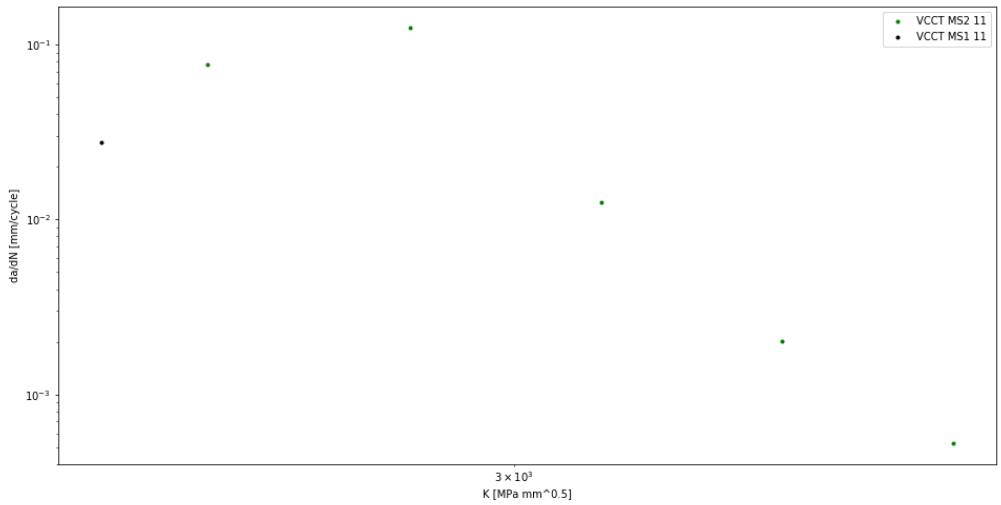


**Figure C.53:** A crack propagation plot showing the crack propagation rate versus the stress intensity factor for a CT specimen with VCCT interactions. In green it is performed for an element size of 2 [mm] and in black for an element size of 1 [mm].

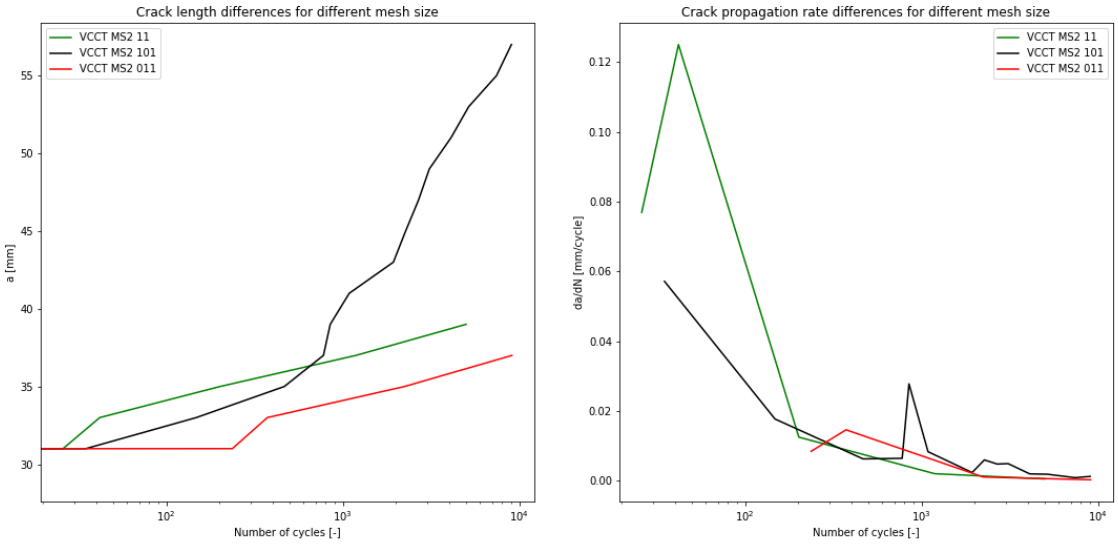


**Figure C.54:** Comparison of the crack propagation for the VCCT interface with mesh refinement. On the left the crack length over the cycles and on the right the crack propagation speed over the cycles. In green it is performed for a VCCT interaction with properties $c_3 = 1$ and $c_4 = 1$, in black for a VCCT interaction with properties $c_3 = 10$ and $c_4 = 1$ and in red for a VCCT interaction with properties $c_3 = 0.1$ and $c_4 = 1$.

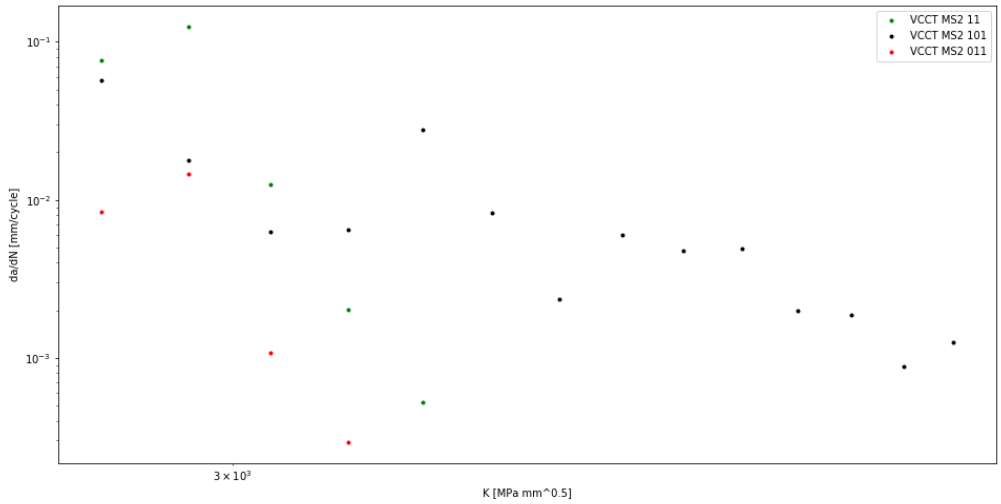


**Figure C.55:** A crack propagation plot showing the crack propagation rate versus the stress intensity factor for a CT specimen with VCCT interactions. In green it is performed for a VCCT interaction with properties $c_3 = 1$ and $c_4 = 1$, in black for a VCCT interaction with properties $c_3 = 10$ and $c_4 = 1$ and in red for a VCCT interaction with properties $c_3 = 0.1$ and $c_4 = 1$.

## C.9. Influence of different load levels

### C.9.1. VCCT MS2 11 U2.5

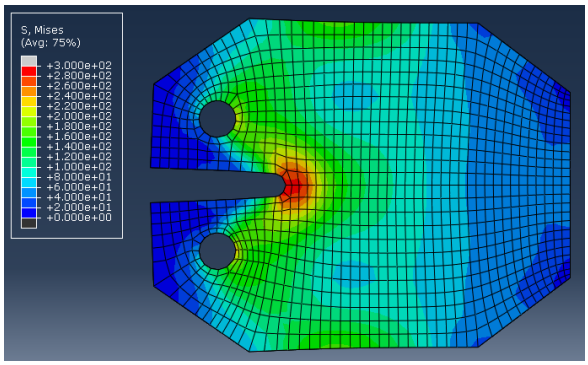


**(a)** One of the plies at cycle 1

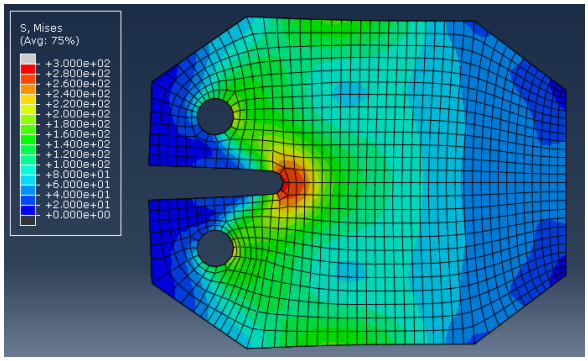


**(b)** One of the plies at cycle 2

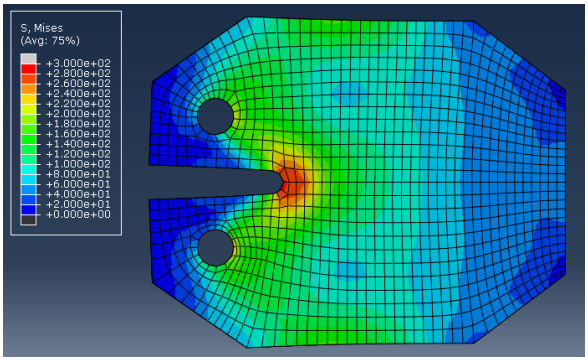


**(c)** One of the plies at cycle 9

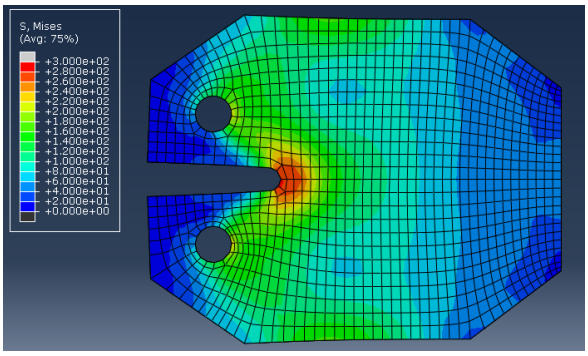


**(d)** One of the plies at cycle 12

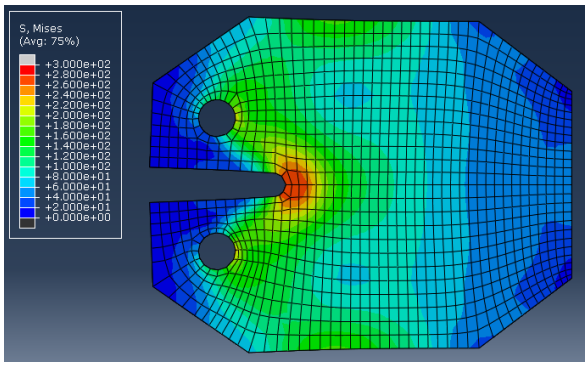


**(e)** One of the plies at cycle 21

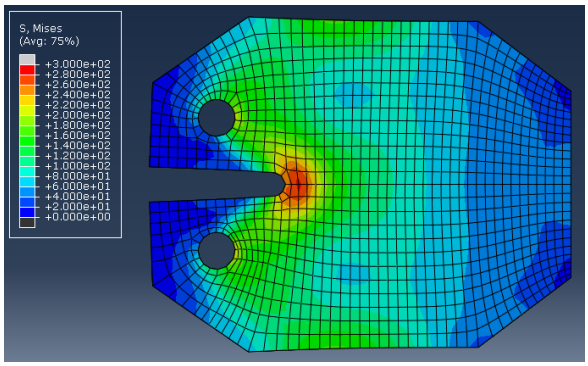


**(f)** One of the plies at cycle 42

**Figure C.56:** VCCT MS2 11 U2.5 part 1

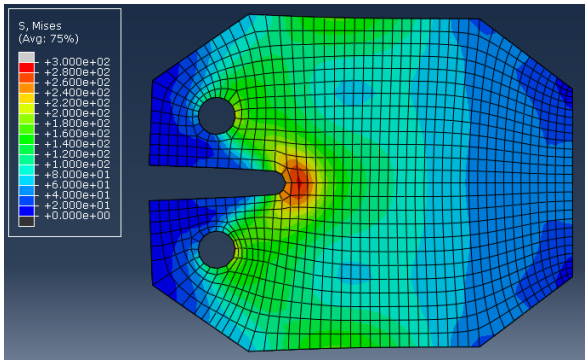


**(a)** One of the plies at cycle 98

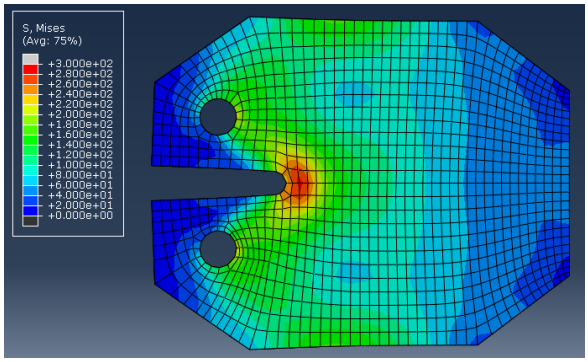


**(b)** One of the plies at cycle 217

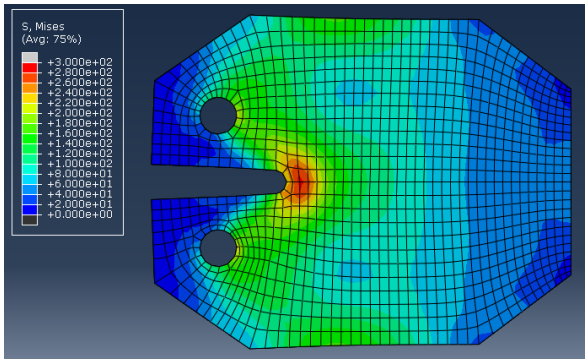


**(c)** One of the plies at cycle 535

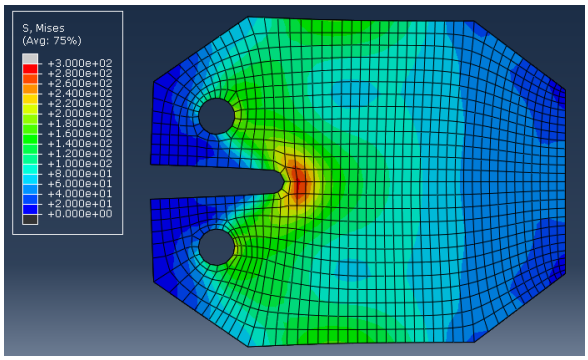


**(d)** One of the plies at cycle 1023

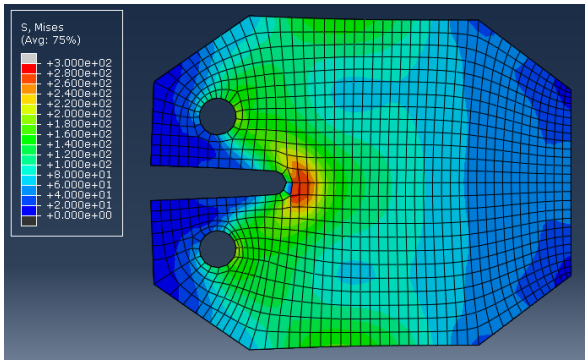


**(e)** One of the plies at cycle 1939

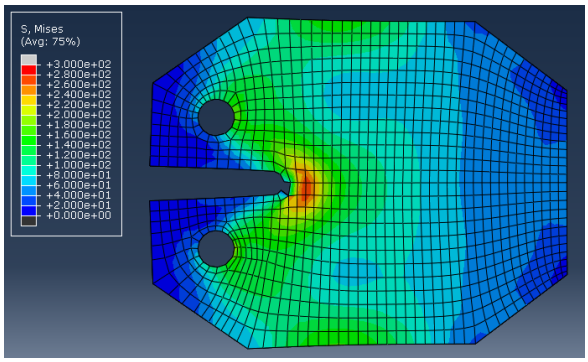


**(f)** One of the plies at cycle 5000

**Figure C.57:** VCCT MS2 11 U2.5 part 2

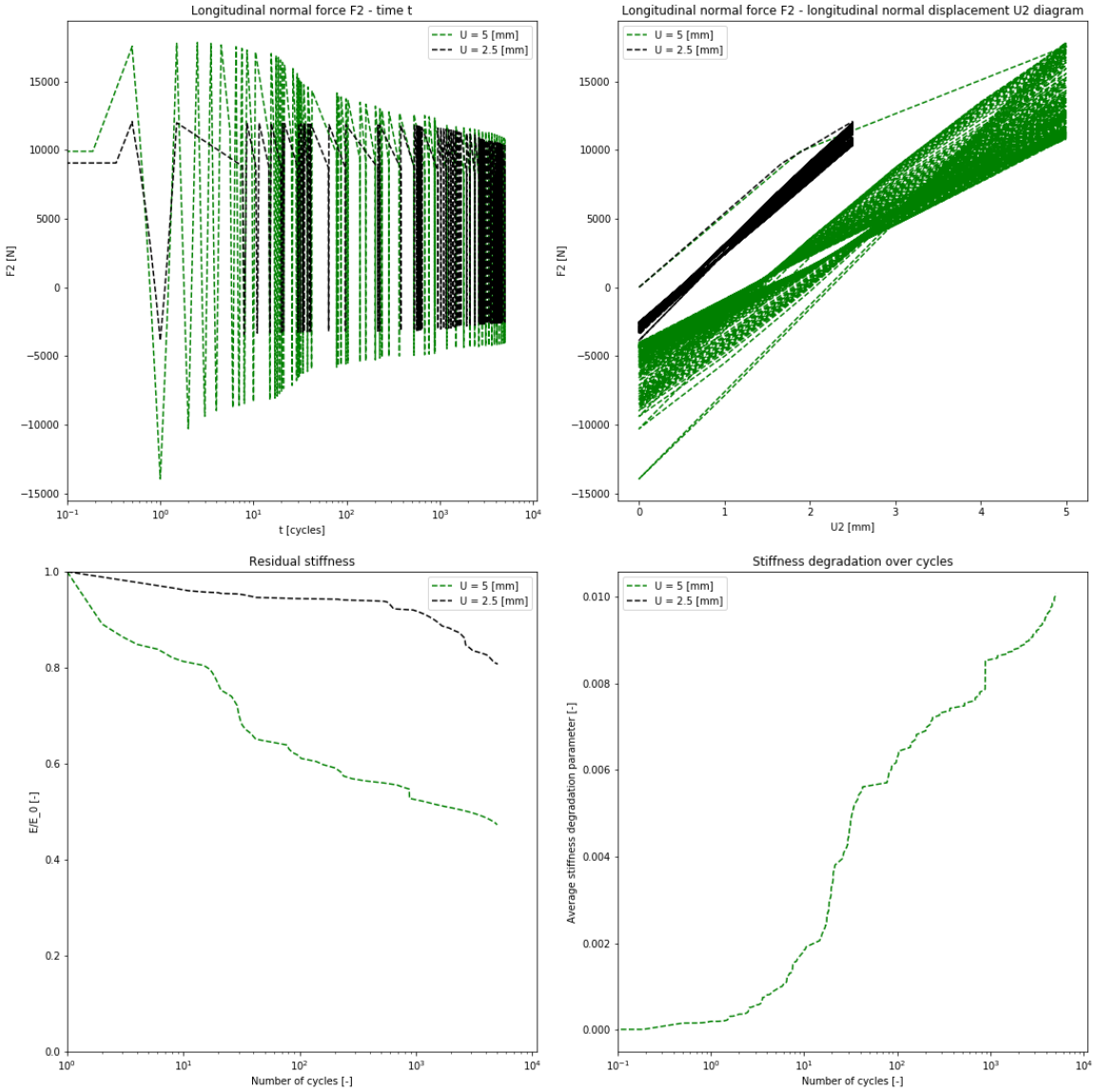


**Figure C.58:** In four plots the output is represented of the fatigue analysis for the compact tension specimen with five quasi-isotropic plies with VCCT interaction. A displacement of 2.5 [mm] is applied. The plots represent the analysis with a compact tension specimen with five plies with a layup $[0|-45|90|45|0]$ for which only the first direction of the quasi-isotropic plies is mentioned. The applied Paris law material constants for the black line are $c_3 = 1$ and $c_4 = 1$ and a mesh size of 2 [mm]. Counting from the left to the right and from the top to the bottom, the load history plot is given first. This plot shows the applied force over time as resultant of a constant applied displacement amplitude. The second plot is the force-displacement diagram which acts as hysteresis plot of the element as structural response. The third plot shows the stiffness of the structure relative to the response of the first cycle. The fourth plot shows the average value of the damage parameters of the individual elements that leads to stiffness degradation, hence it is already normalised with the number of elements. Do recognise that the time axes are now on log scale instead of linear.

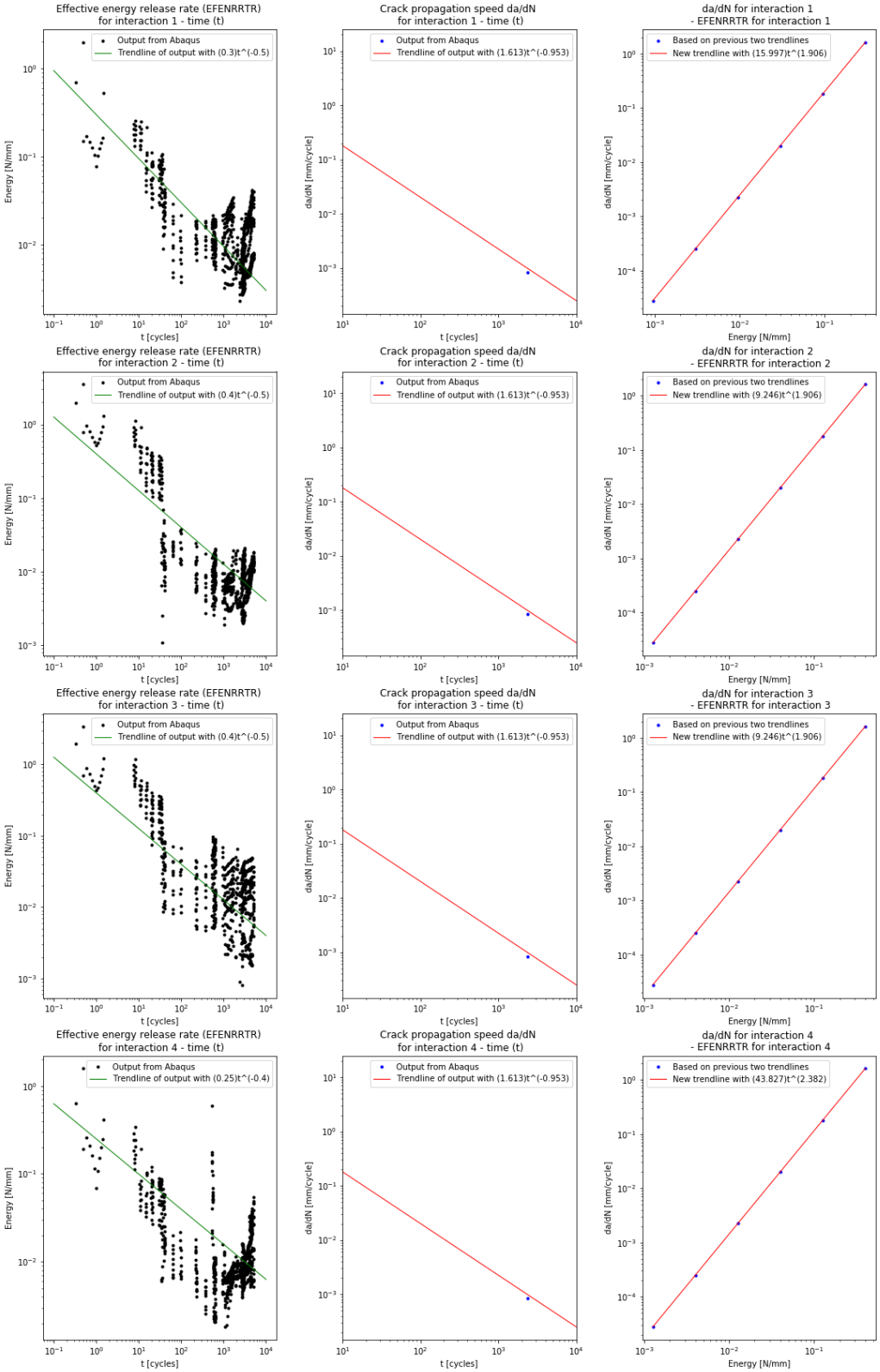


**Figure C.59:** A visualisation of the effect of the Paris law material constants on the fatigue analysis for the compact tension specimen related to figure C.58 with $c_3 = 1$ and $c_4 = 1$ and a load of 2.5 [mm]. Each row is for the next interface from the layup $[0|-45|90|45|0]$ and the fifth is the summation. The first column represents the equivalent energy release rate on the interface for each cycle. The second column provides the crack propagation rate for each 2 [mm] of crack propagation. The third column shows the relation between crack propagation rate and the equivalent energy release rate.

### C.9.2. VCCT MS2 11 U7.5

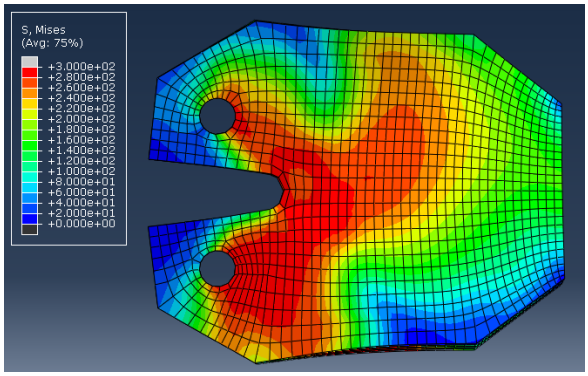


**(a)** One of the plies at cycle 1

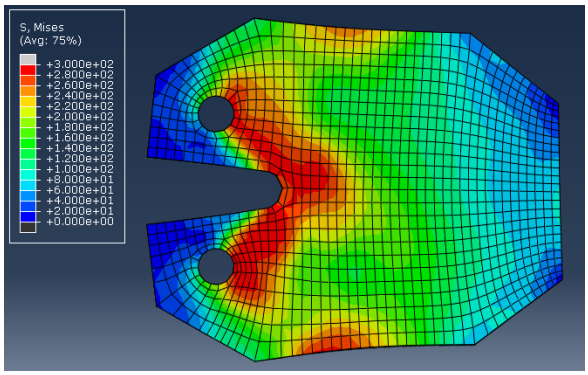


**(b)** One of the plies at cycle 2

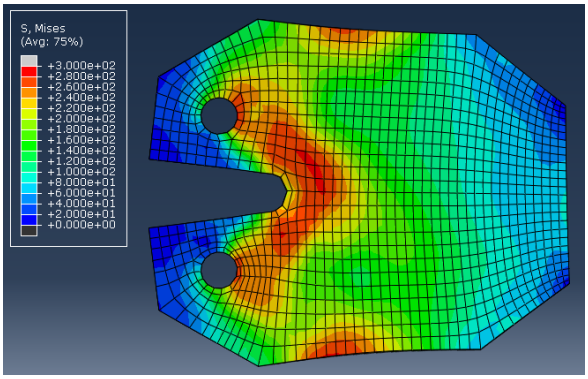


**(c)** One of the plies at cycle 5

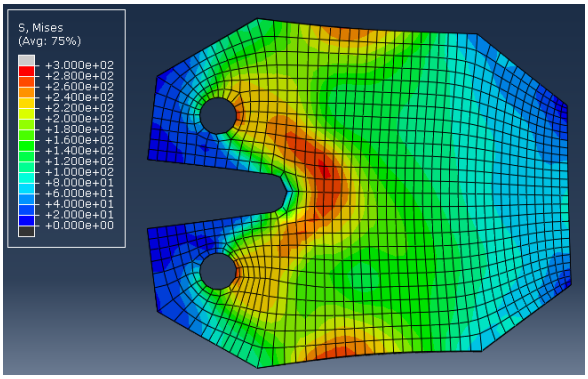


**(d)** One of the plies at cycle 10

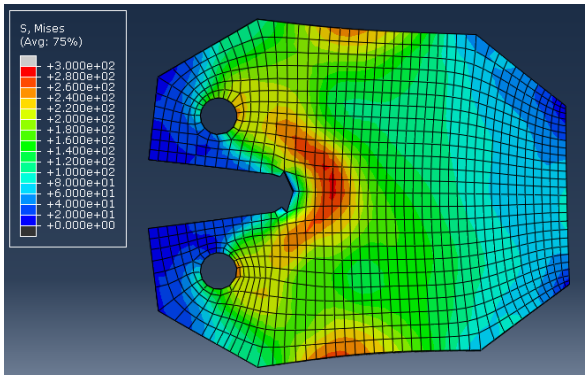


**(e)** One of the plies at cycle 22

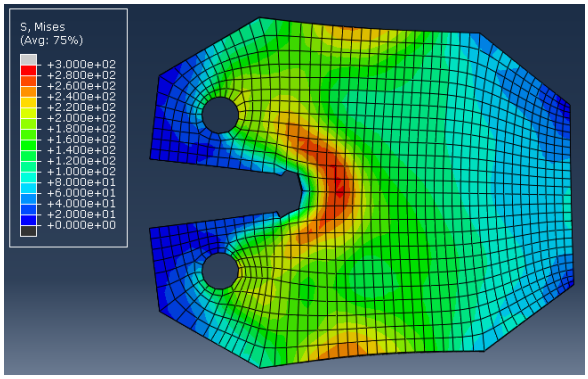


**(f)** One of the plies at cycle 52

**Figure C.60:** VCCT MS2 11 U7.5 part 1

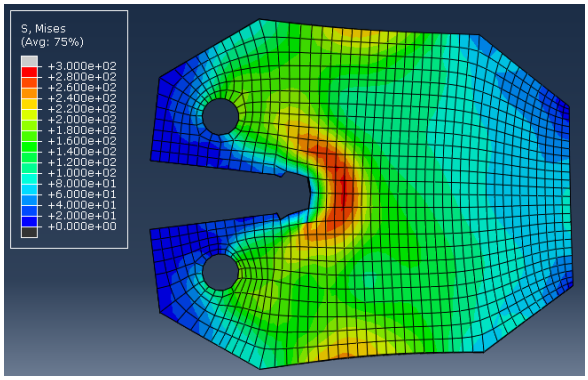


**(a)** One of the plies at cycle 95

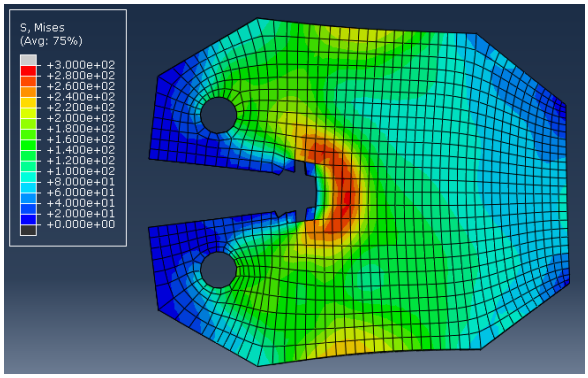


**(b)** One of the plies at cycle 200

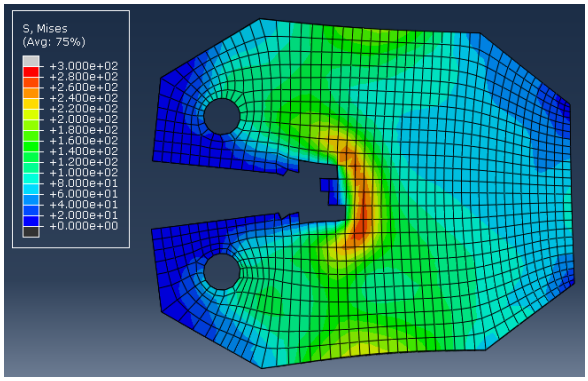


**(c)** One of the plies at cycle 502

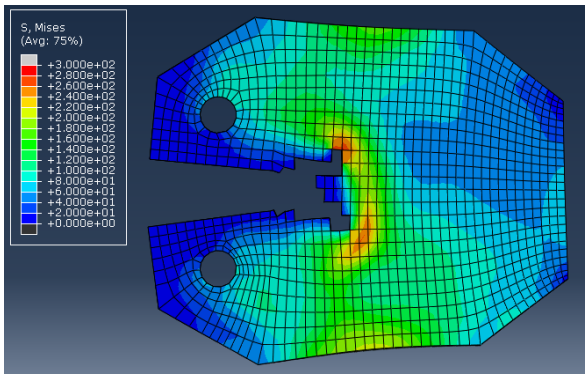


**(d)** One of the plies at cycle 1007

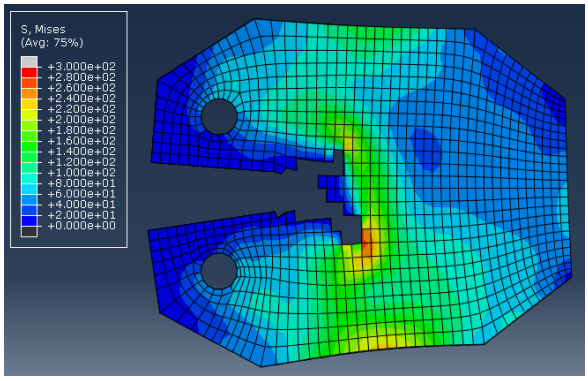


**(e)** One of the plies at cycle 1982

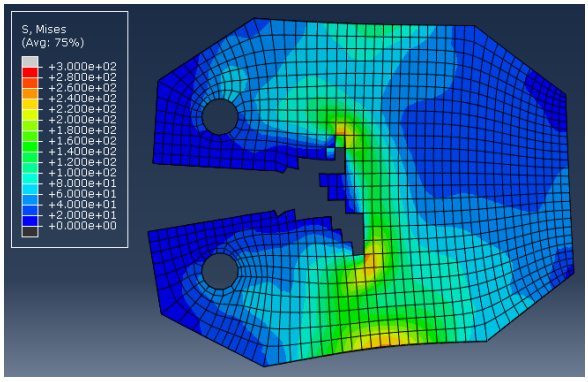


**(f)** One of the plies at cycle 5001

**Figure C.61:** VCCT MS2 11 U7.5 part 2

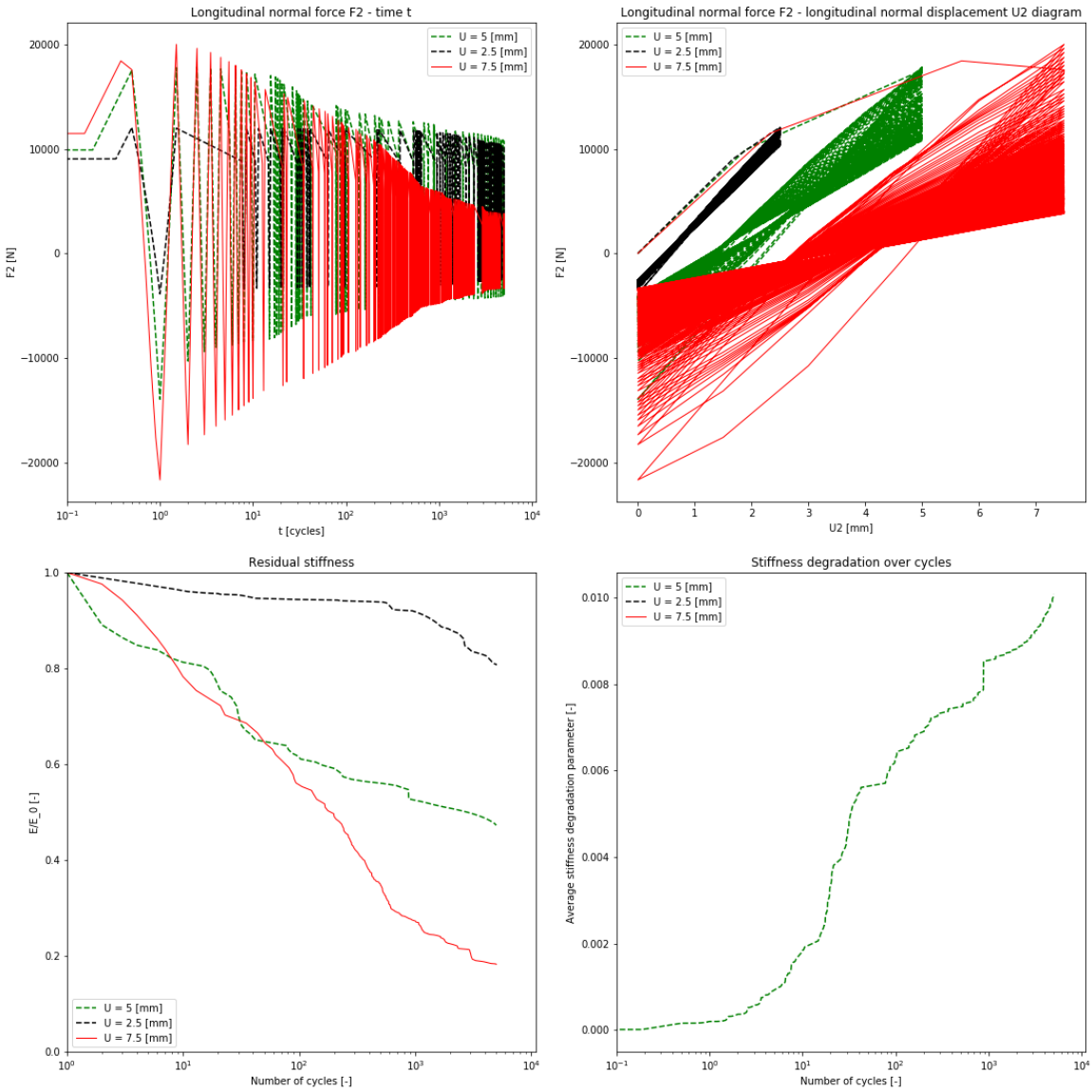


**Figure C.62:** In four plots the output is represented of the fatigue analysis for the compact tension specimen with five quasi-isotropic plies with VCCT interaction. A displacement of 7.5 [mm] is applied. The plots represent the analysis with a compact tension specimen with five plies with a layup $[0|-45|90|45|0]$ for which only the first direction of the quasi-isotropic plies is mentioned. The applied Paris law material constants for the black line are $c_3 = 1$ and $c_4 = 1$ and a mesh size of 2 [mm]. Counting from the left to the right and from the top to the bottom, the load history plot is given first. This plot shows the applied force over time as resultant of a constant applied displacement amplitude. The second plot is the force-displacement diagram which acts as hysteresis plot of the element as structural response. The third plot shows the stiffness of the structure relative to the response of the first cycle. The fourth plot shows the average value of the damage parameters of the individual elements that leads to stiffness degradation, hence it is already normalised with the number of elements. Do recognise that the time axes are now on log scale instead of linear.

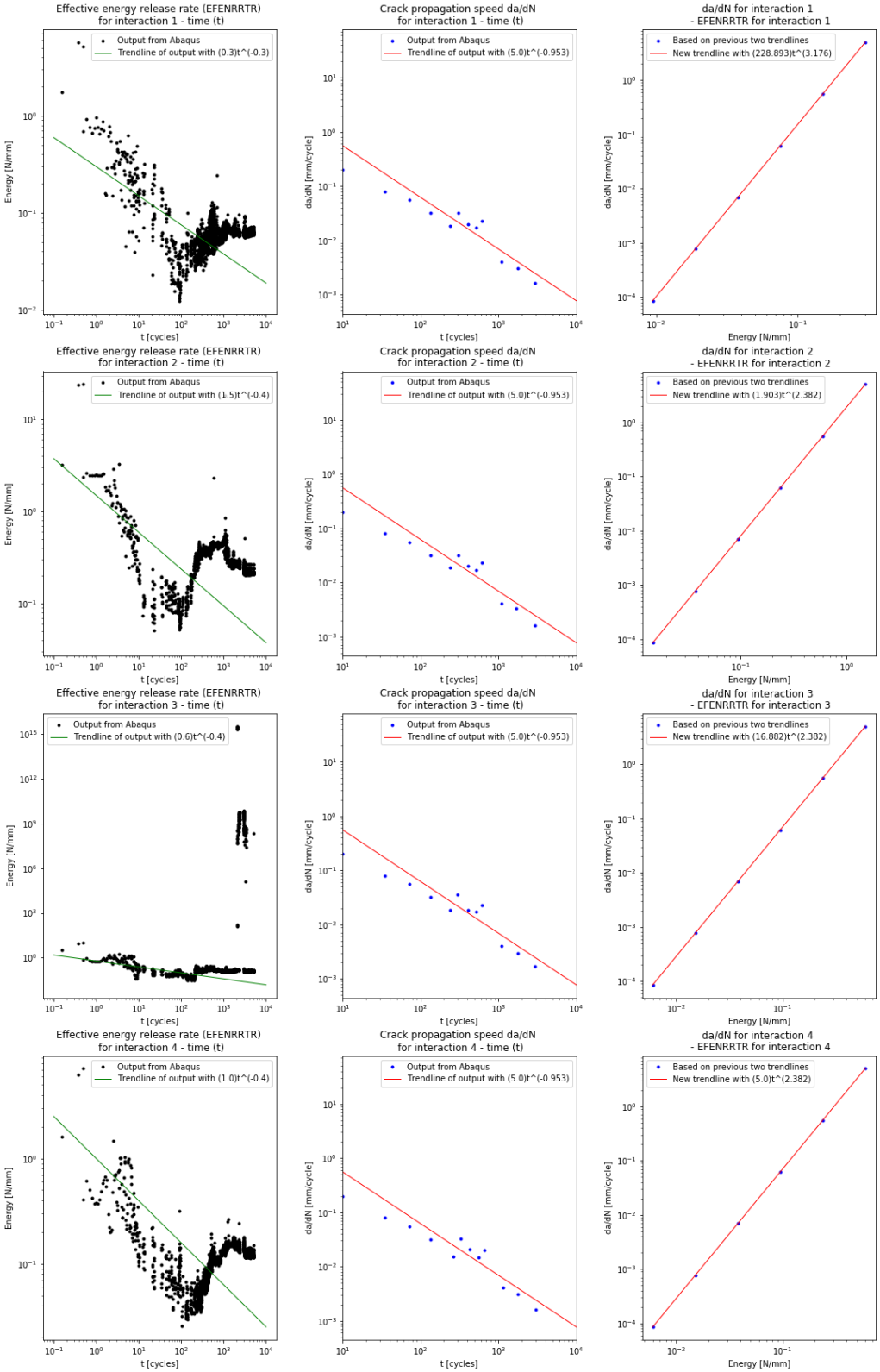


**Figure C.63:** A visualisation of the effect of the Paris law material constants on the fatigue analysis for the compact tension specimen related to figure C.62 with $c_3 = 1$ and $c_4 = 1$ and a load of 7.5 [mm]. Each row is for the next interface from the layup $[0|-45|90|45|0]$ and the fifth is the summation. The first column represents the equivalent energy release rate on the interface for each cycle. The second column provides the crack propagation rate for each 2 [mm] of crack propagation. The third column shows the relation between crack propagation rate and the equivalent energy release rate.

### C.9.3. Comparing results of different load levels for VCCT MS2 11

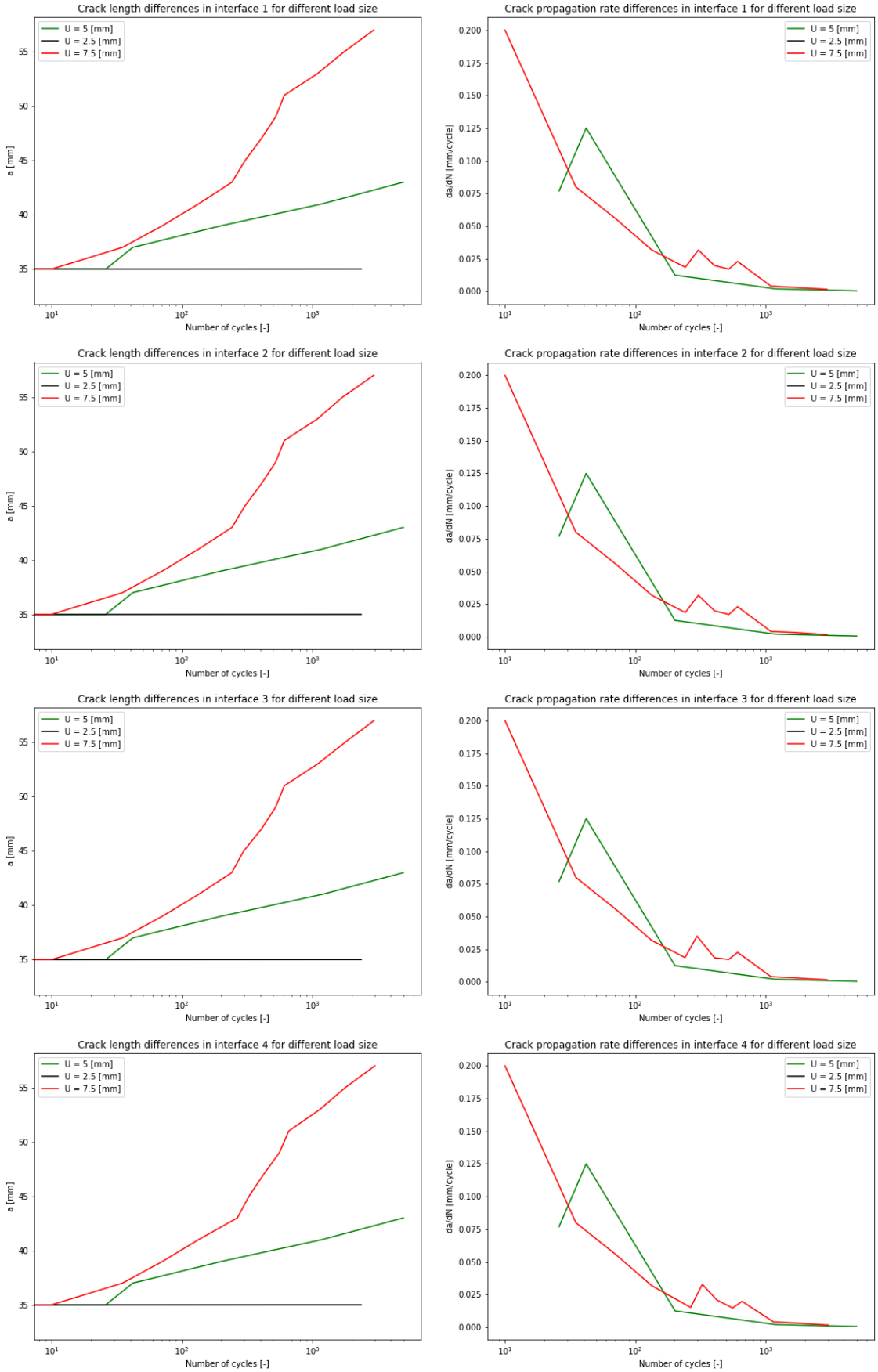


**Figure C.64:** Comparison of the crack propagation for the VCCT interface with load change for each interface. On the left the crack length over the cycles and on the right the crack propagation speed over the cycles. In green it is performed for a 5 [mm] cyclic displacement, in black for a 2.5 [mm] cyclic displacement and in red for a 7.5 [mm] cyclic displacement.

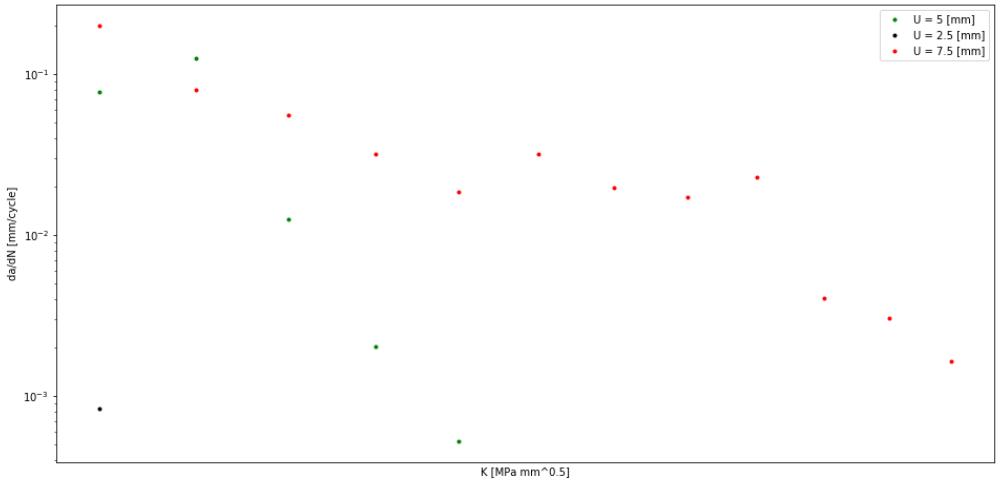


**Figure C.65:** A crack propagation plot showing the crack propagation rate versus the stress intensity factor for a CT specimen with VCCT interactions. In green it is performed for a $5$ [mm] cyclic displacement, in black for a $2.5$ [mm] cyclic displacement and in red for a $7.5$ [mm] cyclic displacement.

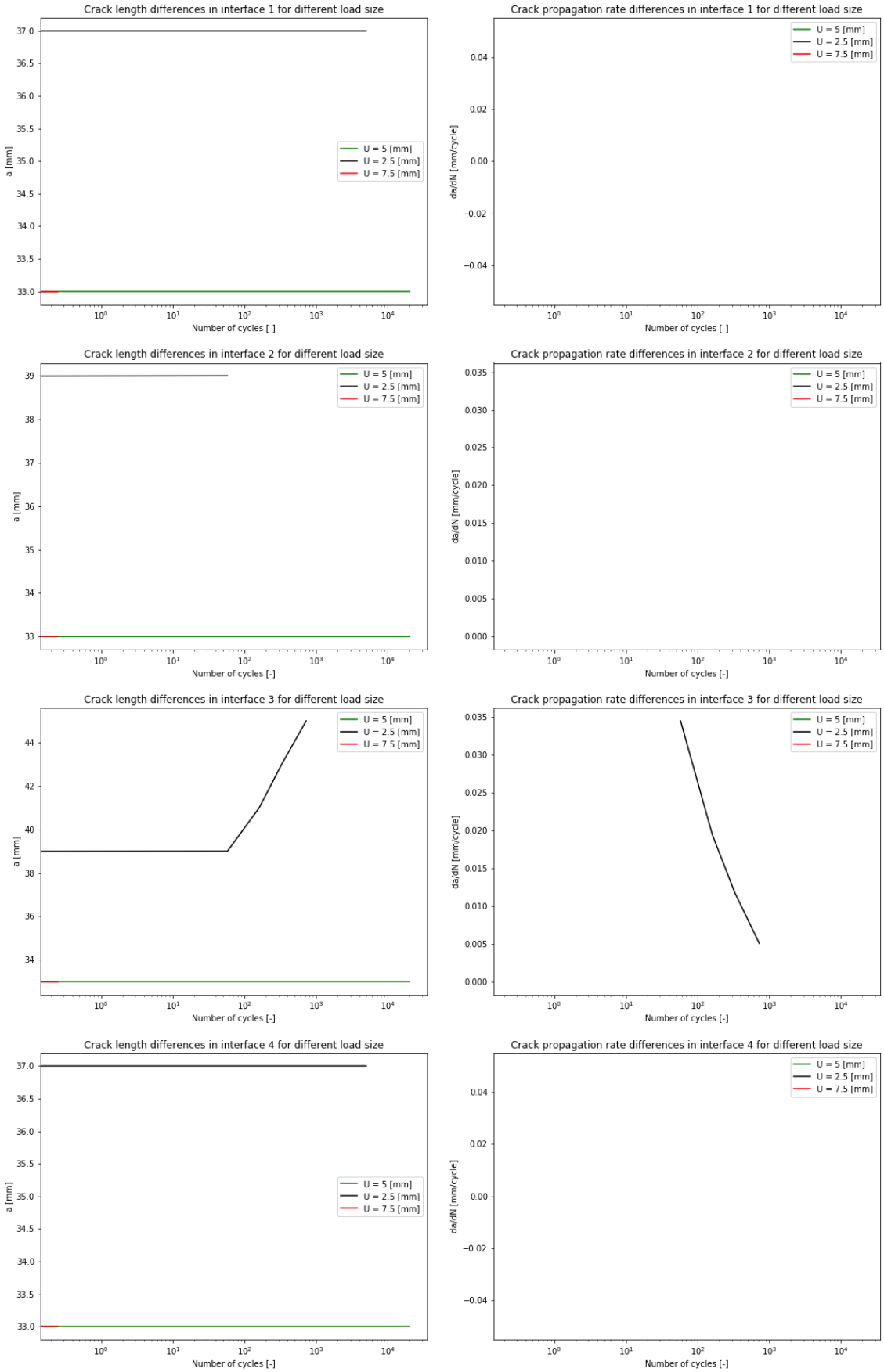


**Figure C.66:** Comparison of the crack propagation for the VCCT interface with load change for each interface. This is if the material is linear elastic, thus isolates the VCCT mechanism. On the left the crack length over the cycles and on the right the crack propagation speed over the cycles. In green it is performed for a 5 [mm] cyclic displacement, in black for a 2.5 [mm] cyclic displacement and in red for a 7.5 [mm] cyclic displacement.